THE ROLE OF FATTY ACID OXIDATION IN DISRUPTION OF MACROPHAGE FUNCTION

By

Alexandra C. Schrimpe Rutledge

Dissertation

Submitted to the Faculty of the

Graduate School of Vanderbilt University

in partial fulfillment of the requirements

for the degree of

DOCTOR OF PHILOSOPHY

in

Chemistry

May, 2009

Nashville, Tennessee

Approved:

Professor David W. Wright

Professor Daniel C. Liebler

Professor David E. Cliffel

Professor Brian O. Bachmann

This dissertation is dedicated to my

parents, Fred and Marie, for

their unconditional love and support

ACKNOWLEDGEMENTS

I recently found a paper entitled “Where I will be in 15 years” that I wrote when I was in the 7th grade. I anticipated that I would be a doctor. Well, I am now a doctor—not a medical doctor like I originally thought that I would become back then—but a doctor, nevertheless. The fact that I am where I am today is a reflection of the guidance and support that I have received over the last 15 years (and the years leading up to my writing that paper).

It goes without saying (but I will say it anyway) that my family is my biggest support. I should begin with the one person who I can honestly say was crucial to my reaching this goal, my husband Ryan. From the moment we met at Vanderbilt, he has influenced my life and become “my everything”. Every single day I am blessed to have him, his love, and his support in all of my endeavors. I cannot express my gratitude enough, but I will try. Thank you Ryan. I only hope that I am to him, what he is to me. I also acknowledge my parents, Fred and Marie Schrimpe, and my brother and sister-in-law, Freddie and LeAnn Schrimpe. I thank them for all of their time, positive energy, and motivation. There is absolutely no way that I would, or could, have done this without them. I must also thank the newest members of my family, Mark, Gayle, Derek, and Ethan Rutledge, for their kind words of encouragement.

Graduate school was by no means what I anticipated it to be. I had no idea of the difficulties, in terms of gaps of knowledge and lack of technical experience, that lie ahead, and I had no idea that the focus of my dissertation research would be, according to Robert Ridley, “an insoluble mass of material that is soul-destroying to work with.”

Consequently, I am indebted to my advisor, David Wright, for his patience and assistance throughout my time here at Vanderbilt. I am extremely fortunate to have had a mentor that cared so much about the success of the science- and the student- at the same time. Thank you for helping me gain the confidence and skills necessary to become the person and scientist that I am today. I only hope that I can lead others like you have led me.

As I mentioned, I had no idea of what graduate school would entail; and, therefore, I had no idea how much time graduate school required. Being that so much time was spent within the confines of SC7870, I have befriended a handful of labmates. I acknowledge Drs. Crystal Miller and Clare Carney for showing me the ropes of studying hemozoin; Drs. Elizabeth Bentzen and Scott Miller for their advice, humor, and friendly conversation; Reese Harry and Kristin Halfpenny for their friendship from our first day of graduate school as partners working through all of the general chemistry labs until the present time; Vanessa Scott for being a great bay-mate and friend outside of lab; Melissa Carter, Rebecca Sandlin, Jonas Perez, Stephen Jackson, and Dr. John Stone for their help and advice; Dr. Catherine Prudom for her knowledge, patience, time, and willingness to help at a moment's notice; one of the most genuine people I have ever known–Josh Swartz–for his cheerfulness, optimism, positive attitude, dedication to complete a task, and curiosity for the depths of science; Goska Broncel, Leila Deravi, and Anh Hoang for daily "tea-times" and wonderful friendships; and Magda Paszewska and Andrzej Balinski for friendship and adventures away from the lab.

Finally, I am grateful for the opportunities, facilities, and people outside of the lab that I have worked with here at Vanderbilt. First and foremost, my committee members, Professors Brian Bachmann, David Cliffel, and Daniel Liebler; I thank them for your

insight, ideas, and knowledge throughout my graduate school career. I am also fortunate for the time spent, and experience gained, using core facilities; I thank Wade Calcutt at the Mass Spectrometry Research Center, Braden Boone at the Vanderbilt Microarray Shared Resource, and both Dave Flaherty and Brittany Matlock at the Flow Cytometry Core Facility.

TABLE OF CONTENTS

LIST OF TABLES

LIST OF FIGURES

CHAPTER I

THE ROLE OF HEMOZOIN IN THE PATHOGENESIS OF MALARIA

Introduction

Malaria is one of the oldest diseases known to mankind; yet, it remains one of the most significant concerns to humanity today, threatening nearly 40% of the world's population.[1] Malaria was first documented centuries ago by Medieval Italians who correlated periodic fevers with exposure to bad marsh air (i.e., mala "bad" and aria "air") that comes to Rome every summer. However, it was not until the late 1800's that the disease was attributed to parasites carried by mosquitoes that often sequester near stagnant water during the summer months.

Malaria is a disease primarily of the tropics, but can also be found in various regions of the Middle East and Asia (Figure 1). Each year between 300 and 500 million people become infected, resulting in over 1 million deaths annually.[1] Although eradicated from most of the world by the mid 1960's, malaria's resurgence in the past decade poses significant social, economical, and health risks on a global scale. This is especially true for third world countries, where poverty assumes both cause and effect roles for disease transmission. Furthermore, malaria infections are becoming progressively more challenging due to parasitic resistance to common antimalarial drugs and vector resistance to insecticides.[2]

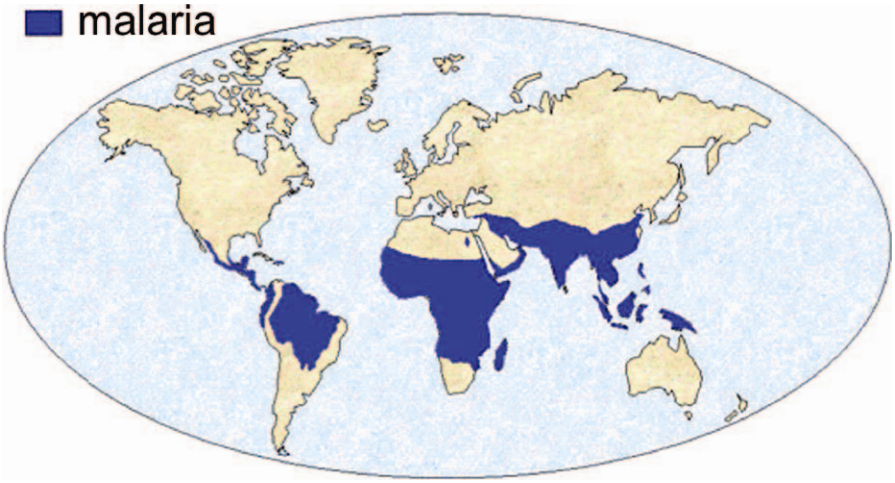

Figure 1. Geographic distribution of malaria.[3]

Lifecycle of *Plasmodium falciparum*

The first major advancement in deciphering the origin of infection was made by Charles Lavaran in 1880 when he observed parasites within erythrocytes collected from malaria victims. Nearly twenty years later, Carlos Finlay and Sir Ronald Ross independently suggested and demonstrated that malaria was transmitted between humans via infected mosquitoes.[4, 5]

Since that time, much has been uncovered related to malaria pathogenesis. Infection is caused by one of four species of *Plasmodium* that target humans: *falciparum*, *vivax*, *ovale*, and *malariae*. The most serious, and often fatal, form of malaria is caused by *P. falciparum*, which is responsible for nearly 80% of malaria cases. Regardless of species, *Plasmodium* parasites have a complex lifecycle with several stages in both the mosquito vector and human host (Figure 2).[6] Transmission occurs when an infected female *Anopheles* mosquito takes a blood-meal and sporozoites, the infective parasite form present in salivary ducts of the mosquito, enter the host's body. Sporozoites quickly (~1 h) target the liver where they reside for 5-15 days while undergoing asexual fission,

resulting in the generation of thousands of merozoites. Hepatic cells eventually rupture and release the merozoites into circulation initiating the intraerythrocytic phase. Within erythrocytes, merozoites mature to a feeding form (i.e., trophozoite) which catabolizes host hemoglobin (Hb) as a source of nutrition essential for development and maturation, ultimately producing another passage of merozoites. After a 48 or 72 h period, RBCs rupture in a synchronized burst and release debris and parasites into circulation. Merozoites complete the asexual phase by differentiating into gametocytes and returning to the mosquito during a subsequent blood meal, or repeat the intraerythrocytic cycle by invading new RBCs. Notably, many clinical manifestations of malaria, including periodic fever, chills, headache, nausea, muscle spasms, and anemia, coincide with this intraerythrocytic phase and synchronized burst.

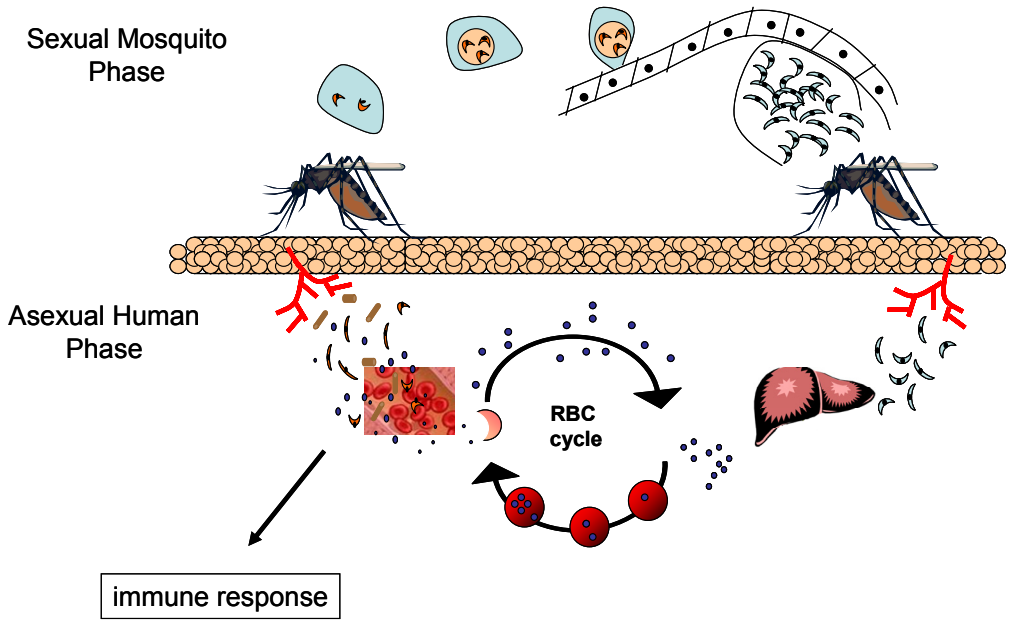

Figure 2. Lifecycle of the malaria parasite. (Top) The sexual cycle produces sporozoites within the body of the mosquito. (Bottom) During a blood-feed, sporozoites are transmitted from the salivary glands of an infected mosquito to a human host. Parasites undergo two asexual reproductions, first within hepatocytes and then within erythrocytes. Hemozoin is formed during the intraerythrocytic cycle.

Hemoglobin Catabolism and Hemozoin Formation

During the intraerythrocytic phase, host Hb is catabolized through a series of enzymatic processes as summarized in Figure 3. By virtue of the indispensable need for nutrition, this process continues repeatedly during infection. Briefly, parasites ingest nearly 80% of host Hb through pinocytosis via cytostomes.[7] Within the digestive vacuole, Hb is initially digested into a mixture of peptides by aspartic acid- (i.e., plasmepsins), cysteine- (i.e., falcipains), and metallo- (falcilysin) proteinases. These peptides are then digested to individual amino acids by exopeptidases within the cytosol of the parasite where they are used for growth and maturation. Given that Hb is degraded to its simplest form, monomeric heme (Fe(II) protoporphyrin IX, Fe(II)-PPIX) is also released into the digestive food vacuole of the parasite.[8, 9]

Although heme is a vital cofactor for a diverse set of proteins involved in respiration, oxygen transport, and drug detoxification, the accumulation of free heme has toxic effects. Heme is capable of binding lipid bilayers, thus inhibiting protease activity and catalyzing lipid peroxidation resulting in cell lysis.[10, 11] Mammalian cells metabolize heme via heme oxygenease (HO-1); however, *Plasmodium* parasites (and several other blood-feeding organisms, including the blood fluke *Schistosoma mansoni* and the kissing bug *Rhodnius prolixus*) lack this enzyme. Detoxification of heme released during hemoglobin catabolism is essential for parasite survival. Consequently, a mechanism has evolved whereby >95% of the free heme is sequestered into the insoluble aggregate hemozoin (Hz) or malaria pigment (Figure 4).[12] As most of the heme is occluded within the crystal, the parasite protected. Several antimalarials (e.g., quinolines) act during the degradation of hemoglobin and subsequent production of Hz and are thought to complex

with the heme, thereby inhibiting the growth of the biomineral and exposing parasites to a toxic environment.[13]

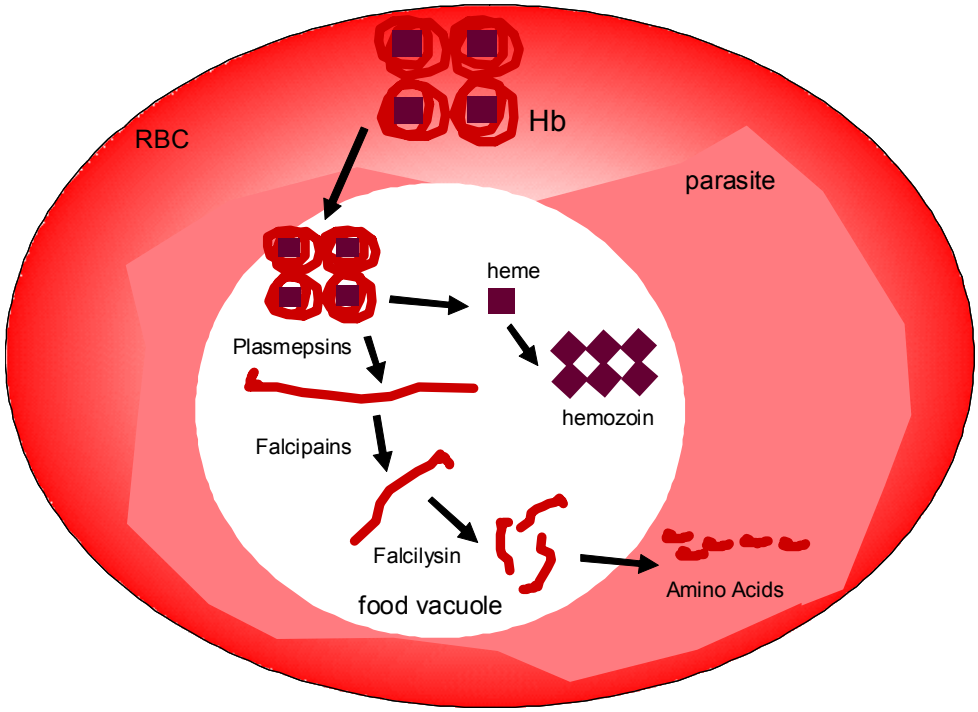

Figure 3. Process of hemoglobin degradation and heme detoxification by intraerythrocytic malaria parasites. Hemoglobin is degraded within the digestive food vacuole of the parasite by a group of aspartic acid proteinases (plasmepsins *Pf*PM1, *Pf*PM2, *Pf*PM4, and *Pf*HAP), cysteine proteinases (falcipains *Pf*FP2, *Pf*FP2′, and *Pf*FP3), and the metalloproteinase falcilysin. As a result of the liberated toxic heme, hemozoin is formed. Adapted from reference 14.

Hemozoin Formation

Slater *et al*. demonstrated that Hz contains bonds between the Fe (III) center of one heme unit and a propionate side chain of another.[16] This result suggested that Hz was a polymer comprised of $[Fe(III)\text{-}PPIX]_n$ chains. The eventual acquisition of a resolved crystal structure by Pagola *et al*., however, led

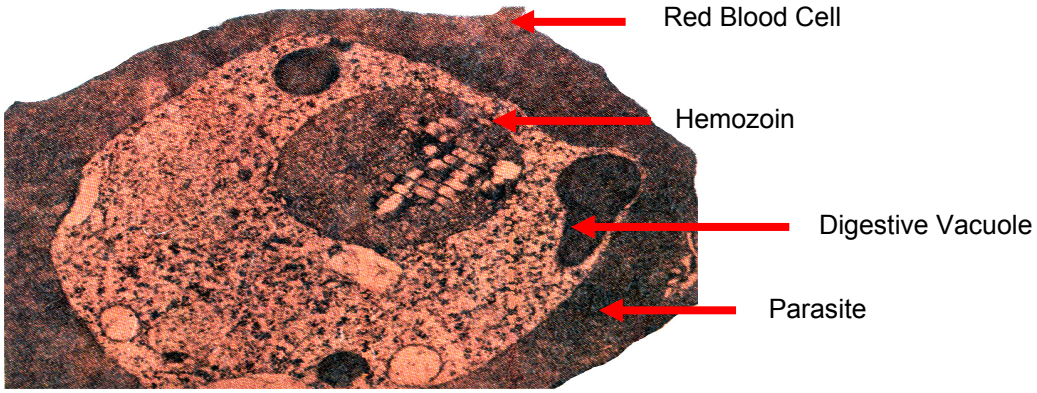

Figure 4. Electron micrograph of a parasitized erythrocyte. Hemozoin is formed within the acidic digestive food vacuole of the parasite.[15]

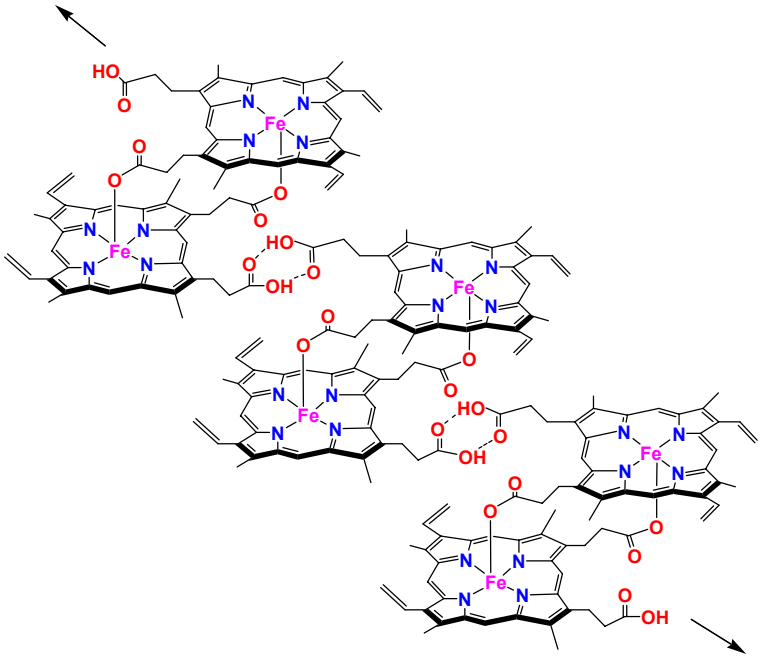

Figure 5. Molecular representation of a growing hemozoin crystal. Structurally, the biomineral is an aggregate of hydrogen bonded five-coordinate Fe (III)-PPIX dimers, joined by reciprocating monodentate carboxylate linkages between the central iron of one monomer and a propionic acid side chain of a second monomer. Adapted from reference 17.

to the determination that the fundamental bonds comprising the Hz dimer (Figure 5) are reciprocal head-to-tail Fe(III)- carboxylate coordinate bonds between the central iron of one heme monomer and the propionic carboxylate side chain of a second heme monomer.[17] Dimeric units are held together by hydrogen bonds, leading to chain extension and crystal growth.

The mechanism of Hz formation *in vivo* is a subject of much debate and, consequently, a topic of active research. Three mechanisms have been proposed thus far: enzymatic activity mediated by a heme polymerase, nucleation by a template protein, and promotion via a lipid-mediated process. Among the first to explore Hz formation, Slater and Cerami reported that *P. falciparum* trophozoite extracts incubated with hematin (Fe(III)-PPIX-OH) under physiological conditions led to Hz formation.[18] The authors proposed that formation was catalyzed by an unknown heat- and sodium dodecyl sulfate (SDS) sensitive-heme polymerase that was present in the extract. Studies performed by Chou and Fitch using *Plasmodium berghei* (murine malaria) extracts supported this theory.[19] However, attempts at identifying and purifying this putative polymerase were unsuccessful. Dorn *et al.* later challenged the presence of a putative heme polymerase by demonstrating that Hz formation occurred spontaneously in the presence of heat-inactivated native Hz and synthetic Hz.[20] The results of these studies suggested that Hz formation was autocatalytic, but were unable to provide a basis for the nucleation of the initial Hz crystal.

The second potential mechanism of Hz formation mentioned above was based on the ability of a protein, specifically histidine-rich proteins II and III (HRP-II and III), to act as a nucleation site for crystal growth.[21] HRPs comprise a family of proteins that

manifest a tandem tripeptide (Ala-His-His) repeat motif that represents a hypothetical biomineralization template. Sullivan and coworkers showed that HRPII was indeed able to promote Hz formation.[21] Furthermore, Ziegler *et al*. utilized a dendrimer to present the tripeptide unit and similarly demonstrated Hz formation.[22] These results indicate that this recurring domain may provide a scaffold which promotes heme nucleation and growth, resulting in Hz formation. Although HRPs mediate Hz formation *in vitro*, their authenticity *in vivo* has been contested, as studies have shown HRPs localize outside of the digestive food vacuole, and thus away from the site of Hz formation. Furthermore, Hz formation in *P. falciparum* clones lacking HRP-II and -III genes was normal.[23] Together, these results suggest that Hz formation proceeds by another mechanism *in vivo*.

The final proposed mechanism of Hz formation was first addressed by Bendrat *et al*., who suggested that lipids are responsible for inducing and mediating biomineral nucleation.[24] The authors specified that the seemingly autocatalytic formation previously observed by synthetic hemozoin was merely a result of contaminating phospholipids from commercial heme preparations (which are prepared by extraction from intact erythrocytes). Several groups have demonstrated the ability of polar membrane lipids[24] and neutral lipid bodies[25-29] to nucleate Hz formation *in vitro*; and recently, neutral lipid nanospheres enveloping hemozoin crystals within *P. falciparum* digestive vacuoles were identified.[26] These observations are intriguing as lipid droplets provide an optimal site for concentrating lipophilic heme from an aqueous environment, furthering the suggestion that lipid promotion appears plays a significant role in Hz formation *in vivo*.

Synthetic Hemozoin

Current malaria research employs the use of two chemically and structurally identical crystal forms of the malaria pigment. The first is native Hz, the biosynthetic material isolated from parasitized erythrocytes, and the second is synthetic Hz, herein referred to as β-hematin (BH).[30] The fundamental difference between the two forms is the array of host- and parasite-derived lipids, proteins, and nucleic acids that are adsorbed onto the surface of native Hz.[31, 32] Given the vast number of pigment preparations that can be derived from these basic forms, the state of the material must be well-defined in order to interpret experimental results. Crude Hz is pigment that is isolated from parasitized erythrocytes and gently washed to remove cellular debris but left with a lipid coat adsorbed onto the hydrophobic porphyrin plane.[33] Purified Hz refers to crude Hz whose lipid coat has been removed by detergent[34] or organic solvent extraction.[35] BH, on the other hand, has been prepared and purified from hemin and is consequently devoid of all biologically-derived components.[36-39] Several groups have reported conflicting results concerning the effects of Hz and BH in both *in vitro* and *in vivo* systems, including pro-inflammatory,[40] anti-inflammatory,[36] and oxidative stress responses . These differences are likely attributable to the purity of the preparation, the amount of biomineral used, and the method of immune cell activation (e.g., lipopolysaccharide (LPS), interferon-γ (IFN-γ), LPS+IFN-γ, or phorbol myristate acetate (PMA)).

BH can be synthesized several ways. Bohle and coworkers reported a dehydrohalogenation reaction that occurs under anhydrous conditions in an inert atmosphere at room temperature over the course of three months.[37] An alternate preparation by Slater *et al.*, referred to as the aqueous acid-catalyzed method, proceeds at

a high temperature (70 ºC) over several hours.[30] Characterization of the products from both synthetic routes demonstrates material that is chemically, spectroscopically, and crystallographically identical to HZ. [39, 41, 42] Morphologically, however, the Bohle method produces BH most similar to hemozoin isolated from *P. falciparum* (Figure 6).[43]

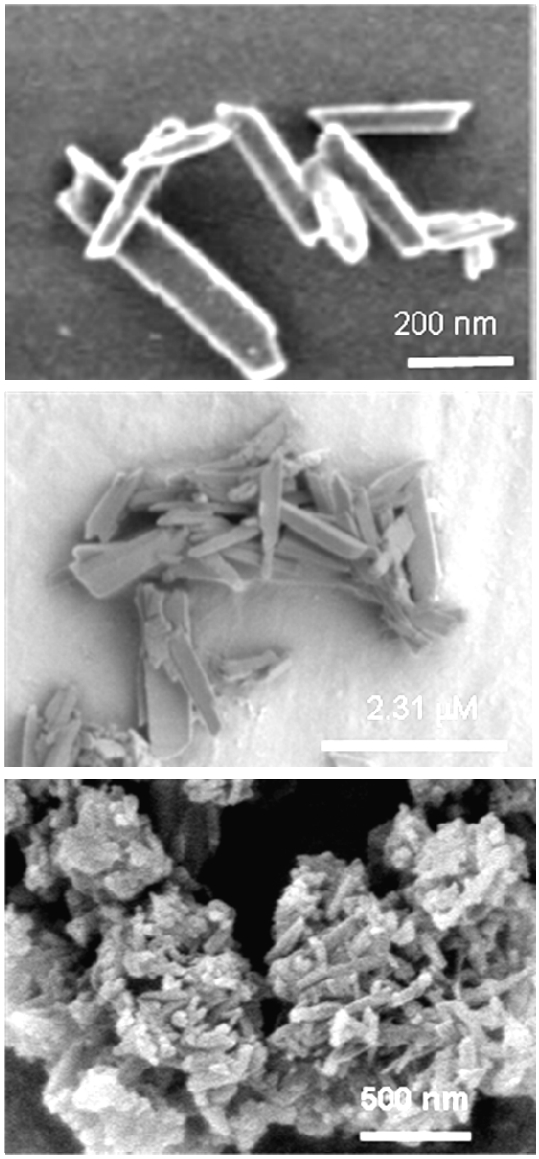

Figure 6**.** Native hemozoin isolated from the parasite *P. falciparum* (top), BH synthesized from a dehydrohalogenation reaction (middle), and BH synthesized from a rapid aqueous acid-catalyzed reaction (bottom).[43, 44]

Immune Response to Malaria

The host immune response to malarial infection is multifactorial, including complex innate and adaptive responses to the parasites, composite native Hz, Hz-derived lipid peroxidation products, and other cellular debris. Not unexpectedly, countless interactions between an array of malaria toxins and host cells result in adverse biological effects (e.g., periodic fever, chills, headache, nausea, muscle spasms, and anemia). Although an early immune response is essential for protective immunity, an over-stimulated response likely contributes to malaria pathogenesis: the destruction of parasites from the body results in considerable tissue damage, and the secretion of soluble factors causes adverse systemic effects.[45, 46] Consequently, the outcome of malarial infection relies upon a delicate balance between under- and over-activation of immune responses.

The release of foreign debris from ruptured RBCs provides a stimulus for innate immune activation and subsequent release of soluble factors including pro-inflammatory cytokines and chemokines. These molecules are responsible for varying levels of disease susceptibility, including cerebral malaria and anemia, and ultimately, disease progression, morbidity, and mortality. TNFα was the first cytokine characterized to play a role during malaria.[47, 48] It has since been demonstrated that TNFα secretion can be induced by macrophages and T cells in response to parasitized RBCs, Hz, and glycolipids (e.g., the glycosylphosphatidylinositol (GPI) moiety).[49] TNFα regulates the production of chemokines and cytokines such as interleukin 1 (IL-1), which is the predominant cytokine responsible for the fever.[50] Notably, anti-TNF therapy reduced the fevers of children infected with *P. falciparum*,[51, 52] demonstrating the synergism that exists during

the inflammatory response. Although other pro-inflammatory molecules, including IL-12, IL-18, and interferon γ (IFNγ),[53-55] are also present in high levels, the production of immune cell effectors is dynamic over the course of infection. The production of several anti-inflammatory cytokines, including IL-4, IL-10, and transforming growth factor (TGF) β is apparent in later stages, indicating an effort to maintain inflammatory balance.[56] However, patients still exhibit inflammation after the clearance of parasites from circulation, demonstrating long-term immune dysregulation.[57]

Biological Activity of Hemozoin

Accumulating evidence suggests that many of the clinical symptoms associated with malaria are not caused directly by the parasite, but by endogenous species generated during interactions with parasite-derived species such as Hz.[53, 58] Each time the intraerythrocytic cycle is completed, parasitized RBCs rupture and release debris, including approximately 200 μmol Hz, into the vasculature.[59] An innate immune response is triggered and phagocytic cells (i.e., monocytes, neutrophils, and macrophages) become activated. Notably, Hz-laden cells, which accumulate in the spleen, liver, and brain, exhibit dysfunctional antigen processing and macrophage functions; Hz-laden macrophages are unable to induce MHC class II molecules, repeat phagocytosis, or generate a microbicidal burst (i.e. reactive oxygen and nitrogen species) upon stimulation. [60]

In light of these factors, the interplay between Hz and the host immune system is of extreme interest. Confocal microscopy studies demonstrate that hemozoin phagocytosed by monocytes is localized within the phagolysosome but remains

undegraded for up to 72 h (Figure 7). From these observations, it was suggested that the persistence of Hz may be either an intrinsic property of the biomineral or immunomodulation mediated by composite Hz. During a typical innate response, foreign material within a phagocytic cell is primarily degraded by the production of microbicidal

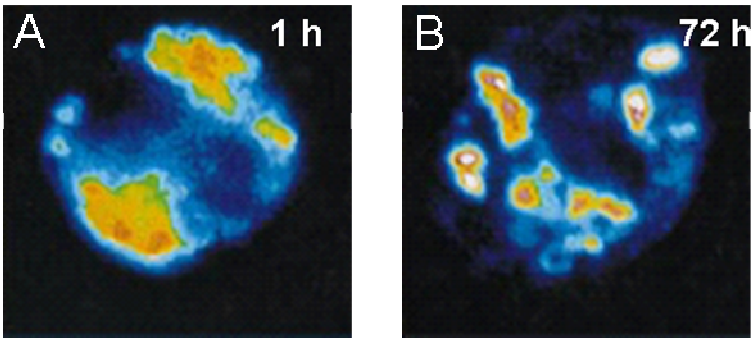

Figure 7. Hz stability. Utilizing the native fluorescence of the heme moiety, confocal microscopy was used to monitor the stability of Hz within phagolysosomes as a function of time. Images show Hz (A) 1 h and (B) 72 h after phagocytosis by human monocytes.[60]

agents including reactive oxygen species (ROS) and reactive nitrogen species (RNS), mediated by NADPH oxidase (NOX) and inducible nitric oxide synthase (iNOS), respectively (Figure 8).[61] Constitutively expressed NOX catalyzes the reduction of O_2 to superoxide anion ($O_2^{\cdot-}$) (Figure 9), which can rapidly be converted to the hydroxyl radical (HO·), hypochlorous acid (HOCl), and hydrogen peroxide (H_2O_2).[62-64] Inducibly expressed iNOS catalyzes the production of nitric oxide (NO)[65] (Figure 10) which reacts with O_2 and forms RNS such as NO_2, N_2O_3, NO_2^- and NO_3^-. Cumulatively, ROS and RNS degrade foreign material.

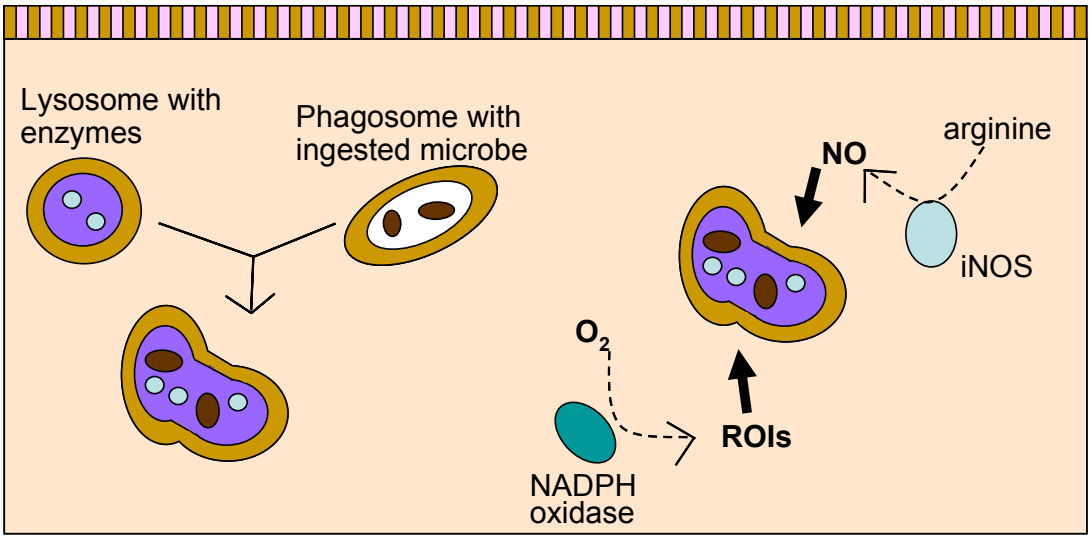

Figure 8. Representation of the pathways mediating microbicidal burst. Upon phagocytosis, foreign material is localized within a phagolysosome. NADPH oxidase and inducible nitric oxide synthase (iNOS) synergize to produce reactive oxygen and nitrogen species that function to degrade the foreign material. Adapted from reference 61.

Given that phagocytosis of Hz markedly decreases production of both ROS and RNS in culture,[33, 66, 67] evidence initially indicated that Hz was not degraded within phagolysosomes because microbicidal burst was impaired. Biochemical studies examining the degradation of BH *in vitro* have since been conducted.[68] It is now known that BH is degraded by physiologically relevant concentrations of ROS (hydrogen peroxide and sodium hypochlorite) and RNS (DeaNo, a nitric oxide releasing agent).[68] Furthermore, macrophage-like cells loaded with opsonized-BH produced normal levels of microbicidal agents and degraded the biomineral nearly 80% within 72 h (Figure 11).[68] These markedly disparate results suggest that the immunological activity resulting from native Hz is not an intrinsic property of the pigment itself, but of a toxin(s) that is presented on its surface.[69]

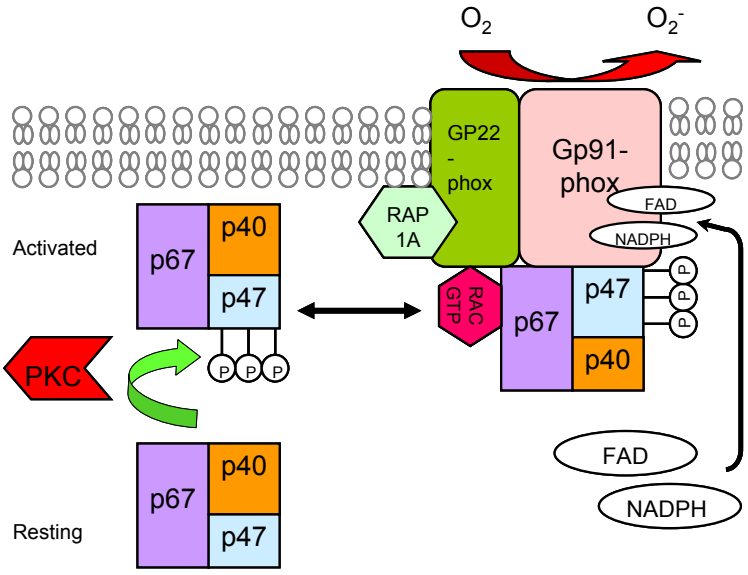

Figure 9. Schematic illustrating the assembly of NADPH oxidase. Upon stimulation, protein kinase C (PKC) phosphorylates the cytosolic phagocyte oxidase complex mediating its translocation to the membrane. This results in activation of the NADPH oxidase complex which subsequently catalyzes the production of reactive oxygen species.

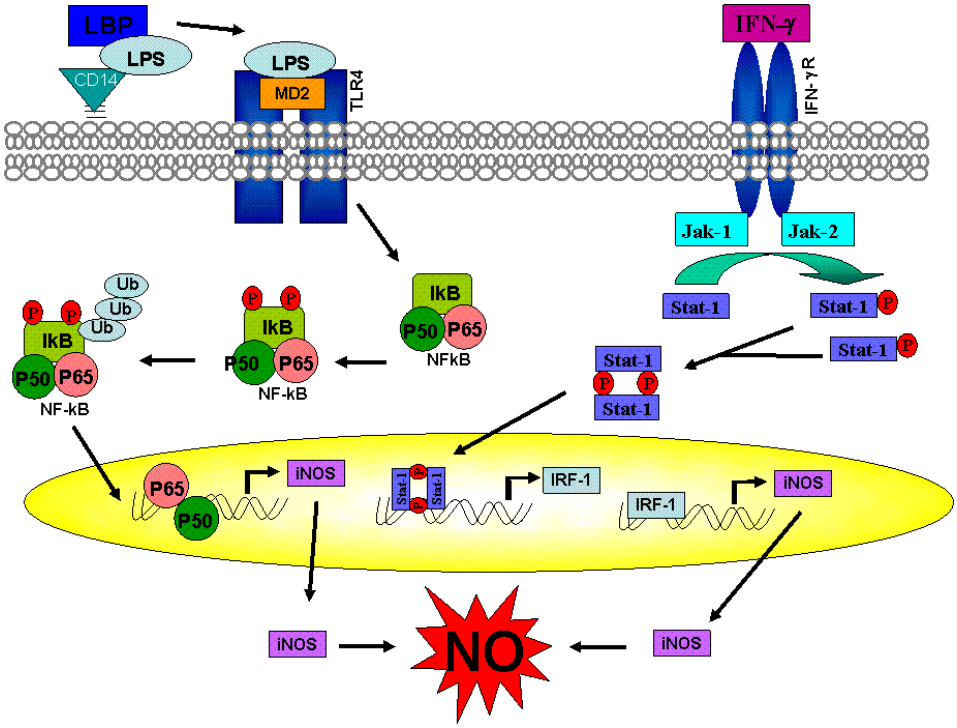

Figure 10**.** Signaling cascades leading to the generation of nitric oxide. LPS and IFN-γ activate the NF-κB and JAK/STAT signaling pathways, respectively, to mediate iNOS expression and subsequent NO production.

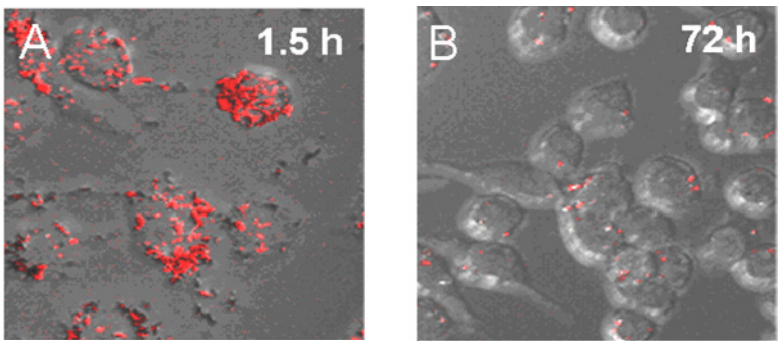

Figure 11. BH stability. Utilizing the native fluorescence of the heme moiety, confocal microscopy was used to monitor the stability of BH within phagolysosomes as a function of time. Images show BH (A) 1.5 h and (B) 72 after phagocytosis by RAW 264.7 macrophage-like cells.[68]

Lipid Peroxidation Products as Non-Specific Malaria Toxins

Lipid peroxidation products represent potential non-specific toxins that are associated with Hz and introduced into the cell during phagocytosis. Extraction of the biological material associate with crude Hz identified an array of host- and parasite-derived lipids, proteins, and nucleic acids.[31] Analysis of the lipid fraction identified secondary lipid peroxidation products including 5-, 8-, 9-, 11-, 12-, and 15-hydroxyeicosatetraenoic acids (HETEs) and 9- and 13- hydroxyoctadecadienoic acids (HODEs), derived form arachidonic acid (AA) and linoleic acids (LA), respectively.[32] Furthermore, Schwarzer *et al*. measured the level of 4-hydroxy-2-nonenal (HNE) in Hz-laden monocytes[70] at the highest intracellular HNE concentration in any biological system observed to date.[71] The biological activity of many of these lipid peroxidation products has been evaluated. For example, 15-HETE mediates several cellular effects including in enhanced vascular permeability and edema, increased chemotaxis and chemokinesis, and RBC adherence to endothelia (all of which are classic features of malarial infection).[32] HNE is highly reactive with nucleophilic sites in biomolecules and

is capable of forming covalent adducts and crosslinks,[72] impairing enzymatic activity,[8, 73-75] and triggering changes in gene expression.[76, 77] Given that Hz is clearly involved in the pathogenesis of malaria, the activity of these Hz-associated lipid peroxidation encourages further investigation of putative roles in the immunomodulation that occurs during malarial infection.

Dissertation Aims

The goal of this dissertation is to investigate the role of fatty acid oxidation in the disruption of macrophage function. The ability of the biologically naïve synthetic analogue of hemozoin, β-hematin (BH), to mediate lipid peroxidation is demonstrated in **Chapter II**. The known biological activity of HNE and 15-HETE suggests possible involvement in malaria pathophysiology. Therefore, **Chapter III** examines the cellular responses to individual components of Hz (BH, HNE, and 15-HETE) in the context of malaria infection using global microarray technology. The ability of HNE to modulate MMP9 regulation and NF-κB signaling was suggested by a number of differentially expressed transcripts and correlates with documented malaria pathophysiology. Thus, **Chapter IV** discusses the ability of HNE to disrupt the programmed functions of a triggered immune response and examines the specific mechanisms leading to altered matrix metalloproteinase 9 (MMP9) and inducible nitric oxide synthase (iNOS) expression.

CHAPTER II

β-HEMATIN-MEDIATED OXIDATION OF POLYUNSATURATED FATTY ACIDS

Introduction

While immune activity is essential for protective immunity, a modulated response contributes to malaria pathogenesis.[53] There is a positive clinical correlation between the severity of infection and the presence of Hz in phagocytic cells, which has led to a myriad of studies investigating the immunological activity of Hz. The identification of a lipid coat adsorbed to Hz prompted several investigations focused on dissecting the make-up of the composite material. Schwarzer *et al*. assessed the isomeric distribution of *P. falciparum* Hz-derived HETEs and identified not only the formation of six structural HETE isomers, but also equivalent stereoisomeric ratios of each structural isomer.[32] Additionally *S. mansoni* Hz-derived HETEs were distributed across all positional and racemic isomers, albeit with a higher level of 12(S)- versus 12(R)-HETE, suggesting the presence of 12-lipoxygenase activity.[78] Together these observations indicate that Hz-mediated lipid peroxidation is non-enzymatic in nature. It is well-established that heme compounds are effective mediators of non-enzymatic lipid oxidation, supporting the premise that reactive lipid peroxidation products arise from the oxidation of lipids by Hz. Consequently, the studies presented in **Chapter II** investigate the ability of BH to drive the oxidation of arachidonic acid and examine the biological activity of the secondary oxidation products.

Lipid peroxidation

The mechanisms associated with lipid peroxidation involve non-enzymatic or enzymatic reactions between molecular oxygen and a lipid molecule. The enzymatic metabolism of AA, a 20 carbon ω-6 fatty acid containing four double bonds (20:4), occurs by three major routes and produces regio- and stereo-specific products: lipoxygenase (LOX) enzymes which form HETEs, leukotrienes, and lipoxins; cyclooxygenase (COX) enzymes which form prostaglandins, prostacyclins, and thromboxanes; and cytochrome P-450 monooxygenase enzymes which form epoxides.[79]

Non-enzymatic oxidation of AA, the focus of Chapter II, results in a mixture comprised of six hydroperoxide species which differ by the position of the hydroperoxide moiety along the carbon backbone: C5, C8, C9, C11, C12, and C15. These primary lipid peroxidation products are referred to as N-HPETEs, where N identifies the carbon atom modified by the hydroperoxide group. Importantly, these intermediates lead to a diverse array of secondary lipid peroxidation species including complex mixtures of regio- and strereo-isomers of isoprostanes, HETEs, HNE, and isoketals (IsoK), among other products (Figure 12).

Non-enzymatic lipid peroxidation in biological systems

Free radical-mediated lipid peroxidation proceeds through a mechanism consisting of three distinct steps: initiation, propagation, and termination (Figure 13). The initiation step begins with the abstraction of a bis-allylic hydrogen atom from a lipid (LH) by an initiator (In) to form a pentadienyl resonance stabilized carbon-centered radical (L•).

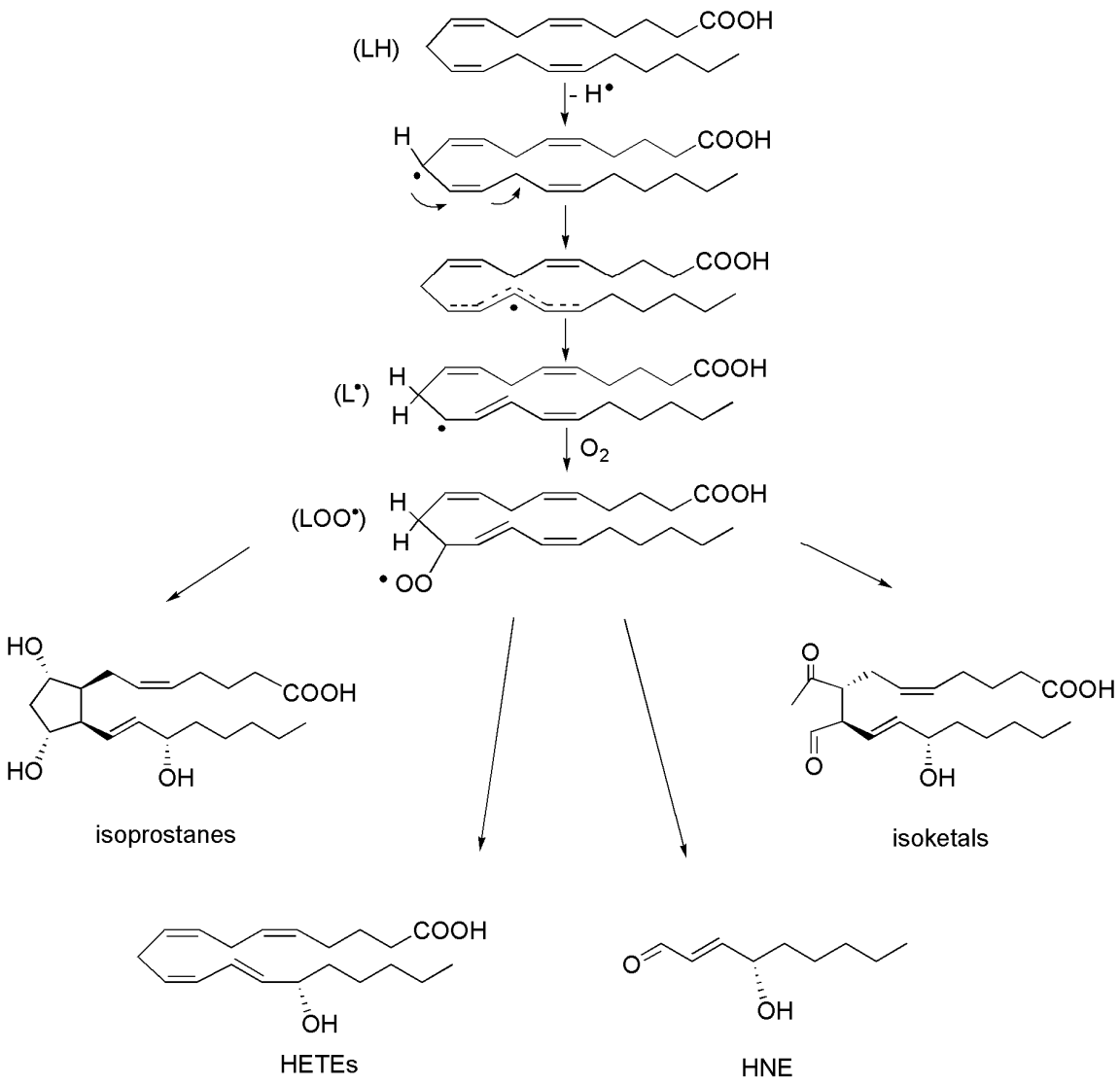

Figure 12. Peroxidation of arachidonic acid. The generation of secondary oxidation products, including isoprostanes, HETEs, HNE, and isoketals, arises from a peroxyeicosatetraenoic acid intermediate.

Mono-allylic and alkyl hydrogens can also be abstracted; however, bis-allylic hydrogens have the weakest C–H bond strength (ΔH = 75 kcal/mol relative to 88 and 101 kcal/mol for mono-allylic and alkyl C–H bonds, respectively) thereby making this abstraction the most favorable.[80] In the presence of molecular oxygen an alkyl radical reacts to form a peroxyl radical (LOO·). LOO· can propagate hydrogen abstraction from another lipid

molecule to form a second L· and a lipid hydroperoxide (LOOH). LOOH can dissociate to form a hydroxyl radical (HO·) and an alkoxyl radical (LO·), the latter of which generates an alcohol (LOH) and L· through yet another hydrogen abstraction. Finally, termination of this chain reaction occurs when two radical species, produced during initiation or propagation, react to form non-radical products. These steps are summarized in Figure 14.

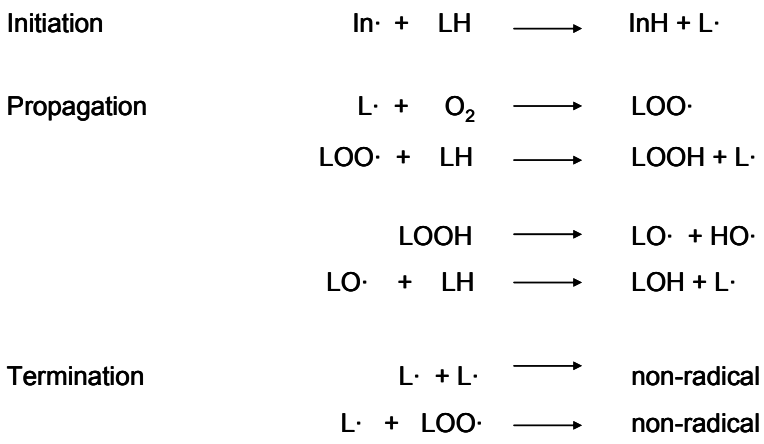

Figure 13**.** Free radical reaction chain involved in the autoxidation of lipids.

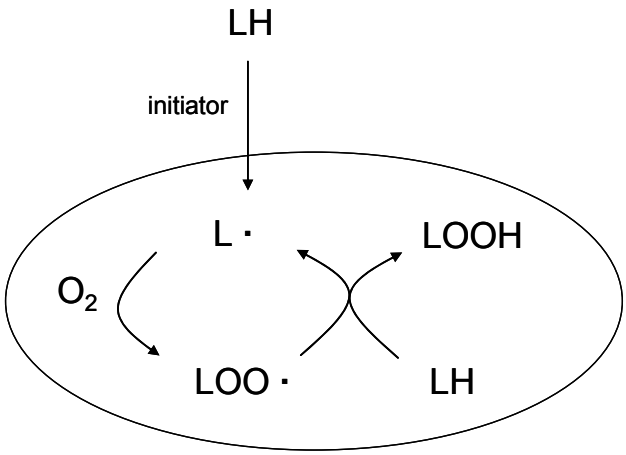

Figure 14. Non-enzymatic lipid peroxidation scheme. The circle represents the propagation cycle.

Iron-mediated lipid peroxidation

Given that iron is essential for both growth and survival, it can be considered the most important metal found in the body. However, it is also well established that iron is intimately associated with lipid peroxidation.[81] Iron and free heme (released during hemoglobin catabolism) mediate the generation of several redox active species including peroxide and both superoxide and hydroxyl radicals. In the presence of iron, lipid peroxides decompose to radicals by a Fenton-type (iron-catalyzed Haber–Weiss) reaction (Figure 15): LOOH reacts with Fe^{2+} to generate LO·. Fe^{3+} has also been shown to generate LOO· which can subsequently react with lipids to propagate additional radical reactions.

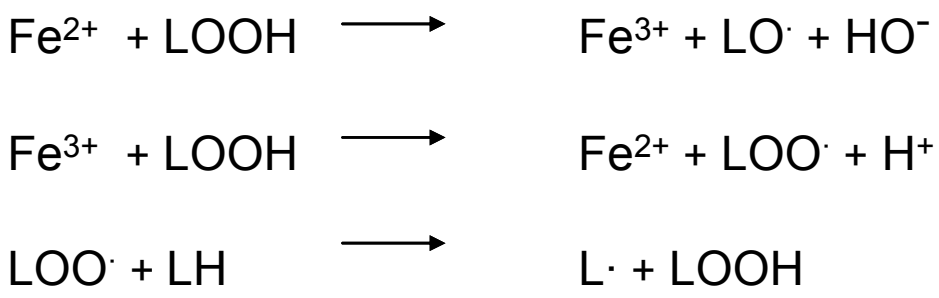

Figure 15**.** Iron-mediated lipid peroxidation.

It is also recognized that redox cycling of heme iron contributes to lipid peroxidation.[82] Heme iron can cycle through multiple oxidation states (Figure 16) including the reactive ferryl (Heme–Fe^{IV}=0) and perferryl (Heme–Fe^{V}=0 or ·Heme–Fe^{IV}=0) complexes ultimately generating lipid radicals and propagating the reactions shown in Figure 15.

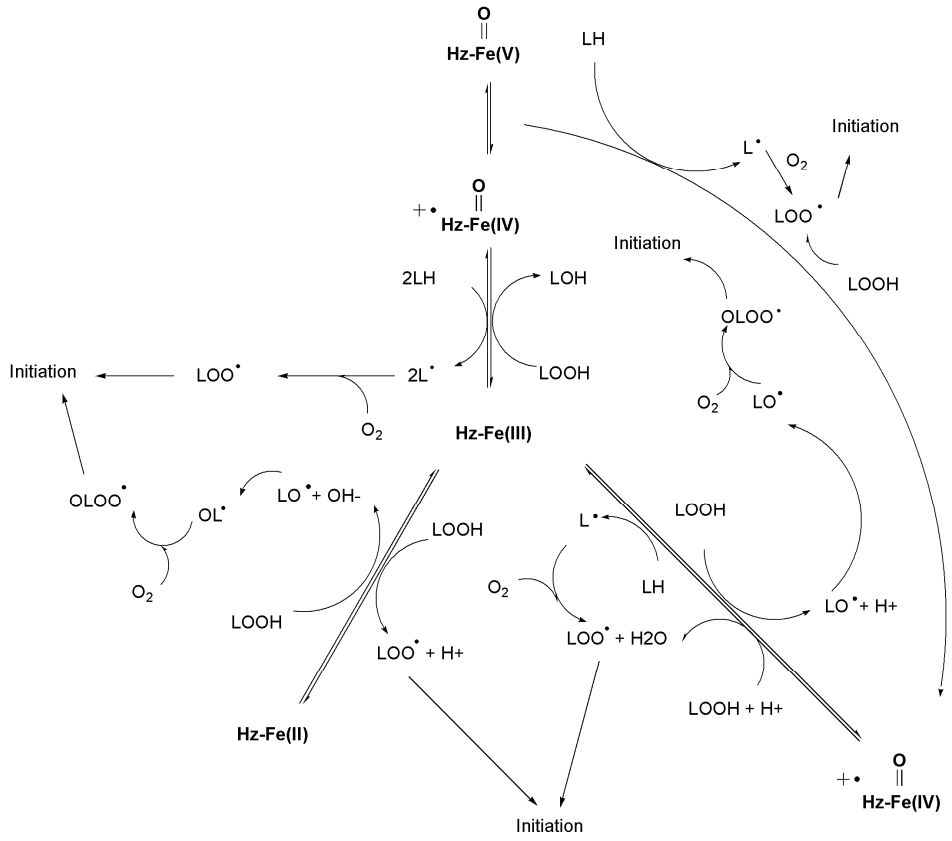

Figure 16. Proposed Hz-mediated lipid peroxidation pathways associated with redox cycling of heme-iron. Adapted from reference 82.

Summary

Lipid peroxidation products are non-specific Hz toxins that are introduced into cells during phagocytosis. Heme compounds are effective mediators of non-enzymatic lipid oxidation, supporting the premise that these products arise from the oxidation of lipids by Hz. Herein, the ability of BH to mediate the peroxidation of arachidonic acid is demonstrated. Additionally, the immunomodulatory activity of native Hz is modeled using constitutive components in a cell culture system. Results indicate that lipid peroxidation products generated during reactions between BH and ghost membranes are biologically active and responsible for impaired PMA-activated NADPH oxidase and LPS-stimulated inducible nitric oxide synthase (iNOS) activities. Furthermore, the results

suggest that Hz-mediated lipid peroxidation products are the underlying basis of Hz immunomodulation.

Experimental

Materials

Sodium bicarbonate, monobasic sodium phosphate, dibasic sodium phosphate, o-phosphoric acid 85%, dimethyl sulfoxide (DMSO), hexane, 2-propanol, acetic acid, and Hepes were obtained from Fisher. N-(1-naphthyl)ethylenediamine (NED), sulfanilimide, hemin chloride (bovine), Pipes, Sepharose 2B, 3,3',5,5'-tetramethylbenzidine liquid substrate (TMB), and lipopolysaccharide (LPS) were obtained from Sigma. Anhydrous methyl alcohol, and 2,6-lutidine were obtained from Acros. Arachidonic acid was obtained from Nu-Chek Prep, Inc. Dulbecco's phosphate buffered saline (PBS) and RPMI 1640 media with 2 g/L sodium bicarbonate were obtained from Gibco. RPMI was supplemented with 10% fetal bovine serum (FBS) (Atlanta Biologicals) and 100 μg/mL penicillin-streptomycin (P/S) (Invitrogen) before use. 4-hydroxy-2-nonenal (HNE) was purchased from Calbiochem. Packed RBC were a donation from the VUMC Blood Bank. All chemicals were used as received unless otherwise noted.

β-hematin synthesis and characterization

β-hematin (BH) was synthesized via a dehydrohalogenation reaction as previously described[37, 68] using purified hemin chloride (Fluka). Briefly, in an inert atmosphere 0.3 g of hemin chloride was dissolved in 5 mL of 2,6-lutidine with stirring. Forty mL of 1:1

DMSO/anhydrous MeOH was added to the flask which was then sealed, covered in foil, and left undisturbed. After 90 days, crude BH was collected via vacuum filtration (0.45 μm filter) and exhaustively washed in MeOH, DMSO, 0.1 M $NaHCO_3$ (pH 9.0), and deionized water. UV-visible spectroscopy was used to monitor BH purity, as determined by baseline absorption of the Soret band for heme in the supernatant of the washes. BH was dried at 150 ºC for 48 h and formation was confirmed by powder X-ray diffraction (XRD), Fourier Transform Infrared (FT-IR) Spectroscopy, and scanning electron microscopy (SEM): XRD studies (0.02 step size, 25s preset time, scan range 4 to 35 º2θ) were performed with a Scintag X1 h/h automated powder diffractometer with a copper target, a Peltier-cooled solid-state detector and a zero-background silica (510) sample support. KBr pellets for IR studies were prepared from dried BH samples and spectra were acquired using an ATI Mattson Genesis Series FT-IR spectrophotometer. For SEM analyses, BH was suspended in ethanol, sonicated, applied to a polished aluminum specimen mount, and dried at 25 ºC overnight. The sample was sputter-coated with gold for 20 s and imaged using a Hitachi S4200 scanning electron microscope at 1.0 kV accelerating voltage. Particles were determined to have an average length of 0.9 ± 0.3 μm.

Cell culture

Murine macrophage-like RAW 264.7 cells (American Type Culture Collection TIB-71, Manassas, VA) were cultured under standard incubation conditions (37 ºC, 5% CO_2) and grown in complete culture media (RPMI supplemented with 5% FBS (Atlanta Biologicals, Atlanta, GA) and 1 μg/mL P/S (Cellgro MediaTech, Herndon, VA)). Cells

were plated at a density of 5×10^5 cells/well in 24 well plates or 4×10^6 cells/well in 6 well plates and incubated for 24 h prior to treatment.

Erythrocyte ghost preparation

Ghosts were prepared according the procedure by Derham *et al*. with minor modifications.[83] Packed red blood cells (RBCs, 3.0 mL) were suspended in 12.0 mL of phosphate buffered saline (PBS, 5 mM NaH_2PO_4 supplemented with 150 mM NaCl, pH 8.0) and centrifuged at 1000 × g for 10 min. The supernatant was discarded and the pellet was resuspended in PBS. After four washes, the pellet was resuspended in phosphate buffer (5 mM NaH_2PO_4, pH 8.0) at a 10% hematocrit. The sample was rigorously shaken and placed on ice for 15 min prior to loading 15.0 mL (6% of the bed volume) onto a Sepharose 2B column (2.5 cm × 50 cm) equilibrated in 15 mM Pipes buffer with 0.1 mM EDTA (pH 6.0) maintained at 4 ºC. Erythrocyte ghosts were eluted with 20 mM Hepes buffer supplemented with 146 mM sodium chloride (pH 7.4) at flow rate of 15 mL/h. The absorbance of fractions was monitored at 280 nm and fractions containing RBC ghosts were pooled and collected by centrifugation (10 700 × g, 15 min, 4 ºC). Ghost membranes were disrupted by alternately vortexing with glass beads (2 min) and resting on ice (2 min) for a total of five cycles.

Reactions between RBC ghosts and BH were prepared in test tubes with a total volume of 2 mL. RBC ghosts, normalized to 1 mg protein/mL via the BioRad Protein Assay, were combined with BH (0.75 mg/mL) in RPMI 1640 complete medium. Samples were stirred for 24 h at RT and centrifuged for 15 min at 5500 rpm. Supernatant was collected and immediately used for experiments.

Cell treatment

Cells were washed once with Dulbecco's PBS (DPBS) and untreated or treated in triplicate with serum-opsonized BH (0.1 mg/mL), HNE (EMD Biosciences, San Diego, CA), 15-S-HETE (Cayman Chemical, Ann Arbor, MI), or BH/ghost membrane reaction supernatant. Opsonization was performed as previously described.[84] Immediately following treatment, LPS was added to all wells at a final concentration of 1 μg/mL.

Generation of lipid peroxides

Arachidonic acid (10 mM) was oxidized in 2 mL of 100 mM phosphate buffer (chelexed, pH 7.4) in the presence of BH (0.48 mM) for 4h at RT. For samples to be assayed for isoketal generation, pyridoxamine dihydrochloride (100 μM) was added at t = 2 h. After extraction of the reaction mixtures with diethyl ether (3 × 2 mL), the organic layers were combined and condensed, and the residue was reconstituted in 200 μL of LC mobile phase.

Liquid chromatography-tandem mass spectrometry (LC-MS/MS)

LC-MS/MS analysis of HETE products was performed using a ThermoFinnigan LTQ linear ion trap mass spectrometer equipped with a Waters Acquity UPLC system. Products were separated on a Thermo Hypersil GOLD C18 column (2.1 × 150 mm, 1.9 μm). Solvent A (10 mM ammonium carbonate in acetonitrile/water (10:90)) and solvent B (10 mM ammonium carbonate in acetonitrile/water (90:10)) were used with a flow rate of 600 μL/min at the following gradient: 0–0.25 min 30% B isocratic phase; 0.25–9 min,

linear gradient from 30–45% B; 9–10 min isocratic phase at 45% B; 10–10.5 min, linear gradient from 45–30% B; 10.5–17 min isocratic phase at 30% B. The sample injection volume was 10 μL. The mass-spectrometer was operated in negative ion mode and tuned as follows: spray voltage of 3.8 kV, a capillary temperature of 300 ºC, capillary voltage of 50 V, and tube lens offset 103.3 V. Product scan spectra of HETE isomers ([M-H^+] *m/z* 319) were acquired from 85 *m/z* to 350 *m/z*. Individual HETE isomer standards were used to establish fragmentation patterns, and unique *m/z* were chosen to extract ion profiles for each isomer.

LC-MS/MS analysis of isoketal products was performed using a ThermoFinnigan TSQ Quantum triple quadrupole equipped with a ThermoFinnigan Surveyor LC. Products were separated on a Magic Bullet C18AQ micro column (3 μm, 100 Å, Michrom BioResources, Auburn, CA) with the gradient programmed from 100% solvent A (5 mM ammonium acetate with 0.1% acetic acid) to 100% solvent B (acetonitrile/methanol 95:5) from 0.5 min to 3 min and then continuing at 100% B for an additional 1.5 min. The column was then equilibrated to 100% A for 2.5 min. The flow rate was set to 190 μL/min and the injection volume was 5 μL. The mass spectrometer was operated in positive ion mode with the following parameters: spray voltage of 3.7 kV, a capillary temperature of 210 ºC, capillary voltage of 35 V, tube lens offset 90 V, source CID of 5 V, and collisional energy of 30 eV. Product scan spectra of the Isok-PM-lactam adduct ([M+H^+] m/z 501) were acquired from 50 m/z to 520 m/z. Selected reaction monitoring was used to confirm m/z 501→ m/z 152 and m/z 501→ m/z 332 transitions, calculated as -17 Da (deamidation by fragmentation of the β-amine) from the

parent Isok-PM-lactam mass. With both instruments, data was acquired and analyzed using Thermo-Finnigan Xcaliber software.

Measurement of reactive oxygen and nitrogen species

Measurement of reactive oxygen species (ROS) was accomplished using luminol-dependent luminescence. Three hours after treatment, cells were washed with PBS and NADPH oxidase was activated by the addition of 1000 mL of 100 nM PMA in PBS. After 4 min, 950 mL of this supernatant was collected into a luminescence tube followed by the addition of 50 mL of 1 mM luminol in PBS. Luminescence was immediately measured using a Monolight 3010 luminometer for 10 s. NO levels were indirectly assessed by measurement of nitrite via the Griess assay. Twenty-four hours after treatment, supernatant (100 μL) was collected and combined with 100 μL Griess reagent (1:1, 1% sulfanilimide in 5% phosphoric acid/0.1% N-(1-naphthyl)ethylenediamine). After five minutes, the absorbance of the azo complex was measured at 540 nm using a Bio-Tek Synergy HT Multidetection Microplate Reader. Nitrite levels were determined by comparison with a standard curve.

Results and Discussion

Native Hz is an immunomodulatory material.[33, 49, 60, 66, 85] Accumulating evidence suggests that the basis of the modulatory activity is not a result of the intrinsic biomineral structure, but of the biomineral's reactivity with endogenous lipids.[32, 68, 86] Consequently, the ability of BH to mediate lipid peroxidation was investigated.

β-hematin (BH) synthesis and characterization

BH was prepared using a modification of the Bohle dehydrohalogenation method.[37] Relying on the differential solubilities of hemin chloride and BH,[87] monomeric heme and small heme aggregates were removed by exhaustive washings in MeOH, DMSO, 0.1 M $NaHCO_3$ (pH 9.0), and deionized water. Purification was assessed by monitoring the absorbance of the Soret band of heme in the washes. As shown in Figure 17, initial MeOH washes (washes 1-3) removed residual hemin chloride, and $NaHCO_3$ (washes 3-5) and DMSO (washes 5-9) solubilized monomeric heme and aggregates.[88]

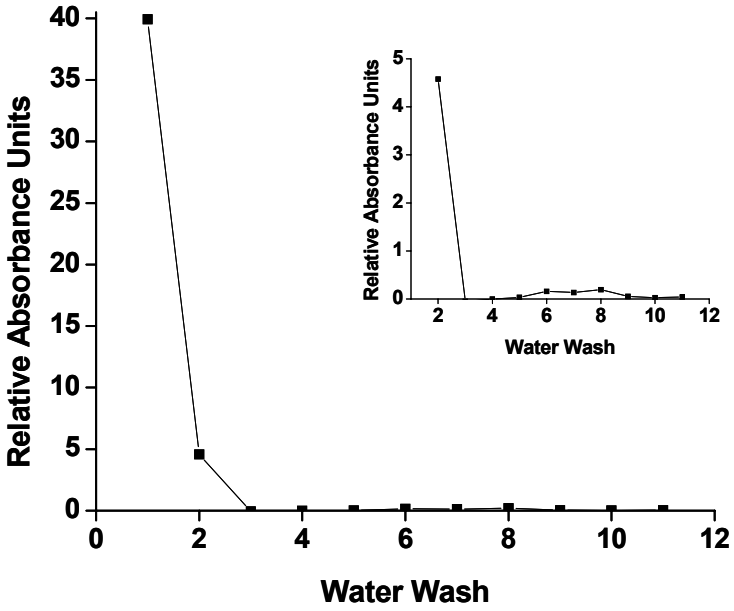

Figure 17. β-hematin purification. Absorbance of the Soret band of heme was measured in MeOH (washes 1-3), $NaHCO_3$ (washes 3-5), DMSO (washes 5-9), and $NaHCO_3$ (washes 10-12) supernatants to monitor the purity of BH. Inset shows detail at low absorbance values.[88]

To ensure that purified BH is spectroscopically and crystallographically identical to Hz, the synthetic material was characterized by FT-IR spectroscopy, SEM, and XRD (Figures 18 and 19).[9, 28, 41] KBr pellets of BH were analyzed by FT-IR, and distinctive bands were observed at 1210 and 1662 cm^{-1}, corresponding to C-O and C=O vibrational stretching of the Fe-carboxylate linkage, respectively. XRD spectra demonstrated the appropriate line pattern distinguished by a peak at 7 º2θ that is nearly double the signals at 22 and 24 º2θ. Finally, SEM micrographs showed needle-like crystals with well-defined facets. BH characterized as described was deemed pure and used for the studies presented herein.

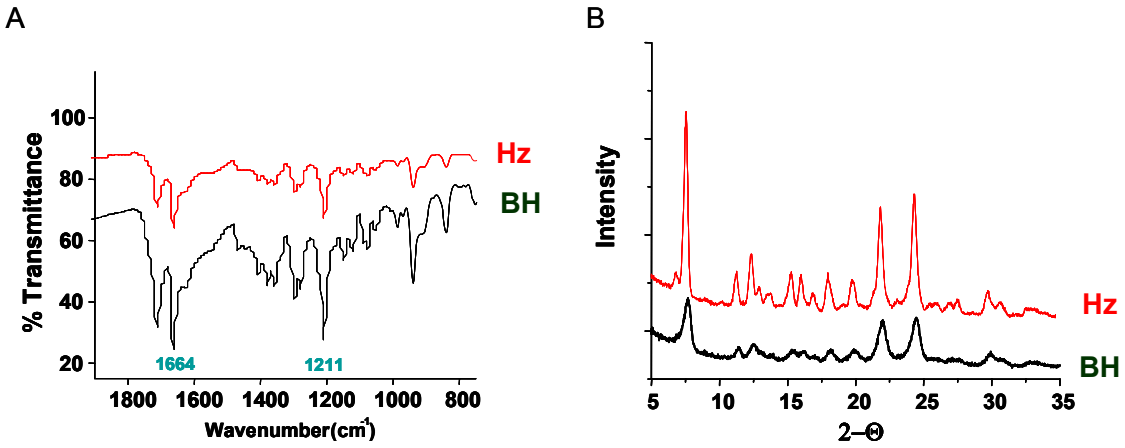

Figure 18. BH characterization. (A) FT-IR spectroscopic analysis and (B) XRD line pattern of the synthetic material. [68]

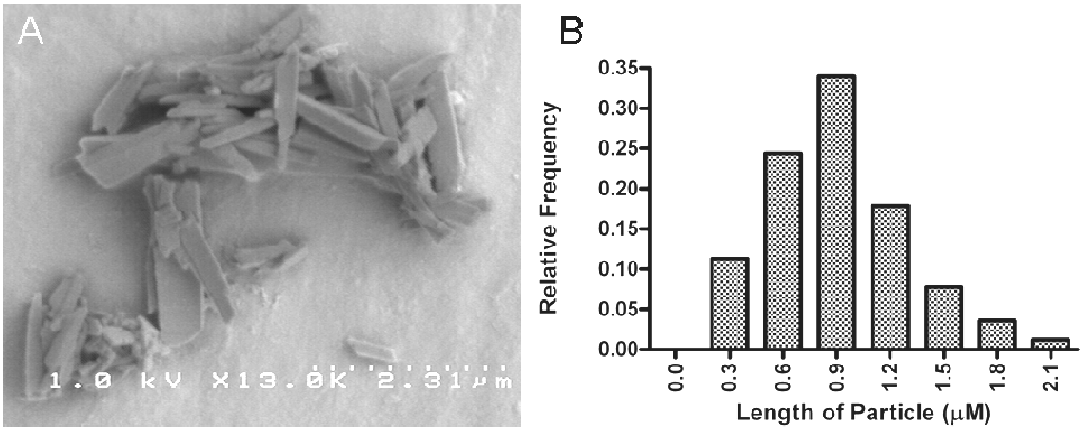

Figure 19. BH crystals. (A) Scanning electron micrograph of synthetic hemozoin crystallites shows needles with well-defined facets. (B)Histogram of BH particle size distribution.[44]

BH-mediated 4-hydroxynonenal (HNE) formation

Transition metals mediate the non-enzymatic decomposition of both arachidonic acid and linoleic acid-derived lipid hydroperoxides.[81, 89-91] Given that this intermediate has been identified as a precursor of HNE, the ability of BH to mediate HNE formation was assessed.[88] BH was incubated with arachidonic acid under either aerobic or anaerobic conditions, and lipid peroxidation products were extracted and analyzed by LC-MS. BH-mediated HNE formation was confirmed by comparison of LC retention time and MS ($M+H^+$ [*m*/*z* 157] and $M+H^+-H_2O$ [*m*/*z* 139]) (Figure 20) with a HNE standard. Quantitation was performed by UV analysis of normal phase liquid chromatograms compared with a standard curve, and relative to autoxidation, BH mediated the generation of HNE in a dose-, time-, and oxygen-dependent manner (Figure 21).[88]

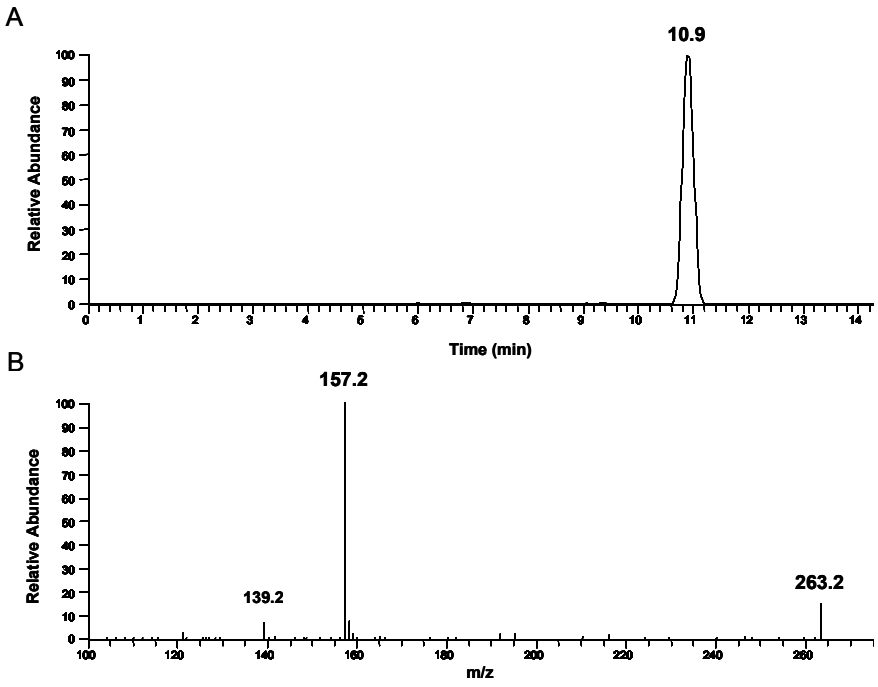

Figure 20. MS analysis of HNE produced from BH-mediated peroxidation of arachidonic acid. (A) Chromatogram showing the elution profile of HNE. (B) The mass spectrum acquired for the peak eluting at 10.9 min demonstrates a singly charged HNE $[M+H]^+$ species at *m/z* 157.[88]

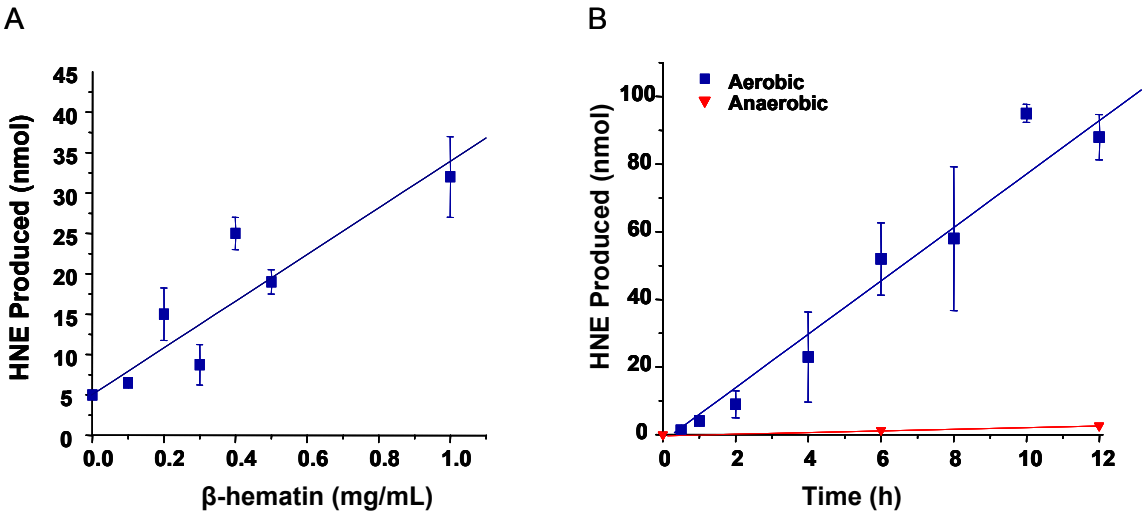

Figure 21. BH-mediated HNE formation. (A) HNE forms as a function of BH concentration. (B) HNE forms as a function of time under aerobic conditions (blue line). Anaerobic conditions (red line) inhibit HNE formation.[88]

BH-mediated hydroxyeicosatetraenoic acid (HETE) formation

The ability of BH to mediate the generation of HNE confirmed the putative reactivity of the dimeric iron core. This result prompted investigation of BH's ability to mediate the formation of HETEs, which are associated with Hz in a native state. During a non-enzymatic reaction, the reduction of a peroxyl radical generates racemic mixtures of hydroxylated fatty acids. Therefore, the distribution of HETE isomers was of interest. Hydrophobic interactions suggest that lipid peroxidation products generated by BH would be preferentially adsorbed to the surface of the biomineral. To confirm this interaction, reactions were centrifuged to pellet BH, supernatant was removed, and BH was washed three times with phosphate buffer prior to extraction. As shown in Figure 22**,** LC-MS/MS analysis revealed that a series of compounds with *m/z* 319 Da ($M\text{-}H^+$) (indicative of the isobaric carboxylate anion of HETE) were associated with the BH pellet. Given that collision-induced disassociation (CID) of positional isomers will yield isomer-specific patterns, all *m/z* 319 species were fragmented, and the products scans were collected. As an example, Figure 23 shows the tandem mass spectrum extracted from the peak at 3.25 min; this peak was determined to be 15-HETE based on the fragmentation pattern, particularly the strong *m/z* 319→219 transition. Specific detection of all six positional HETE isomers (5-, 8-, 9-, 11-, 12-, and 15-HETE) was achieved through MS/MS by monitoring unique *m/z* 319→X transitions, where X represents isomer-specific fragmentation. All isomers were validated by comparison of fragmentation patterns and retention times with standards. The distribution of isomers indicates the preferential formation of 15-HETE relative to all others (15>>11≈5≈12>8>9). Notably, 15- and 5-HETE have been reported to as the

predominant isomers of both iron-catalyzed and Hz-mediated arachidonic acid peroxidation.[86, 92, 93]

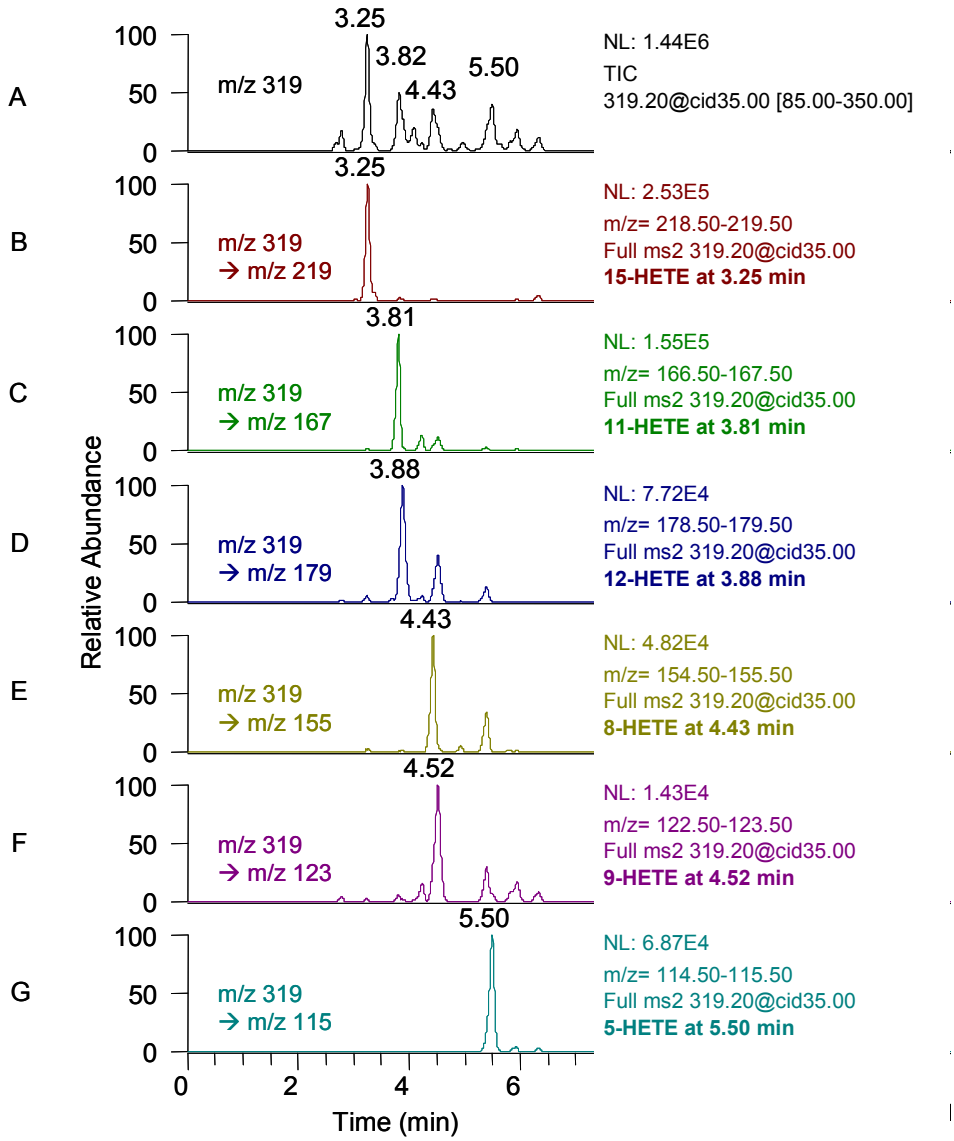

Figure 22. Reverse phase LC-MS/MS analysis of HETEs produced from BH-mediated peroxidation of arachidonic acid. Chromatograms showing (A) total ion current (TIC) of *m/z* 319 and (B-G) MS/MS extracted ion profiles for m/z unique to each isomer.

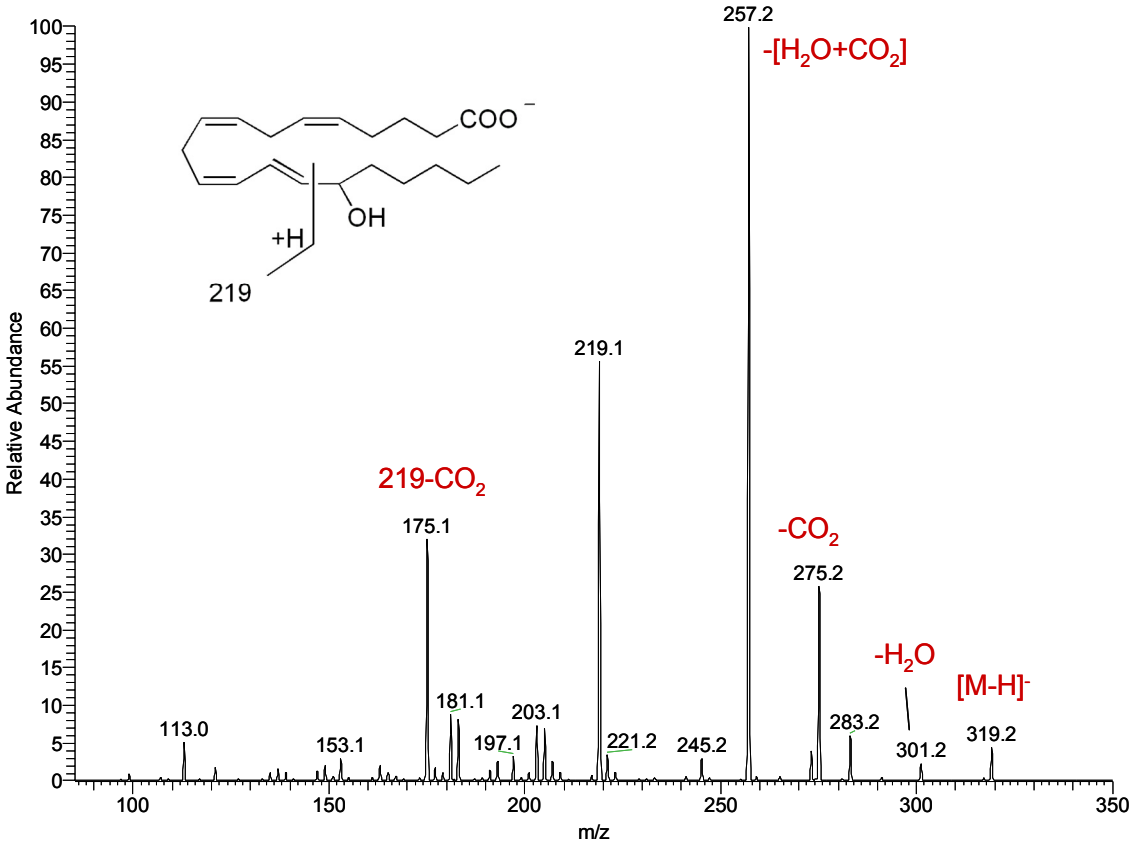

Figure 23. 15-HETE mass spectrum. The M-H$^+$ isobaric ion was subjected to collision induced disassociation, and product ions were scanned from *m/z* 85 to *m/z* 350. The fragmentation pattern of the peak (*m/z* 319) eluting at 3.25 min identifies 15-HETE.

BH-mediated isoketal (IsoK) formation

The non-enzymatic generation of HNE and HETEs mediated by BH mirrors the lipid peroxidation products associated with Hz. As an independent measure of the ability of the dimeric core to generate biologically active species from arachidonic acid, the production of isoketals (IsoK) was assessed. IsoK are 1,4-dicarbonyl compounds and, consequently, are readily reactive with proteins via lysine residues, forming pyrrole, lactam, and hydroxylactam adducts. Pyridoxamine (PM) has proven to be an effective scavenger of IsoK[94] and, therefore, was added to the reactions to scavenge IsoK as they were generated.[95] As shown in Figure 24, BH-mediated the formation of IsoK, and

scavenging of IsoK by PM was readily achieved. Selected reaction monitoring (SRM) confirmed *m/z* 501→152 and 501→332 transitions indicative of a PM/IsoK lactam adduct. To further characterize the species, the molecular ion was subjected to CID, and product ions were scanned from m/z 50 to m/z 520 (Figure 25). The CID spectrum is characteristic of an IsoK/PM lactam adduct: deamidation of PM gives rise to *m/z* 152 and, when accompanied by a loss of H_2O, *m/z* 332, as well as loss of H_2O from the parent and product ions (i.e., *m/z* 314 and 483).

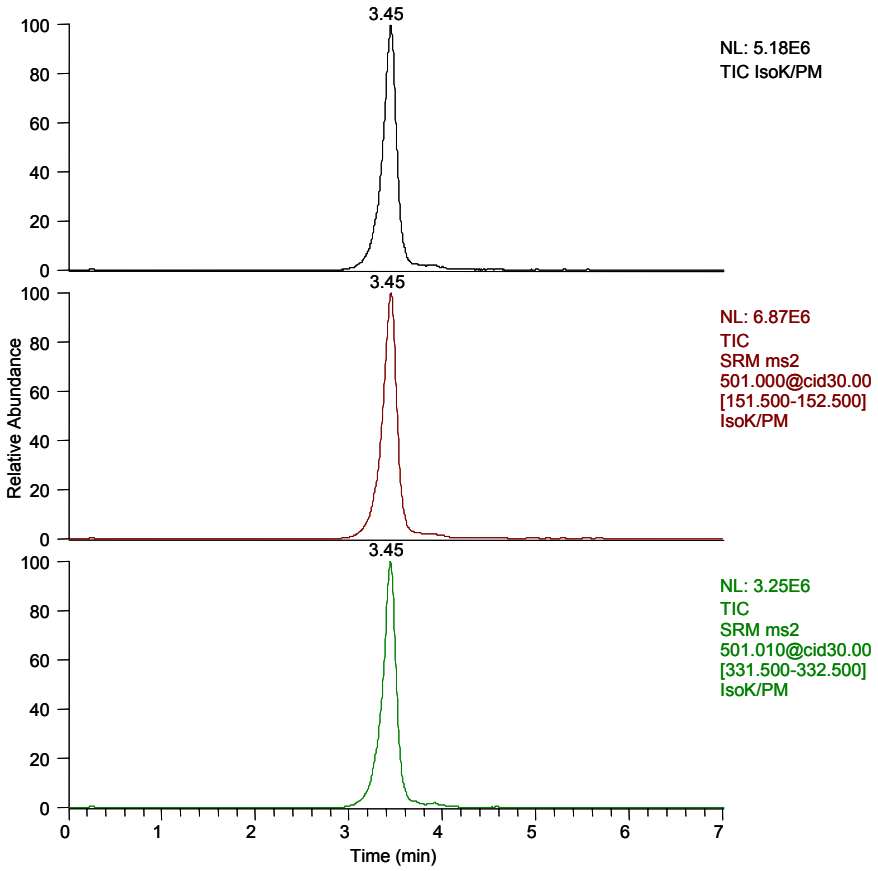

Figure 24. Selected Reaction Monitoring of IsoK/PM lactam adduct. The $[M+H]^+$ ion (*m/z* 501) formed by adduction of isoketal to pyridoxamine was subjected to collision induced disassociation and *m/z* 501→152 and *m/z* 501→332 transitions were monitored.

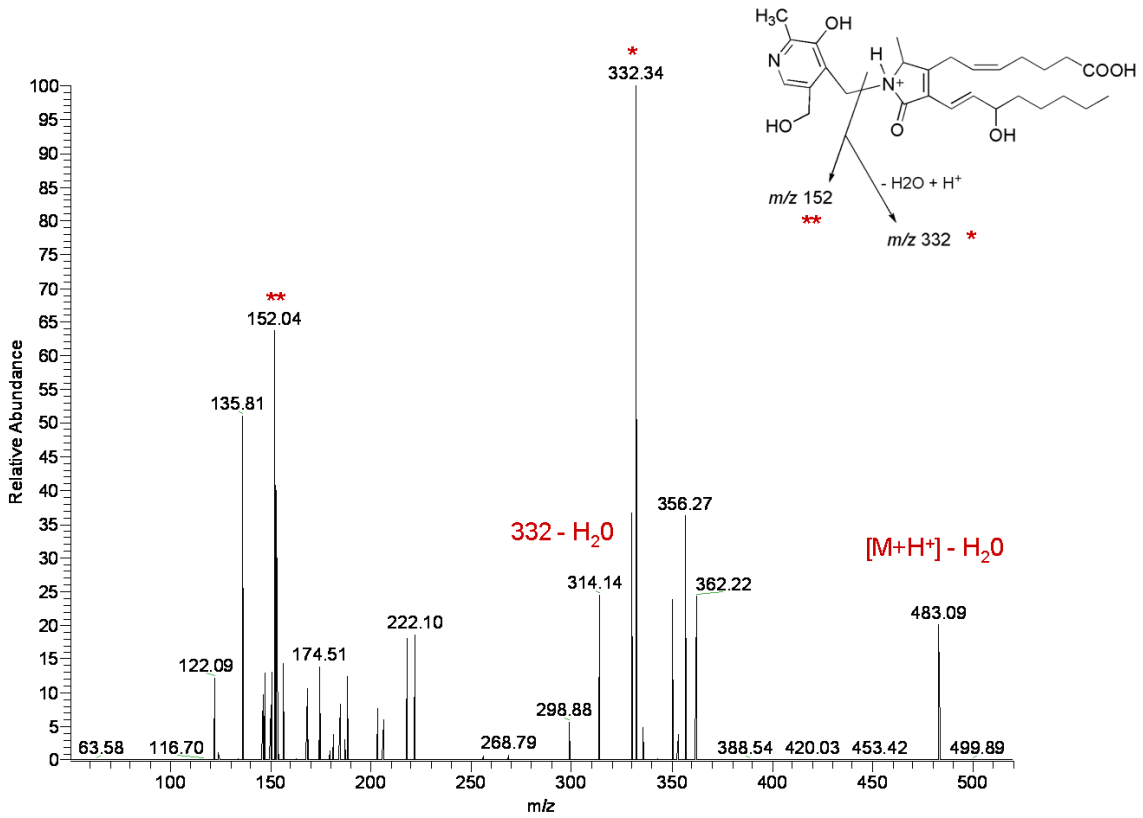

Figure 25. Mass spectrum of IsoK/PM lactam adduct fragmentation. The $[M+H]^+$ ion formed by adduction of Isoketal to pyridoxamine was subjected to collision induced disassociation, and product ions were scanned from *m/z* 50 to *m/z* 520.

BH-mediated ghost membrane peroxidation

In order to examine the reactivity of BH in an appropriate model system, the ability of the biomineral to mediate peroxidation of lipids derived from erythrocyte membranes (i.e., ghost cells) was examined. Ghost cells, obtained by RBC lysis and purified by gel filtration chromatography (Figure 26), were incubated with BH. As shown in Figure 27, BH mediated the generation of a complex array of products. Comparison of the retention times with previous analyses that examined arachidonic acid peroxidation

suggested that several products may be positional HETE isomers. Thus, LC-MS was used to investigate the non-enzymatic formation of HETEs as previously described. Similar to the generation of HETE isomers from arachidonic acid described above, BH-mediated the formation of all six HETE isomers from ghost membranes (Figure 28). Based on peak area, the distribution of isomers was the same as BH-mediated arachidonic acid oxidation (i.e., 15-HETE>>11≈5≈12>8>9).

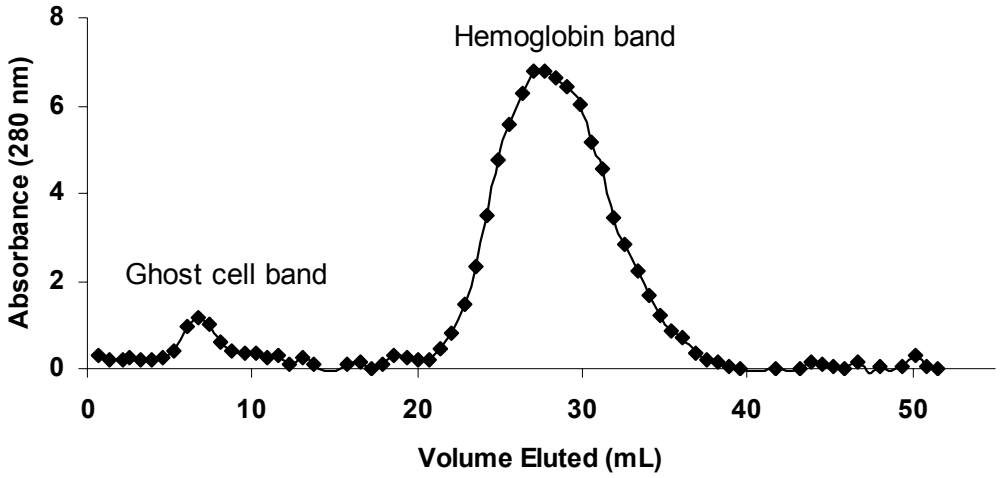

Figure 26. Purification of erythrocyte ghost cells. RBC were lysed and ghost cells were purified by gel filtration chromatography. The absorbance of fractions was monitored (280 nm) to identify ghost cells. Relevant fractions were pooled, and ghost cells were collected by centrifugation.[68]

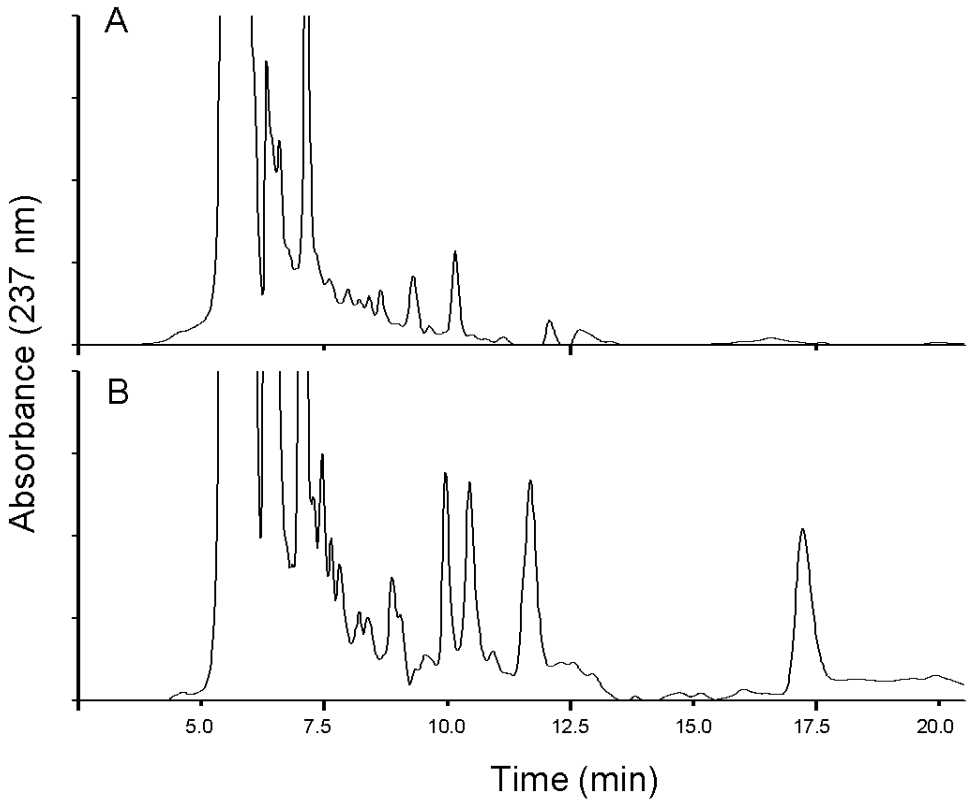

Figure 27. Normal phase HPLC analysis of red blood cell ghost peroxidation. (A) Elution profile of RBC ghost autoxidation. (B) Elution profile of BH-mediated RBC ghost peroxidation. Comparison of chromatogram complexity between autoxidation and BH-mediated oxidation suggests the production of a number of lipid peroxidation species mediated by BH prompting further investigation.

BH-mediated ghost membrane peroxidation reactions were examined for IsoK formation. However, IsoK were not detected in these studies. It should be noted that the prevailing difference between *in vitro* arachidonic acid- and ghost membrane-peroxidation mediated by BH is the presence of protein in ghost membrane samples. It is likely that IsoK were indeed formed but were unable to be detected due to their proclivity to adduct lysine residues of protein. In fact, phospholipid-esterified Isok have been shown to adduct lysine residues of protein (presumably membrane) in an in vivo model of oxidative stress, and Isok directly covalently modified aminophospholipids *in vitro*.[96, 97]

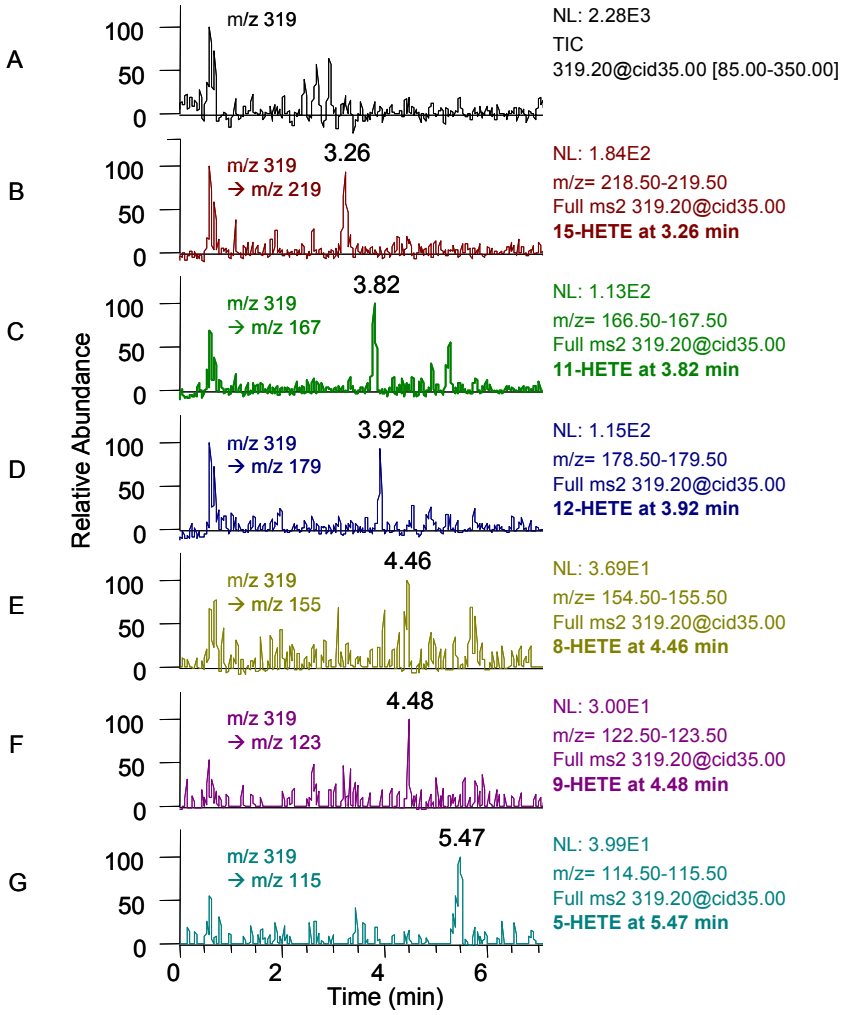

Figure 28. Reverse phase LC-MS/MS analysis of HETEs produced from BH-mediated peroxidation of ghost membranes. Chromatograms showing (A) total ion current (TIC) of *m/z* 319 and (B-G) MS/MS extracted ion profiles for *m/z* unique to each isomer.

Proposed mechanisms of BH-mediated lipid peroxidation

Given that Hz is an insoluble particulate material, mechanistic studies are intrinsically difficult to perform. Although it has been shown that free heme is not liberated from Hz[98] or BH[99] during reactions that generate lipid peroxides, the specific mechanisms mediating lipid peroxidation remain unknown. Accumulating evidence suggests that the oxidizing ability of the Hz is dependent upon the presence of hydroperoxides. Transition metal-mediated decomposition of lipid hydroperoxides likely

occurs by a one electron reduction to an alkoxyl radical.[81, 89-91] In support of this premise, electron paramagnetic resonance (EPR) studies demonstrated the formation of methoxyl and tert-butoxyl radical adducts when purified Hz was incubated with tert-butylhydroperoxide (tert-BuOOH) in the presence of the spin-trap DMPO.[98] BH-mediated HNE formation likely proceeds via a similar pathway.

From a peroxyeicosatetraenoic acid radical intermediate (Figure 12), three major non-enzymatic routes occur. First, the reaction can be quenched and reduced to form HETEs; second, the radical can undergo β-fragmentation and Hock cleavage to produce short chain aldehydes such as HNE; and finally, the radical can undergo two rounds of cyclization with adjacent unconjugated double bonds to form bicycloendoperoxides that are reduced to the PGH_2 intermediate. Schneider *et al*. provide evidence that autoxidation of both HPODE isomers (9*S*- and 13*S*-) forms 4-hydroperoxy-2-nonenal (4-HPNE), the precursor of HNE, by distinct pathways depending on the location of the hydroperoxy group.[93] 13(*S*)-HPODE forms a dihydroperoxide that undergoes Hock cleavage to form HPNE. 9(*S*)-HPODE directly undergoes Hock cleavage which generates an alkenal that oxygenates to form HPNE (Figure 29). Analogous mechanisms describing the formation of HNE from arachidonic acid are proposed using 11- and 15-HPETE as the precursors of 4-HPNE.[93] Alternatively, the non-enzymatic formation of the PGH_2 intermediate leads to the formation of several isoprostanes and isoketals. Figure 30 illustrates the mechanism proposed by Zagorski and Salomon for the rearrangement of PGH_2 to isoketals.[100]

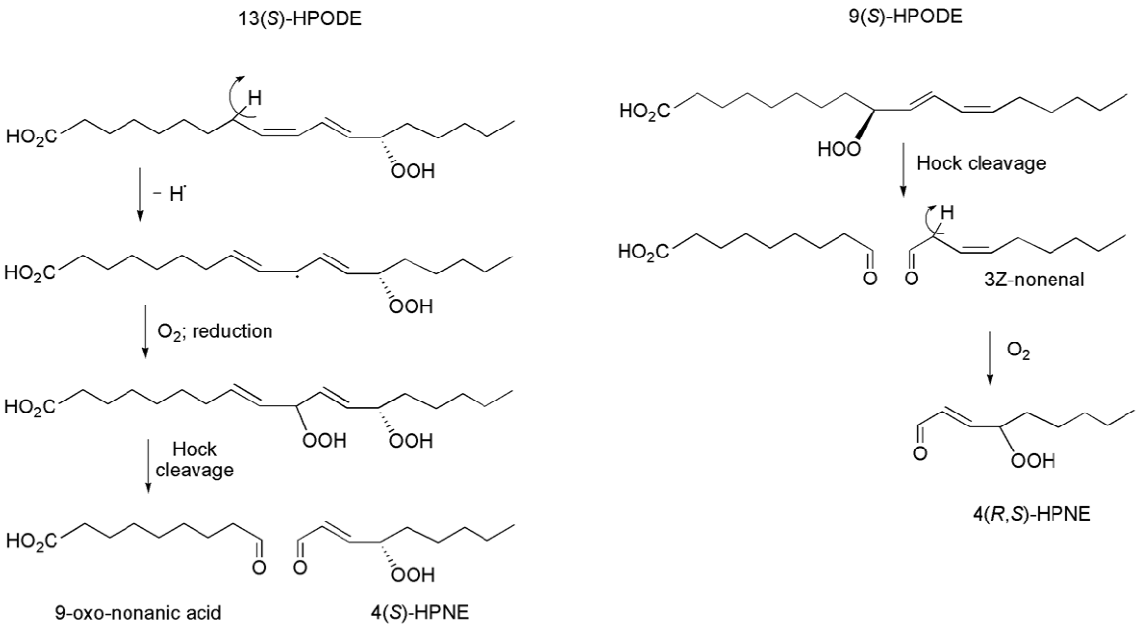

Figure 29. Proposed mechanisms for the formation of HPNE from the non-enzymatic oxidation of 13(*S*)- and 9(*S*)-HPODE.[93]

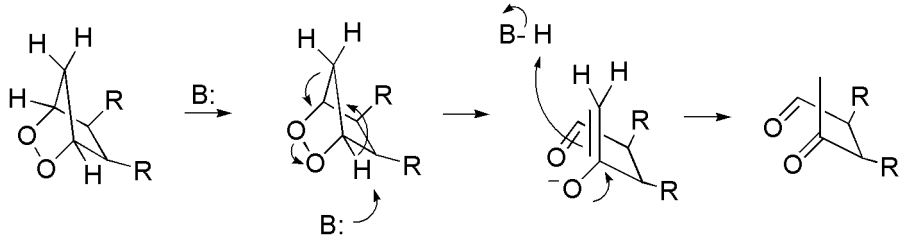

Figure 30. Proposed mechanism for the formation of isoketal from the non-enzymatic oxidation of arachidonic acid via the prostaglandin H_2 intermediate.[93]

Biological activity of lipid peroxidation products

Not all lipid peroxidation products are biologically active; however, those species that are active extend their activity through two major pathways. The first pathway is exemplified by HETE isomers which serve as ligands for the constitutively expressed PPARγ receptor.[101] In monocytes, PPARγ binding triggers signaling involved in differentiation and key regulatory functions. The second pathway results from extremely

reactive lipid peroxidation species that manifest activity through adduction to cellular nucleophiles. HNE is reactive with proteins, forming primarily Michael addition adducts with cysteine residues, and to a lesser extent, lysine and histidine residues. Under physiological conditions, the concentration of cysteine-derived sulfhydryl anions is relatively low, thus establishing the rate limiting step. HNE also forms hemiaminal adducts with lysine residues which dehydrate to form imines, although both of these reactions are reversible, rendering a majority of HNE in a free form (Figure 31). The kinetics of HNE's reactivity with protein was examined by incubating synthetic HNE with a five molar excess of bovine serum albumin (BSA).[102] Within 80 minutes, 50% of the free HNE was depleted demonstrating the potential for disrupted enzyme activity and cellular function.

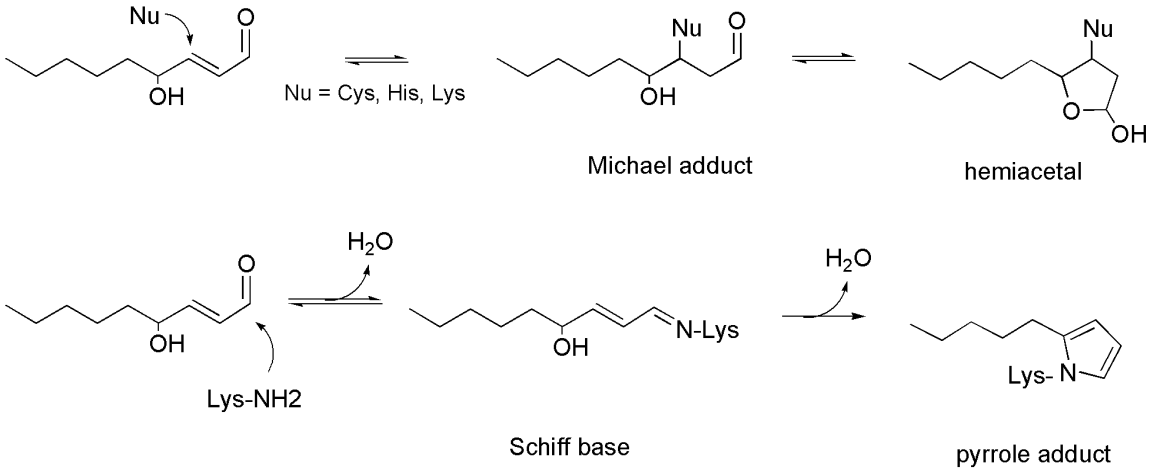

Figure 31. Scheme showing the formation of HNE adducts with protein nucleophiles.

Compared to HNE, IsoK are extensively more reactive with protein. Studies parallel to the HNE reactivity experiment described above examined IsoK reactivity and demonstrated that 50% of free IsoK remained only 20 s after initiating the reaction with

BSA.[102] This rapid decline can be explained by essentially irreversible reactions which drive the reaction of free isoketals to an adducted form.[103] These adducted forms include imine (Schiff base), pyrrole, lactam, and hydroxylactam adducts with lysine residues of proteins, as shown in Figure 32.

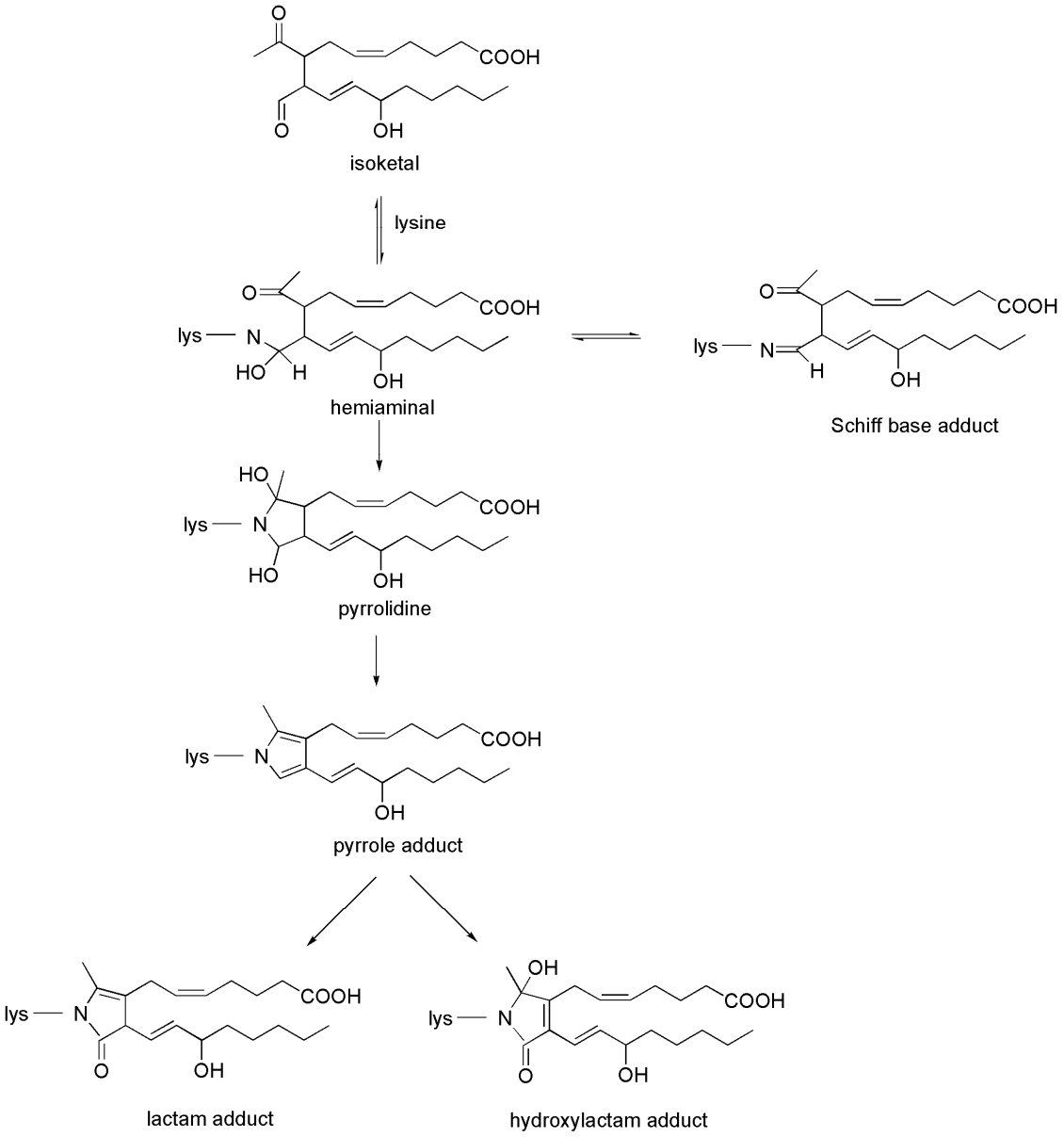

Figure 32. Scheme showing the formation of isoketal adducts with lysine residues. Adapted from reference 103.

Impact of lipid peroxidation products on microbicidal burst

Given the markedly different fates of BH and Hz within phagocytic cells, presumably due to lipid peroxidation products impairing ROS and RNS production,[60, 68] the effects of several constitutive components of Hz (i.e., BH, HNE, and 15-HETE) on microbicidal burst were examined.[68] As illustrated in Figure 33, BH has no inhibitory activity toward the generation of ROS or RNS. These observations are consistent with studies involving cultured B10R, BV2 and N11 microglial cell lines and peritoneal macrophage cells which demonstrated that neither BH nor purified Hz impairs NOX or iNOS activities.[104-106]

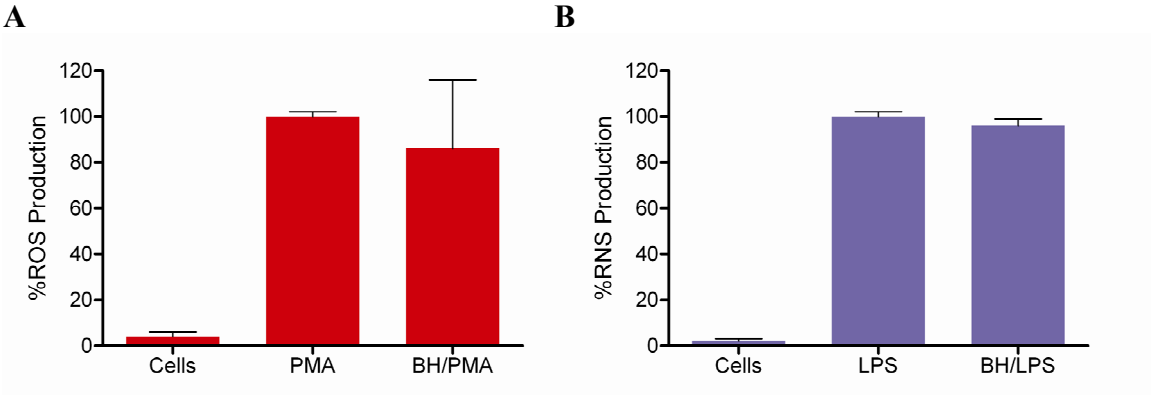

Figure 33. Effect of BH on the production of microbicidal agents.[68] Cells were treated and assayed as described in the experimental procedures. (A) ROS production was measured using the DCF-DA assay. (B) RNS was assessed using the Griess assay. Abbreviations: C, unstimulated cells; PMA, phorbol-12-myristate-13-acetate; BH, β-hematin; LPS, lipopolysaccharide.

In contrast to BH, both HNE and 15-HETE had a significant effect on microbicidal burst. As shown in Figure 34, PMA-stimulated RAW 264.7 cells treated with HNE demonstrated a concentration-dependent inhibition of NOX activity with an EC_{50} value of 45.9 μM; LPS-activated iNOS activity was even more sensitive to HNE

treatment with an EC_{50} value of 9.2 μM. [68] HNE has been shown to alter the activity of protein kinase C, a key signaling protein required for NOX activation in monocyte-derived macrophages[107] and likely explains decreased levels of $O_2^{\cdot-}$ in human neutrophils treated with HNE (EC_{50} 27 μM).[108] Notably, HNE was shown to form covalent adducts to PKC in RAW 264.7 culture (assessed by western blot) and with recombinant PKC βII protein *in vitro* (assessed by proteomic adduct mapping analysis), supporting a role for HNE in the inhibition of NOX activity through PKC inactivation.[109] There is also precedence of HNE impairing iNOS activity in RAW 264.7 cells: serum-withdrawal, which activates cells via NFκB resulting in the production of NO, is unable to mediate NO production when cell are cultured in the presence of HNE.[110] HNE has been shown to covalently adduct to IKK, inhibiting kinase activity[74] which explains decreased levels of NO as a result of impaired NFκB signaling.

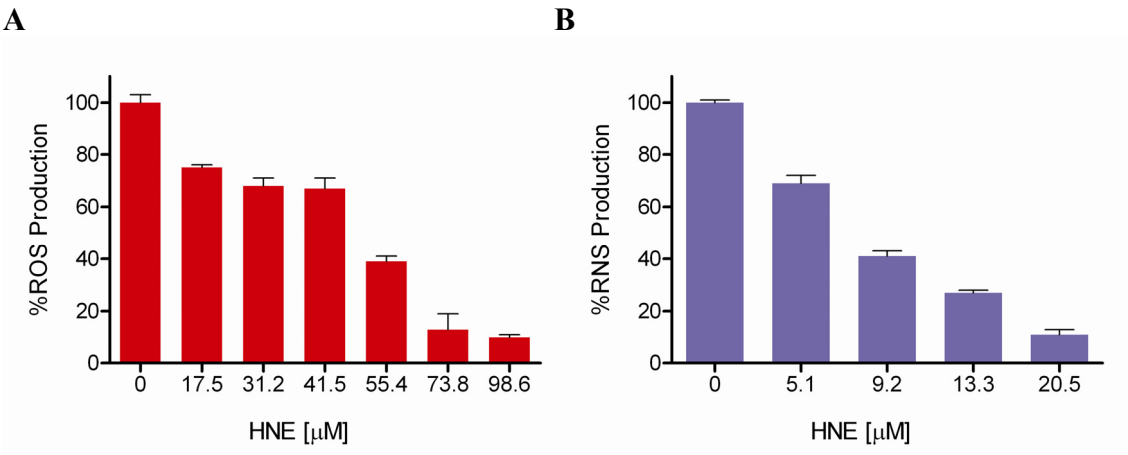

Figure 34. Effect of HNE on the production of microbicidal agents.[68] Cells were treated and assayed as described in the experimental procedures. (A) ROS production was measured using the DCF-DA assay. (B) RNS was assessed using the Griess assay.

Human monocytes treated with 15-HETE exhibit markedly reduced levels of ROS, which approach basal levels by 15 μM.[111] Consistent with this report, 15-HETE significantly impaired PMA-stimulated NOX activity in RAW 264.7 macrophage cells (EC_{50} 8.0 μM) (Figure 35).[68] Although iNOS activity was also affected by 15-HETE, inhibition was less substantial than it was with NOX. While 15-HETE clearly alters ROS and RNS production, albeit to vastly different levels, the specific mechanisms leading to inhibition remain unknown. PPARγ agonists have been shown to antagonize the activity of transcription factors NF-κB and AP-1, thereby inhibiting the expression of iNOS in murine macrophages.[112] iNOS expression was also shown to be abrogated through a PPARγ-independent NF-κB inhibitory mechanism by 15-deoxy-prostaglandin J_2, a PPARγ ligand. [113] Therefore, it is likely that 15-HETE exerts its activity by similar PPARγ-dependent and -independent inhibitory mechanisms.

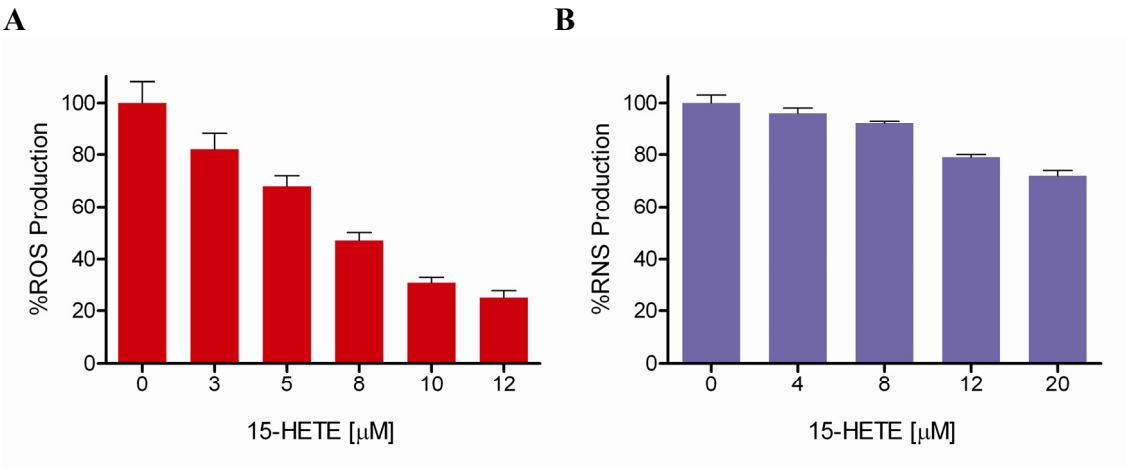

Figure 35. Effect of 15-HETE on the production of microbicidal agents.[68] Cells were treated and assayed as described in the experimental procedures. (A) ROS production was measured using the DCF-DA assay. (B) RNS was assessed using the Griess assay.

Given that both HNE and 15-HETE demonstrated the ability to modulate microbicidal burst, the effects of BH-mediated ghost membrane peroxidation on macrophage response were explored: BH was incubated with ghost cell membranes and activated cells were treated with various amounts of the reaction supernatant. NOX activity in PMA-stimulated RAW cells was inhibited in a concentration-dependent manner, as was the activation of iNOS in LPS-stimulated cells (Figure 36). Importantly, there was no detectable inhibition of ROS or RNS production upon treatment with BH or ghost supernatants alone. These results demonstrate that the inhibitory NOX and iNOS activities within RAW 264.7 cells are due to the products from the reaction between BH and ghosts, not the biomineral itself.

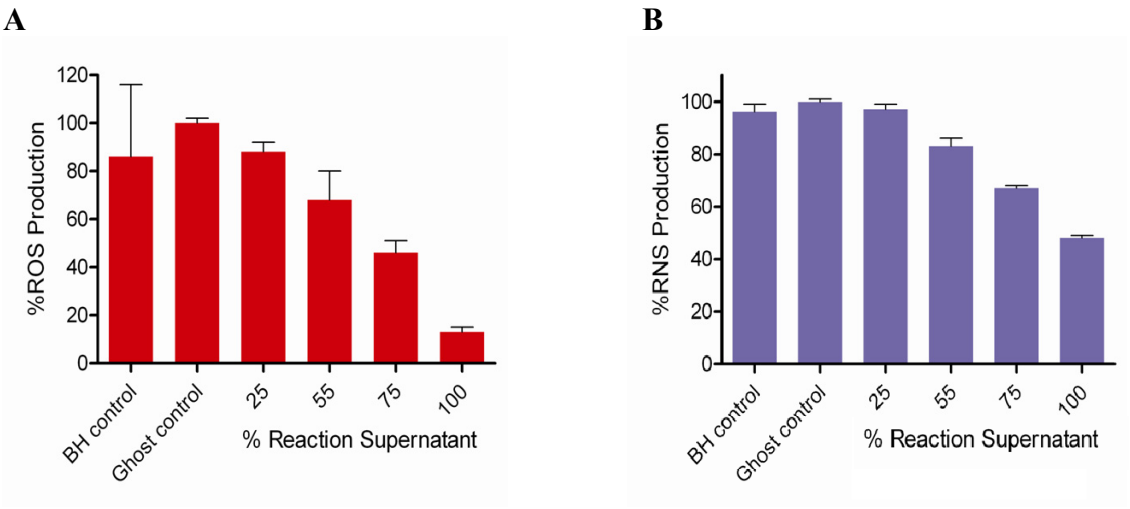

Figure 36. Inhibitory effect of the products generated from the interaction of BH with ghost cells.[68] Cells were treated and assayed as described in the experimental procedures. (A) Inhibition of ROS production was measured using luminol-enhanced chemiluminescence. (B) Inhibition of RNS was assessed using the Griess assay.

Conclusions

In light of the results discussed and the data presented thus far, the following sequence of events is proposed: First, synchronized erythrocyte rupture releases Hz into an environment filled with cellular debris. This setting provides substrate for non-enzymatic Hz-catalyzed peroxidation which results in a gradient of primary and secondary lipid peroxidation products.[32, 70, 78, 86] Next, particulate Hz (laden with biologically active lipid species) triggers a phagocytic response and serves as a vehicle to deliver toxic species into immune cells.[61] Finally, immune cells are rendered functionally impaired, yet viable, resulting in propagation of the infection and immune response.[60, 68, 84, 107, 114]

In order to clarify the basis of Hz-mediated immunomodulation, it is necessary to understand the ways in which cellular functions are perturbed by individual components of Hz. Although an ineffective microbicidal burst illustrates that downstream signaling events can be modulated indirectly by the Hz moiety, the specific mechanisms and cellular targets responsible for the modulation remain unknown. Furthermore, the altered cellular responses represent but two of numerous possible modulations, prompting further exploration of global cellular changes in response to Hz and its components. Consequently, Chapter III focuses on the global impact of individual Hz components.

CHAPTER III

ANALYSIS OF GENE EXPRESSION CHANGES MEDIATED BY INDIVIDUAL CONSTITUENTS OF HEMOZOIN

Introduction

It has been suggested that the immunological activity of hemozoin (Hz) does not stem from the heme moiety itself, but from toxins such as lipid peroxidation products present on the biomineral's surface and introduced into the cell during phagocytosis. In *Chapter II*, the immunomodulatory response to native Hz was recapitulated using constitutive components of Hz in a model system.[68] Macrophage-like cells treated with the reaction supernatant resulted in a dose-dependent impairment of PMA-activated NOX and LPS-stimulated iNOS activities. Neither BH- nor ghost-supernatant alone altered NOX or iNOS activity, indicating that lipid peroxidation products generated during reactions between BH and ghost membranes are responsible for the inhibitory effects. Furthermore, biologically relevant levels of the individual lipid peroxidation products HNE and 15-HETE mimicked the dysfunctional response to hemozoin phagocytosis, suggesting the basis of Hz activity.[68, 114, 115]

Hz toxicity in monocytes is associated with high levels of HNE and 15-HETE.[32, 70] HNE is highly reactive with nucleophilic sites in biomolecules and is capable of forming covalent adducts and crosslinks, impairing enzymatic activity, and triggering changes in gene expression.[8, 72-77] 15-HETE mediates its biological activity upon binding the nuclear PPARγ receptor and has been reported to augment RBC adherence to endothelia, enhance vascular permeability and edema, and increase chemotaxis and

chemokinesis, three hallmarks of malarial infection. [32, 61, 101, 116, 117] In light of these findings, the responses of innate immune cells to specific and nonspecific malaria toxins were of particular interest.

Global effects of the individual components of Hz remain largely unexplored in the context of malaria; therefore, microarray technology was used to explore gene expression changes in activated RAW 264.7 macrophage-like cells exposed to constituent components of native Hz. Chapter III is divided into two parts: expression changes mediated by HNE and BH are presented in *Part I*, and expression changes mediated by 15-HETE are presented in *Part II*. Gene expression patterns were analyzed in the context of biological processes and networks to examine the downstream effects of both specific and non-specific damage, and comparisons were made with cellular alterations that are observed during malarial infection.

Experimental

Cell culture

Murine macrophage-like RAW 264.7 cells (American Type Culture Collection TIB-71, Manassas, VA) were cultured under standard incubation conditions (37 ºC, 5% CO2) and grown in RPMI supplemented with 5% FBS (Atlanta Biologicals, Atlanta, GA) and 1 μg/mL P/S (Cellgro MediaTech, Herndon, VA). Cells were plated at a density of 4 $\times 10^6$ cells/well in 6 well plates and incubated for 24 h prior to treatment.

Cell treatment

Cells were washed once with Dulbecco's PBS (DPBS) and treated with 35 μM HNE (EMD Biosciences, San Diego, CA), 0.1 mg/mL serum-opsonized BH, 10 μL of 0.05% serum-opsonized latex bead (0.1μm), or 40 μM 15(S)-HETE (Cayman Chemicals) per 1×10^6 cells. Opsonization was performed as previously described.[84] Immediately following treatment, LPS was added to all wells at a final concentration of 1 μg/mL. After either 6 or 24 h incubation, cells were washed three times with DPBS and either scraped from wells for RNA extraction or incubated for 15 minutes at 37 ºC in CellStripper non-enzymatic cell dissociation buffer (Cellgro MediaTech) for flow cytometric analysis.

Flow cytometry

Adherent cells (4×10^6/well) were dissociated by a 5-15 minute incubation at 37 ºC with 500 μL CellStripper; cell suspensions were pipetted up and down to release the remaining loosely adhered cells and transferred to round bottom flow cytometry tubes (Falcon). Complete culture media (1000 mL) was added to the suspensions to quench the dissociation buffer. Samples were centrifuged at 1500 RPM for 5 min, media was removed, and cells were washed with PBS. Assays were performed on a BD LSRII Flow Cytometer. Cell death was determined by the Vybrant Apoptosis Assay Kit II (Invitrogen) according to the manufacturer's instructions. Briefly, cells were harvested, resuspended in assay buffer, and stained with Alexa Fluor 488 conjugated Annexin V and propidium iodide (PI). An apoptosis positive control was prepared by treating cells with

10 μM camptothecin (Sigma) for 4 h prior to staining. Single color stains were used as compensation controls, and at least 10 000 events per sample were collected for the determination of cell populations using FACSDiva v6.1-1 software. Sample analysis was performed using FloJo v8.8.2 software (Treestar).

RNA isolation and microarray analysis

Three biological replicates (composed of six pooled wells) per sample were treated as described above. Total RNA was isolated using the Versagene RNA purification and DNase treatment kits, following manufacturer's recommendations. Microarray analysis was performed by the Vanderbilt Microarray Shared Resource. Three biological replicates of each treatment were analyzed for quality (Agilent 2100 Bioanalyzer, Agilent Technologies, Palo Alto, CA). One (1) μg of Total RNA (30ng mRNA) was used to generate First Strand cDNA using the NanoAmp RT-IVT labeling kit according to manufacturer's protocol. Following first strand synthesis,second strand synthesis was completed. The resulting cDNA was then purified using an ABI kit provided column and the entire reaction was used in an IVT reaction to generate cRNA or DIG labeled cRNA. The cRNA was then purified using a kit provided column, assessed for quality on an Agilent Bioanalyzer, and reverse transcribed to make ss cDNA. Samples prepared from 6 h incubations were fragmented, labeled with terminal deoxy transferase with biotin, hybridized to an Affymetrix mouse gene 1.0ST arrays per manufacturer's protocol, and detected with Streptavidin-Phycoerythrin. Samples obtained from 24 h incubations were fragmented, hybridized to an ABI mouse genome survey microarray per manufacturer's protocol, and detected with the addition of the

chemiluminescence reaction substrate. Expression values were quantile normalized and filtered (S/N >3 and flag value <5000, ABI arrays). Partek 6.4 and GeneSpring GX 7.3.1 software were used to determine statistically significant differentially expressed genes from probes altered by ≤ or ≥ 1.8-fold (0.01 p-value cutoff, Benjamini-Hochberg multiple testing correction) in treated stimulated cells (experimental) relative to stimulated cells (control). Genes were classified according to genes ontology (GO) terms using the web-based tool, FatiGO v2.0 (http://www.babelomics.org).[118] In accordance with MIAME procedure, microarray data have been submitted to the NCBI Gene Expression Omnibus and can be found under series GSE13281 and GSE15070.

Pathway and network analysis

Ingenuity Pathways Analysis (IPA) was used for gene expression analysis (Ingenuity Systems®, www.ingenuity.com). A dataset containing gene identifiers and expression values was uploaded into the application. Each identifier was mapped to its corresponding gene object in the Ingenuity knowledge base (IKB). These focus genes were overlaid onto a global molecular network developed from information contained in the IKB, and networks were algorithmically generated based on their connectivity. The Functional Analysis of each network identified the biological functions that were most significant to the genes in the network and Canonical Pathway Analysis identified the pathways from the IPA library of canonical pathways that were most significant to the dataset. Fischer's exact test was used to calculate a *p*-value determining the probability that that each biological function assigned to a network or the association between the genes in the dataset and the canonical pathway are explained by chance alone.

Real-time reverse transcription polymerase chain reaction

Quantitative real-time reverse transcription polymerase chain reaction (qRT-PCR) was used to validate the expression levels of several genes identified as differentially expressed by microarray analysis. Quadruplicate measurements for n = 3 biological replicates per sample were performed. cDNA was reverse-transcribed from 0.5 μg of total RNA using random hexamer primers and Superscript II Reverse Transcriptase (Invitrogen). Reactions were purified using Qiagen's PCR Purification Kit following the manufacturer's protocol. Following RT, all assays were performed with Applied Biosystems TaqMan FAM labeled 20× probes. *Ywhaz* was chosen as the endogenous control based on results obtained from an Applied Biosystems mouse endogenous control array. cDNA amplification was performed using TaqMan 2× Universal PCR Master Mix (Applied Biosystems) according to the manufacturer's directions. Standard Taqman cycling conditions were used as specified by the manufacturer. Cycling and data collection were performed using the Applied Biosystems 7900 HT instrument and analysis performed using the manufacturer's SDS software package to calculate Ct values for each detector. Ct values were processed based on the comparative Ct method, where the relative transcript level of each target gene was calculated according to the equation $2^{-\Delta Ct}$, where ΔCt is defined as $Ct_{\text{target gene}} - Ct_{\text{Ywhaz}}$.

Enzyme-linked immunosorbant assays

Enzyme-linked immunosorbant assays (ELISAs) were used to measure the levels of soluble proteins secreted into culture medium. RAW 264.7 cells (4×10^6 cells/well in 6 well plates) were plated and incubated for 24 h. The cells were washed once with

DPBS and treated in triplicate with LPS (1 μg/mL) or HNE (35 μM) + LPS (1 μg/mL final). Cell culture medium was collected and analyzed using commercial ELISA reagents (R&D Systems) according to protocol using 96-well Immulon 2HB plates (Thermo Electron Corp.). Briefly, capture antibody was added to wells and incubated at 25 ºC overnight. Three washes (300 μL each) were performed after this and all subsequent steps using phosphate buffered saline (PBS) supplemented with 0.05% Tween-20. Wells were blocked with 300 μL of 5% Fraction V bovine serum albumin (Fisher Scientific) in PBS for 1 h at 37 ºC. Three-fold serial dilutions of collected culture medium (1:1–1:2187) in complete medium and two-fold dilutions of recombinant protein in complete medium were added to wells and incubated for 1 h at 37 ºC. Wells were incubated with the appropriate biotinylated detection antibody for 1 h at 37 ºC and subsequently incubated with streptavidin-HRP for 10 min at 37 ºC. After addition of 3,3',5,5',-tetramethylbenzidine liquid substrate (100 μL, Sigma Aldrich), the enzymatic reaction was quenched with 50 μL of 2M H_2SO_4. The absorbance of samples was then measured spectrophotometrically at 450 nm. Culture medium and recombinant protein were used as negative and positive controls, respectively.

Nomenclature

Nomenclature for genes and proteins is as described by the Mouse Genome Informatics (MGI) database guidelines: both murine and human protein names are capitalized (MMP9), murine genes are italicized with the first letter capitalized (e.g., *Mmp9*), and human genes are italicized and capitalized (e.g., *MMP9*).

Results and Discussion

Part I: Comparative Analysis of the Gene Expression Response to HNE, BH, and Latex Beads

The immunomodulation observed during *Plasmodium* blood stage infection is believed to be a result of the host response to parasite products. Although genome-wide expression analyses has been examined in the blood of human victims,[119, 120] malaria positive tissue,[121] and murine[122-124] and monkey[125] malaria models, the specific components responsible for altered expression have not been identified. Given the relationship between high levels of Hz, severity of infection, and disruption of macrophage function, the present study used microarray technology to profile expression changes mediated by Hz-derived components in a model macrophage-like cell line (RAW 264.7 cells). Given the unquestionable reactivity of HNE and ability of the heme moiety to mediate lipid peroxidation, HNE and BH were targeted as the native Hz components

Analysis of gene expression changes in BH- or HNE-treated, LPS-stimulated RAW 264.7 cells

LPS stimulated macrophage-like RAW 264.7 cells were exposed to 0.1 mg/mL BH or 35 μM HNE for 6 or 24 h. The concentrations of BH and HNE were chosen based on reported estimates of Hz (100 μM) in brain capillaries of malaria victims [126] and HNE (40 μM) levels in Hz-fed monocytes.[70] Phagocytosis of opsonized-latex beads and -BH was examined by flow cytometry. Latex bead fluorescence (Figure 37) was detected in

86% and 99% of the gated parent population at 6 and 24 h, respectively, demonstrating the level of phagocytosis.

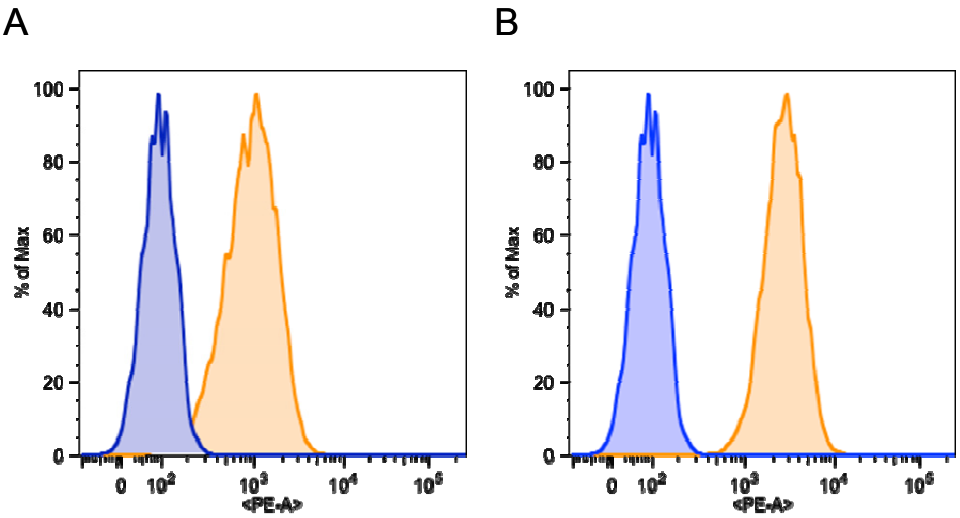

Figure 37. Latex bead phagocytosis. LPS (0.1 µg/mL) stimulated RAW 264.7 cells were treated with serum-opsonized fluorescent red latex beads for (A) 6 h or (B) 24 h and analyzed by flow cytometry. Untreated control cell populations (blue tinted) were overlaid with the latex bead treated cell population (orange tinted) to demonstrate the increase in fluorescence upon phagocytosis.[44]

Accumulation of Hz within monocytes has been shown to considerably increase both depolarized and conventional side scatter.[127] In BH treated cells, phagocytosis of the total population was indicated by a marked increase in conventional side scatter mean fluorescence versus control cells (Figure 38). It was previously shown by confocal microscopy that opsonized BH was ingested by RAW 264.7 cells and localized within the phagolysosome.[68]

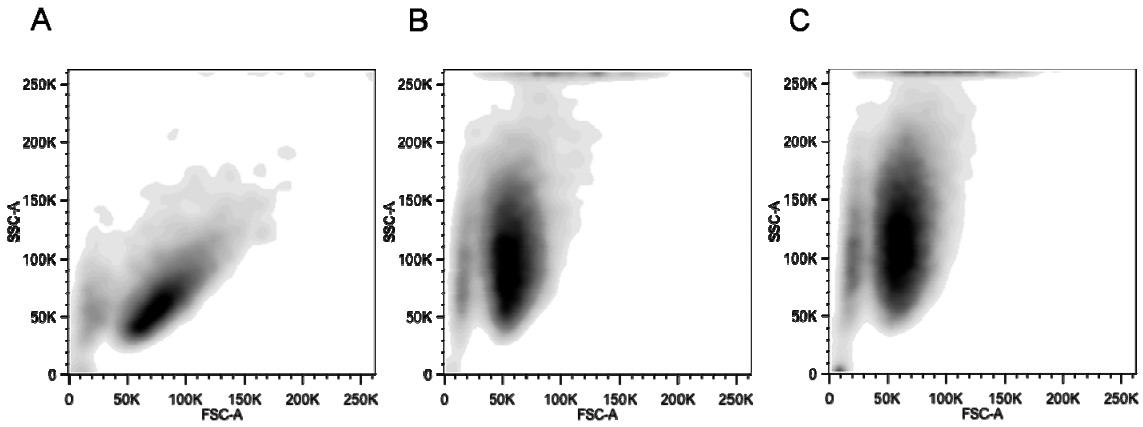

Figure 38. BH phagocytosis. LPS (0.1 μg/mL) stimulated RAW 264.7 cells were (A) untreated or treated with 0.1 mg/mL serum-opsonized BH for (B) 6 h or (C) 24 h and analyzed by flow cytometry. Consistent with phagocytosis of the biomineral, density plots demonstrate that BH treatment markedly increased the side scatter of the total population at both timepoints.[44]

HNE induces cytotoxic and mutagenic effects in several cell types, albeit at differing concentrations.[71] It has been established that the concentration of exogenous HNE necessary to elicit a cellular response can be orders of magnitude higher than an endogenous steady state level.[128] Therefore, the cytotoxicity profiles of HNE in RAW 264.7 cells were evaluated by flow cytometry. LPS-stimulated cells were treated with varying concentrations of HNE for 24 h and changes in viable, apoptotic, and dead cell populations were measured. Figure 39 (A and B) illustrates the analysis of stimulated cells treated 35 μM HNE. The percent of viable cells at increasing concentrations of HNE (0-35 μM) for 24 h was calculated and is shown in Figure 39 (C). Results demonstrate that concentrations of HNE up to 35 μM are well tolerated by RAW 264.7 cells.

Statistically significant ($p \leq 0.01$) gene expression changes (fold change ≥1.8 relative to control), where expression is considered a measurement of the RNA abundance at the time of isolation, were identified by microarray analysis. Within each treatment category,

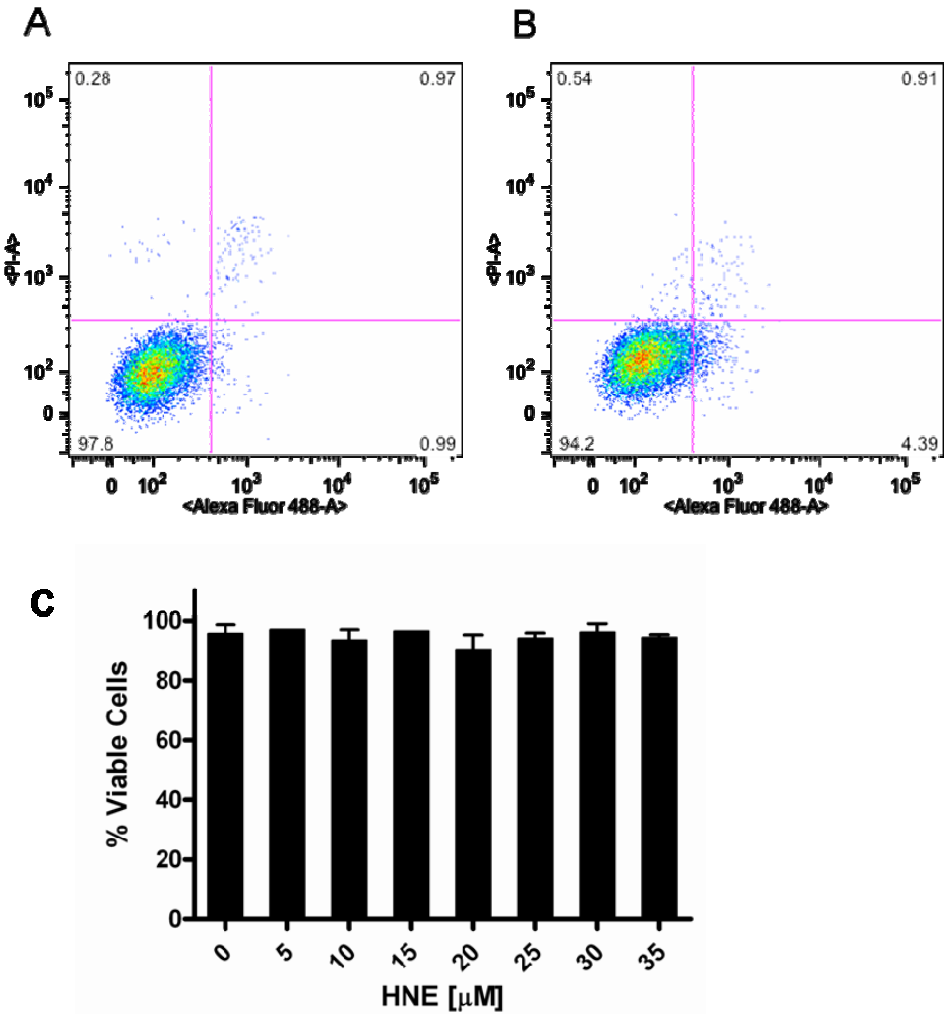

Figure 39. Viability of HNE-treated cells. LPS (0.1 μg/mL) stimulated RAW 264.7 cells were (A) untreated or (B) treated with 35 μM HNE for 24 h and stained with apoptosis and necrosis-specific stains. Three populations were observed by flow cytometric analysis: viable cells, apoptotic cells, and necrotic cells. Viable cells are negative for both Alexa Fluor 488 conjugated annexin V and PI, apoptotic cells are positive for Alexa Fluor 488 conjugated annexin V, and necrotic cells are positive for PI. (C) Viable cells within total cell populations treated with HNE (0-35 μM) for 24 h were determined.

differentially expressed genes were sorted into lists based on the direction of regulation and compared to identify common changes relative to untreated stimulated cells (Figure 40, A-D). In order to identify expression changes dependent on interactions of BH rather than those due to phagocytosis, differentially expressed genes were controlled by a

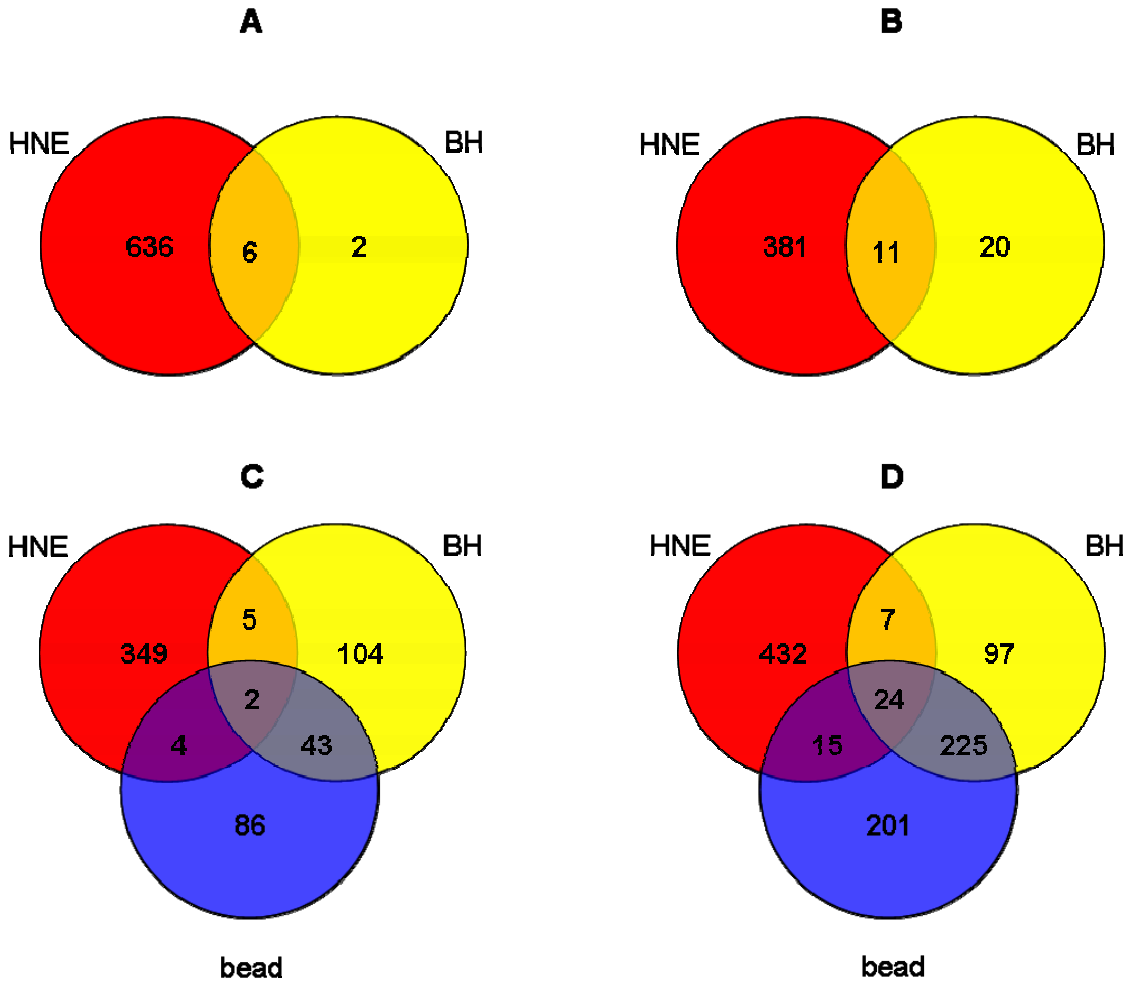

Figure 40. Overlapping genes with significant differential expression mediated by BH and HNE. Venn diagrams show the intersection of genes that were altered by 0.1 mg/mL BH with those altered by either latex bead or 35 μM HNE treatment. Numbers represent statistically significant ($p \leq 0.01$) genes up- or down-regulated ≥1.8-fold relative to LPS stimulated cells at 24 h. (A) down-regulated genes identified at 6 h, (B) up-regulated genes identified at 6 h, (C) down-regulated genes identified at 24 h, (D) up-regulated genes identified at 24 h.[44]

corresponding particulate latex bead challenge. Six hours post-challenge, there were no significant gene expression changes mediated by latex bead phagocytosis, and only a small group (i.e., 39 genes) altered by BH phagocytosis. Steady-state mRNA levels (24 h) demonstrate that nearly 70% of the genes differentially expressed by BH are in common with the 'inert' latex bead control, indicating that the response to BH is predominantly phagocytic.

Consequently, phagocytosis-related genes were identified and disregarded for remaining analyses. The number of genes differentially expressed by HNE or BH treatment indicates the degree of perturbation by each of the native Hz-associated components. HNE treatment altered a significantly larger group of genes than BH treatment, suggesting a more serious impact on cellular function.

Ingenuity Pathway Analysis (IPA) was used to perform a functional analysis of each dataset. IPA functional analysis ranks molecular and cellular functions according to Fischer's Exact Test *p*-value. Those categories exhibiting $p < 0.001$ are shown in Table 1 for both BH and HNE treatment datasets at 6 and 24 h timepoints. The magnitude of response to either BH or HNE treatment is evident from the number of significantly affected biological processes identified by IPA. At 6 h, both BH and HNE affect a diverse group of functions including 'Cell Signaling', 'Cellular Development', 'Molecular Transport', and 'Small Molecule Biochemistry' among others. By 24 h, the cellular response to BH is minimal. Given that BH does not impair microbicidal functions, is sensitive to microbicidal agents, and is degraded upon phagocytosis in RAW 264.7 cells,[68] it was not surprising to find that the steady-state response to BH was modest. The degree of perturbation by HNE at 24 h complements literature observations

regarding its extensive reactivity with cellular nucleophiles.[8, 72-77] Expression changes mediated by BH and HNE indicate differential cellular responses to both treatments as a function of time. There is, however, some overlap in the early and late response to HNE, primarily associated with 'Stress Response', 'Cell Cycle', 'Immune Response', 'Metabolic Process', and 'Gene Expression' (listed within Table 2).

Functional analysis of interaction networks

Biological interaction networks were generated by mapping differentially expressed genes unique to HNE and BH treatment to the molecules in the Ingenuity knowledge database (IKB) based on known interactions in the canonical literature. Each network is associated with a numerical value, a 'score', to indicate the likelihood that the focus genes occur in the network by random chance. Networks scoring 10 or higher (score is defined as –log (*p*-value)) are considered significant.

Among the 39 genes modulated by BH phagocytosis at 6 h, 27 were eligible for analysis based on IPA criteria, mapping to 2 relevant interaction networks. The most significant network (Figure 41 A) has a score of 25 and associates 11 focus genes involved predominantly with 'Carbohydrate Metabolism' ($p = 3.76 \times 10^{-3}$), 'Gene Expression' ($p = 5.93 \times 10^{-3}$), and 'Small Molecule Biochemistry' ($p = 5.98 \times 10^{-3}$). Interestingly, the network predicted interactions with several transcriptional regulators (*Hnf4a*, *Jdp2*, *Jun*, *Mafk*, *Fos*, and *Elk3*). Gene expression alterations of 113 IPA network eligible genes were mediated by BH treatment at 24 h, mapping to eight significant

Table 1. Functional analysis of BH and HNE datasets[a]

Biological Function	*p*-value[a]			
	BH		HNE	
	6 h	24 h	6 h	24 h
Amino Acid Metabolism			$< 10^{-4}$	2.03×10^{-4}
Carbohydrate Metabolism	5.54×10^{-4}			
Cell Cycle	5.54×10^{-4}	7.24×10^{-4}	$< 10^{-4}$	$< 10^{-4}$
Cell Death	2.41×10^{-4}		$< 10^{-4}$	$< 10^{-4}$
Cell Morphology		7.10×10^{-4}	$< 10^{-4}$	$< 10^{-4}$
Cell Signaling	5.61×10^{-4}		$< 10^{-4}$	
Cell-To-Cell Signaling and Interaction	$< 10^{-4}$		$< 10^{-4}$	$< 10^{-4}$
Cellular Assembly and Organization		1.61×10^{-4}	$< 10^{-4}$	$< 10^{-4}$
Cellular Compromise			$< 10^{-4}$	
Cellular Development	5.54×10^{-4}		$< 10^{-4}$	$< 10^{-4}$
Cellular Function and Maintenance	2.84×10^{-4}		$< 10^{-4}$	$< 10^{-4}$
Cellular Growth and Proliferation			$< 10^{-4}$	$< 10^{-4}$
Cellular Movement			$< 10^{-4}$	$< 10^{-4}$
DNA Replication, Recombination, and Repair			$< 10^{-4}$	$< 10^{-4}$
Free Radical Scavenging	5.54×10^{-4}			
Gene Expression			$< 10^{-4}$	$< 10^{-4}$
Lipid Metabolism	5.54×10^{-4}			
Molecular Transport	5.54×10^{-4}		$< 10^{-4}$	
Post-Translational Modification		6.25×10^{-4}	$< 10^{-4}$	$< 10^{-4}$
Small Molecule Biochemistry	5.54×10^{-4}		$< 10^{-4}$	2.03×10^{-4}
Vitamin and Mineral Metabolism			$< 10^{-4}$	

[a] Ingenuity Pathway Analysis uses a right-tailed Fisher Exact Test to calculate *p*-values. Significance values for each dataset indicate the probability that the association between the genes and the given molecular and cellular functions are due to random chance.

functional interaction networks. The network shown in Figure 41 B linked 13 focus genes with 22 additional molecules with a significance score of 21. Of the products encoded by these genes, 17 are localized in the nucleus and 9 are transcriptional regulators. This

particular network associates several genes that are involved in 'Cell Cycle' ($p = 1.87 \times 10^{-4}$). Consistent with this function, the network predicted interactions with several cell division genes (*Bhlbh2, Hdac2, Gas1* and *Cdk4*).

HNE mediated 591 network eligible expression changes at 6 h which mapped to 31 significant networks. The most significant interaction network (Figure 41 C) incorporates 31 focus genes with a score of 45, and is indicative of 'Immunological Disease' ($p = 5.74 \times 10^{-3}$). This network is enriched with focus genes encoding receptor molecules such as *Cxcr4*, *Ccr1*, *Il4r*, *Il13ra1*, and *Fcgr1a* (CD64), and cytokines *Ccl4*, *Il1rn*, *Ccl7*, and *Il10*. Analysis of the genes differentially expressed by HNE treatment at 24 h resulted in 492 network eligible focus genes mapping to 28 significant networks. The interaction network shown in Figure 41 D incorporated 26 focus genes with 9 additional genes by direct interactions with a score of 36, and is primarily related to 'Inflammatory Disease' ($p = 1.67 \times 10^{-14}$), 'Tissue Development' ($p = 1.36 \times 10^{-13}$), and 'Cellular Growth and Proliferation' ($p = 3.40 \times 10^{-12}$). The network contains 11 genes encoding products that are secreted into the extracellular space including cytokines (*Cxcl3, Il6*, and *Tnf)*, growth factors (*Igf1, Pdgfb, Tgfb1,* and *Vegfa*), and peptidases (*F10* and *Mmp9*) among other molecules (*Dcn* and *Timp1*).

HNE-mediated gene expression response

Previously**,** gene expression changes in human ARPE-19[76] and RKO human colorectal carcinoma cells[77] dosed with HNE have been examined by microarray analysis. Albeit under different conditions than the current study (e.g., cell line, concentration of HNE, and presence of stimulant), several commonalities are apparent.

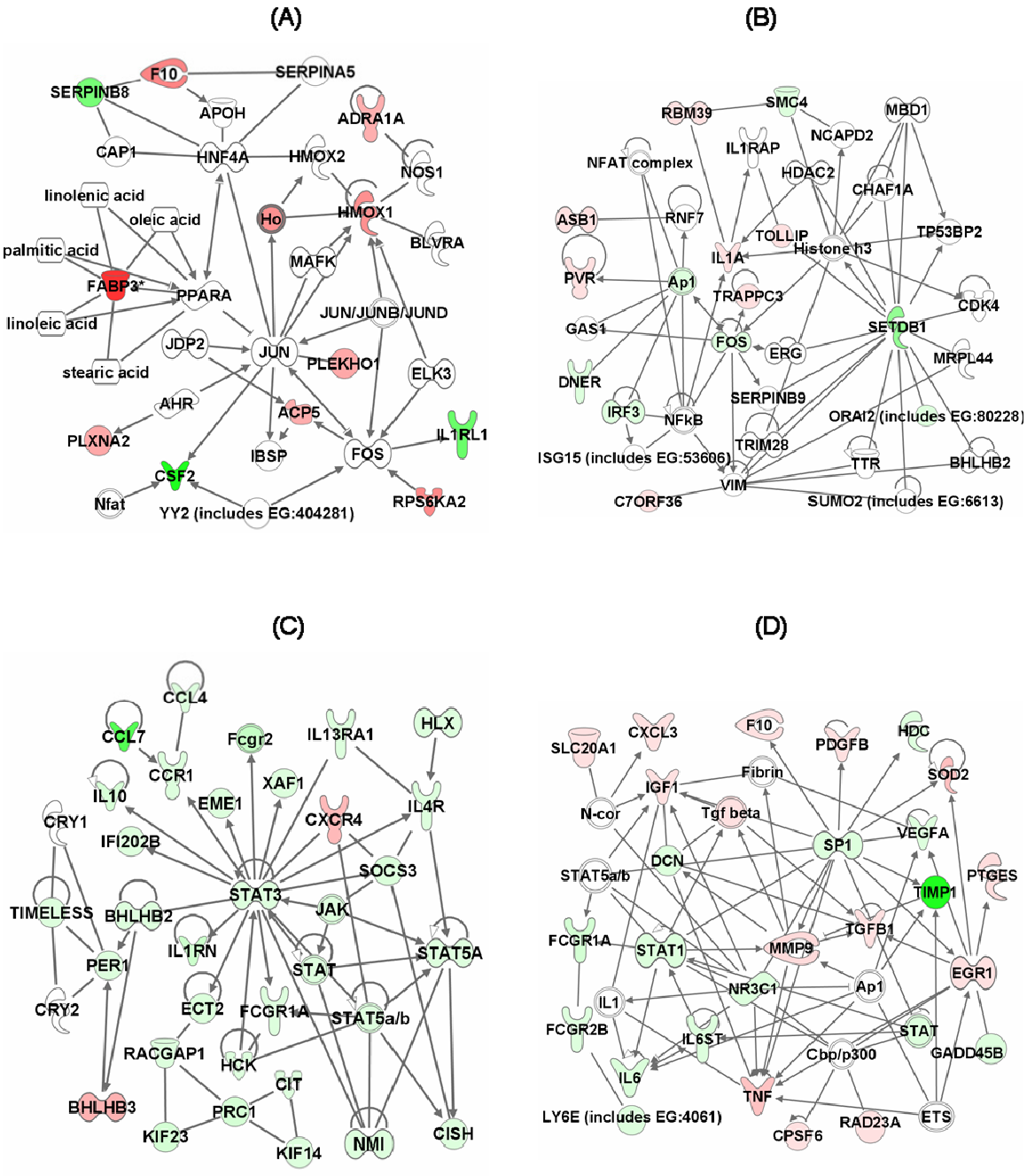

Figure 41. Ingenuity network analysis. Genes altered ≥1.8-fold ($p \leq 0.01$) in either BH- or HNE-treated RAW 264.7 cells (i.e., focus genes) were overlaid onto a global molecular network developed from information contained in the Ingenuity knowledge base (IKB). Networks of these focus genes were then algorithmically generated based on their connectivity. Network showing direct interactions between focus genes altered by (A) BH treatment at 6 h, (B) BH treatment at 24 h, (C) HNE treatment at 6 h, and (D) HNE treatment at 24 h. Genes or gene products are represented as nodes, and the biological relationship between two nodes is represented as an edge (line). The intensity of the node color indicates the degree of up- (red) or down- (green) regulation.

For example, exposure to 4 μM HNE for 4 h repressed the expression of genes whose products are involved in signal transduction, transcriptional regulation/DNA binding, xenobiotic metabolism/stress response, and cell cycle regulation.[76] Comparison with the early response to HNE in the current study demonstrates consistent regulation of a group of identical genes including *Ccna2*, *Cdc25a*, *Ccr1*, *Il18*, *Bcl2l1*, *Ier3*, *Id1*, *Top2a*, *Zfp36*, and *Lyn* (Table 2).

Gene expression responses of RKO human colorectal carcinoma cells to either subcytotoxic (5 or 20 μM) or cytotoxic (60 μM) concentrations of HNE has also been examined.[77] At 20 μM HNE, 6 h post-treatment, the primary observation was an antioxidant response. The present study mirrors several of the expression changes at 6 h, including stress response genes (*Gclm*, *Hmox1*, *Dnajb4*, *Txnrd1*) among others (*Riok3*, *Hbp1*, *Zbtb20*, *Rit1*, *Arrdc3*, *Gabarapl1*,*Ccna2*, *Ccnf*, *Ccnb1*, *Cenpa*, *Fbxo5*, *Mki67*, *Plk1*, *Ier3*, and *Top2a*) (**Table 2**).

Validation of microarray results

qRT-PCR was used to confirm several genes susceptible to differential regulation by HNE and BH at 6 h and 24 h (Table 3). Analysis was focused on selected genes implicated in the host response to malaria. The results shown in Figure 42 are expressed as fold change relative to untreated stimulated cells (control). At 6 h, RT-PCR confirmed that HNE repressed the expression of chemokine (C-C motif) ligand 2 (*Ccl2*), colony stimulating factor 3 (granulocyte) (*Csf3*), tissue inhibitor of metalloproteinase 1 (*Timp1*), matrix metalloproteinase 9 (*Mmp9*), *Csf2,* interleukin (Il) 1 alpha (*Il1a*) and 1 beta (*Il1b*), and BH down-regulated colony stimulating factor 2 (granulocyte-macrophage) (*Csf2*)

relative to untreated stimulated cells. At 24 h, HNE enhanced expression of *Mmp9,* nuclear factor of kappa light polypeptide gene enhancer in B-cells inhibitor, epsilon (*Nfkbie*), inhibitor of kappaB kinase epsilon (*Ikbke*), tumor necrosis factor (*Tnf*), and *Csf3*. Concurrently, *Timp1* and chemokine (C-C motif) ligand 5 (*Ccl5*) genes were repressed. RT-PCR analyses of BH-treated cells at 24 h confirmed *Il1a* stimulation and FBJ osteosarcoma oncogene (*Fos*) suppression. These results are consistent with the microarray data. ELISA studies showed that HNE treatment induced MMP9 and CSF3 translation and release relative to stimulated, untreated cells (Figure 43).

Table 2. Select Gene Expression Changes Mediated by HNE[a]

Gene Symbol	Description	Fold Change		MGI Gene ID
		6 h	24 h	
Cell Cycle				
Atm	ataxia telangiectasia mutated homolog (human)		1.9	107202
Atr	Ataxia telangiectasia and rad3 related		3.8	108028
Bub1	budding uninhibited by benzimidazoles 1 homolog (S. cerevisiae)	-2.7		1100510
Bub1b	budding uninhibited by benzimidazoles 1 homolog, beta (S. cerevisiae)	-2.8		1333889
Ccna2	cyclin A2	-5.1		108069
Ccnb1	cyclin B1	-5.2		88302
Ccnd1	cyclin D1		1.9	88313
Ccnf	cyclin F	-4.1		102551
Ccng2	cyclin G2	-2.9		1095734
Ccr1	chemokine (C-C motif) receptor 1	-3.1		104618
Cdc20	cell division cycle 20 homolog (S. cerevisiae)	-2.3		1859866
Cdc25a	cell division cycle 25 homolog A (S. pombe)	-1.9		103198
Cdc25c	cell division cycle 25 homolog C (S. pombe)	-3.5		88350
Cdk6	cyclin-dependent kinase 6		1.9	1277162
Chek1	checkpoint kinase 1 homolog (S. pombe)	-2.3		1202065
Dbf4	DBF4 homolog (S. cerevisiae)	-2.0		1351328
E2f2	E2F transcription factor 2		2.0	1096341
Fen1	flap structure specific endonuclease 1		2.5	102779

Table 2, continued.

Gadd45a	growth arrest and DNA-damage-inducible 45		2.5	107799
Mki67	antigen identified by monoclonal antibody Ki	-4.0		106035
Msh5	mutS homolog 5 (E. coli)		6.2	1329021
Mutyh	mutY homolog (E. coli)		3.1	1917853
Mxd1	MAX dimerization protein 1	-4.7		96908
Ndc80	NDC80 homolog, kinetochore complex component (S. cerevisia)	-2.4		1914302
Pa2g4	proliferation-associated 2G4		2.3	894684
Pcna	proliferating cell nuclear antigen		2.3	97503
Plk1	polo-like kinase 1 (Drosophila)	-8.6		97621
Rad23a	RAD23a homolog (S. cerevisiae)		2.2	105126
Rad51	RAD51 homolog (S. cerevisiae)		16.3	97890
Rbl1	retinoblastoma-like 1 (p107)		2.7	103300
Riok3	RIO kinase 3	1.9		1914128
Sass6	spindle assembly 6 homolog (C. elegans)	-2.4	-4.6	1920026
Suv39h1	suppressor of variegation 3-9 homolog 1 (Drosophila)		2.4	1099440
Tgfb	transforming growth factor, beta 1		2.0	98725
Xaf1	XIAP associated factor 1	-2.1	-87.4	3772572
Zwilch	Zwilch, kinetochore associated, homolog (Drosophila)	-2.3		1915264
Cell Signaling				
Fcgr1a	Fc fragment of IgG, high affinity Ia, receptor (CD64)	-4.4	-13.6	95498
Fcgr2b	Fc fragment of IgG, low affinity IIb, receptor (CD32)	-7.7	-2.9	95499
Cellular Development				
Cd83	CD83 molecule	-2.4	-2.4	1328316
Ifi16	interferon, gamma-inducible protein 16	-4.1	-11.6	96429
Irf7	interferon regulatory factor 7	-3.4	-51.3	1859212
Mafb	v-maf musculoaponeurotic fibrosarcoma oncogene homolog B (avian)	-4.4	-2.2	104555
Dyserythropoiesis				
Ccl5	chemokine (C-C motif) ligand 5		-22.5	98262
Traf3	Tnf receptor-associated factor 3		-2.3	108041
Tsc22d3	TSC22 domain family, member 3		-3.6	1196284
ECM degradation				
Mmp9	Matrix metalloproteinase 9	-4.0	5.3	97011
Timp1	Tissue inhibitor of metalloproteinase 1	-8.5	-1748.4	98752

Table 2, continued.

Gene Expression				
Axud1	AXIN1 up-regulated 1	-3.0	-1.8	2387989
Batf2	basic leucine zipper transcription factor, ATF-like 2	-1.8	-3.1	1921731
Ddx58	DEAD (Asp-Glu-Ala-Asp) box polypeptide 58	-2.4	-14.2	2442858
Mx1	myxovirus (influenza virus) resistance 1, interferon-inducible protein p78 (mouse)	-7.9	-43.4	97243
Pcgf5	polycomb group ring finger 5	-1.8	-2.1	1923505
Phf11	PHD finger protein 11	-2.9	-13.7	1918441
Sp100	SP100 nuclear antigen	-2.8	-4.4	109561
Glutathione Metabolism				
G6pd2	glucose-6-phosphate dehydrogenase 2	1.8	2.0	105977
G6pdx	glucose-6-phosphate dehydrogenase X-linked	2.1		105979
Gclc	glutamate-cysteine ligase, catalytic subunit	8.6		104990
Gclm	glutamate-cysteine ligase , modifier subunit	7.6		104995
Gss	glutathione synthetase	2.4		95852
Gsta1	glutathione S-transferase, alpha 1 (Ya)	7.2	30.7	1095417
Gstp1	glutathione S-transferase, pi 1	1.8		95865
Idh1	isocitrate dehydrogenase 1 (NADP+), soluble	3.3		96413
Pgd	phosphogluconate dehydrogenase	2.4		97553
Immune Response				
Adrb2	adrenergic, beta-2-, receptor, surface	4.1	2.2	87938
C5r1	complement component 5, receptor 1		3.5	88232
Casp4	caspase 4, apoptosis-related cysteine peptidase	-2.2	-2.4	107700
Ccl17	chemokine (C-C motif) ligand 17		3.1	1329039
Ccl2	chemokine (C-C motif) ligand 2	-44.8		98259
Ccl22	chemokine (C-C motif) ligand 22	-12.3		1306779
Ccl4	chemokine (C-C motif) ligand 4	-2.1		98261
Ccl6	chemokine (C-C motif) ligand 6	-3.1		98263
Ccl7	chemokine (C-C motif) ligand 7	-22.6	-2.3	99512
Ccr1	chemokine (C-C motif) receptor 1	-3.1		104618
Cd14	CD14 antigen		2.2	88318
Cd300lf	CD300 antigen like family member F	-3.9		2442359
Cd40	CD40 antigen	-4.3		88336
Cd44	CD44 antigen	-2.6		88338

Table 2, continued.

Cd86	CD86 antigen	-1.8		101773
Cenpa	centromere protein A	-2.3		88375
Cfb	complement factor B	-7.4		105975
Clec12a	C-type lectin domain family 12, member a	-1.9		3040968
Clec2d	C-type lectin domain family 2, member d	-4.1		2135589
Clec4n	C-type lectin domain family 4, member n	-2.4		1861231
Clec5a	C-type lectin domain family 5, member a	-1.8		1345151
Csf2	colony stimulating factor 2 (granulocyte-macrophage)	-12.1		1339752
Csf3	colony stimulating factor 3 (granulocyte)	-18.2	18.0	1339751
Cxcl1	chemokine (C-X-C motif) ligand 1		2.7	108068
Cxcl14	chemokine (C-X-C motif) ligand 14	-2.7		1888514
Cxcr4	chemokine (C-X-C motif) receptor 4	2.5		109563
Dcn	Decorin		-4.0	94872
Ercc1	excision repair cross-complementing rodent repair deficient	-1.8		95412
F10	coagulation factor X		4.1	103107
Fbxo5	F-box protein 5	-4.0		1914391
Gbp1	Guanylate binding protein 1	-3.1	-16.8	95666
Gbp3	guanylate nucleotide binding protein 3	-3.7		1926263
Gbp5	guanylate nucleotide binding protein 5	-5.9		2429943
H28	histocompatibility 28	-6.3		95975
Hdc	histidine decarboxylase	-8.8	-3.1	96062
Icam1	intercellular adhesion molecule 1	1.8	7.5	96392
Igf1	insulin-like growth factor 1		2.1	96432
Il10	Interleukin 10	-4.7		96537
Il10ra	Interleukin 10 receptor, alpha		3.7	96538
Il13ra1	Interleukin 13 receptor, alpha 1	-3.4		105052
Il18	Interleukin 18	-2.0		107936
Il18rap	interleukin 18 receptor accessory protein	-2.8		1338888
Il1a	Interleukin 1 alpha	-66.6		96542
Il1b	Interleukin 1 beta	-32.7		96543
Il1f6	Interleukin 1 family, member 6	-12.6		1859324
Il1rl1	Interleukin 1 receptor-like 1	-3.6		98427
Il1rn	Interleukin 1 receptor antagonist	-6.8		96547
Il27	Interleukin 27	-6.4		2384409
Il4ra	Interleukin 4 receptor, alpha	-2.9		105367
Il6	Interleukin 6	-43.3	-11.2	96559
Isg20	interferon stimulated exonuclease gene 20kDa	-3.1	-7.6	1928895
Ltb	lymphotoxin B	-1.9		104796
Nlrc4	NLR family, CARD domain containing 4	2.3	2.7	3036243
Oasl2	2'-5' oligoadenylate synthetase-like 2	-5.1		1344390

Table 2, continued.

Pgdfb	platelet derived growth factor, B polypeptide		3.2	97528
Pla2g7	phospholipase A2, group VII (platelet-activating factor acetylhydrolase, plasma)	3.1	10.7	1351327
Pou2f2	POU domain, class 2, transcription factor 2	-1.9		101897
Rsad2	radical S-adenosyl methionine domain containing 2	-4.4		1929628
Tnf	tumor necrosis factor		8.7	104798
Traf3ip2	Traf3 interacting protein 2	-1.8		2143599
Ube2L6	ubiquitin-conjugating enzyme E2L 6	-1.8	-2.3	1914500
Vegfa	vascular endothelial growth factor A		-2.4	103178
Interferon-associated Signaling or Regulation				
H2-Bf	histocompatibility 2, complement component factor B		-51.0	105975
H2-DMb2	histocompatibility 2, class II, locus Mb2		-5.1	95923
H2-Q1	histocompatibility 2, Q region locus 1		-3.2	95928
H2-Q5	histocompatibility 2, Q region locus 5		-2.1	95934
H2-T23	histocompatibility 2, T region locus 23		-9.4	95957
H2-T9/H2-T22	histocompatibility 2, T region locus 9;histocompatibility 2, T region locus 22		-5.2	95965
Ifi202b	interferon activated gene 202B	-3.8		1347083
Ifi203	interferon activated gene 203	-3.7		96428
Ifi204	interferon activated gene 204	-3.7		96429
Ifi205	interferon activated gene 205	-4.3		101847
Ifi47	interferon gamma inducible protein 47	-3.0		99448
Ifih1	interferon induced with helicase C domain 1	-2.0		1918836
Ifit1	interferon-induced protein with tetratricopeptide repeats 1	-3.6		99450
Ifit2	interferon-induced protein with tetratricopeptide repeats 2	-6.3		99449
Ifit3	interferon-induced protein with tetratricopeptide repeats 3	-3.3		1101055
Irf8	interferon regulatory factor 8	-2.6		96395
Jak2	Janus kinase 2	-1.7		96629
Mx2	myxovirus (influenza virus) resistance 2	-7.3		97244
Oas1a	2'-5' oligoadenylate synthetase 1A	-2.0		2180860
Ptges	prostaglandin E synthase		4.7	1927593
Stat1	signal transducer and activator of transcription 1	-2.2	-10.8	103063
Stat3	signal transducer and activator of transcription 3	-2.1		103038
Stat5a	signal transducer and activator of transcription 5A	-2.1		103036

Table 2, continued.

Metabolic Process				
Adh7	alcohol dehydrogenase 7 (class IV), mu or sigma polypeptide	8.0	2.3	87926
Hbp1	high mobility group box transcription factor 1	2.9		894659
Mov10	Mov10, Moloney leukemia virus 10, homolog (mouse)	-2.2	-2.5	97054
Oas3	2'-5'-oligoadenylate synthetase 3, 100kDa	-2.4	-8.3	2180850
Parp12	poly (ADP-ribose) polymerase family, member 12	-2.1	-4.9	2143990
Serpinb1b	serine (or cysteine) peptidase inhibitor, clade B, member 1b	2.8	4.3	2445361
Tiparp	TCDD-inducible poly(ADP-ribose) polymerase	-1.8	-2.9	2159210
NF-kB signaling				
Ikbke	inhibitor of kappaB kinase epsilon		3.2	1929612
Nfkbia	nuclear factor of kappa light chain gene enhancer in B-cells inhibitor, alpha		1.8	104741
Nfkbie	nuclear factor of kappa light polypeptide gene enhancer in B-cells inhibitor, epsilon		3.6	1194908
Oxidative Stress Response				
Abcc1	ATP-binding cassette, sub-family C (CFTR/MRP), member 1	2.1		102676
Akr1a4	aldo-keto reductase family 1, member A4 (aldehyde reductase)	1.8		1929955
Aox1	aldehyde oxidase 1	2.2		88035
Cat	Catalase	3.1		88271
Dnajb4	DnaJ (Hsp40) homolog, subfamily B, member 4	5.3		1914285
Ephx1	epoxide hydrolase 1, microsomal	2.0	3.2	95405
Hmox1	heme oxygenase (decycling) 1	6.0		96163
Mapk14	mitogen-activated protein kinase 14	2.0		1346865
Pik3cb	phosphatidylinositol 3-kinase, catalytic, beta polypeptide	2.3		1922019
Prdx1	peroxiredoxin 1	2.9	3.1	99523
Raf1	v-raf-leukemia viral oncogene 1	2.2		97847
Sod2	superoxide dismutase 2, mitochondrial		1.7	98352
Sqstm1	sequestosome 1	3.1		107931
Txnrd1	thioredoxin reductase 1	2.1		1354175
Xdh	xanthine dehydrogenase	2.0		98973

Table 2, continued.

Signal Transduction				
Fcrl1	Fc receptor-like 1	3.5	3.9	2442862
Lyn	Yamaguchi sarcoma viral (v-yes-1) oncogene homolog	-1.9		96892
Rasgrp3	RAS guanyl releasing protein 3 (calcium and DAG-regulated)	3.9	4.4	3028579
Rit1	Ras-like without CAAX 1	2.1		108053
Small Molecule Biochemistry				
Cp	ceruloplasmin (ferroxidase)	-7.7	-6.0	88476
Slc7A2	solute carrier family 7 (cationic amino acid transporter, y+ system), member 2	-5.2	-5.2	99828
Cell Structure				
Gsn	Gelsolin		2.5	95851
Stmn1	stathmin 1		10.8	96739
Tuba4	tubulin, alpha 4		2.5	1095410
Ubiquitin-Proteasome Pathway				
Fbxl17	F-box and leucine-rich repeat protein 17	1.8		1354704
Fbxl20	F-box and leucine-rich repeat protein 20	2.1		1919444
Fbxo22	F-box only protein 22		3.0	1926014
Fbxo30	F-box protein 30	2.0		1919115
Fbxo31	F-box protein 31	1.8		1354708
Herc3	hect domain and RLD 3	2.3		1921248
Map1lc3b	microtubule-associated protein 1 light chain 3 beta	2.0		1914693
Psmc3ip	proteasome (prosome, macropain) 26S subunit, ATPase 3, interacting protein		6.4	1098610
Psmd12	proteasome (prosome, macropain) 26S subunit, non-ATPase, 12		2.0	1914247
Rnf128	ring finger protein 128	4.2		1914139
Rnf167	ring finger protein 167	1.9		1917760
Ube2d3	ubiquitin-conjugating enzyme E2D 3 (UBC4/5 homolog, yeast)		2.4	1913355
Ube2i	ubiquitin-conjugating enzyme E2I		3.0	107365
Ube2t	ubiquitin-conjugating		7.1	1914446
Ube4b	ubiquitination factor E4B, UFD2 homolog (S. cerevisiae)	1.8		1927086
Uchl1	ubiquitin carboxy-terminal hydrolase L1		4.4	103149
Usp18	ubiquitin specific protease 18		-224.6	1344364
Other				
Arrdc3	arrestin domain containing 3	7.0		2145242

Table 2, continued.

Bcl2l11	BCL2-like 11 (apoptosis facilitator)	2.0		1197519
Epsti1	epithelial stromal interaction 1 (breast)	-2.1	-10.6	1915168
Gabarapl1	gamma-aminobutyric acid (GABA(A)) receptor-associated protein-like 1	2.8		1914980
Id1	inhibitor of DNA binding 1	-2.0		96396
Ier3	immediate early response 3	-2.0		104814
Ifi203	interferon activated gene 203	-3.7	-5.2	96428
Klhl6	Kelch-like 6 (Drosophila)	-1.9	-3.8	2686922
Map1d	methionine aminopeptidase 1D	1.8	1.9	1913809
Ms4A6D	membrane-spanning 4-domains, subfamily A, member 6D	-2.3	-3.9	1916024
Top2a	topoisomerase (DNA) II alpha	13.2		98790
Trim30	tripartite motif-containing 30	-7.2	-31.8	98178
Uvrag	UV radiation resistance associated gene	-1.9	-1.8	1925860
Zak	sterile alpha motif and leucine zipper containing kinase AZK	-1.9	-4.0	2443258
Zbp1	Z-DNA binding protein 1	-5.7	-69.4	1927449
Zbtb20	zinc finger and BTB domain containing 20	3.6		1929213
Zfp36	zinc finger protein 36	-1.9		99180

[a] Genes altered ≥1.8-fold ($p \leq 0.01$) up or down in LPS stimulated HNE-treated cells relative to LPS stimulated cells. Fold changes (FC) represent the average of three independent biological experiments.

Table 3. Taqman Gene Expression Assays Used for Quantitative Real-Time RT-PCR

Treatment	Gene	Assay ID	Amplicon length
6 h BH, 6 h HNE	Csf2	Mm00438328_m1	71
6 h HNE	Ccl2	Mm00441242_m1	74
6 h HNE	Il1b	Mm00434228_m1	90
6 h HNE, 24 h BH	Il1a	Mm00439620_m1	68
6 h, 24 h HNE	Mmp9	Mm00442991_m1	76
6 h, 24 h HNE	Timp1	Mm00441818_m1	90
6 h, 24 h HNE	Csf3	Mm00438334_m1	106
24 h HNE	Ccl5	Mm01302428_m1	71
24 h HNE	Tnf	Mm00443258_m1	81
24 h HNE	Nfkbie	Mm00500796_m1	78
24 h HNE	Ikbke	Mm00444862_m1	66
24 h BH	Fos	Mm00487425_m1	59

[a] Each assay consists of two unlabeled PCR primers and a FAM dye-labeled TaqMan MGB (minor groove binder) probe.

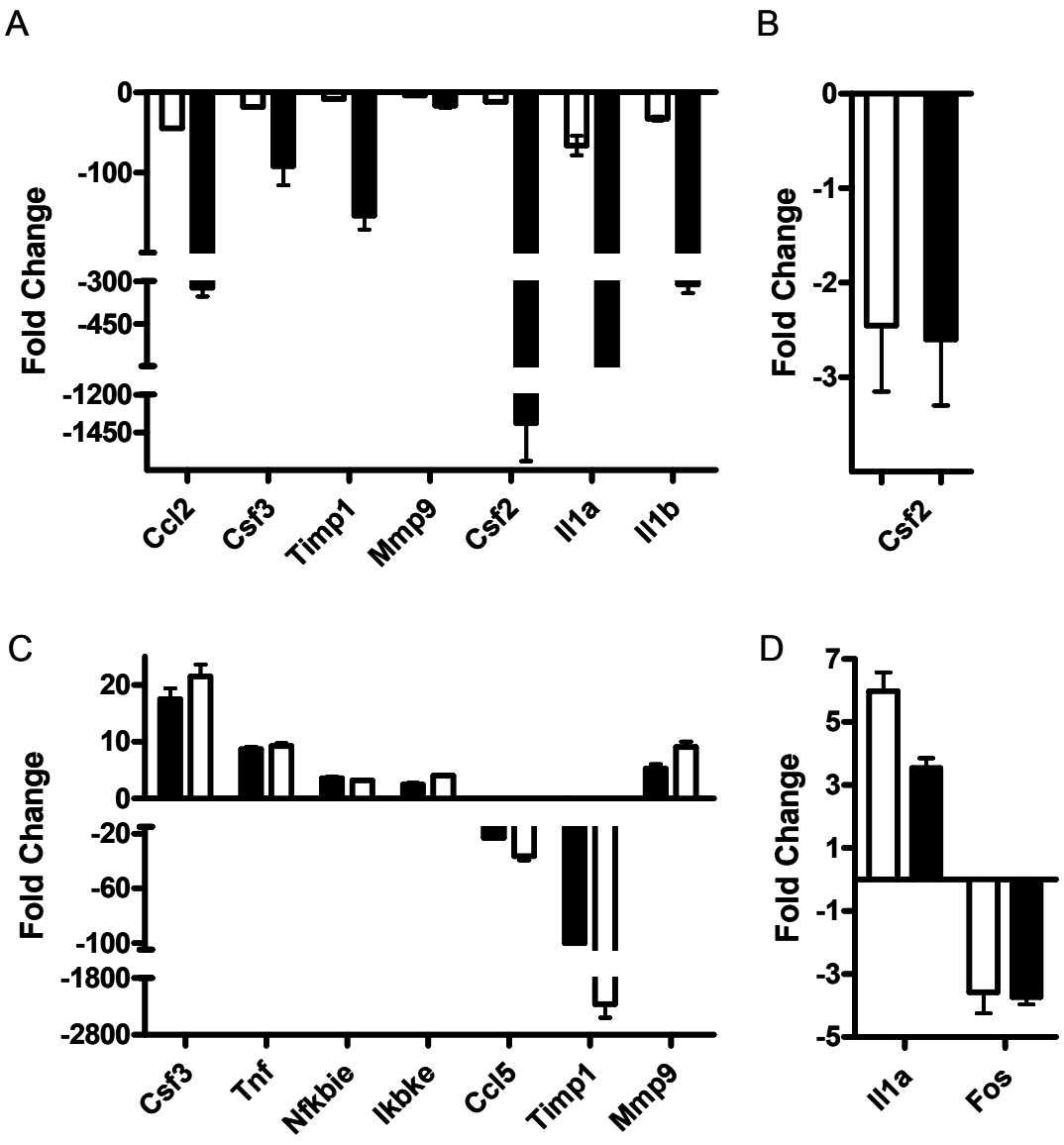

Figure 42. Quantitative real-time RT-PCR validation of microarray results. RAW 264.7 cells were stimulated with 0.1 μg/mL LPS and untreated or treated with (A) 35 μM HNE for 6 h, (B) 0.1 mg/mL BH for 6 h, (C) 35 μM HNE for 24 h, or (D) 0.1 mg/mL BH for 24 h. White bars represent vsalues determined by microarray experiments for comparison. Black bars represent fold-changes assessed by qRT-PCR (treated, stimulated cells relative to stimulated controls) ($\bar{X}$ ± 99% confidence interval for quadruplicate measurements of n = 3 biological replicates). Abbreviations: chemokine (C-C motif) ligand (*Ccl*); colony stimulating factor (*Csf*); tissue inhibitor of metalloproteinase 1 (*Timp1*); matrix metalloproteinase 9 (*Mmp9*); interleukin 1 (*Il1*); tumor necrosis factor (*Tnf*); nuclear factor of kappa light polypeptide gene enhancer in B-cells inhibitor, epsilon (*Nfkbie*); inhibitor of kappaB kinase, epsilon (*Ikbke*); and FBJ osteosarcoma oncogene (*Fos*).[44]

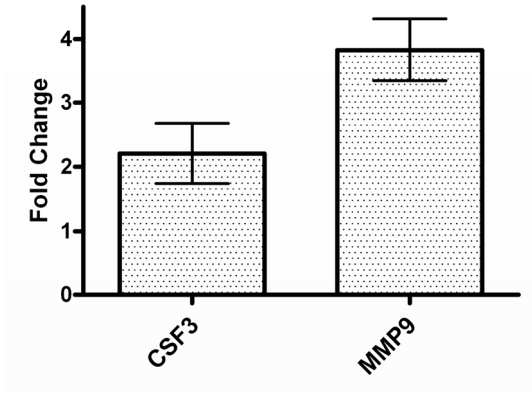

Figure 43. ELISA validation of microarray results. Equivalent numbers of cells (4×10^6/well) were stimulated with LPS (1 μg/mL) in the absence or presence of 35 μM HNE for 24 h. CSF3 (colony stimulating factor 3 [granulocyte]) and MMP-9 (matrix metalloproteinase 9) released into the culture medium were analyzed by ELISA. Fold changes (HNE-treated stimulated cells relative to stimulated controls) are shown ($\overline{X} \pm$ SD for triplicate measurements, representative of three independent experiments).[44]

Differential gene expression in the context of malaria pathogenesis

Microarray data from this study were compared to two groups of genes. The first group consists of specific genes or gene products that are associated with human[120, 121] or murine[122, 124] models of malarial infection, and/or BH or Hz[85, 129] exposure. The second group includes genes that are classified with specific biological processes that are over-expressed in a murine *P. yoelii* model [124] and/or naturally-acquired *P. falciparum* infections[119] (e.g., cell-cell signaling, defense response, immune response, inflammatory response, and signal transduction, among others). Complete lists of differentially expressed genes altered by either HNE or BH treatment that fall within these categories are listed in **Appendix A**.

Stress response

Regulation of antioxidant response element (ARE) gene expression is controlled by the transcription factor NRF2, whose activity is suppressed through the formation of a complex with its inhibitor Keap1. Disruption of NRF2/Keap1 complex liberates NRF2, allowing its nuclear translocation and subsequent transactivation of ARE-dependent gene expression. Consistent with previous findings in a variety of cell types,[71, 77] a potent "oxidative stress response mediated by Nrf2" was observed at both 6 h and 24 h following HNE treatment, suggesting an effort to reduce cellular damage (Table 2). Expression of genes encoding phase I and II metabolizing enzymes and antioxidant response proteins was significantly enhanced by HNE. Activation of a stress response is consistent with an increase of *Prdx1* in the spleens of *P. berghei* infected mice[122] and *Sod2* and *Hmox1* in both the blood of acute pediatric malaria victims[120] and Hz-loaded placental tissue.[121] A common stress response is heme oxygenase (decycling) 1 (*Hmox1*) induction. In the current study *Hmox1* expression is induced by both HNE and BH at 6 h. This observation is in agreement with up-regulated *Hmox1* expression in mouse peritoneal macrophages (PM) treated with BH.[105]

Cell cycle checkpoint signaling

The present data indicate a broad 'DNA replication, Recombination, and Repair' response to HNE at 6 and 24 h. Early expression of several genes associated with checkpoint control is repressed. By 24 h, however, a dramatic DNA damage response including the induction of a number of genes associated with G1/S cell cycle checkpoint regulation was observed (Figure 44 and Table 2). Since HNE can form adducts with

deoxyguanosine residues,[130] activation of cell cycle checkpoint signaling genes suggests an effort to ameliorate DNA injury. The presence of damaged DNA is consistent with enhanced expression of excision repair (*Fen1, Rad23a, Rad51*, and *Gadd45a*), and mismatch repair (*Msh5, Pcna*, and *Mutyh*) genes at 24 h. Notably, increased *ATM* and *RAD23A* expression has also been identified in whole blood of *P. falciparum* infected children.[120]

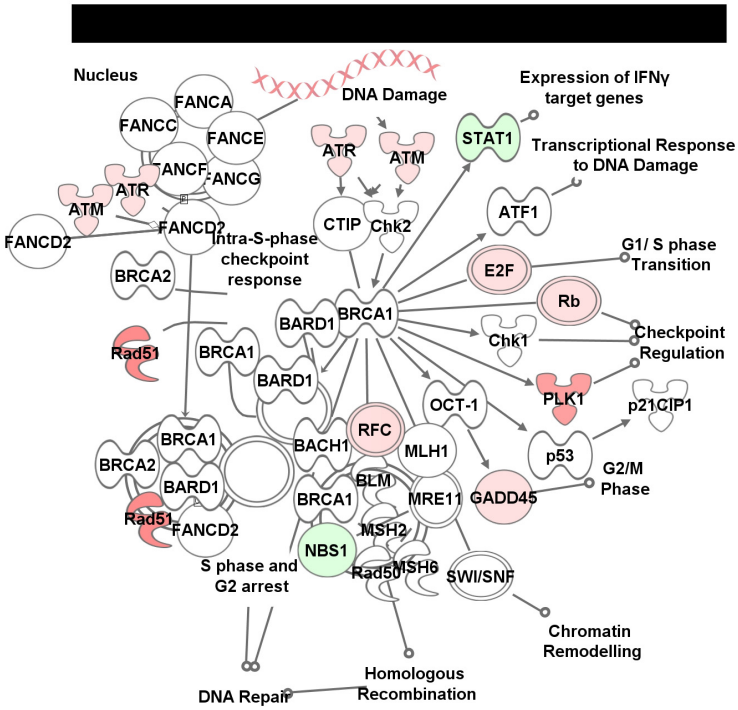

Figure 44. Ingenuity canonical pathway analysis. Differentially expressed genes were mapped to the Ingenuity Canonical Pathway library to identify significantly altered canonical signaling pathways. 'IL-10 Signaling' was influenced by 35 µM HNE at 6 h. Genes or gene products are represented as nodes and the intensity of the node color indicates the degree of up- (red) or down- (green) regulation.[44]

Ubiquitin-proteasome pathway

In addition to its reactivity with DNA, HNE readily modifies proteins through adduction to cysteine, histidine, and lysine residues.[72] In some cases, these covalent

modifications have been shown to impair enzymatic activity.[8, 73-75] One route for clearance of damaged or misfolded proteins is through the ubiquitin proteasome pathway, and proteosomal degradation of HNE-modified ubiquitinated alcohol dehydrogenase has been demonstrated.[131] In the present study, HNE mediated the induction of several ubiquitin- and 26S proteasome-associated genes at 6 h and 24 h (Table 2). Furthermore, HNE mediated the repression of a deubiquitinating enzyme, *Usp18*, which is purported to remove ubiquitin adducts from a wide range of substrates. Taken together, these alterations indicate activation of the ubiquitin-proteasome pathway, which may represent an effort to degrade HNE-modified protein.

Structural genes

Several cytoskeleton organization and biogenesis genes were susceptible to induction by BH and HNE. Analysis of the steady-state expression changes showed that BH treatment led to the induction of *Tuba4* and *Pstpip2* (Table 4), and HNE up-regulated *Gsn, Tuba4*, and *Stmn1* expression (Table 2). Although tubulin is up-regulated, stathmin has been shown to sequester tubulin and disrupt polymerization.[83] Studies have shown tubulin-HNE adducts and disrupted microtubule organization in Neuro 2A cells,[132] and HNE-mediated cytoskeletal alterations in both bovine lung microvascular endothelial[133] and P19 neuroglial cultures.[134] In the context of malaria infection, *GSN* and *PSTPIP2* are induced in the blood of pediatric malaria victims[120] suggesting cellular cytoskeletal alterations.

Table 4. Select Gene Expression Changes Mediated by BH[a]

Gene Symbol	Description	Fold Change		MGI Gene ID
		6 h	24 h	
Interferon-associated Signaling or Regulation				
H2-Ab1	histocompatibility 2, class II antigen A, beta 1		-1.8	103070
H2-Q1	histocompatibility 2, Q region locus 1		-4.8	95928
Immune Response				
Ccl2	chemokine (C-C motif) ligand 2		2.2	98259
Ccl6	chemokine (C-C motif) ligand 6		5.4	98263
Cd2	CD2 antigen		102.4	88320
Csf2	colony stimulating factor 2 (granulocyte-macrophage)	-12.1		1339752
Cxcl2	chemokine (C-X-C motif) ligand 2		1.9	1340094
Ereg	Epiregulin		13.2	107508
Fos	FBJ osteosarcoma oncogene		-3.6	95574
Il1a	interleukin 1 alpha		6.0	96542
Il20	interleukin 20		2.4	1890473
Oxidative Stress Response				
Hmox1	heme oxygenase (decycling) 1	6.0		96163
Cell Structure				
Pstpip2	proline-serine-threonine phosphatase interacting protein 2		6.1	1335088
Tuba4	tubulin, alpha 4		1.9	1095410

[a] Genes altered ≥1.8-fold ($p \leq 0.01$) up or down in LPS stimulated BH-treated cells relative to LPS stimulated cells. Fold changes (FC) represent the average of three independent biological experiments.

Macrophage activation

An exacerbated inflammatory response is assumed to play a significant role in malaria pathogenesis. In an effort to uncover the basis of the inflammatory activity, Hz has been examined as a contributing agent. Previously, in vitro studies have shown that Hz phagocytosis reduces IL6 and stimulates TNFα,[85] in concord with HNE treatment in

the current study. Both purified Hz and synthetic Hz (i.e., BH) led to the induction of *Ccl3* (*Mip1a), Ccl4 (Mip1b)*, and *Tnf* in murine macrophages and human peripheral mononuclear cells.[129] Later work demonstrated that BH induced the expression and secretion of chemokines (MIP-1α, MIP-1β, MIP-2 (CXCL2), MCP-1 (CCL2), RANTES), chemokine receptors (CCR1, CCR2, CCR5, CXCR2, and CXCR4), cytokines (IL-1β and IL-6), and myeloid related proteins (S100A8, S100A9,and S100A8/A9) in vivo.[40] This microarray analysis demonstrates that BH had a modest effect on the induction of immune response genes at 6 h and 24 (Table 4). HNE treatment, however, drastically repressed expression of immune/inflammatory response genes (Figure 45) and

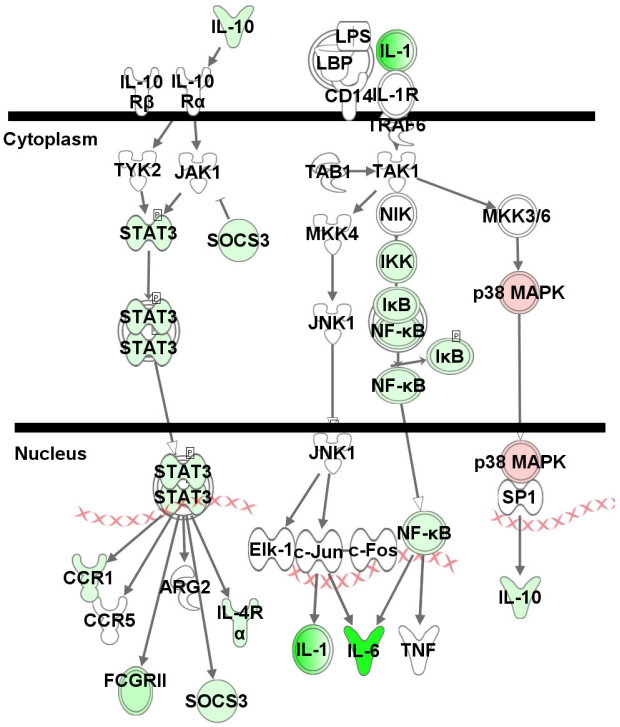

Figure 45. Ingenuity canonical pathway analysis. Differentially expressed genes were mapped to the Ingenuity Canonical Pathway library to identify significantly altered canonical signaling pathways. 'Role of BRCA1 in DNA Damage Response' was influenced by 35 μM HNE at 24 h. Genes or gene products are represented as nodes and the intensity of the node color indicates the degree of up- (red) or down- (green) regulation.[44]

interferon-signaling and -regulated genes at 6h. By 24 h, the response was reversed and the induction of a large group of immune/inflammatory response genes was identified (Table 2). Notably, this change in response over time may explain the often contradictory interpretation of Hz and immune cell interactions reported in the literature.[33, 36, 40, 49, 85, 135, 136]

A number of specific studies probing the inflammatory response to malaria are consistent with the observed HNE-mediated gene expression changes: murine kidneys infected with *P. berghei* parasites display increased expression of TNFα,[137] and *P. falciparum* exposed CHO cells exhibit increased levels of TNFα, GCSF (CSF3), and TGFβ.[138] Several individual expression changes also correspond with responses observed in microarray analyses of genuine or experimental malaria. For example, messages for *LY96*, *CD14* and *C5R1* in whole blood of pediatric victims [120] *CD2*, *C5R1* and *IL10RA* in placental malaria,[121] and *Cd2* in a *P. yoelii* infected mice[124] are consistent with enhanced expression by HNE in the current microarray analysis.

Although HNE and BH augment the expression of genes involved in mounting an immune response, they repress the expression of a number of genes central to a cell's antigen presenting ability (Tables 2 and 4). The present study identified significant ($p < 0.05$) steady-state repression of antigen major histocompatibility complex (MHC) class II-associated genes in both HNE- and BH-treated cells (*H2-Q1/H2-Q2*). Likewise, HNE decreased expression of *H2-T23*, *Cfb* (*H2-Bf*), *H2-DMb2*, *H2-Q5*, and *H2-T22/H2-T9*, while BH down-regulated *H2-Ab1* expression. Notably, Hz loading has been implicated as a factor contributing to both impaired monocyte MHC class II antigen presentation[84] and defective dendritic cell function.[101, 139] The ability of HNE, and to a lesser extent BH,

to suppress MHC II expression implies two Hz components involved in the defective responses. Furthermore, elevated levels of TGF-β and PGE_2 are associated with T-cell inhibition.[140] HNE enhanced the expression of genes encoding *Tgfb* and *Ptges* and may contribute to the impaired T-cell activity observed upon Hz phagocytosis.

NF-κB signal transduction

The LPS mediated pathway to produce nitric oxide (NO) is well characterized and entails NF-κB signal transduction. In quiescent cells, NF-κB is sequestered by inhibitory proteins (IκB) in the cytoplasm. Upon activation, IκB kinase (IKK) phosphorylates IκB, triggering its polyubiquitination and subsequent degradation. Once NF-κB is liberated from IκB, NF-κB translocates to the nucleus and regulates gene expression, including iNOS.

It has been shown that serum withdrawal in RAW 264.7 cells results in the activation of NF-κB, expression of iNOS, and synthesis of NO. However, serum withdrawal-mediated IκB phosphorylation and downstream signaling was abolished in HNE treated cells.[110] In accord with this data, HNE prevented NO production in LPS-stimulated RAW 264.7 cells.[68] HNE has been shown to covalently adduct to IKK, inhibiting kinase activity thus preventing the phosphorylation of IκB.[74] As a result, IκB degradation and NF-κB translocation are impaired.

Unlike HNE, there are a wide range of observations regarding the effects of Hz and BH on iNOS activity and NO synthesis. For example, both BH and purified Hz do not inhibit IFNγ mediated NO in B10R murine macrophage cells.[35] Similarly, RAW 264.7 cells stimulated by LPS and loaded with BH exhibit normal NO levels.[68] In

contrast, LPS-mediated NO production is reduced in BH treated murine PM.[105] Skorokhod et al. found that levels of NO are not impaired in several murine phagocytic cell lines after crude Hz or BH loading, but determined that human monocytes are unable to produce NO when stimulated with either LPS or IFNγ.[141] Furthermore, native Hz decreases NO in LPS or IFNγ stimulated murine PM suggesting that a non-heme moiety component is responsible for the dysfunction.[67] This varied group of results demonstrates the need for careful extrapolation of NO production data based on cell type, stimulatory molecule, and the state of the Hz preparation.

In the present study, HNE, and not BH, had an impact on NF-κB related gene expression (Table 2). Early changes in expression indicate repression of the NF-κB pathway (down-regulated *Cd40, Nfkb1,* and *Nfkbiz* levels) by HNE. However, at 24 h, IKK (i.e., *Ikbke*) and IκB (*Nfkbia, Nfkbie*) expression is enhanced. Notably, transcript abundance does not necessarily correlate with protein level or kinase activity. In accord with the HNE studies mentioned above, IKK expression may be increased because the available enzyme is inactivated by HNE. Due to the numerous gene expression modulations mediated by HNE, it seems probable that most are a result of downstream effects of HNE interactions. The increase of IKK expression, however, may be a direct response to dysregulated kinase activity.

Extracellular matrix degradation

A current hypothesis is that expression changes of ECM genes may have direct involvement in malaria pathogenesis, particularly in cases of cerebral malaria (CM). CM is a severe complication of *P. falciparum* infection that is characterized by adherence of

parasitized RBC to the cerebral microvasculature. Analysis of the brain vessels from CM mouse models reveals Hz accumulation not only within parasites, but also free and within phagocytic cells.[142] Furthermore, examination of the cortex of post-mortem CM victims shows inflammation, swelling, and a slate-gray discoloration, commonly attributed to Hz deposition.[143] Compelling evidence indicates that both systemic and local cytokine release contribute to the disease pathophysiology, particularly in the brain of CM victims. Blood brain barrier (BBB) destruction is a major factor associated with CM.[144] Matrix metalloproteinases (MMPs), secreted enzymes involved in ECM remodeling, are able to degrade basal lamina leading to BBB damage.[145] Interestingly, Hz increases the transcription, translation, and activity of MMP9 in monocytes.[146] Activation of MMP9 is also observed during *P. falciparum* infection[120] and may contribute to the disruption of endothelial basement membranes and extravasation of blood cells.[146]

The activity of MMP9 is controlled by its cognate inhibitor, TIMP1. HNE exposure initially repressed *Mmp9* expression; however, by 24 h the level of mRNA was significantly increased. Notably, both 6 h and steady-state mRNA levels of HNE treated samples indicate severely impaired *Timp1* expression (–2000-fold at 24 h by qRT-PCR). Taken together, *Mmp9* induction coupled with *Timp1* repression indicates a steady state MMP9/TIMP1 imbalance that may lead to increased proteolysis of the ECM (Table 3).[146] *Mmp9* expression can be regulated through a variety of signaling cascades including NF-κB, p38 MAPK, and ERK1/2 pathways.[147-149] Given that HNE abrogates NF-κB mediated iNOS expression in both LPS stimulated- and serum deprived-RAW 264.7 cells,[68, 110] *Mmp9* up-regulation in the present study is not a result of NF-κB activation.

Active MMP9 is capable of pro-TNF-α cleavage which releases the active cytokine and promotes *Mmp9* expression.[150] Thus, the increased expression of *Tnf* discussed previously may enhance a positive feedback cycle in this study. Importantly, analyses of postmortem brain tissue of CM patients identified elevated TNF mRNA and protein,[151] and immunostaining studies identified significant cerebrum, brainstem, and cerebellar localization.[152] These observations, along with the up-regulation of several collagen genes involved in ECM repair during malaria infection,[122] are consistent with the occurrence of ECM damage.

CM patients possess several traits including obstructed microvascular flow, attributable to the sequestration of blood cells including parasitized RBC and leukocytes.[153] Intercellular adhesion molecule 1 (ICAM1), one of the most important receptors involved in cytoadherence,[154] is upregulated in naturally-acquired malaria and may contribute to ECM degradation.[154, 155] In the current study, HNE up-regulated *Icam1* expression at 6 and 24 h (Table 2). Through cell adhesion, ICAM1 aids ECM binding and may trigger macrophage accumulation and localized MMP9 activity. This hypothesis is supported by evidence that during septic shock, ICAM1 is involved in leukocyte influx and subsequent tissue damage.[156]

Dyserythropoiesis

The specific mechanism(s) leading to malarial anemia have not been clearly defined, but several factors including dyserythropoiesis are thought to play a role.[157] Casals-Pascual *et al*. provide evidence correlating dyserythropoiesis with Hz.[158] Further, HNE and the supernatant of native Hz-fed monocytes have both been shown to dose-

dependently inhibit erythroid-progenitor growth in culture.[159] Repressed CCL5 has been correlated with dyserythropoiesis and may be a contributing factor.[160] Interestingly, CM victims, which have been found with significant Hz accumulation in their brains,[143] exhibit decreased levels of CCL5.[161] The significant repression of *Ccl5* expression by HNE at 24 h supports a potential role for HNE in dyserythropoiesis. Moreover, impaired expression of two upstream regulators of *Ccl5*, namely *Traf3* and *Tsc22d3*, may be directly involved in *Ccl5* repression in the current study (Table 2).

Part Two: Gene expression analysis of the response to 15-HETE

Given the myriad of HNE-mediated gene expression changes presented in *Part I* of this chapter, it seems probable that other biologically active lipid oxidation products generated by Hz, including 15-HETE, may be also active in macrophage immunomodulation. Consequently, *Part II* focuses on steady-state gene expression changes induced by 15-HETE in activated RAW 264.7 cells in the context of a nonspecific malaria toxin that may be involved in disease pathophysiology.

Functional analysis of gene expression changes induced by 15-S-HETE

Cytotoxicity profiles of 15-HETE treated RAW 264.7 cells were determined by flow cytometry: LPS-stimulated cells were treated with increasing concentrations of 15-HETE for 24 h, and changes in viable, apoptotic, and dead cell populations were measured. Figure 46 shows that concentrations up to 45 μM have no impact on cell viability. LPS stimulated macrophage-like RAW 264.7 cells were treated for 24 h with 40

μM 15-S-HETE, based on the estimate that trophozoites and Hz contained 33-39 μmol 15-HETE/L RBC.[32] Statistically significant ($p \leq 0.025$) changes in gene expression (fold change ≥1.8 relative to stimulated cells) were identified by microarray analysis. Differentially expressed genes were sorted into lists based on the direction of regulation, and corresponding Gene Ontology (GO) categories were identified. Given that this study aims to explore potential alterations in gene expression that are incurred by 15-HETE during hemozoin phagocytosis, differentially expressed mRNAs were controlled by a particulate latex bead challenge under the same conditions (Figure 47). 15-HETE had a much greater effect on induction of gene expression than repression (293 transcripts versus 100 transcripts, respectively).

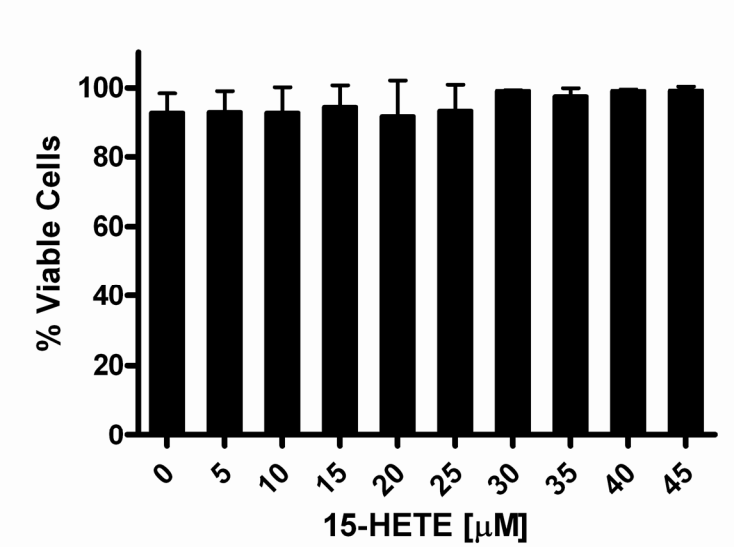

Figure 46. Viability of 15-HETE-treated cells. LPS (0.1 μg/mL) stimulated RAW 264.7 cells were untreated or treated with 15-HETE (0-45 μM) for 24 h and stained with apoptosis and necrosis-specific stains. Three populations were observed by flow cytometric analysis: viable cells, apoptotic cells, and necrotic cells. Viable cells are negative for both Alexa Fluor 488 conjugated annexin V and PI, apoptotic cells are positive for Alexa Fluor 488 conjugated annexin V, and necrotic cells are positive for PI. (C) The plot illustrates the % of viable cells within total cell populations treated with increasing concentrations of15-HETE.

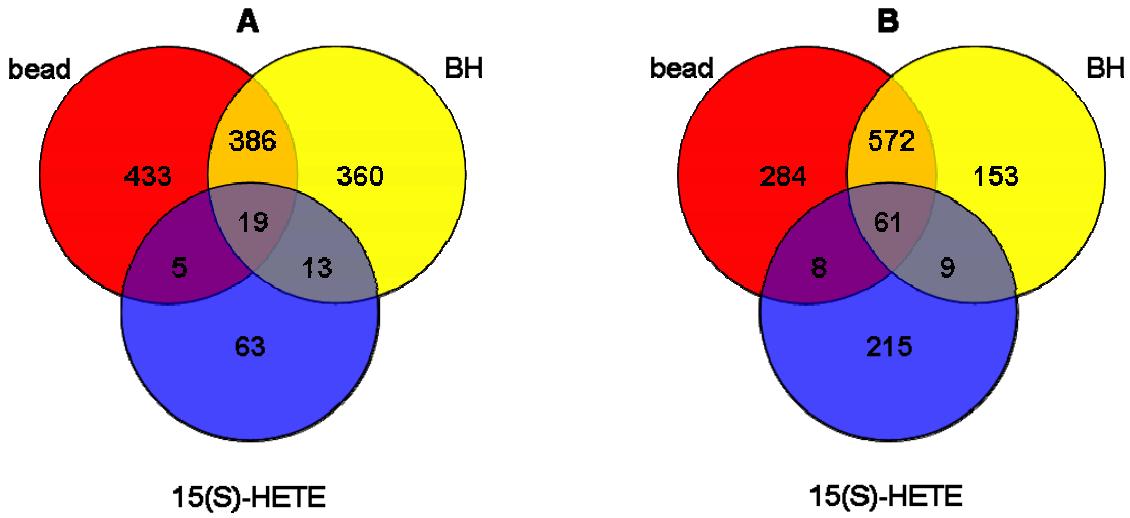

Figure 47. Genes with significant differential expression mediated by 15-S-HETE. Venn diagrams show the intersection of genes that were transcriptionally altered by 40 μM 15-HETE with those altered by latex bead treatment and serum-opsonized BH (0.1 mg/mL). Numbers represent statistically significant ($p \leq 0.025$) transcripts up- or down-regulated ≥1.8-fold in 2 of 3 samples, relative to LPS stimulated, untreated cells at 24 h. (A) Decreased and (B) increased expression are shown separately.[162]

Ingenuity Pathway Analysis (IPA) was used to identify biological interaction networks associated with 15-HETE mediated expression changes. Identifiers and relative levels of altered genes were imported and mapped by IPA for comparison to molecules within the Ingenuity knowledge base (IKB). Focus genes (i.e., imported genes that are eligible for generating interaction networks based on incorporation in IKB) were used to identify relationships based on known interactions in the literature. Each network is associated with a score indicating the likelihood that the focus genes occur in the network by random chance. Networks scoring 10 or higher (score is defined as –log (*p*-value)) are considered significant.

Among the transcripts modulated by 15-HETE exposure, 263 were eligible for analysis based on IPA criteria, mapping to 11 relevant interaction networks. The most significant network (Figure 48 A) has a score of 51 and associates 27 focus genes. Transcriptional regulators are among the products encoded by these genes (*Bclaf1, Med1, Noc2l, Rnf4*, and *Zfp36l1*). This network also contains *Il1b, Cyp3a4, Gnas,* and *Adfp*, all of which are involved in 'lipid metabolism' as well as 'small molecule biochemistry' ($p = 1.27 \times 10^{-4}$).

The second most significant interaction network (Figure 48 B) incorporates 18 focus genes with a score of 29, and is indicative of 'molecular transport' ($p = 9.42 \times 10^{-7}$) and 'cellular movement' ($p = 9.77 \times 10^{-6}$). This network is enriched with focus genes encoding molecules associated with the plasma membrane such as *Pkd2, Cd300a, Cldn11, Gypc,Klra4,* peptidase *Adam9* and transporters *Atp1a2, Slc16a1,*and *Slc16a3*. Consistent with these genes, the network predicted interactions with several other plasma membrane molecules (*Tjp2, Bsg, Cdh1, Tspan3, Tspan4, Cd247, Itgb1,* and *Atp1b2*) that were not present in the data file.

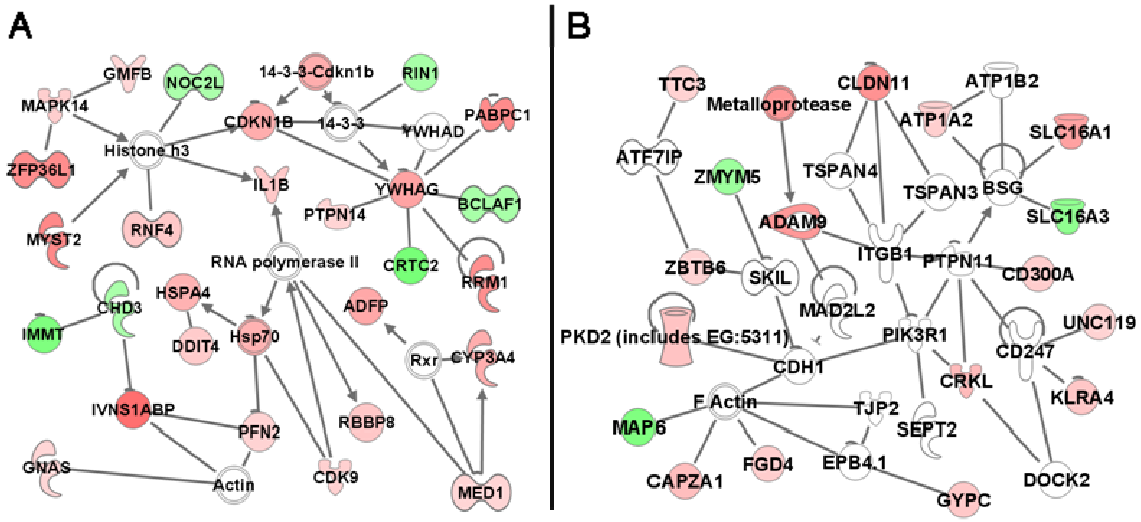

Figure 48. Ingenuity Pathway network analysis. Transcripts altered ≥1.8-fold ($p \leq 0.025$) in 15-HETE treated RAW 264.7 cells (i.e., focus genes) were overlaid onto a global molecular network developed from information contained in the Ingenuity knowledge base (IKB). Networks of these focus genes were then algorithmically generated based on their connectivity. Networks show direct interactions between focus genes altered by 15-HETE treatment and associated molecules within IKB. Genes or gene products are represented as nodes, and the biological relationship between two nodes is represented as an edge (line). White nodes represent IKB molecules that are associated with focus genes. All edges are supported by at least one reference from the literature, from a textbook, or from canonical information stored in the IKB. The intensity of node color indicates the degree of up- (red) or down- (green) regulation. Networks reflect (A) lipid metabolism and small molecule biochemistry and (B) molecular transport and cellular movement.[162]

Molecular and cellular functions controlled by 15-S-HETE

It is thought that Hz impairs cellular function through the generation and introduction of toxic species such as lipid peroxidation products into cells. Previously, the ability of BH and HNE to stimulate a transcriptional response was examined in macrophage-like cells.[44] HNE significantly impacted a wide range of steady-state responses (e.g., macrophage activation, immune and inflammatory responses, NF-κB signal transduction, ECM degradation, and dyserythropoiesis) while BH, induced a modest, primarily phagocytic, response. Comparison of the number of gene expression

changes influenced by 15-HETE with HNE indicates that 15-HETE modulates a number of mRNA targets, but is a much less potent agent than HNE (Figure 49).

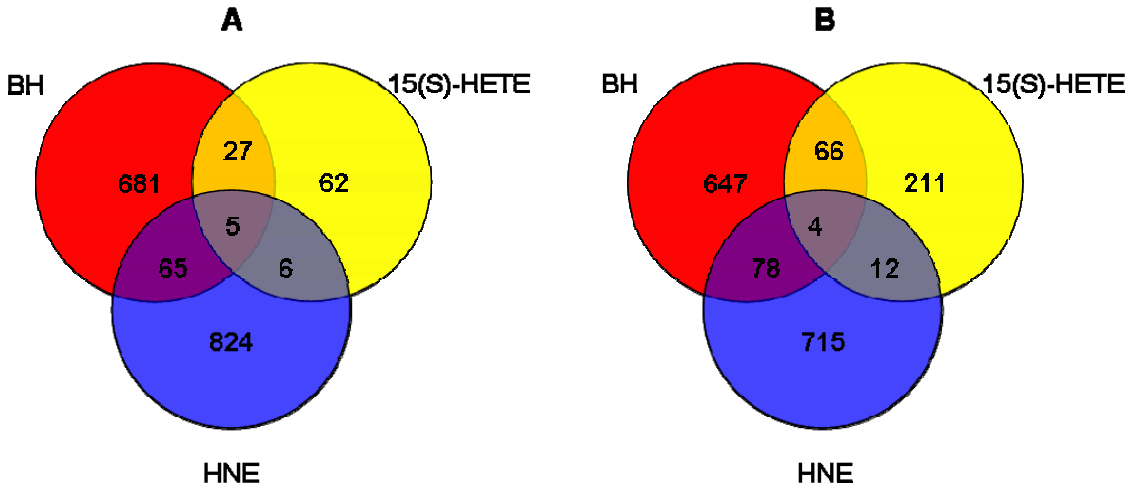

Figure 49. Overlapping genes with significant differential expression. Datasets for each treatment (15-HETE, HNE, BH, and latex bead) group were generated from statistically significant ($p \leq 0.01$) transcripts up- or down-regulated ≥1.8-fold in 2 of 3 samples relative to untreated LPS-stimulated cells. Venn diagrams show intersections of the resulting 15-HETE, HNE, and BH data subsets. (A) Increased and (B) decreased expression are shown separately.[162]

Comparison of the biological functions modulated by 15-HETE (Table 5) with those affected by BH and HNE[44] reveals that all three Hz constituents affected 'Cell Cycle', 'Cell Morphology', and 'Cellular Assembly and Organization' genes at 24 h. Although 15-HETE modulated a considerably smaller group of transcripts than HNE, a comparable response was observed for both the number of molecular and cellular functions and the specific categories affected. Both 15-HETE and HNE altered 'Cell Death', 'Cellular Development', 'Cell Growth and Proliferation', 'Gene Expression', and 'Small Molecule Biochemistry'. Additionally, 15-HETE affected several unique categories including 'Carbohydrate Metabolism', 'Cellular Compromise', 'Drug

Metabolism', 'Lipid Metabolism', 'Molecular Transport', 'RNA Damage and Repair', and 'RNA Post-Translational Modification'.

Table 5. Functional analysis of 15-S-HETE dataset[a]

Biological Function	*p*-value
Carbohydrate Metabolism	6.42×10^{-6}
Cell Cycle	1.28×10^{-4}
Cell Death	1.93×10^{-5}
Cell Morphology	2.53×10^{-4}
Cellular Assembly and Organization	5.30×10^{-4}
Cellular Compromise	4.52×10^{-4}
Cellular Development	3.42×10^{-5}
Cellular Growth and Proliferation	3.81×10^{-4}
Drug Metabolism	3.81×10^{-4}
Gene Expression	2.22×10^{-4}
Lipid Metabolism	1.25×10^{-3}
Molecular Transport	3.81×10^{-4}
RNA Damage and Repair	3.79×10^{-4}
RNA Post-Transcriptional Modification	3.79×10^{-4}
Small Molecule Biochemistry	3.81×10^{-4}

[a] Ingenuity Pathway Analysis uses a right-tailed Fisher Exact Test to calculate *p*-values. Significance values for each dataset indicate the probability that the association between the genes and the given molecular and cellular functions are due to random chance.

It was not surprising that IPA analysis identified a large group of lipid metabolism' and 'carbohydrate metabolism' expression changes. Given that *Il1b* acts upstream of *Cyp3a4*, *Ugdh*, *Gnas*, *Gm2a*, *Psen1*, and *Il15*, stimulated expression of *Il1b* may be indirectly involved in the up-regulation of each of these genes in the current study. Additionally, expression of several 'small molecule biochemistry' transcriptional regulators including *Bclaf1, Med1, Rnf4, Noc2l,* and *Zfp36l1* was identified.

Validation of microarray results

qRT-PCR was used to confirm several genes susceptible to differential regulation by 15-HETE; analysis focused on selected genes implicated in the host response to malaria (Table 6). The results shown in Figure 50 are expressed as fold change relative to LPS-stimulated cells. In agreement with the microarray results in terms of magnitude and direction of change, 15-HETE stimulated the expression of *Arf3* (ADP-ribosylation factor 3), *Cldn11* (claudin 11), *Cxcl11* (chemokine (C-X-C motif) ligand 11), *Mapk14* (mitogen-activated protein kinase 14), *Prdx1* (peroxiredoxin 1), and *Sdc1* (syndecan 1), and repressed the expression of *Egr1* (early growth response 1).

Table 6. Taqman Gene Expression Assays Used for Quantitative Real-Time RT-PCR[a]

Gene	Assay ID	Amplicon length
Arf3	Mm00500194_m1	93
Cldn11	Mm00500915_m1	86
Cxcl11	Mm00444662_m1	82
Mapk14	Mm00442497_m1	56
Prdx1	Mm01621996_s1	70
Sdc1	Mm00448918_m1	131
Egr1	Mm00656724_m1	182

[a] Each assay consists of two unlabeled PCR primers and a FAM dye-labeled TaqMan MGB (minor groove binder) probe.

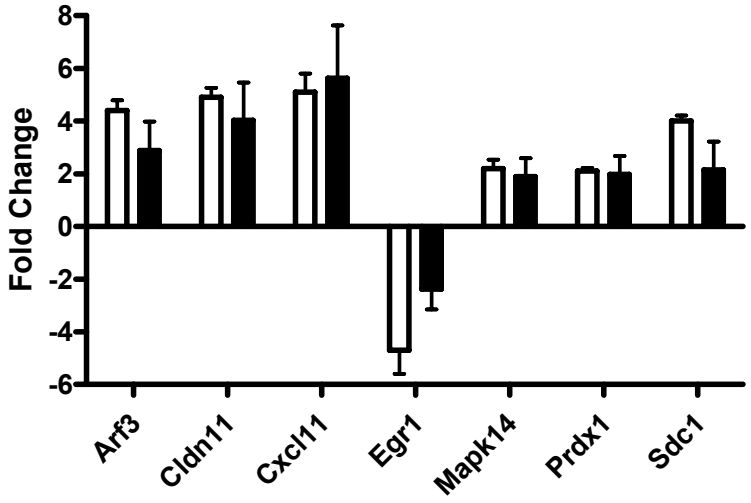

Figure 50. Quantitative real-time RT-PCR validation of microarray results. RAW 264.7 cells were stimulated with 0.1 μg/mL LPS and treated with 40 μM 15-HETE for 24 h prior to RNA extraction. Black bars represent fold-changes (treated, stimulated cells relative to stimulated cells) assessed by qRT-PCR ($\overline{X}$ ± 99% confidence interval for quadruplicate measurements of n = 3 biological replicates). White bars represent values determined by microarray analysis for comparison. Abbreviations: *Arf3* (ADP-ribosylation factor 3), *Cldn11* (claudin 11), *Cxcl11* (chemokine (C-X-C motif) ligand 11), *Egr1* (early growth response 1), *Mapk14* (mitogen-activated protein kinase 14), *Prdx1* (peroxiredoxin 1), and *Sdc1* (syndecan 1).[162]

Differential gene expression in the context of malaria pathogenesis

Gene expression alterations induced by 15-HETE in the current study were compared to two groups of transcripts. The first group consists of specific genes or gene products that are associated with human[120] or murine[122, 123] models of malarial infection, or Hz exposure[136]. The second group includes genes that are classified under specific GO processes that are over-expressed in the *P. yoelii* model[124] and/or naturally-acquired *P. falciparum* infections[119] (e.g., cell-cell signaling, defense response, immune response, inflammatory response, and signal transduction, among others). Differential expression mediated by 15-HETE treatment that correlates with either of the two groups described

above is listed in Table 7. Common transcripts were primarily associated with 'cell-to-cell signaling and interaction' and 'immune response' (e.g., *Fcgrt*, *Cd86*, *C5ar1*, *Ccr4*, *Mapk14*, *Pik3ap1*, *Tapbp*, and *Tnfaip6*).

Table 7. Selected genes affected by 40 μM 15-HETE[a]

Symbol	FC	AB Probe ID	Description	Entrez ID	Ref
Electron transport [119]					
Ugdh	1.9	500013	UDP-glucose dehydrogenase	22235	
Cyp3a11	3.6	516253	cytochrome P450, family 3, subfamily a, polypeptide 11	13112	
Smox	5.1	560410	spermine oxidase	228608	
Regulation of transcription, DNA-dependent [119]					
Rab11a	2.0	359489	RAB11a, member RAS oncogene family	53869	
Cdk9	2.1	392872	cyclin-dependent kinase 9 (CDC2-related kinase)	107951	
Fli1	2.3	407869	Friend leukemia integration 1	14247	
Zfp482	2.0	435236	Zinc finger protein 482	241322	
Fbxl11	-2.9	464056	F-box and leucine-rich repeat protein 11	225876	
Pspc1	2.0	474771	paraspeckle protein 1	66645	
Myst2	5.4	494053	MYST histone acetyltransferase 2	217127	
Mxd1	2.1	520449	MAX dimerization protein 1	17119	
Egr1	-4.7	524988	early growth response 1	13653	
Bclaf1	-1.9	549609	BCL2-associated transcription factor 1	72567	
Pparbp	1.9	553770	peroxisome proliferator activated receptor binding protein	19014	
Rnf4	2.5	567180	Ring finger protein 4	19822	
Tsc22d3	2.0	700170	TSC22 domain family 3	14605	
Fliih	4.6	706377	flightless I homolog (Drosophila)	14248	
Creg1	1.9	760346	cellular repressor of E1A-stimulated genes 1	433375	
Pou2f2	-4.4	911620	POU domain, class 2, transcription factor 2	18987	
Hlx1	2.1	915372	H2.0-like homeo box 1 (Drosophila)	15284	

Table 7, continued.

Protein biosynthesis [119, 124]					
Eprs	4.9	455664	glutamyl-prolyl-tRNA synthetase	107508	
Protein folding [119]					
Hspa4	3.5	578003	heat shock protein 4	15525	
Clpx	2.4	733670	caseinolytic peptidase X (E.coli)	270166	
Ubiquitin cycle [119]					
Ube2l6	2.0	401185	ubiquitin-conjugating enzyme E2L 6	56791	[120]
Cul7	0.4	742757	cullin 7	66515	
Fbxo3	1.9	832607	F-box only protein 3	57443	
Intracellular protein transport [119]					
Sort1	2.4	339169	Sortilin 1	20661	
Ap1s2	2.0	605927	adaptor-related protein complex 1, sigma 2 subunit	108012	
Arf3	4.4	652348	ADP-ribosylation factor 3	11842	
Response to stress [119]					
Prdx1	2.1	530413	peroxiredoxin 1	18477	[122]
Mapk14	2.2	755610	mitogen activated protein kinase 14	26416	[120]
Prdx6	-2.0	825043	peroxiredoxin 6	11758	
Defense response [119, 124]					
Klra18	2.5	806675	killer cell lectin-like receptor, subfamily A, member 18	93970	
Bst1	2.1	837914	bone marrow stromal cell antigen 1	12182	
Inflammatory response [119, 124]					
Card12	2.2	336709	caspase recruitment domain family, member 12	268973	
Abcb1a	2.6	677412	ding cassette, sub-family B (MDR/TAP), member 1A	97570	
Ca2	4.0	574832	carbonic anhydrase 2	88269	
Cdkn1b	3.7	516253	cytochrome P450, family 3, subfamily a, polypeptide 11	104565	
Clu	4.0	379462	Clusterin	88423	

Table 7, continued.

Cr1l	1.9	538208	complement component (3b/4b) receptor 1-like	88513	
Cyp3a11	3.7	516253	cytochrome P450, family 3, subfamily a, polypeptide 11	88609	
Fyn	2.50	766362	Fyn proto-oncogene	95602	
H2-Q8	1.8	712519	histocompatibility 2, Q region locus 8	95937	
Hnrnpa3	4.8	903894	heterogeneous nuclear ribonucleoprotein A3	1917171	
Mrc1	2.9	331550	Mannose receptor, C type 1	97142	
Pole4	2.3	508321	polymerase (DNA-directed), epsilon 4 (p12 subunit)	1914229	
Ppp3r1	2.7	716541	protein phospatase 3, regulatory subunit B, alpha isoform (calcineurin B, type I)	107172	
Procr	2.0	431405	protein C receptor, endothelial	104596	
Rrm1	5.6	865694	ribonucleotide reductase M1	98180	
Serpinb2	4.0	860577	serine (or cysteine) proteinase inhibitor, clade B, member 2	97609	
Leukocyte extravasation and signaling					
Arhgap12	2.2	465731	Rho GTPase activating protein 12	1922665	
Crkl	3.0	389169	v-crk sarcoma virus CT10 oncogene homolog (avian)-like	104686	
Ptk2b	2.6	867483	PTK2 protein tyrosine kinase 2 beta	104908	
Immune response [119, 124]					
Gbp3	3.0	405120	guanylate nucleotide binding protein 4	55932	[122, 124]
Ddx58	7.1	438990	DEAD (Asp-Glu-Ala-Asp) box polypeptide 58	230073	
Gbp1	2.9	586296	guanylate nucleotide binding protein 1	14468	[120, 123, 124]
Il1a	5.1	595893	interleukin 1 alpha	96542	
Il1b	2.4	734612	interleukin 1 beta	16176	

Table 7, continued.

Il15	1.9	876196	interleukin 15	16168	
Ifit3	3.2	888038	interferon-induced protein with tetratricopeptide repeats 3	15959	
Cxcl11	5.1	921243	chemokine (C-X-C motif) ligand 11	56066	
Cell cycle [124]					
Pmp22	1.9	616997	peripheral myelin protein	18858	
Cdkn1b	3.7	704876	cyclin-dependent kinase inhibitor 1B (P27)	12576	
Ccnf	2.4	767163	cyclin F	12449	
Rhob	-2.2	925472	ras homolog gene family, member B	11852	
Cell adhesion [119]					
Cldn11	4.9	338333	claudin 11	18417	
Scarb2	2.5	561450	scavenger receptor class B, member 2	12492	
Signal transduction [124]					
Rin1	-1.9	478326	Ras and Rab interactor 1	225870	
Ms4a4c	2.4	495283	membrane-spanning 4-domains, subfamily A, member 4C	64380	
Prkrir	3.4	561755	protein-kinase, interferon-inducible double stranded RNA dependent inhibitor, repressor of (P58 repressor)	72981	
Olfr472	-2.2	591718	olfactory receptor 472	258770	
Ywhag	4.1	606287	3-monooxygenase/tryptophan 5-monooxygenase activation protein, gamma polypeptide	22628	
Gnas	1.8	646267	GNAS (guanine nucleotide binding protein, alpha stimulating) complex locus	14683	
Ms4a4c	3.2	791872	membrane-spanning 4-domains, subfamily A, member 4C	64380	
Ptger2	3.0	912597	prostaglandin E receptor 2 (subtype EP2)	19217	
G-protein coupled receptor protein signaling pathway [119]					
Olfr1303	-2.0	366625	olfactory receptor 1303	258397	

Table 7, continued.

Slc19a2	1.9	763767	solute carrier family 19 (thiamine transporter), member 2	116914	
Olfr435	-3.2	810459	olfactory receptor 435	258647	
Olfr316	-1.9	903210	olfactory receptor 316	258064	
Cell-cell signaling [119]					
Wnt6	2.0	590115	wingless-related MMTV integration site 6	22420	
Development [119]					
Lrp6	-2.3	691244	low density lipoprotein receptor-related protein 6	16974	
Egfl4	-2.2	914308	EGF-like-domain, multiple 4	269878	
Pgf	2.9	932795	placental growth factor	18654	
Metabolism [124]					
Hsd17b4	2.2	303973	hydroxysteroid (17-beta) dehydrogenase 4	15488	
Echdc3	2.2	331450	enoyl Coenzyme A hydratase domain containing 3	67856	
Atp2c1	2.0	388850	ATPase, Ca++-sequestering	235574	
Atp1a2	2.1	684165	ATPase, Na+/K+ transporting, alpha 2 polypeptide	98660	
Oas3	-3.0	487213	2'-5' oligoadenylate synthetase 3	246727	[120]
carbohydrate transport [119]					
Slc35a4	2.5	318829	Solute carrier family 35, member A4	67843	
Protein transport [119]					
Rab20	2.0	410549	RAB20, member RAS oncogene family	19332	
Rap2b	2.2	471908	RAP2B, member of RAS oncogene family	74012	
Exoc2	3.0	498825	exocyst complex component 2	66482	
Rheb	1.9	653270	RAS-homolog enriched in brain	19744	
Zfyve20	2.9	669220	zinc finger, FYVE domain containing 20	78287	
Nupl2	2.1	868036	Nucleoporin like 2	231042	

Table 7, continued.

Protein ubiquitination [119]					
Trim12	2.7	454451	tripartite motif protein 12	76681	
Trim34	2.9	600486	tripartite motif protein 34	94094	
Cell differentiation [119]					
Ndrg2	2.1	468211	N-myc downstream regulated gene 2	29811	

[a] Transcripts altered ≥1.8-fold ($p \leq 0.025$) in 15-S-HETE-treated RAW 264.7 cells that are associated with (1) specific genes or gene products correlated to malarial or (2) genes that are classified with specific over-expressed GO biological processes in malaria models, are shown in the table. Fold changes (FC) represent the average of three independent biological experiments.

Global responses to malaria infection have been examined at the molecular level in the blood of human victims,[119, 120] malaria positive tissue,[121] and murine[122-124] and monkey[125] malaria models using microarray technology. Perturbation of gene expression associated with erythropoiesis, glycolysis, metabolism, B-cell activation, and inflammation was frequently identified in these analyses; however, the specific agents responsible for mediating these expression changes remain unknown. Accumulating evidence led to the hypothesis that many of the adverse effects of malaria are not caused directly by the parasite, but by endogenous toxins generated during interactions with parasite-derived species such as Hz.[58]

Unlike the mode of action behind the of HNE's biological activity (forming adducts to cellular nucleophiles and subsequently modulating cell signaling) 15-HETE serves as a ligand for the nuclear PPARγ receptor,[101] a ligand-activated transcription factor. In the current study, activated RAW 264.7 macrophage-like cells were treated with 15-HETE, and gene expression changes were identified. The number of expression

changes mediated by 15-HETE is modest relative to the global response to HNE (Figure 49). mRNA levels were assessed at 24 h in the model to mimic a steady state response to 15-HETE that would be relevant to malaria infection. Consequently, not only are downstream PPARγ signaling transcripts (e.g., *Adfp*, *Ca2*, *Cyp3a4*, *M6pr*, *M6prbp1*, *Med1*, *Med7*, and *Sdc1*) elevated in response to 15-HETE, but several secondary cascades are also stimulated (Table 7).

Cytoadherence

The balance between the removal of *Plasmodia* from circulation and their sequestration inside host cells is crucial for parasite survival during infection. Sequestration is mediated by cytoadherence, specifically the adherence of parasitized RBCs (PRBCs) and leukocytes to capillary and postcapillary venular endothelial cells (EC). This cytoadherance reduces blood flow and causes metabolic dysfunction[163] and is thought to be a major factor associated with cerebral malaria (CM). Mechanism(s) used for adhesion and migration involve the expression of ligands and receptors on PRBCs or leukocytes and EC. In addition to constitutive adhesion molecules, cell-cell and cell-matrix interactions are also mediated by cytokines or microbial products which enhance the expression of inducible adhesion molecules

Investigation of potential arachidonic acid metabolite involvement in cytoadherence identified 15-HETE as an agent capable of stimulating basal adhesion of erythrocytes[117] and monocytes to EC[164, 165]. In the current study, 15-HETE induced the expression of several integrin signaling transcripts (e.g., *Crkl*, *Rap2b*, *Arf3*). Furthermore, the expression of genes encoding *Pkd2* and *Sdc1*, which are involved in cell-cell and

cell-matrix interactions, and *Ptpn14*, which has alleged involvement in cell adhesion, was also induced by 15-HETE.

Leukocyte extravasation and chemotaxis

The inflammatory response to malaria, both acute and chronic, follows a predictable sequence of events. Following initial vascular changes, permeability increases resulting in edema. Enhanced cytoadherence results in the accumulation, adherence, and emigration of leukocytes through vascular endothelium, subsequently releasing molecular mediators which contribute to both the immune response and recruitment/activation of effector cells. Overwhelming evidence demonstrates that the pathophysiology of malaria involves both systemic and local cytokine release. The recruitment of phagocytes around cerebral capillaries has been observed in CM and likely explains increased chemotaxis and chemokinesis.[166] CM is a severe complication of *P. falciparum* infection that is characterized by cytoadherence in cerebral microvasculature. Accumulation of Hz-loaded monocytes has been observed in brains of CM victims[155] and may contribute to the disruption of endothelial basement membrane and subsequent extravasation of blood cells.[146] Importantly, blood brain barrier (BBB) destruction and enhanced vascular permeability/edema are major factors associated with CM.[144, 167]

A potential contribution of 15-HETE toward increased vascular permeability has been examined in the lung. Administration of this hydroxylated fatty acid was shown to increase respiratory edema fluid production,[168] suggesting a role as an inflammatory mediator. The current analysis identified the 'Leukocyte Extravasation Signaling' pathway as being significantly ($p = 0.015$) affected by 15-HETE. Specifically, the steady-

state expression of *Arhgap12*, *Cldn11*, *Crkl*, *Mapk14*, and *Ptk2b* is up-regulated. Although 15-HETE is generally considered to have anti-inflammatory properties, activation of a large group of genes encoding inflammatory response molecules was observed (Table 7).

15-HETE and MMP9 regulation

15-HETE was recently shown to enhance IL1B expression and MMP9 activity in human monocytes.[115] Comparison of these results with the current study identified a different response: While *Il1b* mRNA is elevated by 15-HETE, *Mmp9* mRNA is down-regulated (-4.8–fold by qRT-PCR). *Mmp9* expression can be regulated through a variety of signaling cascades including NF-κB, p38 MAPK, and ERK1/2 pathways.[149] It was proposed that the enhanced regulation of IL1B and MMP9 regulation in human monocytes may be associated with NF-κB signalling based on reports demonstrating NF-κB-mediated MMP9 expression in LPS-stimulated RAW 264.7 cells.[149] This hypothesis seems unlikely in LPS-stimulated RAW 264.7 cells as 15-HETE has been shown to impair NF-κB-mediated expression of *iNOS*.[68, 78] Furthermore, PPARγ ligands (other than 15-HETE) have been shown to inhibit *MMP9* expression, secretion, and activity in macrophages and vascular smooth muscle cells[169-171] and repress NF-κB signal transduction.[172, 173] Consequently, NF-κB regulated transcription is not likely to be the basis of enhanced *MMP9* expression in 15-HETE-treated human monocytes.[115]

Conclusions

The host immune response to malarial infection is multifactorial, including complex innate and adaptive immune responses to the parasites, composite native Hz, Hz-derived lipid peroxidation products, and other cellular debris. Not unexpectedly, countless interactions between an array of malaria toxins and host cells result in adverse biological effects, prompting a reductionist examination of such complex systems. The survival strategy for parasites requires the detoxification of free heme released during RBC catabolism, and consequently the synthesis of Hz. The oxidation of fatty acids by Hz (or BH) is a rich chemistry which only now is being elucidated. Of these oxidation products (all R,S isomers of HETE's, HODE's, and HNE), HNE is unquestionably the most reactive. Additionally, concentrations of HNE found in Hz laden monocytes are the highest reported in any biological system.[71] Consequently, HNE was chosen to begin exploration of the cellular response to the lipid component of Hz.

A wide range of substantive modulations occurred in activated cells following HNE treatment at both 6 and 24 h. The early response predominantly involves an oxidative stress activity that involves induction of ARE and glutathione metabolism genes. Steady state gene expression changes are associated with a variety of documented malaria responses such as macrophage activation, immune and inflammatory responses, NF-κB signal transduction, ECM degradation, and dyserythropoiesis. The modest, primarily phagocytic, response to BH supports the hypothesis that Hz predominantly functions as a vehicle to generate and introduce toxic mediators (e.g., HNE, hydroxylated fatty acids) that are closely associated with the biomineral into phagocytic cells.[69]

In response to the large number of gene expression alterations mediated by HNE, the global response to 15-HETE was examined in macrophage-like cells. 15-HETE has previously been implicated as having a functional role in a variety of cellular processes such as inflammation, asthma, carcinogenesis, and atherosclerosis, however its precise role remains unknown. 15-HETE can be incorporated into membrane lipids, and alter vascular tone and EC permeability.[116] Analyses demonstrated that the response to 15-HETE was predominantly associated with altered expression of 'lipid metabolism' as well as 'small molecule biochemistry' genes. Notably, several genes related to cytoadherance, leukocyte extravasation, and inflammatory response were also differentially regulated by 15-HETE treatment. However, the small number of expression changes indicates that 15-HETE does not elicit a marked. Although these results add insight and detail to 15-HETE's effect on gene expression in macrophage-like cells, it should be noted that there are limitations to any model system. 15-HETE represents but one structural HETE isomer that is associated with Hz; 5-, 8-, 9-, 11-, and 12-HETE have also been identified.[78, 86] Although 5- and 15-HETE are reported to be the predominant isomers formed during iron catalyzed or Hz-mediated oxidation of AA,[86, 92] 12-HETE may exert greater biological activity.[78] These findings suggest that upon hemozoin phagocytosis, the sum of individual HETE PPARγ ligands may mediate a synergistic immunomodulatory response.

CHAPTER IV

HNE-MEDIATED DYSREGULATION OF SIGNAL TRANSDUCTION

Introduction

Hemozoin has long been suspected of contributing to immunomodulations that occur during *Plasmodia* infection. The Hz-associated lipid peroxidation product HNE exerts activity that parallels Hz. Specifically, several gene expression alterations associated with MMP9 and NF-κB regulation described in *Chapter III* suggest that HNE is a major contributor of the immunomodulation caused by native Hz.

Sequestered Hz has been detected in brain tissue of cerebral malaria (CM) victims[143] and has been suggested as a factor that contributes to inflammation, swelling, disruption of the blood brain barrier, and extravasation of blood cells.[146] Notably, transcriptional activation of MMP9 was observed in human blood during *P. falciparum* infection,[120] and Hz was shown to induce the expression, translation, and activity of MMP9 in human monocytes.[146] In *Chapter III* it was shown that HNE up-regulated *Mmp9* mRNA in macrophage-like cells.[44]

MMP9 (gelatinase-B) is a member of the MMP family of zinc-dependent endoproteinases involved in ECM remodeling.[144-146] The primary substrates of MMP9 are elastin and type IV collagen, major constituents of the basement membrane and ECM.[174] Canonical transcriptional regulation of MMP9 (Figure 51) is mediated by a variety of growth factors and cytokines (e.g., tumor necrosis factor (Tnf), interleukin 1 beta (Il-1b), epidermal growth factor (Egf), and transforming growth factor, beta 1 (Tgf-b1) that can

trigger a number of signaling cascades.[147-149, 175] Post translation, several additional forms of MMP9 regulation are at play including spatial localization, extracellular zymogen activation, and binding with cognate tissue inhibitor of metallopeptidases (TIMP) protein. This tightly regulated system is essential to prevent tissue damage.

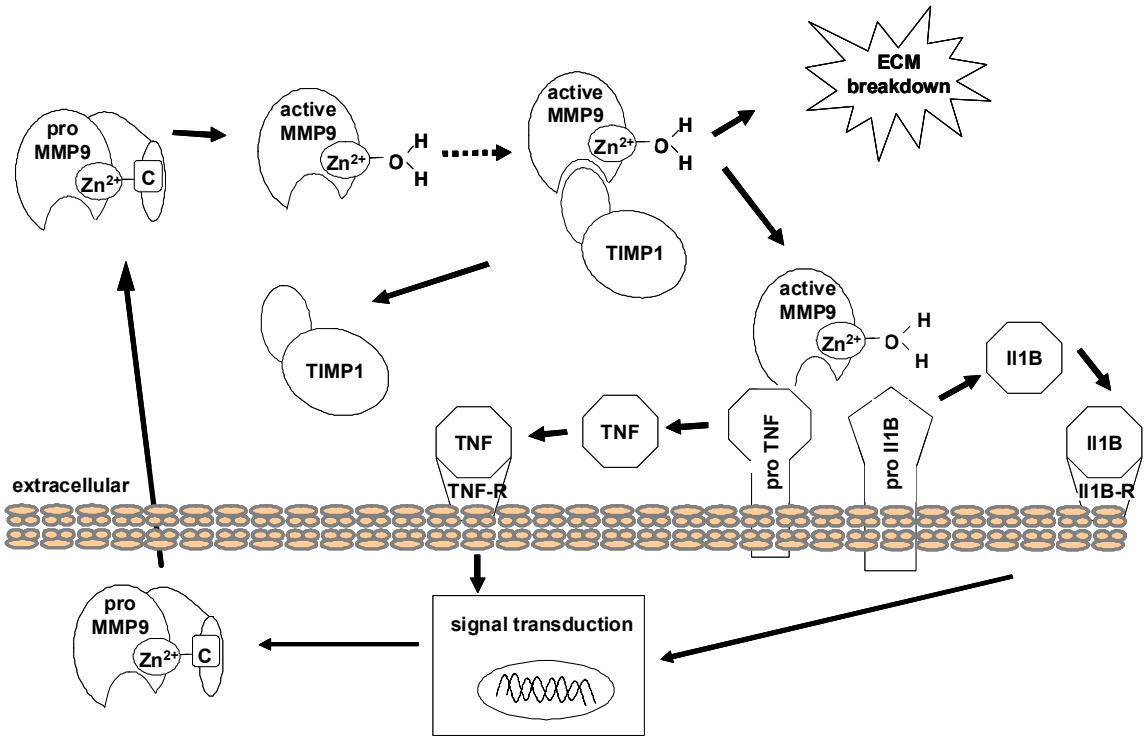

Figure 51. Canonical regulation of MMP9. *MMP9* is expressed and processed as an inactive pro-enzyme. Upon proteolysis, MMP9 is activated. Although active, the proteolytic activity of MMP9 is maintained through the formation of a complex with MMP9's cognate inhibitor, TIMP1. Active MMP9 can cleave both pro-TNF and pro-IL1B from membrane bound forms to a soluble cytokines. Both of these cytokines have been shown to mediate signal transduction leading to expression of *MMP9*, thus completing a positive feedback loop.

In addition to perturbed MMP9 regulation, the microarray results presented in *Chapter III* also highlighted alterations of NF-κB signal transduction. The LPS mediated

pathway to produce NO is well characterized and entails NF-κB signal transduction (Figure 52). In quiescent cells, NF-κB is sequestered by the inhibitor of κB (IκB)

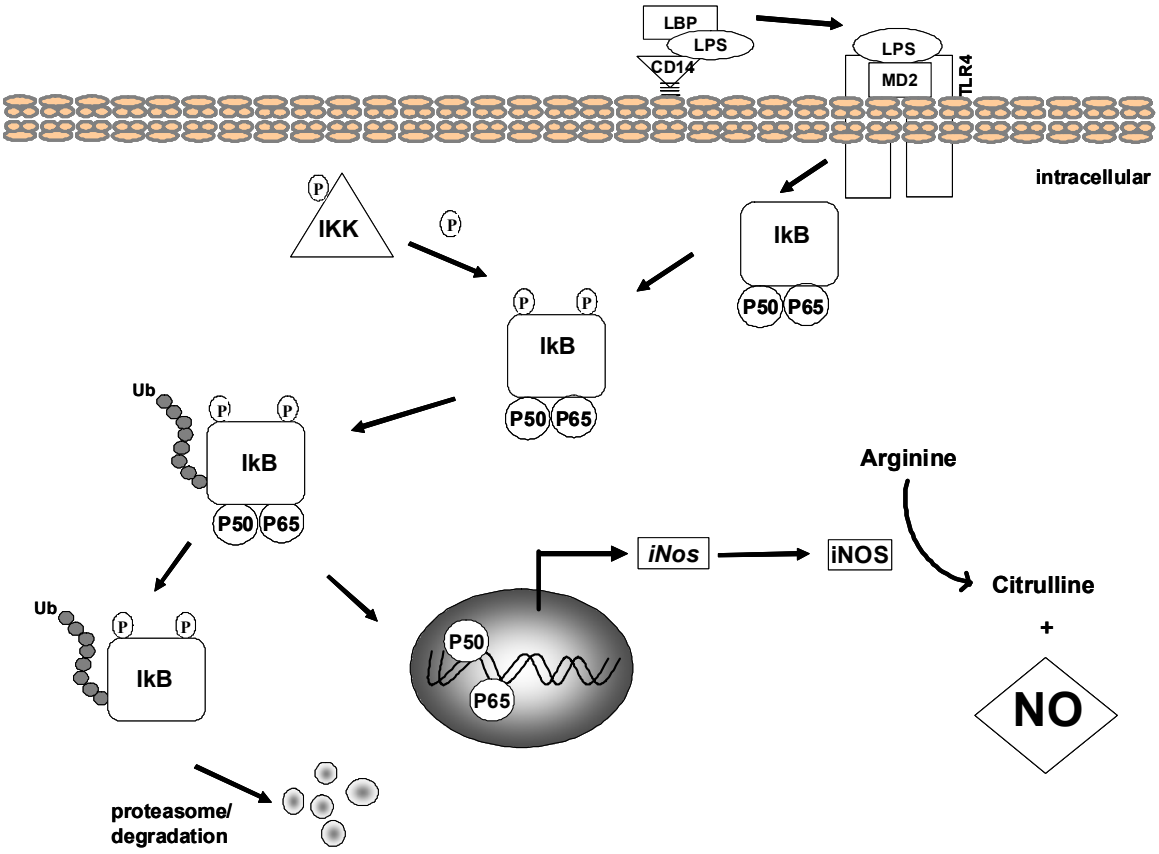

Figure 52. Canonical NF-κB signal transduction. LPS binding to Toll-like receptor 4 (TLR4) recruits adapter proteins (e.g., TRAF) which recruit the IKK complex. Active IKK phosphorylates IκB, triggering its polyubiquitination and subsequent degradation. NF-κB is then free to translocate to the nucleus and mediate the expression of iNOS, which ultimately generates NO.

in the cytoplasm. Upon receiving an appropriate signal leading to its activation, IκB kinase (IKK) phosphorylates IκB leading to its degradation and subsequent release of the NF-κB complex. Once NF-κB is liberated from IκB, NF-κB translocates to the nucleus

and regulates gene expression including iNOS which is responsible for the production of NO.

Given the suggestions of altered MMP9 regulation and NF-κB signal transduction in *Chapter III*, biochemical approaches were used to explore the mRNA and protein levels of members of these canonical pathways. Chapter IV is divided into two parts: the effects of HNE and 15-HETE on MMP9 regulation are presented in *Part I*, and the effect of HNE on NF-κB is presented in *Part II*.

Experimental

Cell Culture

Murine macrophage-like RAW 264.7 cells (ATCC, TIB-71) were maintained in RPMI 1640 medium (Cellgro) supplemented with 5% fetal bovine serum (Atlanta Biologicals) and 1 μg/mL penicillin-streptomycin (Cellgro) under standard incubation conditions (37 ºC, 5% CO2). Cells were plated 18-24 h prior to treatment at a density of 4 × 106 cells/well in 6 well plates (qRT-PCR experiments) or 5 × 105 cells/well in 24 well plates (ELISA experiments).

Cell Treatment

Cells were washed once with Dulbecco's PBS (DPBS) and treated with 10-35 μM HNE (Calbiochem) or 20-40 μM 15-S-HETE (Cayman Chemical) and LPS (1 μg/mL final concentration, Sigma) for 24 or 48 h. For inhibition studies, cells were pre-incubated for 1.5 h with 10 nM-30 μM of the appropriate inhibitor before HNE treatment and LPS

stimulation. U0126, SB203580, SP600125, and PDTC (Calbiochem) were added to cells to inhibit ERK1/2, p38, JNK, and NF-κB signaling cascades, respectively. Active MMP9 was inhibited with 10 nM-30 μM of MMP9 inhibitor I (Calbiochem) at the time of HNE+LPS treatment. TNF signaling was blocked with a neutralizing TNFα antibody (Abcam) according to the manufacturer's protocol at the time of treatment.

RNA Isolation

Cells were washed three times with DPBS and scraped from the wells. Three biological replicates (composed of 6 pooled wells each) per sample were prepared. Total RNA was isolated using the VersaGene cultured cell RNA purification and DNase treatment kits, following manufacturer's recommendations and analyzed for quality (Agilent 2100 Bioanalyzer, Agilent Technologies, Palo Alto, CA).

Real-Time Reverse Transcription Polymerase Chain Reaction

Quantitative real-time reverse transcription polymerase chain reaction (qRT-PCR) was used to validate the expression levels of *Mmp9* (Taqman assay Mm00442991_m1), *Timp1* (Mm00441818_m1), *Tnf* (Mm00443258_m1), and *Il1b* (Mm00434228_m1) in HNE and 15-HETE treated cells. Triplicate measurements for n = 3 biological replicates per sample were performed. cDNA was reverse-transcribed from 0.5 μg of total RNA using random hexamer primers and Superscript II Reverse Transcriptase (Invitrogen). Reactions were purified using Qiagen's PCR Purification Kit following the manufacturer's protocol. Following RT, all assays were performed with Applied Biosystems TaqMan FAM labeled 20× probes (Table 1). *Ywhaz* was chosen as the

endogenous control based on results obtained from an Applied Biosystems mouse endogenous control array. cDNA amplification was performed using TaqMan 2× Universal PCR Master Mix (Applied Biosystems) according to the manufacturer's directions. Standard Taqman cycling conditions were used as specified by the manufacturer. Cycling and data collection were performed using the Applied Biosystems 7900 HT instrument and analysis performed using the manufacturer's SDS software package to calculate Ct values for each detector. Ct values were processed based on the comparative Ct method, where the relative transcript level of each target gene was calculated according to the equation $2^{-\Delta Ct}$, where ΔCt is defined as $Ct_{\text{target gene}} - Ct_{\text{Ywhaz}}$.

Enzyme-linked immunosorbant assays

Enzyme-linked immunosorbant assays (ELISAs) were used to measure the levels of soluble proteins secreted into culture medium. Cell culture medium was collected and analyzed using commercial ELISA reagents (R&D Systems) according to protocol using 96-well Immulon 2HB plates (Thermo Electron Corp.). Briefly, capture antibody was added to wells and incubated at 25 ºC overnight. Three washes (300 µL each) were performed after this and all subsequent steps using phosphate buffered saline (PBS) supplemented with 0.05% Tween-20. Wells were blocked with 300 µL of 5% Fraction V bovine serum albumin (Fisher Scientific) in PBS for 1 h at 37 ºC. Three-fold serial dilutions of collected culture medium (1:1–1:2187) in complete medium and two-fold dilutions of recombinant protein in complete medium were added to wells and incubated for 1 h at 37 ºC. Wells were incubated with the appropriate biotinylated detection antibody for 1 h at 37 ºC and subsequently incubated with streptavidin-HRP for 10 min at

37 ºC. After addition of 3,3',5,5',-tetramethylbenzidine liquid substrate (100 µL, Sigma Aldrich), the enzymatic reaction was quenched with 50 µL of 2M H_2SO_4. The absorbance of samples was then measured spectrophotometrically at 450 nm. Culture medium and recombinant protein were used as negative and positive controls, respectively.

Zymography

LPS stimulated cells were treated 10 or 35 µM HNE and culture medium was collected at 48 h. Equal total protein was resolved on 10 % Novex-Zymogram gel containing gelatin (Invitrogen) under non-denaturing and non-reducing conditions. Post electrophoresis, gels were washed 2× with 2.5% Triton-X 100 for 30 min and then incubated with substrate buffer (50 mM Tris-HCl pH 7.5, 200 mM NaCl, 50 mM CaCl2, and 0.2% BRIJ-35) for 16 h at 37 ºC. Gels were stained with 10% acetic acid, 30% methanol, and 0.5% Coomassie Brilliant Blue (R-250) for 1 h, followed by destaining. Proteins with gelatinolytic activity were visualized as clear bands on a blue background. Apparent molecular weight was determined by comparison with Precision Plus Protein pre-stained Kaleidoscope standard (Bio-Rad). Zymograms were imaged (Bio-Rad Chemidoc XRS System) and the data analyzed using Quantity One software (Bio-Rad). The area and average intensity were measured for each band representing MMP9 activity.

Determination of NO synthesis

NO levels were estimated indirectly by the accumulation of the stable NO metabolite nitrite via the Griess assay. Twenty-four hours after treatment, supernatant (100 µL) was collected and combined with 100 µL Griess reagent (1:1, 1% sulfanilimide

in 5% phosphoric acid/0.1% N-(1-naphthyl)ethylenediamine). After five minutes, the absorbance of the azo-complex was measured at 540 nm using a Bio-Tek Synergy HT Multidetection Microplate Reader. Nitrite levels were determined by comparison with a standard curve.

Immunoprecipitation

Cells (4×10^6/well) were incubated with 0 or 35 μM HNE for 1 h under standard incubation conditions, and subsequently lysed as described above. Anti-IKKα (3 μg) was incubated with 50 μL of MagnaBind amine-derivatized beads (Pierce) with 4 mM bis(sulfosuccinimidyl)suberate (BS^3) in PBS for 1 h at RT mixing end-over-end. Reactions were quenched with 20 mM Tris (pH 8.5) for 15 min. Antibody cross-linked beads were separated using a magnet, and unbound antibody was removed by three washes with lysis buffer. Crude lysate (400 μg in 200 μL) was added to the beads and incubated with mixing overnight. Unbound lysate was removed and beads were washed 3× with lysis buffer. IKKα was eluted with 4× LDS buffer (with 2% β-mercaptoethanol) at 70 ºC for 10 min.

Immunoblotting

Cells were washed three times with ice-cold DPBS and lysed in 50 mM Tris-HCl (pH 7.4), 120 mM NaCl, 0.5% Nonidet P-40 (BioAffinity Systems Inc, Roscoe, IL), and 1mM EDTA, supplemented with complete mini protease inhibitor tablet (Roche) and phosphatase inhibitor cocktails I and II (Sigma) on ice for 15 min, followed by sonication (30% amplitude, 8 sec). Cell lysates were cleared by centrifugation at 13,200 × g for 10

min. Protein concentration was determined with the BioRad DC protein assay. Protein (20-50 μg) was resolved on a 4-12% NuPAGE Bis-Tris gel (Invitrogen) and electrophoretically transferred to a polyvinylidene difluoride membrane (0.2 μM, Invitrogen). Membranes were blocked overnight at 4 ºC with 5% nonfat dry milk in Tris-buffered saline (25 mM Tris-HCl (pH 7.4), 137 mM NaCl, 2.7 mM KCl) containing 0.1% Tween 20 (TBST). Blots were incubated with anti-phospho-IκB, anti-IκB, anti-IKKα, anti-IKKβ, or anti-iNOS (Santacruz Biotechnology) in 5% nonfat milk in TBST for 2 h at RT. Membranes to be probed for HNE-protein adducts were treated with 265 mM $NaBH_4$ in MOPS buffer (100 mM, pH 8) for 10 minutes at room temperature with gentle shaking and subsequently washed 6 × 5 min with TBST. Blots were then blocked and incubated with anti-HNE-Michael Adduct (Reduced) Rabbit pAb antibody (Calbiochem) as described above. Primary antibody complexes were stained with goat anti-rabbit horseradish peroxidase secondary antibody (Santacruz Biotechnology) in 5% nonfat milk in TBST for 1 h at RT. Protein bands were visualized by enhanced chemiluminescence (Pierce ECL Western Blotting substrate).

Peptide synthesis

The IKKα and IKKβ protein sequences were digested *in silico* with trypsin to determine the peptides containing the purportedly sensitive cysteine-178 and cysteine-179, respectively: DVDQGSLCTSFVGTLQYLAPELFENK (IKKα) and ELDQGSLCTSFVGTLQYLAPELLEQQK (IKKβ).[176-179] These model peptides were synthesized via a continuous flow fmoc solid phase peptide synthesis method on an Advanced Chemtech peptide synthesizer, purified by reverse phase HPLC, and

lyophilized as previously described.[180] Identification of the peptides was confirmed by MALDI mass spectrometry.

Peptide Adduction and analysis

Peptides (90 μL, 1 mM) dissolved in 75:25 acetonitrile/50 mM phosphate buffer (pH 7.4) were incubated with 10 μL of 5 mM HNE (stock solution 64 mM in ethanol) for 3 h at 37 ºC. Control reactions were prepared in parallel with an equivalent volume of ethanol as the experimental samples. Reaction mixtures were reduced with 10 μL of 1M $NaBH_4$ for 10 min, neutralized with 10 μL of 1M HCl, and purified by reverse phase HPLC (Nova-Pak C_{18}, 3.9×150 mm, Waters) monitoring an absorbance of 210 nM. Mobile phase A was 0.05% trifluoroacetic acid (TFA) in H_2O, mobile phase B was 0.05% TFA in acetonitrile. The gradient (500 μL/min) was as follows: 0–1 min, isocratic phase 5% B; 1–5 min, gradient to 15%B; 5–30 min, gradient to 35% B; 30–45 min, gradient to 90% B; 45–55 min, held at 90% B; 55–65 min, gradient to 5% B. Fractions were collected and analyzed by a Thermo Finnigan LCQ ion trap mass spectrometer (Thermo Fisher Scientific, Waltham, MA). MS/MS scans were acquired using an isolation width of 2 m/z and 30% normalized collision energy. The mass spectrometer was tuned prior to analysis using each synthetic peptide. Resulting MS/MS spectra were compared to simulated MS/MS fragmentation data using GPMAW 6.01.1 (Lighthouse Data).

Nomenclature

Nomenclature for genes and proteins is as described by the Mouse Genome

Informatics (MGI) database guidelines: both murine and human protein names are capitalized (MMP9), murine genes are italicized with the first letter capitalized (e.g., *Mmp9*), and human genes are italicized and capitalized (e.g., *MMP9*).

Results and Discussion

Part I: Effects of Lipid Peroxidation Products on Matrix Metalloproteinase-9 Regulation in LPS stimulated RAW 264.7 Cells

It was recently reported that phagocytosis of Hz by human monocytes increased MMP9 mRNA, protein, and activity.[146] The authors demonstrated that 10 μM 15-S-HETE increased MMP9 activity and IL1B mRNA and secreted protein in monocytes. In contrast, 0.1 μM HNE had no effect on MMP9 activity, and an inhibitory effect at 1-10 μM. Consequently, the source of Hz activity was attributed to the lipid peroxidation product 15-S-HETE.[115] These observations are in opposition to the gene expression results presented in *Chapter III* that implicated HNE, not 15-HETE, in severe dysfunction of MMP9 regulation.[44, 162]

Effects of HNE and 15-HETE on mRNA expression

Since microarray results are semiquantitative by nature, quantitative real time RT-PCR (qRT-PCR) analyses of stimulated cells treated with either HNE or 15-HETE were performed. Several genes encoding proteins associated with *Mmp*9 expression and activity were chosen for validation and fold changes were calculated relative to LPS-

stimulated cells. As shown in Figure 53, HNE significantly up-regulated the levels of *Mmp9* and *Tnf* mRNA, in direct contrast to decreased levels of *Mmp9* and *Tnf* mediated by 15-HETE. *Timp1* transcription was drastically reduced (-2000–fold) by HNE, yet unaltered by 15-HETE. Neither HNE nor 15-HETE treatment significantly altered *Il1b* levels. These expression results indicate that HNE stimulates canonical MMP9 pathways; however mRNA levels do not necessarily correlate with protein levels.

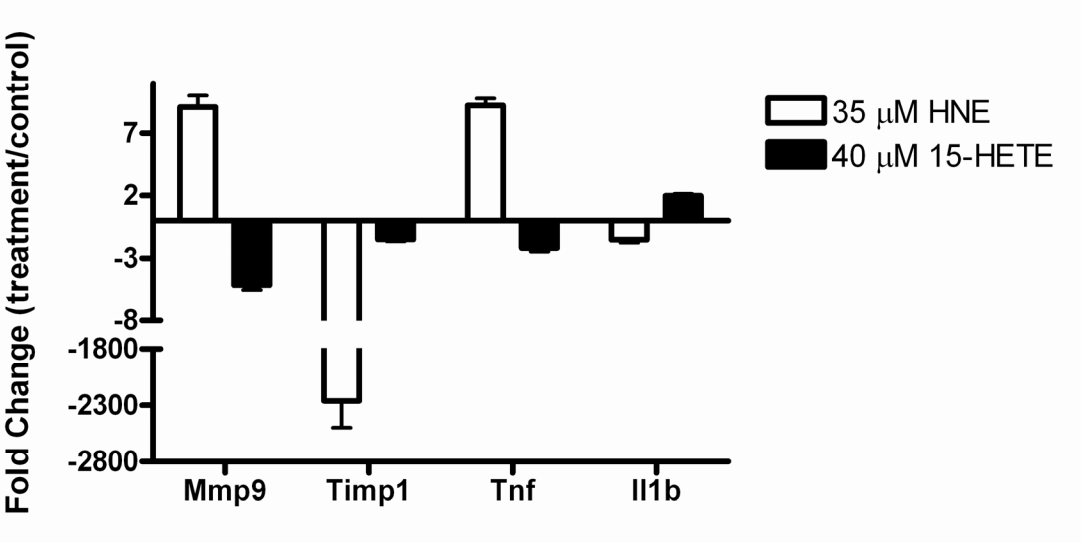

Figure 53. Quantitative real-time RT-PCR validation. RAW 264.7 cells were stimulated with 0.1 μg/mL LPS and untreated (control) or treated with either 35 μM HNE (white bars) or 40 μM 15-HETE (black bars) for 24 h prior to RNA extraction. Fold-changes (treated, stimulated cells relative to untreated, stimulated cells) are shown ($\overline{X}$ ± 99% confidence interval for triplicate measurements of n = 3 biological replicates). Abbreviations: *Mmp9*, matrix metalloproteinase 9; *Timp1*, tissue inhibitor of metalloproteinase 1; *Tnf*, tumor necrosis factor; *Il1b* interleukin 1 beta.

Effects of HNE and 15-HETE on Mmp9 and Timp1 secretion

Protein secretion of MMP9 induced by 10 or 35 μM HNE or 20 or 40 μM 15-HETE was measured by ELISA in the culture medium at 24 or 48 h (Figure 54). In the

absence of LPS stimulation, MMP9 secretion was below detectable limits in untreated, HNE treated, or 15-HETE treated cells. LPS stimulation, however, resulted in a significant increase of Mmp9 in all samples. In agreement with the qRT-PCR data, HNE further enhanced the level of MMP9 as a function of time, indicating that HNE synergized with LPS signaling. 15-HETE did not alter MMP9 secretion in LPS stimulated cells.

TIMP1 is a critical regulator of MMP9 activity in the extracellular space. Consequently, the level of TIMP1 secreted from cells was investigated (Figure 55). LPS stimulation resulted in a marked increase in TIMP1 protein. In accord with qRT-PCR data, HNE treatment severely impaired protein secretion, nearly to the level of unstimulated cells by HNE. 15-HETE, however, increased the level of TIMP1 measured. These results indicate that while 15-HETE seemingly imposes additional control of MMP9, HNE induces changes in favor of MMP9 activity, altering an otherwise exceptionally tightly regulated system. Similar to altered MMP regulation in these studies, HNE has been reported to induce the expression of MMP13 and repress the expression of TIMP1 in osteoarthritic tissues contributing to cartilage destruction.[181]

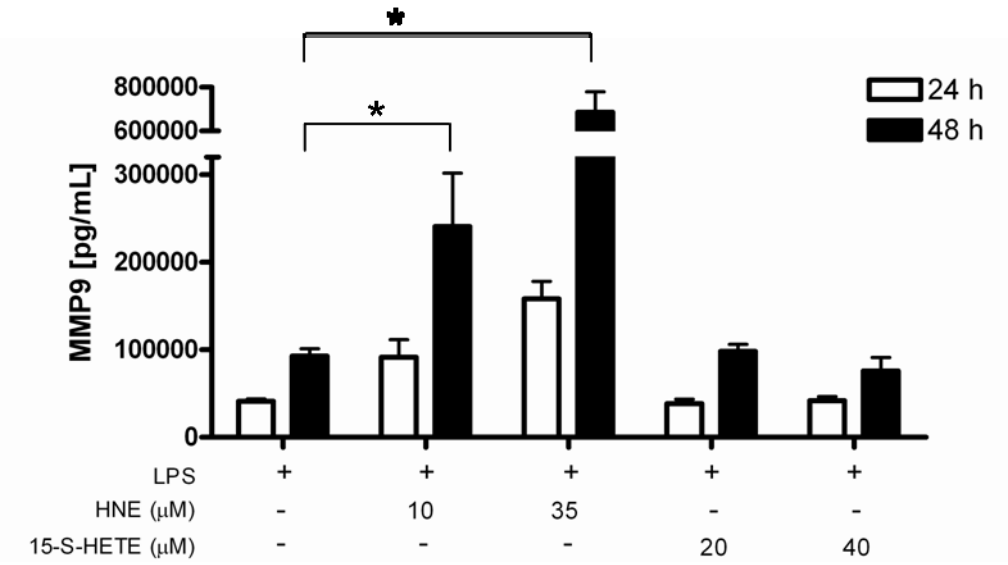

Figure 54**.** Determination of MMP9 levels by ELISA. RAW 264.7 cells were stimulated with 0.1 μg/mL LPS and treated with HNE or 15-HETE for 24 h (white bars) or 48 h (black bars). MMP9 secreted in the culture medium was assayed by ELISA, and levels were determined using a standard curve prepared with recombinant mouse MMP9 ($\overline{X}$ ± stdev, n≥3). Asterisks represent significant ($p < 0.05$) changes.

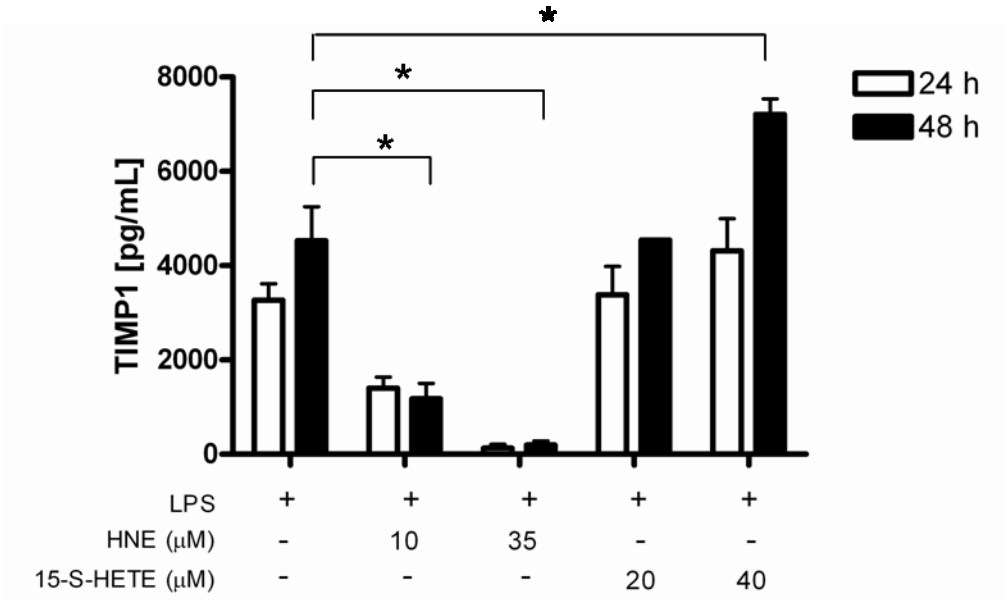

Figure 55. Determination of TIMP1 levels by ELISA. RAW 264.7 cells were stimulated with 0.1 μg/mL LPS and treated with HNE or 15-HETE for 24 h (white bars) or 48 h (black bars). TIMP1 secreted in the culture medium was assayed by ELISA, and levels were determined using a standard curve prepared with recombinant mouse TIMP1 ($\overline{X}$ ± stdev, n≥3). Asterisks represent significant ($p < 0.05$) changes.

Measurement of MMP9 Activity by Zymography

Given the shift in balance between elevated levels of MMP9 and decreased TIMP1, the activation state of MMP9 was examined. Since both pro- and active-forms of MMP9 are detected by ELISA, MMP9 protein levels do not necessarily correlate with activity. Thus, LPS stimulated cells were treated with 10 or 35 μM HNE for 48 h, and culture medium was tested by zymography using gelatin as a substrate (Figure 56). As shown by the clear bands against the dark background, MMP9s proteolytic activity increases with increasing HNE concentration.

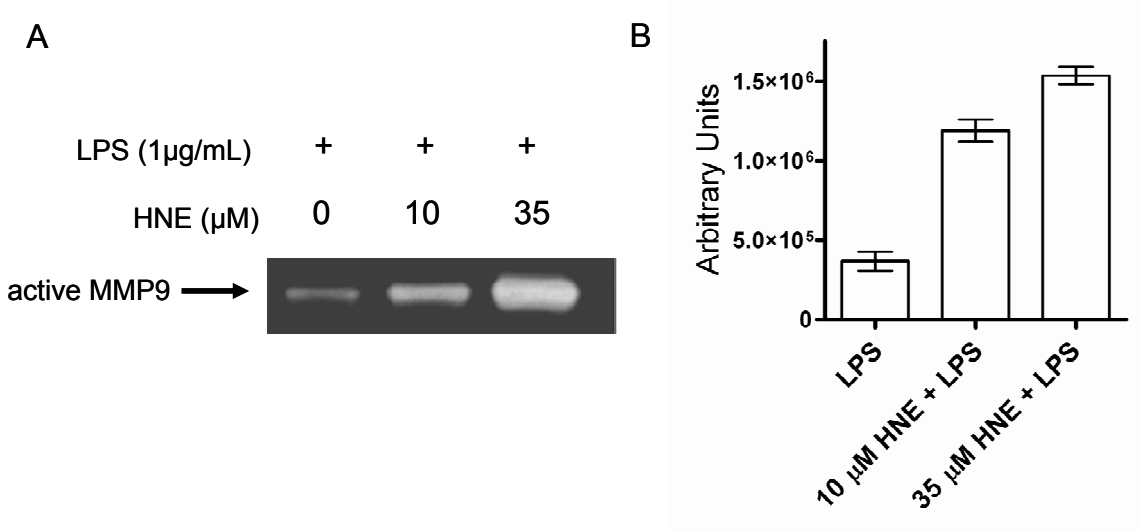

Figure 56. HNE stimulates MMP9 secretion and activity. Cells were treated with HNE and immediately stimulated with LPS. (A) Culture medium was collected after 48 h and subjected to SDS-PAGE zymography. (B) The bands were quantified by scanning densitometry. Data shown are representative of three independent experiments. Asterisks represent significant ($p < 0.05$) changes.

Role of active MMP9 in Mmp9 Regulation

Active MMP9 has been shown to participate in a positive feedback loop mediating *Mmp9* expression. Therefore, an MMP9 inhibitor was added during the

incubation of stimulated HNE treated cells to prevent proteolytic activity and determine whether active MMP9 activity contributes to MMP9 secretion. These experiments revealed that active MMP9 does in fact participate in downstream *Mmp9* expression, translation, and secretion. As shown in Figure 57, MMP9 secretion mediated by HNE in LPS-stimulated cells was reduced by the inhibitor, whereas MMP9 secretion mediated by LPS stimulation was not. This is likely a consequence of the decreased level of TIMP1, and subsequent active state of MMP9, when cells are exposed to HNE, in contrast to the inactive MMP9 bound to TIMP1 in LPS-treated cells.

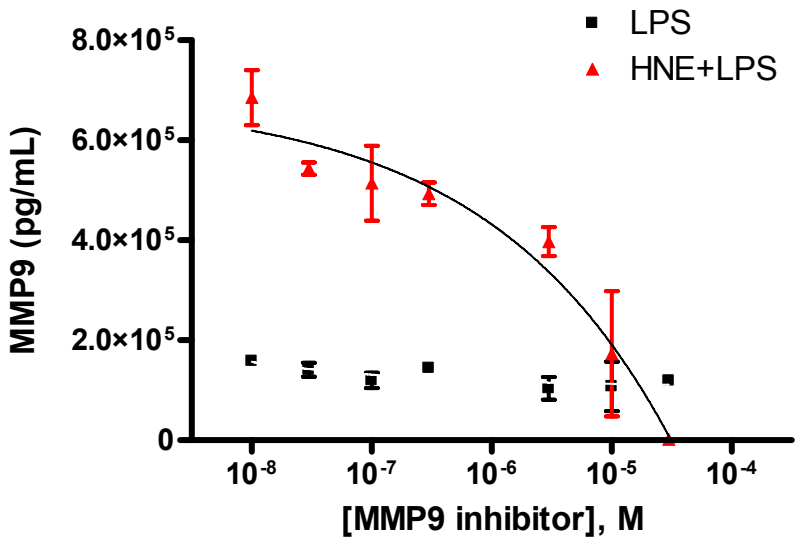

Figure 57. Active MMP9 mediates MMP9 Regulation. RAW 264.7 cells were stimulated with 0.1 µg/mL LPS and treated with an MMP9 inhibitor in the absence (black points) or presence (red points) of 35 µM HNE for 48. MMP9 secreted in the culture medium was assayed by ELISA, and levels were determined using a standard curve prepared with recombinant mouse MMP9 ($\overline{X}$ ± stdev, n≥3).

Effects on HNE and 15-HETE on Il1b and Tnf secretion

There is considerable evidence that active MMP9 plays a role in the shedding of TNFα[150] and IL-1β[182] from membrane-anchored precursors. In turn, both of these cytokines can ultimately induce *Mmp9* expression, initiating a positive feedback cycle.[183] Protein validation of secreted IL1B demonstrated that while HNE-treatment decreased the level of the cytokine, 15-HETE had no effect (Figure 58). The decrease of TNFα secretion influenced by 15-HETE was consistent with mRNA levels. However, while HNE increased *Tnfa* mRNA, secreted TNFα protein was decreased (Figure 59). This result may not necessarily be due to impaired translation, but to impaired cleavage of the membrane bound form. A second explanation may be that TNFα is bound to its cognate receptor and thus not in a soluble form for detection. Regardless, similar findings were observed in human monocytes where TNFα secretion was markedly increased by LPS, but inhibited by HNE in a dose-dependent manner.[184]

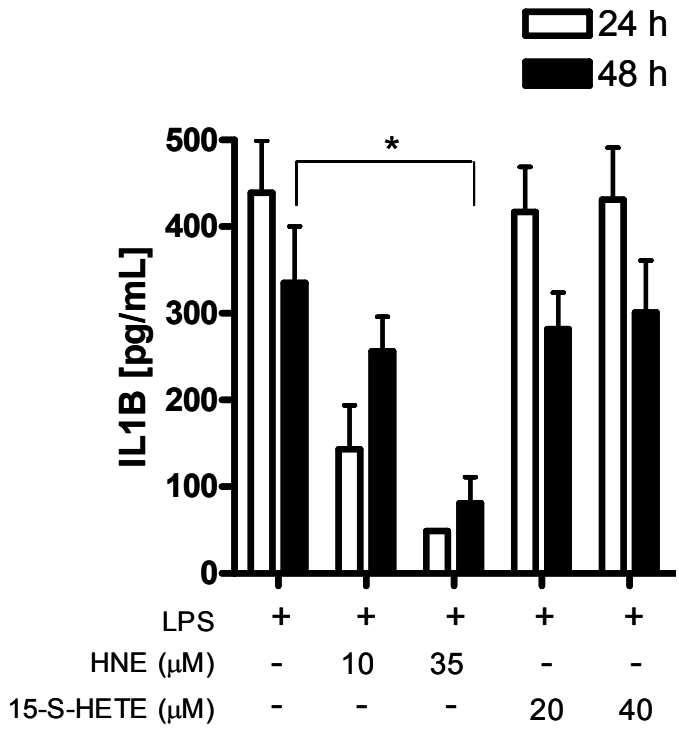

Figure 58. Determination of IL1B levels by ELISA. RAW 264.7 cells were stimulated with 0.1 μg/mL LPS and treated with HNE or 15-HETE for 24 h (white bars) or 48 h (black bars). IL1B secreted in the culture medium was assayed by ELISA, and levels were determined using a standard curve prepared with recombinant mouse IL1B ($\overline{X}$ ± stdev, n≥3). Asterisks represent significant ($p < 0.05$) changes.

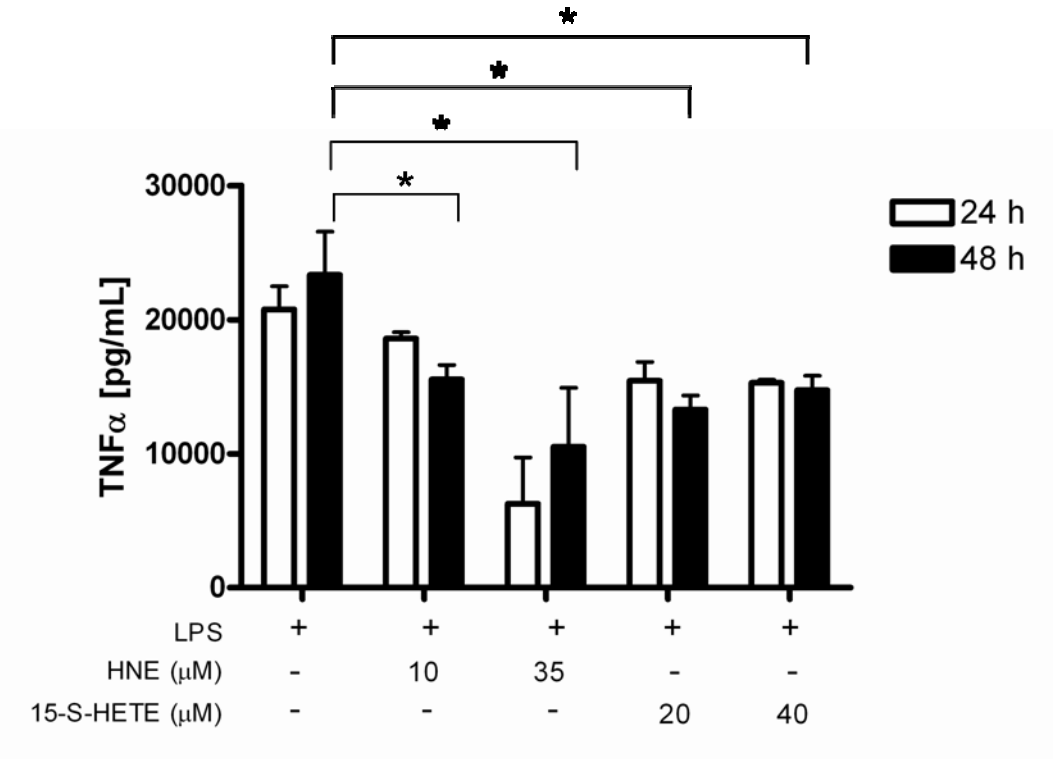

Figure 59. Determination of TNF levels by ELISA. RAW 264.7 cells were stimulated with 0.1 μg/mL LPS and treated with HNE or 15-HETE for 24 h (white bars) or 48 h (black bars). TNF secreted in the culture medium was assayed by ELISA, and levels were determined using a standard curve prepared with recombinant mouse TNF ($\overline{X}$ ± stdev, n≥3). Asterisks represent significant ($p < 0.05$) changes.

MMP9 feedback

The mechanisms involved in TNF and IL1B secretion described above remain unknown. However, active MMP9 has previously been shown to cleave both TNF and IL1B from their membrane bound pro-form to their soluble active form.[150, 182] Given that an ELISA will only detect soluble forms of these cytokines, LPS stimulated cells were treated with both HNE and the MMP9 inhibitor, and culture medium was assayed for secreted TNFα and IL1B. As shown in Figure 60, the presence of the MMP9 inhibitor reduced the levels of TNF, but not IL1B. These results suggest that active MMP9 cleaves

TNF, which subsequently binds its receptor leading to signal transduction and, ultimately, *Mmp9* expression.

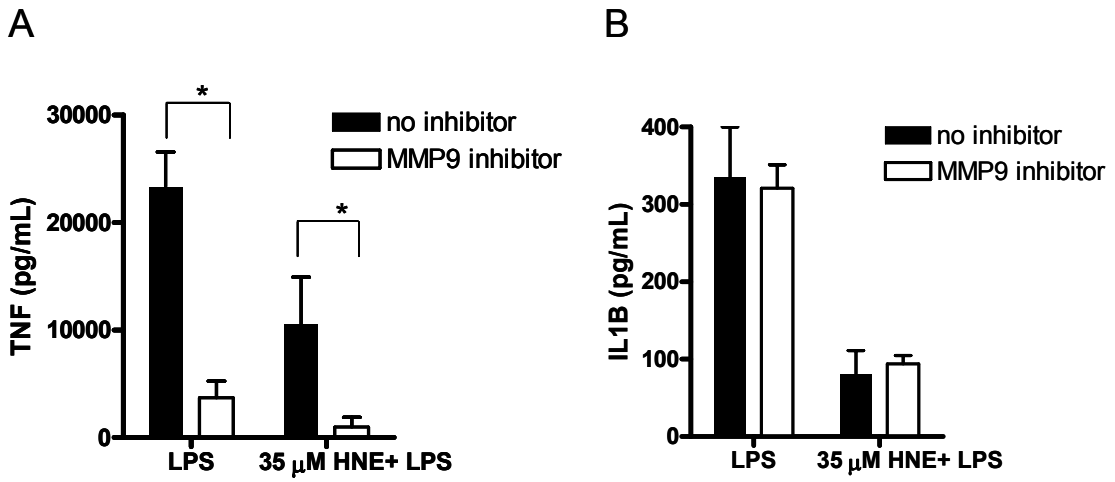

Figure 60. MMP9-mediated cytokine secretion. Stimulated cells were treated with HNE in the absence and presence of an MMP9 inhibitor. After 48 h (a) TNF and (b) IL1B secreted in the culture medium were assayed by ELISA ($\bar{X}$ ± stdev, n≥3). (black bars no MMP9 inhibitor, white bars MMP9 inhibitor). Asterisks represent significant ($p < 0.05$) changes.

Tnf-mediated Mmp9 expression

Although the level of TNF was lower then anticipated in HNE treated cells, there was still considerable amount of TNF secreted into culture medium. Given that TNFα signaling can contribute to *Mmp9* expression, neutralizing Tnfα antibodies were used to block soluble Tnfα from mediating signal transduction (Figure 61). Without any lipid peroxidation product present, neutralization decreased LPS mediated Mmp9 secretion nearly to that of unstimulated cells. In the presence of HNE, MMP9 was reduced, but still present in a much greater quantity than the LPS control. This indicates that TNF synergizes with other mediators for MMP9 secretion in HNE treated cells. Blocking TNFα in 15-HETE treated LPS stimulated cells reduced MMP9 protein to that of the LPS

control, demonstrating that MMP9 secretion in 15-HETE treated stimulated cells is a consequence of LPS signal transduction.

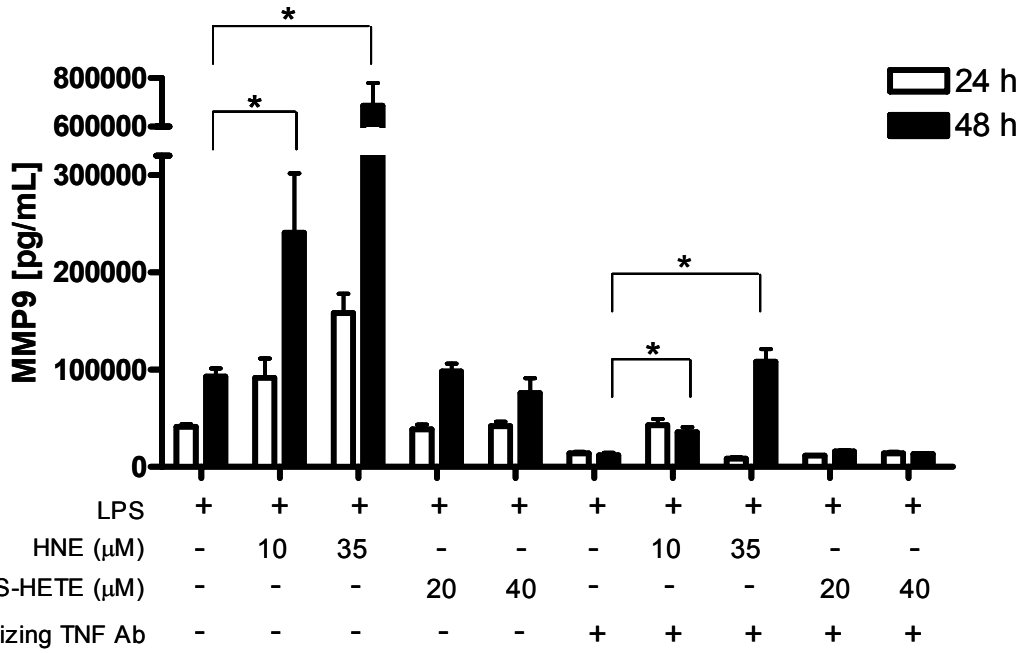

Figure 61. Cytokine mediated Mmp9 expression. RAW 264.7 cells were stimulated with 0.1 μg/mL LPS and treated with HNE or 15-HETE for 24 h (white bars) or 48 h (black bars) in the absence or presence of a neutralizing TNF antibody. MMP9 secreted in the culture medium was assayed by ELISA, and levels were determined using a standard curve prepared with recombinant mouse MMP9 ($\overline{X}$ ± stdev, n≥3). Asterisks represent significant ($p < 0.05$) changes.

Role of NF-κB and MAP Kinases in Mmp9 regulation

MMP9 is primarily regulated at the level of transcription by a number of pathways (i.e., NF-κB, p38, ERK1/2, and JNK), depending on cell type and source of stimulation; therefore, the specific signaling cascades leading to HNE-mediated MMP9 expression in RAW 264.7 cells were investigated. Prior to HNE treatment and LPS stimulation, cells were incubated with chemical inhibitors, namely PDTC, SP600125, U0126, or SB203580, to prevent signaling through NF-κB, JNK, ERK1/2, or p38, respectively. Inhibitor concentrations were chosen according to literature values and the

range was extended in both directions to ensure pathway inhibition. After 48 h, culture medium was assayed for MMP9 secretion. While inhibition of NF-κB and JNK had no effect on the level of MMP9 (Figure 62, A and B), ERK1/2 inhibition decreased the level of MMP9 detected in both LPS and HNE+LPS treated cells (Figure 62, C). Importantly, p38 inhibition only attenuated MMP9 secretion in the presence of HNE (Figure 62, D). In agreement with previous studies, HNE promoted the activation of p38,[110, 181] which synergized with ERK1/2 signaling mediated by LPS-stimulation.

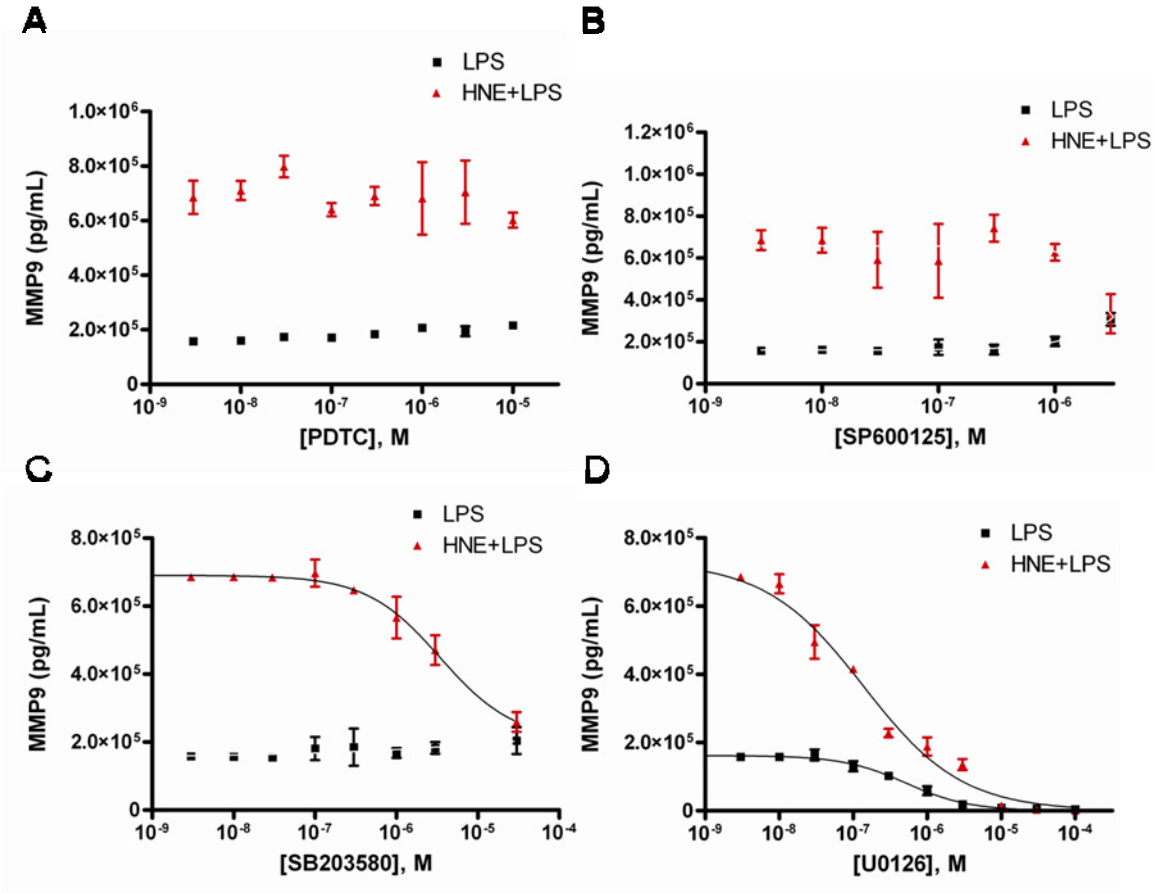

Figure 62. Effects of chemical inhibitors on MMP9 secretion. Cells were pre-treated with increasing concentrations of PDTC, SP600125, SB203580, and U0126 to inhibit NF-κB, JNK, p38, and ERK1/2, respectively. After 1.5 h, cells were treated with LPS in the absence or presence of 35 μM HNE for 48 h. Supernatant was assayed by ELISA to determine the level of secreted MMP9 ($\overline{X}$ ± stdev, n≥3).

Part 2: 4-Hydroxynonenal Impairs LPS-Mediated Expression of Inducible Nitric Oxide Synthase

Nitric oxide (NO) is a potent molecule that mediates several physiological responses including the degradation of foreign material within phagolysosomes via microbicidal burst. As demonstrated in *Chapter II*, however, RAW 264.7 cells incubated with HNE are unable to generate NO. Additionally, HNE was proven capable of altering the gene expression of several NF-kB pathway members, as was presented in Chapter III. Taken together, these results indicate that modulated NF-κB signaling impaired the generation of NO. Furthermore, these results suggest this NO deficiency as one possible explanation for the lack of Hz degradation within phagocytic cells.[60] In order to investigate the regulation of NO, RAW 264.7 and J774 macrophage-like cells were treated with increasing concentrations of HNE in order to monitor the effects on NF-κB pathway.

HNE impairs nitric oxide generation and inducible nitric oxide synthase expression in macrophage-like cells

RAW 264.7 and J774 macrophage-like cells were treated with increasing concentrations of HNE (0-35 μM) and immediately stimulated with LPS to activate NF-κB signal transduction. A time course of the effects of HNE on the generation of NO from macrophage-like cells is shown in Figure 63. While LPS stimulated NO in both model cell lines, incubation with HNE inhibited LPS-mediated NO production in a dose- and time-dependent manner. To determine whether inhibition of NO was a consequence of decreased iNOS expression, lysate was collected from LPS-stimulated cells cultured in the presence of HNE. In accord with the levels of NO detected at 24 h, Figure 64 shows

that iNOS expression is inhibited by HNE in a dose-dependent manner on both model cells lines.

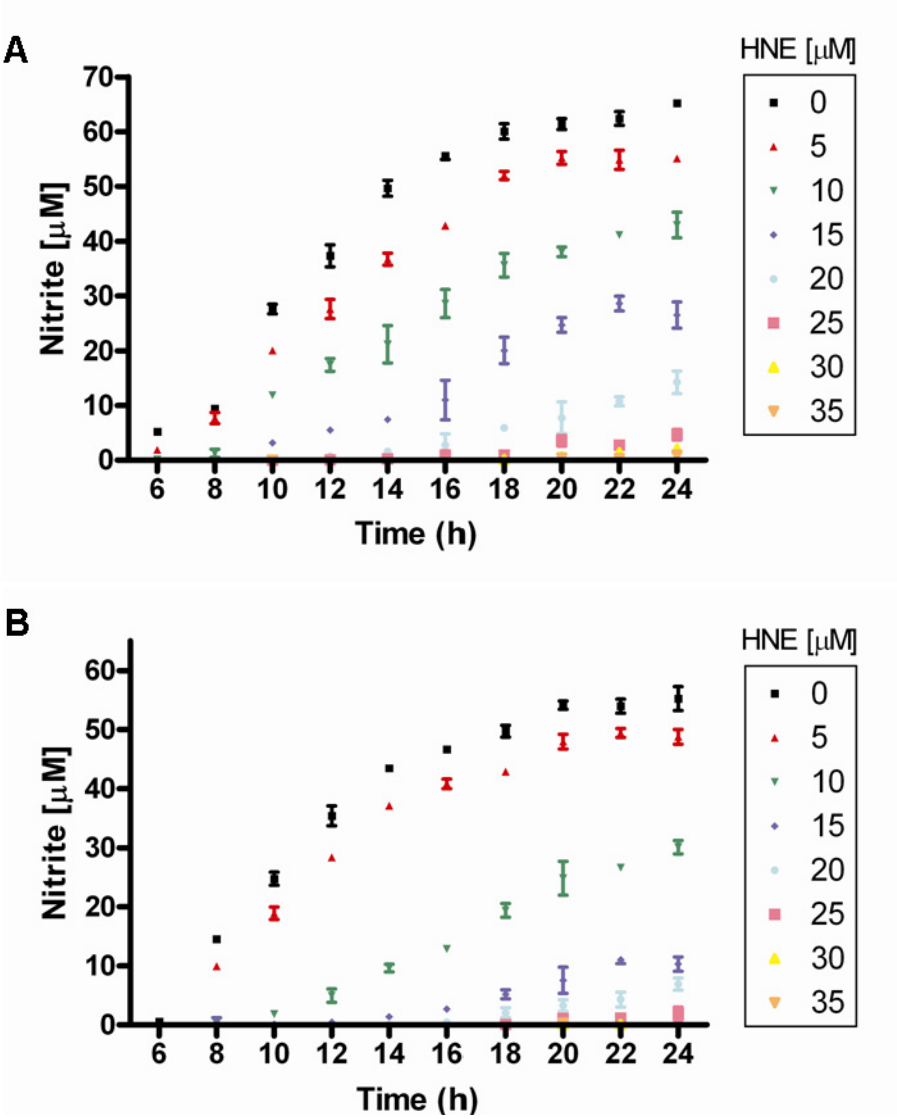

Figure 63. Time course of inhibition of NO production by HNE. (A) RAW 264.7 and (B) J774 macrophage-like cells were treated with HNE (0-35 μM) and immediately stimulated with LPS (1 μg/mL). Supernatants were collected every two hours and nitrite levels were determined via the Griess assay using a standard curve prepared with sodium nitrite ($\overline{X}$ ± stdev, n=3).

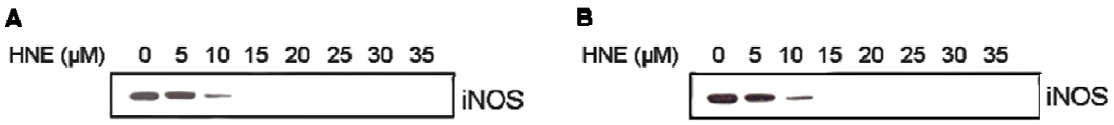

Figure 64**.** HNE impairs LPS-mediated iNOS expression. (A) RAW 264.7 and (B) J774 macrophage cells were treated with increasing concentrations of HNE and immediately stimulated with LPS to initiate NF-κB signaling. After 24 h, cells were lysed and the expression of iNOS within cytosolic extracts was assessed by immunobloting. Data are representative of at least 3 independent experiments.

HNE inhibits the phosphorylation and degradation of IκBα

LPS-mediated expression of iNOS signals through the NF-κB cascade. A critical step in this cascade is the tightly regulated degradation of IκB, a process that is initiated by phosphorylation of Ser-32 and -36 on IκBα and Ser-19 and -23 on IκBβ by the IκB Kinase (IKK) complex. In order to determine if iNOS expression is impaired as a result of impaired IκB degradation, the level of IκBα was assessed. Figure 65 (A and B) show that IκBα is degraded within 10 min of LPS stimulation in RAW 264.7 and J774 cells, respectively. In the presence of 35 μM HNE, however, degradation is inhibited. Since degradation is a direct consequence of IκB phosphorylation, levels of phosphorylated Ser-32 of IκB were determined using an antibody against phospho-Ser-32 of IκBα. As shown in Figure 65 (C and D), HNE treatment inhibits the phosphorylation of LPS-stimulated RAW 264.7 and J774 IκB, respectively. Thus, HNE appears to prevent IκB degradation through impaired IκB phosphorylation, in accord with impaired IκB phosphorylation and abolished NO generation in serum-deprived RAW 264.7 cells treated with HNE.[110]

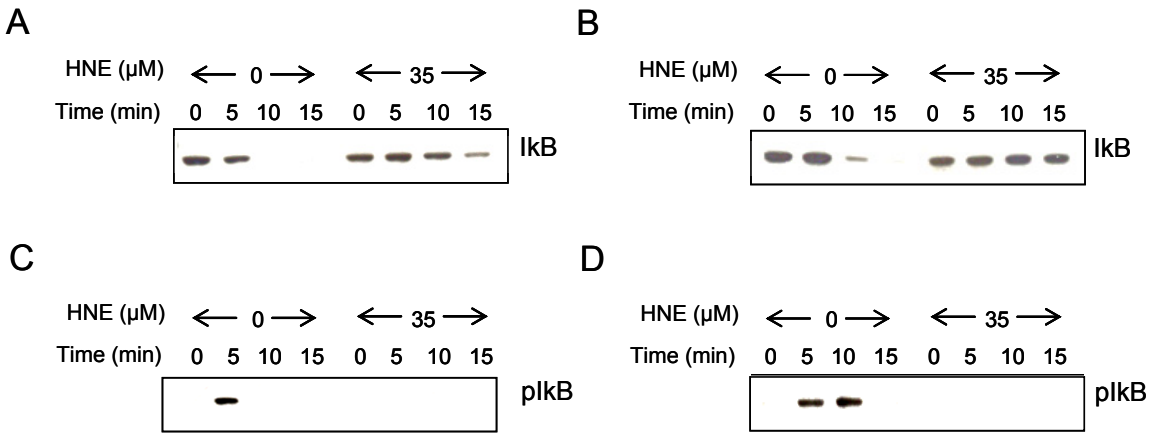

Figure 65. HNE inhibits LPS-mediated phosphorylation and degradation of IκBα. (A, C) RAW 264.7 and (B, D) J774 cells were untreated or treated with 35 μM HNE and stimulated with LPS for 0, 5, 10, or 15 min prior to lysing and the expression of total IκB and phosphorylated-IκB was determined by immunoblotting. Data are representative of at least 3 independent experiments.

Phosphorylation of IκB is mediated by an active IκB kinase (IKK) complex. This complex is composed of three subunits, namely IKKα, IKKβ (which comprise the catalytic domain), and IKKγ (which serves a regulatory function). Because IKK appears inactive in HNE-treated cells, a trend that has also been reported for cells exposed to acrolein[185] and 15-deoxyprostaglandin J_2[113, 186] which are structurally related to HNE, the levels of IKKα and IKKβ 2 h after HNE-treatment were assessed by immunoblotting. While IKKα and IKKβ levels appear stable, immunoblotting against reduced HNE-Michael adducts demonstrates HNE-modified protein in the molecular weight range of IKKα and IKKβ (Figure 66 A). Figure 66 B shows that 12 h after HNE-treatment IKKα protein decreases with increasing concentration of HNE, yet IKKβ maintains a stable level. Given that HNE-modified protein can be cleared from cells through degradation,[131] it was proposed that IKKα may be modified by HNE. The schematic shown in Figure 67

illustrates the workflow used to assess HNE-modified IKKα. Briefly, IKKα was purified from crude lysate by immunoprecipitation with an antibody against IKKα, and the IKKα eluent was examined for the presence of an HNE adduct by immunoblotting with an antibody against reduced HNE-Michael adducts. The results demonstrate that HNE does target IKKα in culture but provide no information regarding the site of HNE adduction.

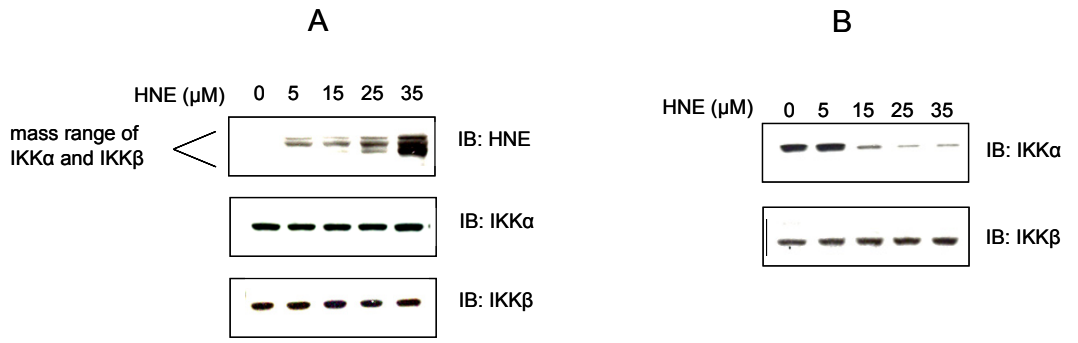

Figure 66. HNE alters IKK protein levels. RAW 264.7 cells were stimulated with LPS and treated with increasing concentrations of HNE (0-35 μM) (A) Immunoblots against HNE-modified protein, IKKα, and IKKβ 2 h after HNE treatment (B) Immunoblots against IKKα and IKKβ 12 h after HNE treatment.

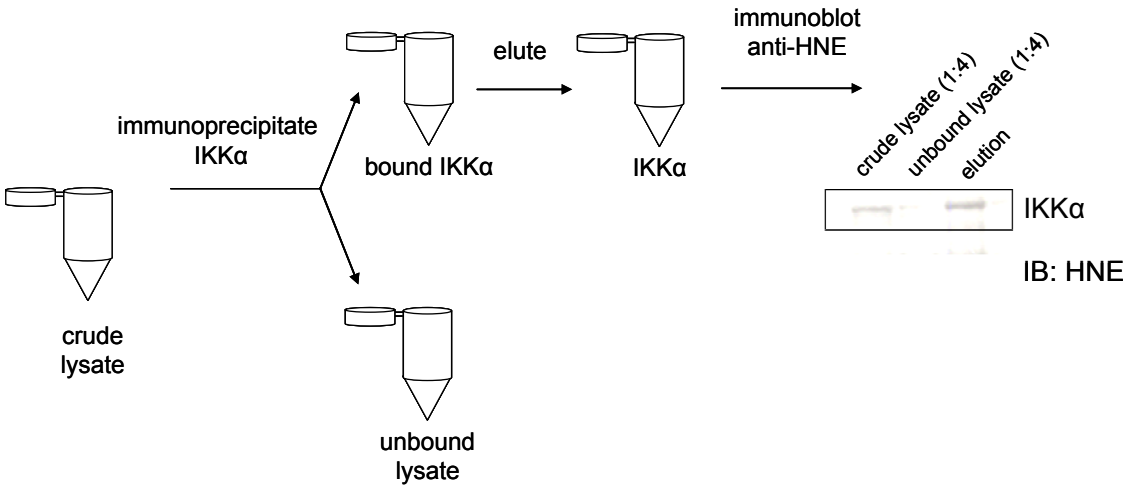

Figure 67. Scheme showing the identification of HNE-adducted IKKα. IKKα was purified from lysate using IKKα cross-linked magnetic beads. Bound IKKα was eluted, reduced to stabilize adducts, and immunoblotted using an antibody against reduced HNE Michael adducts.

HNE-IKK adduct mapping

Structurally, IKKα and IKKβ are very similar (Figure 68): each subunit contains an N-terminal kinase domain, a leucine zipper region, and a C-terminal helix-loop-helix domain.[187] Previous studies using RAW 264.7 demonstrated that the activity both IKKα and -β is abolished in the presence of auranofin, a thiol-reactive metal compound, suggesting that both IKK subunits contain a sensitive cysteine residue.[179] The location of a sensitive cysteine within the activation loop of IKKβ was since demonstrated via site-directed mutagenesis; substitution of Cys-179 with alanine (C179A) reversed the activity of auranofin and several other inhibitory compounds in independent studies.[176, 177, 188] Consequently, Cys178 and Cys179 within the activation loops of IKKα and IKKβ, respectively, are potential targets of HNE adduction.

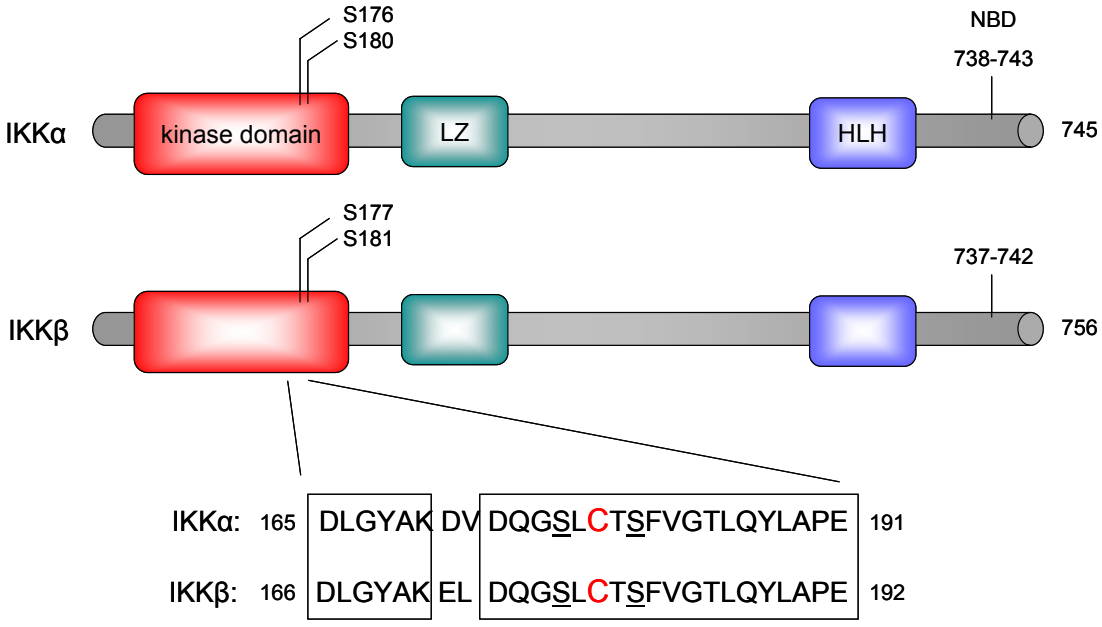

Figure 68. Schematic representation of IKKα and IKKβ and alignment of the activation loops. Phosphorylation sites that are critical for kinase activation are indicated and underlined. Invariant residues are boxed and putative HNE binding sites are colored red. Adapted from references 177 and 189.

Synthetic peptides representing tryptic cleavages of both activation loops were individually incubated with HNE for 3 h at 37ºC, reduced with $NaBH_4$, neutralized, and purified by reverse-phase HPLC. The ability of HNE to adduct the cysteine residues of both IKKα and IKK β peptides was investigated using mass spectrometry. Full scan MS analyses (Figure 69) demonstrated mass additions of 158 m/z for the molecular ions of both HNE-treated peptide samples, consistent with reduced HNE adduction via Michael addition (Table 8).

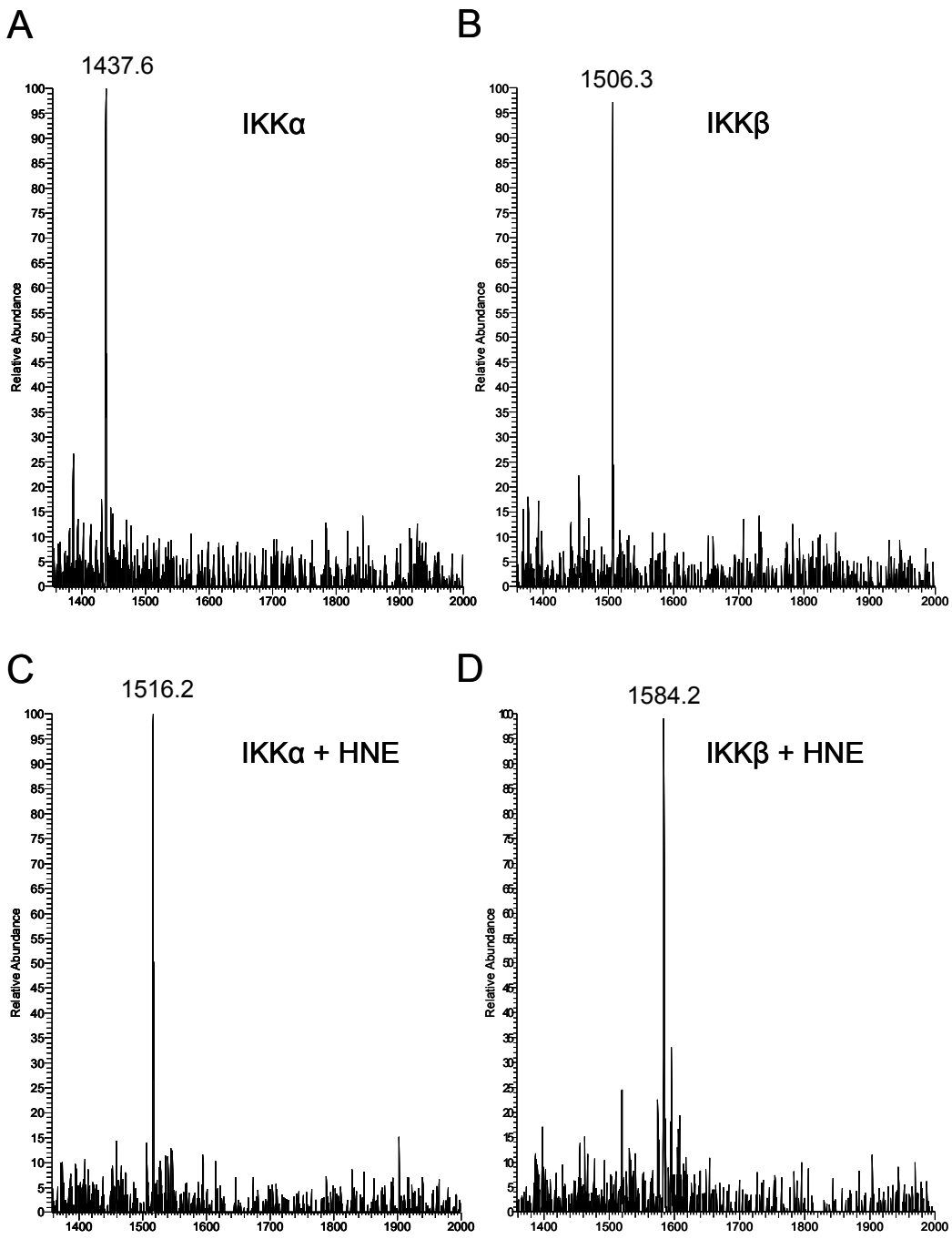

Figure 69. MS spectra of IKKα and IKKβ peptides. Full scan MS spectra were acquired for (A) IKKα peptide, (B) IKKβ peptide, (C) IKKα peptide incubated with HNE, and (D) IKKβ peptide incubated with HNE showing the doubly charged parent masses $[M+2H]^{2+}$. The mass increases of both peptides incubated with HNE are consistent with the addition of a single reduced Michael adduct (158 Da) on each parent peptide $[M+2H]^{2+}$.

Table 8. MS analysis of IKK activation loop peptides

Sample	Observed Molecular Ion (2+)	Predicted Molecular Ion (2+)
IKKα	1437.6	1437.7
IKKα + HNE	1516.2	1517.7
IKKβ	1506.3	1505.8
IKKβ + HNE	1584.2	1584.8

The molecular ions were selected to undergo CID, the product ions were scanned, and the fragmentation patterns were analyzed. MS/MS spectra of the IKKα peptide DVDQGSLCTSFVGTLQYLAPELFENK and IKKβ peptide ELDQGSLCTSFVGTLQYLAPELLEQQK incubated with HNE are shown in Figures 70 and 71, respectively. Given the high molecular weight of these tryptic peptides, low molecular weight species (<20% of the precursor m/z) were unable to be identified due to the low mass cutoff inherent to ion traps. However, inspection of the fragmentation patterns confirms an HNE adduct on the cysteine residue of both peptides: there is an addition of 158 Da on all b-ions C-terminal to the modified residue, and on all y-ions N-terminal to the modified residue. Fragmentation patterns of control peptides were assessed for comparison and used to validate the formation of an HNE adduct at both cysteine residues. Based upon these results, it was determined that cysteine-178 and cysteine-179 was modified with a reduced HNE Michael adduct.

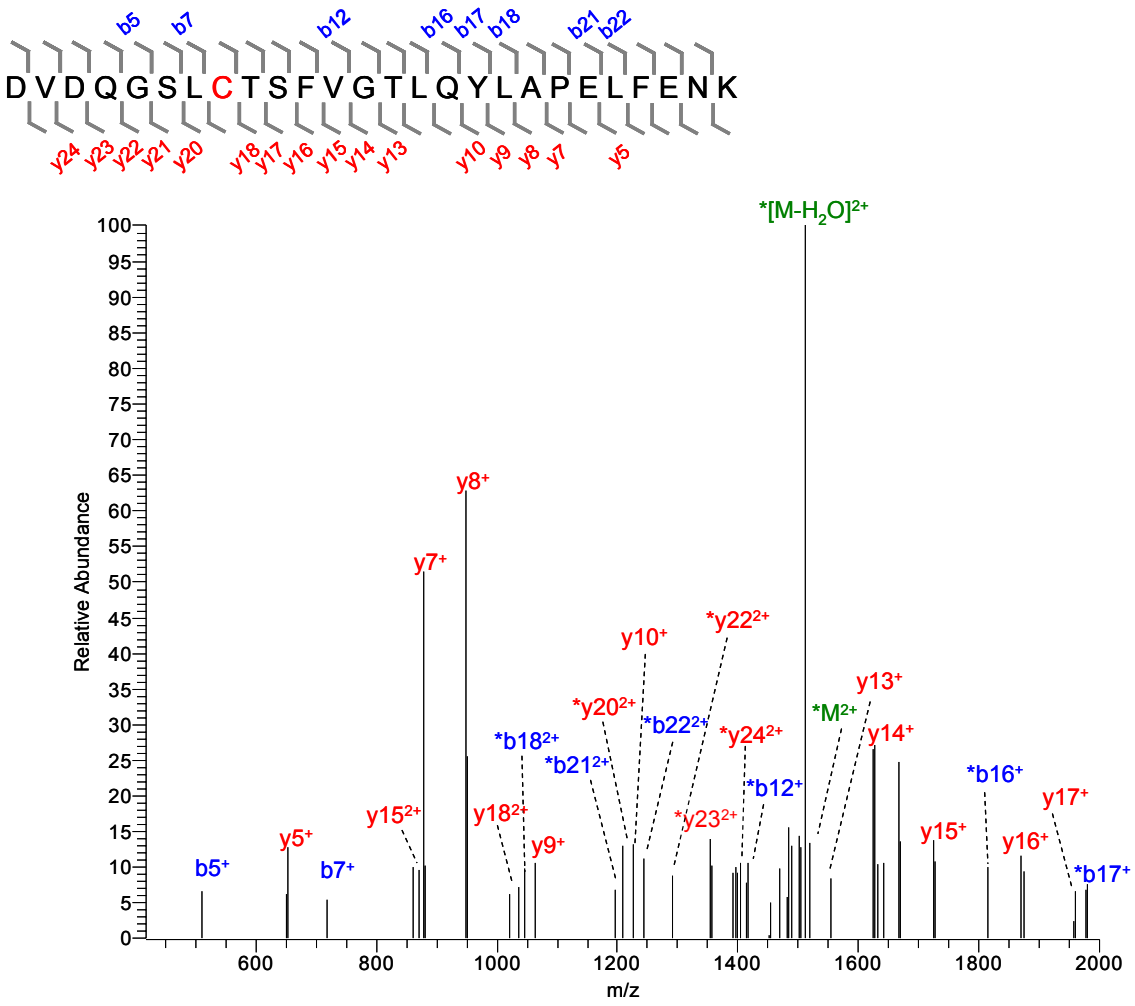

Figure 70. MS/MS spectrum of the synthetic peptide DVDQGSLCTSFVGTLQYLAPELFENK from IKKα incubated with HNE. The fragmentation pattern of the molecular ion $[M+2H]^{+2}$ 1516.2 is shown and is consistent with a reduced Michael adduct on the cysteine residue. Fragments containing an HNE-modified residue are indicated with an asterisk.

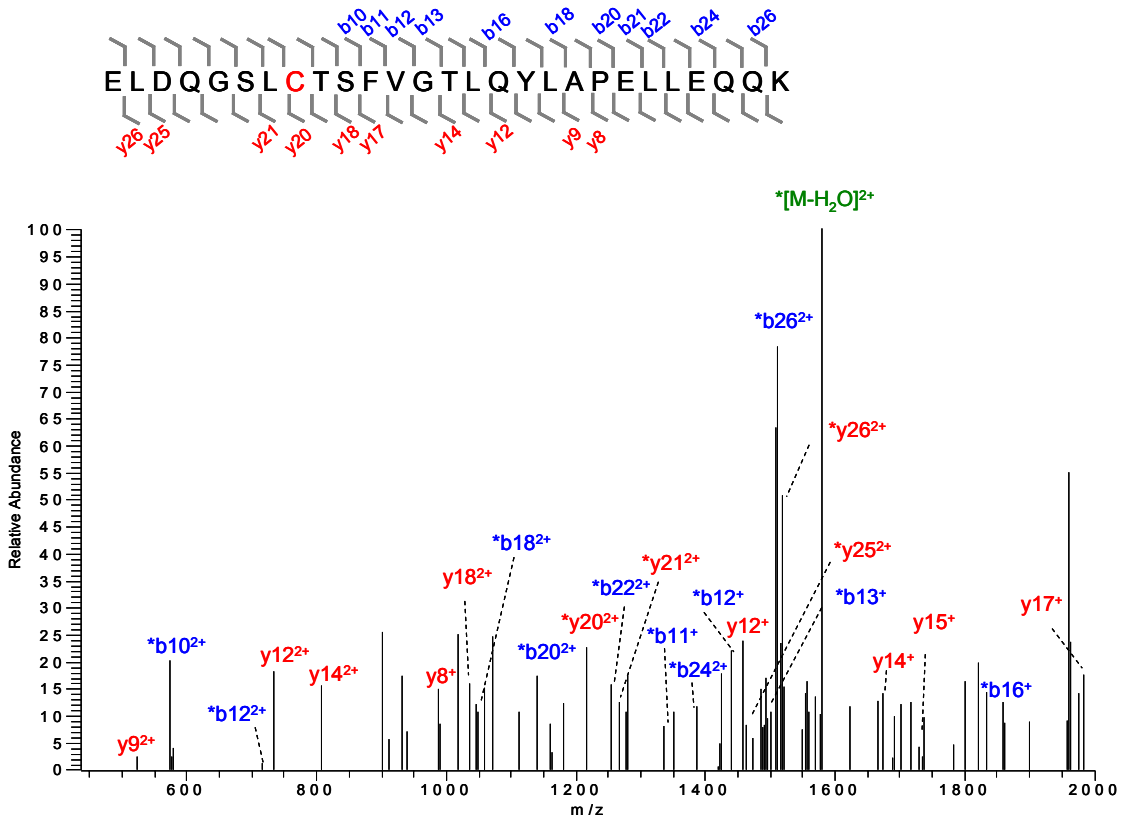

Figure 71. MS/MS spectrum of the synthetic peptide ELDQGSLCTSFVGTLQYLAPELLEQQK from IKKβ incubated with HNE. The fragmentation pattern of the molecular ion $[M+2H]^{+2}$ 1584.2 is shown and is consistent with a reduced Michael adduct on the cysteine residue. Fragments containing an HNE-modified residue are indicated with an asterisk.

Conclusions

It is generally accepted that lipid peroxidation products associated with native Hz are a major contributor of Hz activity. Consistent with these results, HNE has been reported to differentially influence signal transduction.[71] The data presented within this chapter provide insight regarding the biological activity of HNE and its ability to stimulate (e.g., p38 MAPK) as well as inhibit (e.g., NF-κB) immune responses. The

ability of Hz to enhance MMP9 activity[146] and the altered expression of several genes involved in *Mmp9* regulation by HNE[44] prompted exploration of the roles of lipid peroxidation products on MMP9 activity. The studies presented in *Part I* indicated that HNE, not 15-HETE, alters MMP9 regulation at multiple levels in activated immune cells (Figure 72). Stimulation of MMP9 by HNE occurs at the transcriptional level, primarily by the p38 MAPK cascade. Simultaneously, the expression of MMP9's cognate inhibitor, TIMP1, is severely repressed by HNE, thus enhancing the activity of MMP9. *Timp1* is regulated by STAT3 signaling,[190, 191] and *Stat3* (along with *Stat1* and *Stat5*) is differentially expressed in response to HNE (Table 2). Therefore, altered expression of STAT3 may be responsible for repressed levels of TIMP1. Altered *Mmp9* and *Timp1* expression changes indicate an imbalance in favor of ECM destruction.[146] Inhibition of active MMP9 decreased shedding of TNFα and repressed MMP9 secretion, indicating that active MMP9 participates in a positive feedback cycle. These results suggest possible mechanisms mediating ECM degradation in CM and other pathogeneses where lipid peroxidation is active.

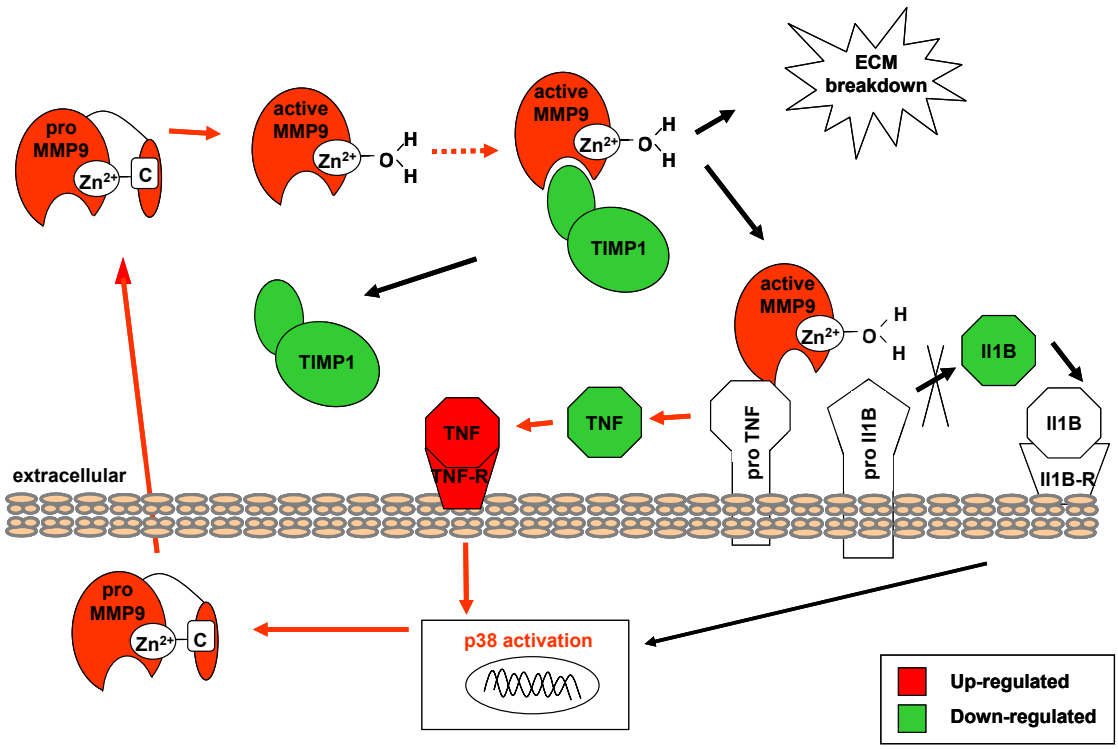

Figure 72. Schematic depicting the proposed mechanism of MMP9 regulation by HNE in LPS-stimulated RAW 264.7 macrophage-like cells. p38 MAPK synergizes with LPS-mediated ERK1/2 MAPK signaling initiating a positive feedback cycle: MMP9 secreted into the extracellular matrix (ECM) is in a pro-form. Upon cleavage of the cysteine-switch motif, MMP9 becomes activated. Repressed expression of *Timp1* results in basal levels of TIMP1 and, therefore, no inhibition of active MMP9. Active MMP9 cleaves TNF from its membrane-bound form to produce a soluble cytokine that enhances *Mmp9* expression.

Studies described in *Part II* demonstrate that the production of NO, which is essential for robust microbicidal burst and innate immune activity, is inhibited by HNE. Data support that HNE inhibits murine macrophage NF-κB signaling at level of IKK activity (Figure 73). The lack of IκB degradation results in inhibition of NF-κB translocation, a trend observed in H1299 and Jurkat T cells,[74] and impaired NF-κB-mediated iNOS expression and NO production. The ability of HNE to modulate enzyme activity is well-established* and provides a rational explanation for the inactivation of IKK. The identification of sensitive cysteines within the activation loop of IKKα and

IKKβ suggest that HNE can impair IKK activity through the formation of adducts within the kinase domain. Furthermore, other cysteine residues (in addition to histidine and lysine) of IKK are also potential targets for modification that may result in IKK inactivation.

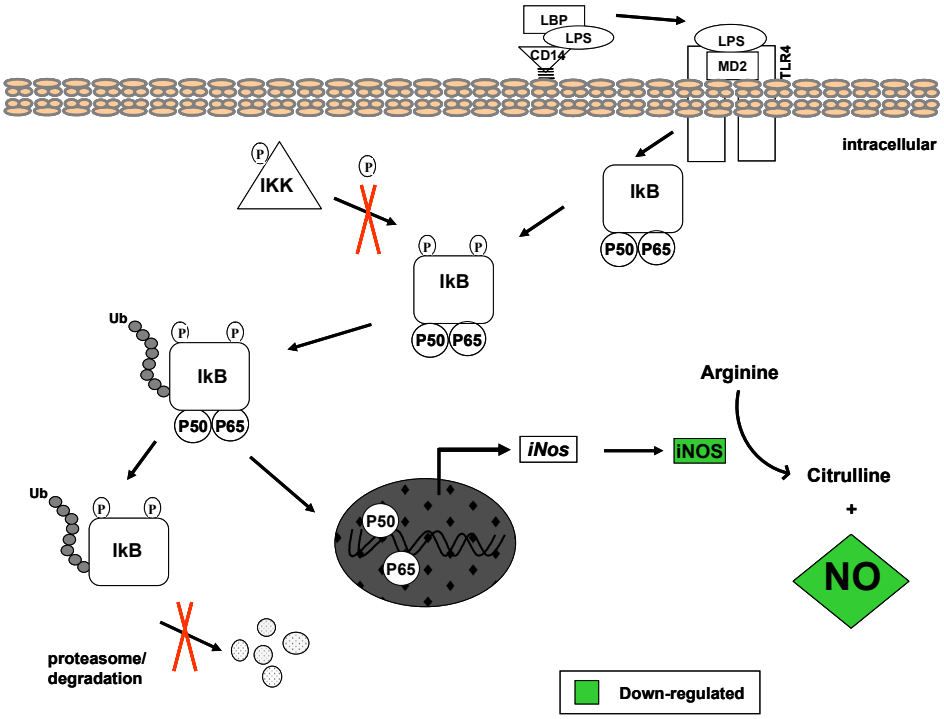

Figure 73. Schematic depicting the proposed mechanism of NF-κB inhibition in LPS-stimulated RAW 264.7 and J774 macrophage-like cells. LPS mediates the activation of IKK and subsequent phosphorylation of IκB. Release and degradation of IκB liberates NF-κB to mediate the expression of iNOS and, therefore, generation of NO. Treatment of cells with HNE, however, prevents the phosphorylation of IκB and all downstream signal transduction. Evidence indicates that HNE directly inhibits the activity of IKK through the formation of an adduct, likely in the activation loop of the IKK's kinase domain.

Synopsis and Future Directions

In the preceding chapters, the biological activity of fatty acid oxidation products was explored in the context of macrophage immunomodulation. BH was shown to

mediate non-enzymatic lipid peroxidation resulting in the formation of HNE, HETEs, isoketals, and ghost membrane-derived oxidation products. The global responses to BH, HNE and 15-HETE were identified, and gene expression alterations suggested that HNE was likely a major source of Hz's activity. Finally, the ability of HNE to simultaneously stimulate and inhibit signal transduction pathways was demonstrated. These results provide a wealth of knowledge about the heme moiety, HNE, and 15-HETE and their activity on macrophage-like cells, however, they also highlight several research challenges. While the effects of several constituent components of composite Hz on LPS-stimulated cells are presented in this dissertation, the response to Hz during infection is exponentially more complicated with multiple stimuli activating innate immune cells and synergism occurring between biologically active species. Several studies are currently underway: the mechanisms leading to HNE-mediated repression of TIMP1 mRNA and protein (presented in Chapter IV Part I) are being examined, and IKK protein is being mapped for HNE adduction sites (suggested by the immunoprecipitation studies presented in Chapter IV Part II). A more complete understanding of the effects of individual Hz components should establish the molecular basis of native Hz mediated immunomodulation. Future research will likely be focused on integrating the complex, interacting pathways that govern immune responses by known, and as of yet unknown, components of Hz. Furthermore, this knowledge may provide the basis for new insights into approaches to treat malaria.

APPENDIX A

MALARIA-RELEVANT GENE EXPRESSION CHANGES

Selected genes that are associated with (A) specific genes or gene products correlated to malarial infection or (B) genes that are classified under specific overexpressed biological processes in malaria models that are modulated ≥1.8-fold by 35 μM HNE or 0.1 mg/mL BH at 6 or 24 h are listed in Tables 1-9. Each table includes the gene symbol, gene description, fold-change relative to LPS-stimulated cells, Probset ID number, and literature reference, if applicable.

Table 9. Selected genes up-regulated by 35 μM HNE at 6 h[a]

Gene Symbol	Description	Fold Change	Affymetrix Probeset ID	MGI Gene ID	Ref
Apoptosis[123.124]					
Dap	death-associated protein	1.8	10423498	1918190	
Dnase2a	deoxyribonuclease II alpha	1.8	10573461	1329019	
Sgpl1	sphingosine phosphate lyase 1	1.8	10369413	1261415	
Cell Cycle[124]					
Plk2	polo-like kinase 2 (Drosophila)	3.7	10407126	1099790	
Pdcd4	programmed cell death 4	3.6	10463997	107490	
Trp53inp1	transformation related protein 53 inducible nuclear pr	3.4	10503259	1926609	
Plekho1	pleckstrin homology domain containing, family O member 1	2.3	10500295	1914470	
Ccng1	cyclin G1	2.2	10385271	102890	
Riok3	RIO kinase 3	1.9	10453900	1914128	
Nek3	NIMA (never in mitosis gene a)-related expressed kinase 3	1.8	10577492	1344371	
Cell-Cell Signaling[123]					
Trpv4	transient receptor potential cation channel, subfamily V,	2.0	10532839	1926945	
Cldn11	claudin 11	1.8	10491313	106925	
Defense Response[123.124]					
Als2	amyotrophic lateral sclerosis 2 (juvenile) homologue (human)	2.0	10354979	1921268	
Nlrp10	NLR family, pyrin domain containing 10	1.9	10566709	2444084	
Immune Response[123.124]					
Procr	protein C receptor, endothelial	4.3	10477717	104596	
Sqstm1	sequestosome 1	3.2	10385572	107931	
Il7r	interleukin 7 receptor	3.1	10427628	96562	
Tnfrsf10b	tumor necrosis factor receptor superfamily, member 10b	2.4	10416230	1341090	

Table 9, continued.

Pglyrp3	peptidoglycan recognition protein 3	2.1	10493842	2685266	
Cd300lb	CD300 antigen like family member B	2.0	10392796	2685099	
Clec4d	C-type lectin domain family 4, member d	1.9	10541614	1298389	
Cd300a	CD300A antigen	1.9	10382438	2443411	
Inppl1	inositol polyphosphate phosphatase-like 1	1.9	10565996	1333787	
Icam1	intercellular adhesion molecule 1	1.8	10583519	96392	
Inflammatory Response[123.124]					
Pla2g7	phospholipase A2, group VII (platelet-activating factor a	3.2	10445293	1351327	
Lipa	lysosomal acid lipase A	2.9	10467139	96789	
Ly96	lymphocyte antigen 96	2.3	10344966	1341909	120
Nlrc4	NLR family, CARD domain containing 4	2.3	10452879	3036243	
Intracellular Protein Transport					
Zmat3	zinc finger matrin type 3	2.6	10497673	1195270	
Chml	choroideremia-like	2.0	10360460	101913	
Napb	N-ethylmaleimide sensitive fusion protein attachment protei	1.9	10488387	104562	
Metabolic Process[124]					
Blvrb	biliverdin reductase B (flavin reductase (NADPH))	3.6	10551347	2385271	121
Htatip2	HIV-1 tat interactive protein 2, homologue (human)	3.0	10553403	1859271	
Hbp1	high mobility group box transcription factor 1	2.9	10399897	894659	
Camk1d	Calcium	2.6	10479852	2442190	
Pgd	phosphogluconate dehydrogenase	2.4	10518570	97553	120
Mocos	molybdenum cofactor sulfurase	2.4	10454353	1915841	
Alox5ap	arachidonate 5-lipoxygenase activating protein	2.3	10527638	107505	120
Crot	carnitine O-octanoyltransferase	2.3	10528102	1921364	
Pik3cb	phosphatidylinositol 3-kinase, catalytic, beta polypeptide	2.3	10595924	1922019	

Table 9, continued.

Lpin1	lipin 1	2.2	10399478	1891340	
Gsr	glutathione reductase	2.1	10571274	95804	
Mtmr10	myotubularin related protein 10	2.1	10553897	2142292	
Ulk1	Unc-51 like kinase 1 (C. elegans)	2.1	10532472	1270126	
Calr3	calreticulin 3	2.0	10579691	1920566	
Atp6v1a	ATPase, H+ transporting, lysosomal V1 subunit A	1.9	10439566	1201780	
Aldh6a1	aldehyde dehydrogenase family 6, subfamily A1	1.9	10401473	1915077	
Ephx1	epoxide hydrolase 1, microsomal	1.9	10360684	95405	
Pgm2l1	phosphoglucomutase 2-like 1	1.9	10555303	1918224	
Adi1	Acireductone dioxygenase 1	1.9	10395058	2144929	
Pcyox1	prenylcysteine oxidase 1	1.9	10545910	1914131	
Hsd17b11	hydroxysteroid (17-beta) dehydrogenase 11	1.8	10531919	2149821	
Rpp38	Ribonuclease P	1.8	10479749	2443607	
Protein Folding[123]					
Dnajb4	DnaJ (Hsp40) homologue, subfamily B, member 4	4.9	10502823	1914285	
Fkbpl	FK506 binding protein-like	2.0	10444436	1932127	
Fkbp14	FK506 binding protein 14	1.8	10544885	2387639	
Regulation of Apoptosis[123]					
Serpinb9	serine (or cysteine) peptidase inhibitor, clade B, memb	2.5	10404429	106603	
Bid	BH3 interacting domain death agonist	2.2	10547531	108093	
Bcl2l11	BCL2-like 11 (apoptosis facilitator)	2.0	10475866	1197519	
Regulation of Transcription, DNA-Dependent[123]					
Zbtb20	zinc finger and BTB domain containing 20	**3.6**	10435789 10435769	1929213	
Creg1	cellular repressor of E1A-stimulated genes 1	3.5	10351347	1344382	120
Nr1d2	nuclear receptor subfamily 1, group D, member 2	3.2	10417734	2449205	

Table 9, continued.

Bhlhb3	basic helix-loop-helix domain containing, class B3	3.1	10549276	1930704	
Eid3	EP300 interacting inhibitor of differentiation 3	2.8	10365286	1913591	
Phf21a	PHD finger protein 21A	2.4	10474006	2384756	
Zscan29	zinc finger SCAN domains 29	2.4	10486712	2139317	
Myst1	MYST histone acetyltransferase 1	2.1	10557831	1915023	
Nfic	nuclear factor I	1.9	10371176	109591	
Maf1	MAF1 homologue (S. cerevisiae)	1.9	10424833	1916127	
Mafg	v-maf musculoaponeurotic fibrosarcoma oncogene family, prot	1.9	10393881	96911	
Mapk14	mitogen-activated protein kinase 14	1.8	10443391	1346865	120
Cep290	centrosomal protein 290	1.8	10366073	2384917	
Snapc5	small nuclear RNA activating complex, polypeptide 5	1.8	10586176	1914282	
Rxra	retinoid X receptor alpha	1.8	10470446	98214	
Bbx	bobby sox homologue (Drosophila)	1.8	10439854	1917758	
Response to Stress[123]					
Srxn1	sulfiredoxin 1 homologue (S. cerevisiae)	10.3	10477061	104971	
Gclm	glutamate-cysteine ligase , modifier subunit	7.4	10495763	104995	
Gsta1	glutathione S-transferase, alpha 1 (Ya)	**6.8**	10587323 10587331	1095417	
Hmox1	heme oxygenase (decycling) 1	6.0	10572897	96163	120 121
Dnajb4	DnaJ (Hsp40) homologue, subfamily B, member 4	5.3	10502823	1914285	
Adrb2	adrenergic receptor, beta 2	3.9	10459288	87938	
Prdx1	peroxiredoxin 1	**3.1**	10507328 10436048	99523	122
Idh1	isocitrate dehydrogenase 1 (NADP+), soluble	3.1	10355214	96413	
Hspa1b	heat shock protein 1B	2.6	10450367	99517	
Hspa4l	heat shock protein 4 like	2.1	10491780	107422	
Txnrd1	thioredoxin reductase 1	2.1	10365260	1354175	

Table 9, continued.

Hsph1	heat shock 105kDa/110kDa protein 1	2.1	10535904	10535904	120
G6pdx	glucose-6-phosphate dehydrogenase X-linked	2.0	10605338	105979	
Apex1	Apurinic	1.8	10414522	88042	
Ahsa2	AHA1, activator of heat shock protein ATPase homologue 2 (ye	1.8	10384672	1916133	
Signal Transduction[124]					
Kitl	kit ligand	3.9	10366052	96974	
Rasgrp3	RAS, guanyl releasing protein 3	3.7	10446965	3028579	
Cebpa	CCAAT	3.4	10552140	99480	
Olfr26	olfactory receptor 26	3.4	10584470	109309	
Nrp1	neuropilin 1	3.0	10576639	106206	
Plekhm1	pleckstrin homology domain containing, family M (with RU	3.0	10391918	2443207	
Cxcr4	chemokine (C-X-C motif) receptor 4	2.8	10357472	109563	
Ralgps1	Ral GEF with PH domain and SH3 binding motif 1	2.7	10481804	1922008	
Olfr933	olfactory receptor 933	2.5	10584479	3030767	
Rasgef1b	RasGEF domain family, member 1B	2.5	10531610	2443755	
Nkiras1	NFKB inhibitor interacting Ras-like protein 1	2.5	10412900	1916971	
Arhgap22	Rho GTPase activating protein 22	2.4	10413951	2443418	
Spa17	sperm autoantigenic protein 17	2.2	10592336	1333778	
Bcl6	B-cell leukemia	2.2	10438738	107187	120
Raf1	v-raf-leukemia viral oncogene 1	2.2	10547034	97847	
Tgfbr1	transforming growth factor, beta receptor I	2.1	10504817	98728	120
Rit1	Ras-like without CAAX 1	2.1	10493309	108053	
Calcoco1	calcium binding and coiled coil domain 1	2.1	10433057	1914738	
Arhgap27	Rho GTPase activating protein 27	2.0	10391895	1916903	
Csf1r	colony stimulating factor 1 receptor	2.0	10456071	1339758	

Table 9, continued.

Ick	intestinal cell kinase	1.9	10587299	1934157	
Srpk2	Serine	1.9	10528484	1201408	
Pld2	phospholipase D2	1.9	10377859	892877	
Cd36	CD36 antigen	1.9	10528207	107899	
Ptpra	protein tyrosine phosphatase, receptor type, A	1.9	10476163	97808	
Gnat3	guanine nucleotide binding protein, alpha transducing 3	1.9	10519905	3588268	
Mtss1	metastasis suppressor 1	1.8	10428857	2384818	
Lpar1	lysophosphatidic acid receptor 1	1.8	10513256	108429	
Tbc1d8b	TBC1 domain family, member 8B	1.8	10602020	1918101	
Cacna1a	calcium channel, voltage-dependent, P	1.8	10573348	109482	
Edg5	endothelial differentiation, sphingolipid G-protein-coupled	1.8	10591412	99569	
Translation					
Impact	imprinted and ancient	2.1	10454039	1098233	
Eif2c3	eukaryotic translation initiation factor 2C, 3	1.8	10516348	2446634	
Ubiquitin-Dependent Protein Catabolic Process[124]					
Gclc	glutamate-cysteine ligase, catalytic subunit	8.2	10587266	104990	120
Rnf128	ring finger protein 128	4.0	10602009	1914139	
Fbxl20	F-box and leucine-rich repeat protein 20	2.2	10390574	1919444	
Herc3	hect domain and RLD 3	2.1	10538658	1921248	
Map1lc3b	microtubule-associated protein 1 light chain 3 beta	2.1	10576056	1914693	
Fbxo31	F-box protein 31	1.8	10582231	1354708	
Fbxo30	F-box protein 30	1.8	10361748	1919115	
Fbxl17	F-box and leucine-rich repeat protein 17	1.8	10452430	1354704	
Rnf167	ring finger protein 167	1.8	10377927	1917760	
Ube4b	ubiquitination factor E4B, UFD2 homologue (S. cerevisiae)	1.8	10518642	1927086	

Table 9, continued.

Other					
Arrdc3	arrestin domain containing 3	7.0	10406407	2145242	
Zdhhc18	zinc finger, DHHC domain containing 18	2.9	10517070	3527792	120
Gabarapl 1	gamma-aminobutyric acid (GABA(A)) receptor-associated protein-like 1	2.8	10542200	1914980	120
Lrrfip2	leucine rich repeat (in FLII) interacting protein 2	1.8	10589723	1918518	

[a] Genes up-regulated ≥1.8-fold ($p \leq 0.01$) at 6 h in HNE-treated RAW 264.7 cells that are associated with (1) specific genes or gene products correlated to malarial infection or HNE exposure (references listed by gene in column 7), or (2) specific over-expressed biological processes in malaria models (references listed with ontology in column 1), are shown in the table. Fold changes (FC) represent the average of three independent biological experiments. **Bold** FC indicate that multiple probes gave analogous results (average FC is shown).

Table 10. Selected genes down-regulated by 35 μM HNE at 6 h[a]

Gene Symbol	Description	Fold Change	Affymetrix Probeset ID	MGI Gene ID	Ref
Apoptosis[123.124]					
Phlda1	pleckstrin homology-like domain, family A, member 1	-2.6	10366346	1096880	
Bcl2a1c	B-cell leukemia	-2.5	10589884	1278327	
Ddit4	DNA-damage-inducible transcript 4	-2.5	10369290	1921997	
Stk17b	Serine	-2.4	10354588	2138162	
Bcl2a1b	B-cell leukemia	**-2.3**	10587683 10587690 10595633	1278326	
Tnfaip8	tumor necrosis factor, alpha-induced protein 8	-2.2	10455647	2147191	
Xaf1	XIAP associated factor 1	-2.1	10378068	3772572	
Cell Cycle[124]					
Lif	leukemia inhibitory factor	-11.6	10373918	96787	
Plk1	polo-like kinase 1 (Drosophila)	-8.6	10557156	97621	
Kif11	kinesin family member 11	-8.3	10462796	1098231	
Anln	anillin, actin binding protein (scraps homologue, Drosophila)	-7.3	10591781	1920174	
Nuf2	NUF2, NDC80 kinetochore complex component, homologue (S. cerevisia)	-6.8	10359890	1914227	
Kif20b	kinesin family member 20B	-5.8	10462632	2444576	
Ccnb1	cyclin B1	**-5.3**	10411739 10562637 10515836	88302	
Ccna2	cyclin A2	-5.1	10497831	108069	
Sgol2	shugoshin-like 2 (S. pombe)	-4.8	10346365	1098767	
Cdca2	cell division cycle associated 2	-4.7	10421029	1919787	
Aspm	asp (abnormal spindle)-like, microcephaly associated (Drosophilia)	-4.5	10350392	1334448	
Ccnf	cyclin F	-4.1	10448506	102551	
Nek6	NIMA (never in mitosis gene a)-related expressed kinase 6	-4.1	10471844	1891638	
Fbxo5	F-box protein 5	-4.0	10361375	1914391	

Table 10, continued.

Mki67	antigen identified by monoclonal antibody Ki 67	-4.0	10568714	106035	
Cdc25c	cell division cycle 25 homologue C (S. pombe)	-3.9	10458195	88350	
Sgol1	shugoshin-like 1 (S. pombe)	-3.3	10451805	1919665	
Nek2	NIMA (never in mitosis gene a)-related expressed kinase 2	-3.2	10352767	109359	
Ccng2	cyclin G2	-3.1	10523297	1095734	
Spag5	sperm associated antigen 5	-3.1	10379127	1927470	
Bub1b	budding uninhibited by benzimidazoles 1 homologue, beta (S. cerevisia)	-2.9	10474769	1333889	
Smc4	structural maintenance of chromosomes 4	-2.7	10492558	1917349	
Gsg2	germ cell-specific gene 2	-2.6	10388234	1194498	
Cks2	CDC28 protein kinase regulatory subunit 2	**-2.5**	10353004 10405185 10424779	1913447	
Espl1	extra spindle poles-like 1 (S. C)	-2.5	10427166	2146156	
Ndc80	NDC80 homologue, kinetochore complex component (S. cerevisia)	-2.5	10452709	1914302	
Birc5	baculoviral IAP repeat-containing 5	-2.4	10382998	1203517	
Ercc6l	excision repair cross-complementing rodent repair deficient	-2.4	10606071	2654144	
Sass6	spindle assembly 6 homologue (C. elegans)	-2.4	10495574	1920026	
Cdkn2d	cyclin-dependent kinase inhibitor 2D (p19, inhibits CDK4)	-2.3	10591517	105387	
Cenpa	centromere protein A	-2.3	10520521	88375	
E2f8	E2F transcription factor 8	-2.3	10563780	1922038	
Sesn2	sestrin 2	-2.3	10516932	2651874	
Cdc25a	cell division cycle 25 homologue A (S. pombe)	-2.2	10589420	103198	
Dbf4	DBF4 homologue (S. cerevisiae)	-2.2	10528077	1351328	
Fancd2	Fanconi anemia, complementation group D2	-2.2	10540738	2448480	
Nusap1	nucleolar and spindle associated protein 1	-2.1	10474984	2675669	
Cks1b	CDC28 protein kinase 1b	-1.8	10499639	1889208	
Nsl1	NSL1, MIND kinetochore complex component, homologue S. cerev	-1.8	10352709	2685830	

Table 10, continued.

Cell-Cell Signaling[123]					
Pxk	PX domain containing serine	-3.3	10412624	1289230	
Agrn	agrin	-2.0	10519270	87961	
Dlg7	discs, large homologue 7 (Drosophila)	-1.9	10419323	2183453	
Metabolic Process[123]					
Hdc	Histidine decarboxylase	-8.8	10487238	96062	
Pbk	PDZ binding kinase	-4.6	10416037	1289156	
Abca1	ATP-binding cassette, sub-family A (ABC1), member 1	-4.5	10512949	99607	
Mmp9	matrix metalloproteinase 9	-4.1	10478633	97011	
Lipg	lipase, endothelial	-3.1	10459772	1341803	
Fgr	Gardner-Rasheed feline sarcoma viral (Fgr) oncogene homologue	-3.0	10508772	95527	
Dgkh	diacylglycerol kinase, eta	-2.2	10421774	2444188	
Neil3	nei like 3 (E. coli)	-2.2	10578690	2384588	
Src	Rous sarcoma oncogene	-2.2	10477970	98397	
Fbxo15	F-box protein 15	-2.0	10457077	1354755	
Fen1	flap structure specific endonuclease 1	-2.0	10465912	102779	
Alpk1	alpha-kinase 1	**-1.9**	10502042 10502050 10502052	1918731	
Cry2	cryptochrome 2 (photolyase-like)	-1.9	10485170	1270859	
Mthfs	5, 10-methenyltetrahydrofolate synthetase	**-1.9**	10587695 10595630	1340032	
Rara	retinoic acid receptor, alpha	-1.9	10381082	97856	
Anp32a	acidic (leucine-rich) nuclear phosphoprotein 32 family, m	-1.8	10586064	108447	
Nab2	Ngfi-A binding protein 2	-1.8	10373313		
Pdss1	prenyl (solanesyl) diphosphate synthase, subunit 1	-1.8	10469712	1889278	
Pgs1	phosphatidylglycerophosphate synthase 1	-1.8	10383012	1921701	
Psmb10	proteasome (prosome, macropain) subunit, beta type 10	-1.8	10581378	1096380	
Rad54l	RAD54 like (S. cerevisiae)	-1.7	10515257	894697	

Table 10, continued.

Cytokine and Chemokine Mediated Signaling Pathway[124]					
Stat1	signal transducer and activator of transcription 1	-2.2	10346191	103063	
Stat5a	signal transducer and activator of transcription 5A	-2.1	10381172	103036	
Stat3	signal transducer and activator of transcription 3	-2.0	10391301	103038	
Jak2	Janus kinase 2	-1.8	10462363	96629	
Defense Response[123.124]					
Mx2	myxovirus (influenza virus) resistance 2	-7.9	10437224	97244	
Saa3	serum amyloid A 3	-7.3	10563597	98223	
Ccr1	chemokine (C-C motif) receptor 1	-3.2	10598004	104618	
Sp110	Sp110 nuclear body protein	**-2.6**	10347928 10356278 10582874	1923364	
Hck	Hemopoietic cell kinase	-2.3	10477250	96052	
Penk1	preproenkephalin 1	-2.0	10511363	104629	
Sbno2	strawberry notch homologue 2 (Drosophila)	-2.0	10370721	2448490	
Immune Response[123.124]					
Il1a	interleukin 1 alpha	-67.1	10487588	96542	
Il6	interleukin 6	-46.9	10520452	96559	
Il1b	interleukin 1 beta	-33.7	10487597	96543	
Il1f6	interleukin 1 family, member 6	-12.8	10469793	1859324	
Cfb	Complement factor B	-7.4	10450325	105975	
H28	histocompatibility 28	-6.9	10502801	95975	
Il1rn	interleukin 1 receptor antagonist	-6.9	10469816	96547	
Il27	interleukin 27	-6.5	10567987	2384409	
Gbp5	guanylate nucleotide binding protein 5	-6.3	10496539	2429943	
Il10	interleukin 10	-5.4	10349603	96537	
Oasl2	2'-5' oligoadenylate synthetase-like 2	-5.1	10524621	1344390	
Clec2d	C-type lectin domain family 2, member d	-4.7	10542156	2135589	

Table 10, continued.

Rsad2	radical S-adenosyl methionine domain containing 2	-4.7	10399710	1929628	
Cd40	CD40 antigen	-4.3	10478678	88336	
Il1rl1	interleukin 1 receptor-like 1	-4.0	10345791	98427	
Cd300lf	CD300 antigen like family member F	-3.9	10392845	2442359	
Gbp3	guanylate nucleotide binding protein 3	-3.8	10496580	1926263	
Ccl6	chemokine (C-C motif) ligand 6	-3.4	10389222	98263	
Irf7	interferon regulatory factor 7	-3.4	10569102	1859212	
Gbp1	guanylate nucleotide binding protein 1	-3.1	10496555	95666	
Il18rap	interleukin 18 receptor accessory protein	-3.0	10345824	1338888	
Il4ra	interleukin 4 receptor, alpha	-2.9	10557326	105367	
Cxcl14	chemokine (C-X-C motif) ligand 14	-2.8	10409579	1888514	
Clec4n	C-type lectin domain family 4, member n	-2.7	10541605	1861231	
Irf8	interferon regulatory factor 8	-2.5	10576034	96395	
Il18	interleukin 18	-2.3	10585194	107936	
Pou2f2	POU domain, class 2, transcription factor 2	-2.1	10560964	101897	
Clec12a	C-type lectin domain family 12, member a	-2.0	10542164	3040968	
Clec5a	C-type lectin domain family 5, member a	-1.9	10544273	1345151	
Ercc1	excision repair cross-complementing rodent repair deficient	-1.8	10550650	95412	
Ltb	Lymphotoxin B	-1.8	10444752	104796	
Traf3ip2	Traf3 interacting protein 2	-1.8	10362615	2143599	
Inflammatory Response[123.124]					
Ccl2	chemokine (C-C motif) ligand 2	-47.2	10379511	98259	
Ccl7	chemokine (C-C motif) ligand 7	-22.6	10379518	99512	
Ccl22	chemokine (C-C motif) ligand 22	-13.0	10574213	1306779	
Fcgr2b	Fc receptor, IgG, low affinity IIb	-7.7	10360028	95499	
Fcgr1	Fc receptor, IgG, high affinity I	-4.4	10500335		

Table 10, continued.

Cd44	CD44 antigen	-2.7	10485405	88338	
Aoah	acyloxyacyl hydrolase	-2.3	10403871	1350928	
Ccl4	chemokine (C-C motif) ligand 4	-2.2	10379721	98261	
Cd86	CD86 antigen	-1.8	10439312	101773	
Jmjd3	jumonji domain containing 3	-1.8	10387372	2448492	
Intracellular Protein Transport					
Ap1s3	adaptor-related protein complex AP-1, sigma 3	-2.2	10355967	1891304	
Tacc3	transforming, acidic coiled-coil containing protein 3	-2.1	10521090	1341163	
Kpna2	karyopherin (importin) alpha 2	**-2.0**	10392284 10453512 10497503	103561	
Rffl	ring finger and FYVE like domain containing protein	-1.8	10389087	1914588	
Regulation of Apoptosis[123]					
Csf2	colony stimulating factor 2 (granulocyte-macrophage)	-14.0	10385912	1339752	
Bcl2l1	Bcl2-like 1	-3.7	10488655	88139	
Notch1	Notch gene homologue 1 (Drosophila)	-3.5	10481056	97363	
Casp4	caspase 4, apoptosis-related cysteine peptidase	-2.2	10582997	107700	
Casp7	caspase 7	-2.0	10464128	109383	
Hells	helicase, lymphoid specific	-2.0	10462973	106209	
Ier3	immediate early response 3	-2.0	10444890	104814	
Regulation of Transcription, DNA-Dependent[123]					
Trim30	tripartite motif-containing 30	-7.2	10566358	98178	
Mxd1	MAX dimerization protein 1	-4.7	10545921	96908	
Jdp2	Jun dimerization protein 2	-4.3	10397351	1932093	
Top2a	topoisomerase (DNA) II alpha	-3.7	10390707	98790	
Nfkbiz	nuclear factor of kappa light polypeptide gene enhancer i	-3.4	10439936	1931595	
Nr1d1	nuclear receptor subfamily 1, group D, member 1	-3.4	10390691	2444210	

Table 10, continued.

Axud1	AXIN1 up-regulated 1	-3.0	10597758	2387989	
Bhlhb2	basic helix-loop-helix domain containing, class B2	-3.0	10540472	1097714	
Osm	Oncostatin M	-3.0	10373912	104749	
Klf7	Kruppel-like factor 7 (ubiquitous)	-2.6	10355141	1935151	
Foxm1	forkhead box M1	-2.5	10542079	1347487	
Asf1b	ASF1 anti-silencing function 1 homologue B (S. cerevisiae)	-2.4	10573261	1914179	
Foxp1	forkhead box P1	-2.4	10546661	1914004	
Nr4a1	nuclear receptor subfamily 4, group A, member 1	-2.3	10427035	1352454	
Carhsp1	calcium regulated heat stable protein 1	**-2.1**	10437590 10497752	1196368	
Hivep3	human immunodeficiency virus type I enhancer binding prot	-2.0	10507677	106589	
Id1	inhibitor of DNA binding 1	-2.0	10477169	96396	
Zfp367	zinc finger protein 367	-2.0	10410092	2442266	
Plagl2	pleiomorphic adenoma gene-like 2	-1.9	10488697	1933165	
Zfp36	zinc finger protein 36	-1.9	10561453	99180	
Akna	AT-hook transcription factor	-1.8	10513666	2140340	
Arid5a	AT rich interactive domain 5A (Mrf1 like)	-1.8	10345445	2443039	
Batf2	basic leucine zipper transcription factor, ATF-like 2	-1.8	10460767	1921731	
Hivep2	human immunodeficiency virus type I enhancer binding prot	-1.8	10361807	1338076	
Hlx	H2.0-like homeobox	-1.8	10360834	96109	
Ikzf1	IKAROS family zinc finger 1	-1.8	10374333	1342540	
Nfkb1	nuclear factor of kappa light polypeptide gene enhancer in	-1.8	10502299	97312	
Nufip1	nuclear fragile X mental retardation protein interacting	-1.8	10416510	1351474	
Pcgf5	Polycomb group ring finger 5	-1.8	10462683	1923505	
Thra	thyroid hormone receptor alpha	-1.8	10381006	98742	
Response to Stress[123]					
F3	coagulation factor III	-5.6	10495675	88381	
Gen1	Gen homologue 1, endonuclease (Drosophila)	-5.2	10399391	2443149	

Table 10, continued.

Blm	Bloom syndrome homologue (human)	-3.4	10564978	1328362	
Ifi47	interferon gamma inducible protein 47	-3.0	10375515	99448	
Ddx58	DEAD (Asp-Glu-Ala-Asp) box polypeptide 58	-2.5	10512067	2442858	
Trip13	thyroid hormone receptor interactor 13	-2.4	10410560	1916966	
Dhx58	DEXH (Asp-Glu-X-His) box polypeptide 58	-2.2	10391207	1931560	
Polq	polymerase (DNA directed), theta	-2.2	10435581	2155399	
Ifih1	interferon induced with helicase C domain 1	-2.0	10483110	1918836	
Eme1	essential meiotic endonuclease 1 homologue 1 (S. pombe)	-1.9	10390050	3576783	
Atad5	ATPase family, AAA domain containing 5	-1.8	10379363	2442925	
Cry1	cryptochrome 1 (photolyase-like)	-1.8	10371400	1270841	
Rad51	RAD51 homologue (S. cerevisiae)	-1.8	10474902	97890	
Signal Transduction[124]					
Gpr109a	G protein-coupled receptor 109A	-10	10533720	1933383	
Edn1	Endothelin 1	-9.2	10404783	95283	
Rnd1	Rho family GTPase 1	-6.7	10432236	2444878	
Adora2b	adenosine A2b receptor	-5.5	10376832	99403	
Ms4a6c	membrane-spanning 4-domains, subfamily A, member 6C	-3.6	10461614	2385644	
Itgal	integrin alpha L	-3.1	10557591	96606	
Arhgef3	Rho guanine nucleotide exchange factor (GEF) 3	-3.0	10413419	1918954	
Bcar3	breast cancer anti-estrogen resistance 3	-3.0	10495781	1352501	
Cish	cytokine inducible SH2-containing protein	-3.0	10588577	103159	
Rassf2	Ras association (RalGDS	-2.9	10487894	2442060	
Arhgap11a	Rho GTPase activating protein 11A	-2.7	10485963	2444300	
Cysltr1	cysteinyl leukotriene receptor 1	-2.7	10606355	1926218	
Pscd4	pleckstrin homology, Sec7 and coiled	-2.6	10425092	2441702	
Mt2	metallothionein 2	-2.5	10574023	97172	
Itgam	integrin alpha M	-2.3	10557862	96607	

Table 10, continued.

Ms4a6d	Membrane-spannin 4-domains, subfamily A, member 6D	-2.3	10466210	1916024	
Wdr67	WD repeat domain 67	-2.2	10424221	2684931	
P2ry2	purinergic receptor P2Y, G-protein coupled 2	-2.1	10565962	105107	
Pik3cd	phosphatidylinositol 3-kinase catalytic delta polypeptide	-2.1	10518686	1098211	
Bcl3	B-cell leukemia	-2.0	10560685	88140	
Ccl17	chemokine (C-C motif) ligand 17	-2.0	10574226	1329039	
Fpr3	formyl peptide receptor 3	-2.0	10442098	1194495	
Irak3	interleukin-1 receptor-associated kinase 3	-2.0	10372781	1921164	
Eif2ak2	eukaryotic translation initiation factor 2-alpha kinase	-1.9	10452980	1353449	
Lyn	Yamaguchi sarcoma viral (v-yes-1) oncogene homologue	-1.9	10503098	96892	
Hus1	Hus1 homologue (S. pombe)	-1.8	10384322	1277962	
Per1	period homologue 1 (Drosophila)	-1.8	10377439	1098283	
Ptger4	prostaglandin E receptor 4 (subtype EP4)	-1.8	10427461	104311	
Translation[123.124]					
Denr	density-regulated protein	-2.3	10525657	1915434	
Ppp1r15b	protein phosphatase 1, regulatory (inhibitor) subunit 1	-1.8	10349868	2444211	
Ubiquitin-Dependent Protein Catabolic Process[124]					
Socs3	suppressor of cytokine signaling 3	**-5.1**	10383010 10393449	1201791	
Usp18	Ubiquitin specific peptidase 18	-3.7	10541307	1344364	
Tnfaip3	tumor necrosis factor, alpha-induced protein 3	-3.0	10368144	1196377	
Herc5	hect domain and RLD 5	-2.5	10538590	1914388	
Cdc20	cell division cycle 20 homologue (S. cerevisiae)	-2.2	10515744	1859866	
Isg15	ISG15 ubiquitin-like modifier	-2.2	10451287	1855694	
Ube2c	Ubiquitin-conjugating enzyme E2C	-2.0	10478572	1915862	
Uhrf1	ubiquitin-like, containing PHD and RING finger domains, 1	-1.9	10446074	1338889	
Rabgef1	RAB guanine nucleotide exchange factor (GEF) 1	-1.8	10526133	1929459	

Table 10, continued.

Ube2l6	ubiquitin-conjugating enzyme E2L 6	-1.8	10473356	1914500	
Usp37	Ubiquitin specific peptidase 37	-1.8	10355582	2442483	
Other					
Ifit2	interferon-induced protein with tetratricopeptide repeats 2	-6.5	10462613	99449	
Ifi205	interferon activated gene 205	-4.3	10360406	101847	
Ifit1	interferon-induced protein with tetratricopeptide repeats 1	-4.0	10462623	99450	
Ifi202b	interferon activated gene 202B	-3.9	10360398	1347083	
Ifi204	interferon activated gene 204	-3.9	10360382	96429	
Ifit3	interferon-induced protein with tetratricopeptide repeats 3	-3.8	10462618	1101055	
Ifi203	interferon activated gene 203	-3.7	10360391	96428	
Samsn1	SAM domain, SH3 domain and nuclear localization signals, 1	-3.5	10440393	1914992	
Ifitm2	interferon induced transmembrane protein 2	-1.9	10553299	1933382	

[a] Genes down-regulated ≤1.8-fold ($p \leq 0.01$) at 6 h in HNE-treated RAW 264.7 cells that are associated with specific over-expressed biological processes in malaria models (references listed with ontology in column 1) are shown in the table. Fold changes (FC) represent the average of three independent biological experiments. **Bold** FC indicate that multiple probes gave analogous results (average FC is shown).

Table 11. Selected genes down-regulated by 35 μM HNE at 24 h[a]

Gene Symbol	Description	Fold Change	ABI Probeset ID	MGI Gene ID
Apoptosis[123.124]				
Sgk	serum/glucocorticoid regulated kinase	-6.6	929684	1340062
Axud1	AXIN1 up-regulated 1	-1.8	907214	2387989
Cell Cycle[124]				
Slfn1	schlafen 1	-15.0	371033	1313259
Sass6	spindle assembly 6 homologue (C. elegans)	-4.6	881483	1920026
Nbn	Nibrin	-3.4	430613	1351625
Plekho1	pleckstrin homology domain containing, family O member 1	-2.4	624539	1914470
Als2cr2	amyotrophic lateral sclerosis 2 (juvenile) chromosome region, candidate 2 (human)	-2.3	358886	2144047
Pols	polymerase (DNA directed) sigma	-1.9	732359	2682295
Cell-Cell Signaling[123]				
Kif1b	kinesin family member 1B	-5.8	744344	108426
Tsc1	tuberous sclerosis 1	-3.1	550748	1929183
Gata3	GATA binding protein 3	-2.3	580073	95663
Ly6e	lymphocyte antigen 6 complex, locus E	-2.3	927958	106651
Metabolic Process[124]				
Avil	Advillin	-8.1	530983	1333798
Dio2	deiodinase, iodothyronine, type II	-6.9	738397	1338833
Cytokine and Chemokine Mediated Signaling Pathway[124]				
Stat1	signal transducer and activator of transcription 1	-10.8	433757	103063
Il6st	interleukin 6 signal transducer	-2.7	647028	96560
Defense Response[123.124]				
[1]	myxovirus (influenza virus) resistance 2	-43.4	837469	97244
Irgm	immunity-related GTPase family, M	-15.0	804608	107567
Dhx58	DEXH (Asp-Glu-X-His) box polypeptide 58	-7.9	659648	1931560
B2m	beta-2 microglobulin	-2.5	501966	88127

Table 11, continued.

Immune Response[123.124]				
Irf7	interferon regulatory factor 7	-51.3	345690	1859212
Ddx58	DEAD (Asp-Glu-Ala-Asp) box polypeptide 58	-17.4	439516	2442858
Ibrdc3	IBR domain containing 3	-2.2	695308	1922484
Inflammatory Response[123.124]				
Ccl5	chemokine (C-C motif) ligand 5	-22.7	516139	98262
Fcgr1	Fc receptor, IgG, high affinity I	-13.6	922856	95498
Il6	interleukin 6	-11.2	924312	96559
Fcgr2b	Fc receptor, IgG, low affinity IIb	-2.9	930585	95499
Ccl7	chemokine (C-C motif) ligand 7	-2.3	562485	99512
Regulation of Apoptosis[123]				
Ern1	endoplasmic reticulum (ER) to nucleus signalling 1	-12.3	749047	1930134
Tsc22d3	TSC22 domain family 3	-3.6	700170	1196284
Traf3	Tnf receptor-associated factor 3	-2.3	613464	108041
Casp1	Caspase 1	-2.0	924714	96544
Regulation of Transcription, DNA-Dependent[123]				
Gatad2b	GATA zinc finger domain containing 2B	-3.9	332294	2443225
Ssbp3	single-stranded DNA binding protein 3	-2.7	602705	1919725
Tspyl2	TSPY-like 2	-2.5	526767	106244
Usf2	upstream transcription factor 2	-2.1	532994	99961
Pcgf5	polycomb group ring finger 5	-2.1	315886	1923505
Zfp30	zinc finger protein 30	-2.0	919271	99178
Response to Stress[123]				
Gna13	Guanine nucleotide binding protein, alpha 13	-2.5	576697	95768
Insig2	insulin induced gene 2	-2.3	603014	1920249
Signal Transduction[124]				
Rassf8	Ras association (RalGDS/AF-6) domain family 8	-5.0	704046	1918573
Rgs1	regulator of G-protein signaling 1	-3.9	923224	1354694
Nr3c1	nuclear receptor subfamily 3, group C, member 1	-3.0	477364	95824
Tbc1d12	TBC1D12: TBC1 domain family, member 12	-2.6	360619	2384803
Spry1	Sprouty homologue 1 (Drosophila)	-1.9	404045	1345139

Table 11, continued.

Translation[123.124]				
Mknk1	MAP kinase-interacting serine/threonine kinase 1	-5.5	679668	894316
Eif2c2	eukaryotic translation initiation factor 2C, 2	-5.2	526883	2446632
Impact	imprinted and ancient	-4.4	627739	1098233
Eif2c3	eukaryotic translation initiation factor 2C, 3	-3.6	526537	2446634
Ubiquitin-Dependent Protein Catabolic Process[124]				
Usp18	ubiquitin specific peptidase 18	-100.0	446807	1344364
Fbxo39	F-box protein 39	-87.4	642750	3505735
Fem1c	Fem-1 homologue c (C.elegans)	-4.1	762818	2444737
Wsb2	WD repeat and SOCS box-containing 2	-2.6	740571	2144041
Ube2l6	ubiquitin-conjugating enzyme E2L 6	-2.3	401185	1914500
Sumo3	SMT3 suppressor of mif two 3 homologue 3 (yeast)	-2.0	463700	1336201
Fbxl20	F-box and leucine-rich repeat protein 20	-2.0	331560	1919444

[a] Genes down-regulated ≤1.8-fold ($p \leq 0.01$) at 24 h in HNE-treated RAW 264.7 cells that are associated with specific over-expressed biological processes in malaria models (references listed with ontology in column 1) are shown in the table. Fold changes (FC) represent the average of three independent biological experiments.

Table 12. Selected genes up-regulated by 35 μM HNE at 24 h[a]

Gene Symbol	Description	Fold Change	ABI Probeset ID	MGI Gene ID	Ref
Apoptosis[123.124]					
Pdcd8	programmed cell death 8	2.1	26926	1349419	
Stk3	serine/threonine kinase 3 (Ste20, yeast homologue)	1.9	56274	1928487	
Tnfaip8	tumor necrosis factor, alpha-induced protein 8	1.9	106869	2147191	
Cell Cycle[124]					
Nek2	NIMA (never in mitosis gene a)-related expressed kinase 2	17.0	18005	109359	
Psmc3ip	proteasome (prosome, macropain) 26S subunit, ATPase 3, interacting protein	6.4	19183	1098610	
Zbtb36	zinc finger and BTB domain containing 36	2.3	207259	2443302	
Atm	ataxia telangiectasia mutated homologue (human)	1.9	11920	107202	120
Cell-Cell Signaling[123]					
Dlg7	discs, large homologue 7 (Drosophila)	12.1	218977	2183453	
Wnt6	wingless-related MMTV integration site 6	4.4	22420	98960	
Cadps	Ca<2+>dependent activator protein for secretion	2.2	27062	1350922	
Hprt1	hypoxanthine guanine phosphoribosyl transferase 1	1.9	15452	96217	
Metabolic Process[124]					
Asf1b	ASF1 anti-silencing function 1 homologue B (S. cerevisiae)	9.7	66929	1914179	
Car12	carbonic anyhydrase 12	4.7	76459	1923709	
Defense Response[123.124]					
Cias1	cold autoinflammatory syndrome 1 homologue (human)	8.3	216799	2653833	
Ccl17	chemokine (C-C motif) ligand 17	3.1	20295	1329039	
Fgr	Gardner-Rasheed feline sarcoma viral (Fgr) oncogene homologue	2.8	14191	95527	
Immune Response[123.124]					
Csf3	colony stimulating factor 3 (granulocyte)	17.5	12985	1339751	

Table 12, continued.

Tnf	tumor necrosis factor	8.7	21926	104798	129 85 124 161
Clec5a	C-type lectin domain family 5, member a	5.0	23845	1345151	
Raet1e	retinoic acid early transcript 1E	3.8	379043	2675273	
Il10ra	Interleukin 10 receptor, alpha	3.7	340636	96538	120
Cxcl1	chemokine (C-X-C motif) ligand 1	2.7	14825	108068	
Nfam1	Nfat activating molecule with ITAM motif 1	**2.7**	623312 489525	1921289	
Tgfb1	transforming growth factor, beta 1	2.0	21803	98725	
Inflammatory Response[123.124]					
Pla2g7	phospholipase A2, group VII (platelet-activating factor acetylhydrolase, plasma)	10.7	27226	1351327	
C5r1	Complement component 5, receptor 1	3.4	338868	88232	120 121
Nlrc4	NLR family, CARD domain containing 4	2.7	268973	3036243	
Cd14	CD14 antigen	2.2	12475	88318	120
Intracellular Protein Transport[123]					
Nup85	Nucleoporin 85	3.3	445007	3046173	
Prdx1	peroxiredoxin 1	**2.9**	18477 545161	99523	122
Pcna	proliferating cell nuclear antigen	2.3	18538	97503	
Pex7	Peroxisome biogenesis factor 7	2.0	18634	1321392	
Nup210	Nucleoporin 210	1.9	54563	1859555	
Metabolic Process[124]					
Echdc3	enoyl Coenzyme A hydratase domain containing 3	5.4	67856	1915106	
Gnaq	guanine nucleotide binding protein, alpha q polypeptide	3.0	14682	95776	
Suclg1	succinate-CoA ligase, GDP-forming, alpha subunit	1.8	56451	1927234	
Protein Folding[123]					
Ppid	peptidylprolyl isomerase D (cyclophilin D)	3.3	67738	1914988	
Ppil1	peptidylprolyl isomerase (cyclophilin)-like 1	2.5	68816	1916066	
Regulation of Apoptosis[123]					
Birc5	baculoviral IAP repeat-containing 5	27.4	11799	1203517	
Mmp9	matrix metalloproteinase 9	5.2	17395	97011	120
Igf1	insulin-like growth factor 1	2.1	16000	96432	

Table 12, continued.

Regulation of Transcription, DNA-Dependent[123]					
Top2a	topoisomerase (DNA) II alpha	13.2	21973	98790	
Mcm6	minichromosome maintenance deficient 6 (MIS5 homologue, S. pombe) (S. cerevisiae)	6.0	17219	1298227	
Tbl1xr1	transducin (beta)-like 1X-linked receptor 1	3.5	81004	2441730	
Bzw1	basic leucine zipper and W2 domains 1	2.9	66882	1914132	
Hmga2	High mobility group AT-hook 2	2.1	15364	101761	
Response to Stress[123]					
Rad51	RAD51 homologue (S. cerevisiae)	16.4	19361	97890	
Pole	polymerase (DNA directed), epsilon	15.4	18973	1196391	
Sod2	superoxide dismutase 2, mitochondrial	9.1	20656	98352	120 121
Tacc3	transforming, acidic coiled-coil containing protein 3	7.3	21335	1341163	
Trip13	thyroid hormone receptor interactor 13	7.1	69716	1916966	
Msh5	mutS homologue 5 (E. coli)	6.1	17687	1329021	
Signal Transduction[124]					
Pilra	paired immunoglobin-like type 2 receptor alpha	13.5	640067	2450529	
Rasgrp3	RAS, guanyl releasing protein 3	4.4	240168	3028579	
Rab11a	RAB11a, member RAS oncogene family	4.3	53869	1858202	
Igbp1b	immunoglobulin (CD79A) binding protein 1b	2.8	50540	1354380	
Gpr183	G protein-coupled receptor 183	2.3	321019	2442034	
Translation[123.124]					
Eif4e	eukaryotic translation initiation factor 4E	4.2	13684	95305	
Eif4e2	eukaryotic translation initiation factor 4E member 2	3.4	26987	1914440	
Pa2g4	proliferation-associated 2G4	2.3	18813	894684	
Eif5a	eukaryotic translation initiation factor 5A	**1.9**	549097 925942	106248	
Pet112l	PET112-like (yeast)	1.8	229487	2442496	
Ubiquitin-Dependent Protein Catabolic Process[124]					
Ube2t	ubiquitin-conjugating enzyme E2T (putative)	7.1	67196	1914446	
Fbxo5	F-box only protein 5	4.4	67141	1914391	
Ggnbp1	gametogenetin binding protein 1	3.5	70772	3055306	

Table 12, continued.

Fbxo22	F-box only protein 22	3.0	71999	1926014	
Ube2i	ubiquitin-conjugating enzyme E2I	3.0	22196	107365	
Ube2d3	ubiquitin-conjugating enzyme E2D 3 (UBC4/5 homologue, yeast)	2.4	66105	1913355	
Bre	brain and reproductive organ-expressed protein	1.9	107976	1333875	
Other					
Gsn	Gelsolin	2.5	437857	95851	120
Rad23a	RAD23a homologue (S. cerevisiae)	2.2	330310	105126	120

[a] Genes up-regulated ≥1.8-fold ($p \leq 0.01$) at 24 h in HNE-treated RAW 264.7 cells that are associated with (1) specific genes or gene products correlated to malarial infection or HNE exposure (references listed by gene in column 7), or (2) specific over-expressed biological processes in malaria models (references listed with ontology in column 1) are shown in the table. Fold changes (FC) represent the average of three independent biological experiments. **Bold** FC indicate that multiple probes gave analogous results (average FC is shown).

Table 13. Selected genes up-regulated by 0.1 mg/mL BH at 6 h[a]

Gene Symbol	Description	Fold Change	Affymetrix Probeset ID	MGI Gene ID	Ref
Cell Cycle[124]					
Rps6ka2	ribosomal protein S6 kinase, polypeptide 2	2.6	10441565	1342290	
Plk2	polo-like kinase 2 (Drosophila)	2.2	10407126	1099790	
Plekho1	pleckstrin homology domain containing, family O member 1	1.9	10500295	1914470	
Immune Response[123.124]					
Fabp3	fatty acid binding protein 3, muscle and heart	**4.2**	10371502 10508614	95476	
F10	coagulation factor X	2.7	10570291	103107	
Il7r	interleukin 7 receptor	2.6	10427628	96562	
Hmox1	heme oxygenase (decycling) 1	2.5	10572897	96163	120 121
Aadacl1	arylacetamide deacetylase-like 1	1.9	10491083	2443191	
Eno2	enolase 2, gamma neuronal	1.8	10547807	95394	
Mtmr10	myotubularin related protein 10	1.8	10553897	2142292	
Signal Transduction[124]					
Gprc5a	G protein-coupled receptor, family C, group 5, member A	2.3	10542335	1891250	
Bcar3	breast cancer anti-estrogen resistance 3	1.9	10495781	1352501	
Plxna2	plexin A2	1.9	10352867	107684	
Adra1a	adrenergic receptor, alpha 1a	1.8	10416099	104773	
Plekhm1	pleckstrin homology domain containing, family M (with RU	1.8	10391918	2443207	
Gpr176	G protein-coupled receptor 176	1.7	10486102	2685858	
Other					
Slamf7	SLAM family member 7	3.4	10360173	1922595	121
Hk3	hexokinase 3	1.8	10409376	2670962	120

[a] Genes up-regulated ≥1.8-fold ($p \leq 0.01$) at 6 h in BH-treated RAW 264.7 cells that are associated with (1) specific genes or gene products correlated to malarial infection or HNE exposure (references listed by gene in column 7), or (2) specific over-expressed biological processes in malaria models (references listed with ontology in column 1) are shown in the table. Fold changes (FC) represent the average of three independent biological experiments. **Bold** FC indicate that multiple probes gave analogous results (average FC is shown).

Table 14. Selected genes down-regulated by 0.1 mg/mL BH at 6 h[a]

Gene Symbol	Description	Fold Change	ABI Probeset ID	MGI Gene ID
Immune Response[123.124]				
Csf2	colony stimulating factor 2 (granulocyte-macrophage)	-3.0	10385912	1339752
Il1rl1	Interleukin 1 receptor-like 1	-2.0	10345791	98427
Metabolic Process[124]				
Dusp2	dual specificity phosphatase 2	-1.8	10475782	101911
Gfod1	glucose-fructose oxidoreductase domain containing 1	-1.8	10408879	2145304
Phlda1	pleckstrin homology-like domain, family A, member 1	-1.8	10366346	1096880

[a] Genes down-regulated more than 1.8-fold ($p \leq 0.01$) at 6 h in BH-treated RAW 264.7 cells that are associated with specific over-expressed biological processes in malaria models (references listed with ontology in column 1) are shown in the table. Fold changes (FC) represent the average of three independent biological experiments.

Table 15. Selected genes down-regulated by 0.1 mg/mL BH at 24 h[a]

Gene Symbol	Description	Fold Change	ABI Probeset ID	MGI Gene ID
Cell Cycle[124]				
Hectd3	HECT domain containing 3	-70.8	567598	1923858
Smarcb1	SWI/SNF related, matrix associated, actin dependent regulator of chromatin, subfamily b, member 1	-3.0	889629	1328366
Mre11a	meiotic recombination 11 homologue A (S. cerevisiae)	-2.6	553944	1100512
Smc4l1	SMC4 structural maintenance of chromosomes 4-like 1 (yeast)	-2.1	789567	1917349
Camk2g	calcium/calmodulin-dependent protein kinase II gamma	-2.0	390021	88259
Camk2b	calcium/calmodulin-dependent protein kinase II, beta	-1.9	868597	88257
Cell-Cell Signaling[123]				
Rab3a	RAB3A, member RAS oncogene family	-2.1	914789	97843
Metabolic Process[124]				
Alas2	aminolevulinic acid synthase 2, erythroid	-9.3	880116	87990
Rpap1	RNA polymerase II associated protein 1	-7.8	587339	1916175
Pdgfb	platelet derived growth factor, B polypeptide	-6.0	788848	97528
Pomt1	protein-O-mannosyltransferase 1	-3.4	914042	2138994
Regulation of Apoptosis[123]				
Tnfsf13b	Tumor necrosis factor (ligand) superfamily, member 13b	-4.7	386868	1344376
Bok	Bcl-2-related ovarian killer protein	-4.3	364104	1858494
Regulation of Transcription, DNA-Dependent[123]				
Setdb1	SET domain, bifurcated 1	-47.8	751594	1934229
Fos	FBJ osteosarcoma oncogene	-3.6	463565	95574
Esrra	estrogen related receptor, alpha	-2.6	923547	1346831
Yeats2	YEATS domain containing 2	-2.0	654721	2447762
Asxl2	additional sex combs like 2 (Drosophila)	-1.9	540321	1922552

Table 15, continued.

Signal Transduction[123]				
Wfikkn2	WAP, follistatin/kazal, immunoglobulin, kunitz and netrin domain containing 2	-24.5	419373	2669209
Olfr112	olfactory receptor 112	-6.1	690941	2177495
Cdgap	Cdc42 GTPase-activating protein	-4.7	827470	1333857
Ms4a6b	membrane-spanning 4-domains, subfamily A, member 6B	-3.5	920843	1917024
Dner	delta/notch-like EGF-related receptor	-2.9	618695	2152889
Frag1	FGF receptor activating protein 1	-1.9	431551	2385286
Irf3	interferon regulatory factor 3	-1.8	925384	1859179
Translation[123.124]				
Eif2s3x	eukaryotic translation initiation factor 2, subunit 3, structural gene X-linked	-4.1	772876	1349431
Pars2	prolyl-tRNA synthetase (mitochondrial)(putative)	-1.9	606179	2386296
Ubiquitin-Dependent Protein Catabolic Process[124]				
Pja2	praja 2, RING-H2 motif containing	-50.5	656636	2159342
Ube2r2	ubiquitin-conjugating enzyme E2R 2	-2.6	546015	1914865

[a] Genes down-regulated more than 1.8-fold ($p \leq 0.01$) at 6 h in HNE-treated RAW 264.7 cells that are associated with specific over-expressed biological processes in malaria models (references listed with ontology in column 1) are shown in the table. Fold changes (FC) represent the average of three independent biological experiments.

Table 16. Selected genes up-regulated by 0.1 mg/mL BH at 24 h[a]

Gene Symbol	Description	Fold Change	ABI Probeset ID	MGI Gene ID	Ref
Cell Cycle[124]					
Ereg	Epiregulin	12.8	593765	107508	
Cops5	COP9 (constitutive photomorphogenic) homologue, subunit 5 (Arabidopsis thaliana)	1.9	330594	1349415	
Metabolic Process[124]					
Pcsk2	proprotein convertase subtilisin/kexin type 2	7.4	732125	97512	
Ppie	peptidylprolyl isomerase E (cyclophilin E)	3.6	530121	1917118	
Stard4	StAR-related lipid transfer (START) domain containing 4	3.1	551930	2156764	
Blvra	biliverdin reductase A	2.2	664457	88170	
Dusp14	dual specificity phosphatase 14	2.1	928759	1927168	
Immune Response[123.124]					
Il1a	interleukin 1 alpha	6.0	595893	96542	
Ccl6	chemokine (C-C motif) ligand 6	5.3	928327	98263	
Tollip	toll interacting protein	2.5	858428	1891808	
Il20	interleukin 20	2.4	879278	1890473	
H2-T23	histocompatibility 2, T region locus 23	2.2	558496	95957	
Intracellular Protein Transport[123]					
Srp9	signal recognition particle 9	2.1	927925	1350930	
Metabolic Process					
Gpt1	glutamic pyruvic transaminase 1, soluble	2.6	556768	95802	
Regulation of Transcription, DNA-Dependent[123]					
Irf4	Interferon regulatory factor 4	4.6	386166	1096873	
Taf7	TAF7 RNA polymerase II, TATA box binding protein (TBP)-associated factor	3.4	535868	1346348	
Rnpc2	RNA-binding region (RNP1, RRM) containing 2	3.0	528719	2157953	
Rqcd1	rcd1 (required for cell differentiation) homologue 1 (S. pombe)	1.8	686770	1928902	
Signal Transduction[124]					
Rab33a	RAB33A, member of RAS oncogene family	2.8	732409	109493	

Table 16, continued.

Olfr313	olfactory receptor 313	2.2	721885	3030147	
Gipc1	GIPC PDZ domain containing family, member 1	2.1	794773	1926252	
Rhebl1	Ras homolog enriched in brain like 1	1.9	456283	1916409	
Ubiquitin-Dependent Protein Catabolic Process[124]					
Rbx1	ring-box 1	3.2	494826	1891829	
Asb1	ankyrin repeat and SOCS box-containing protein 1	2.1	569408	1929735	
Ube2l3	ubiquitin-conjugating enzyme E2L 3	2.0	336987	109240	
Other					
Cd2	CD2 antigen	95.7	919536	88320	121 124
Pstpip2	proline-serine-threonine phosphatase-interacting protein 2	6.1	725778	1335088	120

[a] Genes up-regulated more than 1.8-fold ($p \leq 0.01$) at 6 h in HNE-treated RAW 264.7 cells that are associated with (1) specific genes or gene products correlated to malarial infection or HNE exposure (references listed by gene in column 7), or (2) specific over-expressed biological processes in malaria models (references listed with ontology in column 1) are shown in the table. Fold changes (FC) represent the average of three independent biological experiments.

Table 17. Common genes differentially regulated by 0.1 mg/mL BH and 35 μM HNE[a]

Gene Symbol	Description	Probe ID	Time (h)	Fold Change		MGI Gene ID
				BH	HNE	
Il1rl1	interleukin 1 receptor-like 1	10345791	6	-2.0	-4.0	98427
Phlda1	pleckstrin homology-like domain, family A, member 1	10366346	6	-1.8	-2.6	1096880
Csf2	colony stimulating factor 2 (granulocyte-macrophage)	10385912	6	-3.0	-14.0	1339752
Cd80	CD80 antigen	10435712	6	-1.8	-2.5	101775
Trem1	triggering receptor expressed on myeloid cells 1	10445746	6	-2.4	4.5	1930005
Dusp2	dual specificity phosphatase 2	10475782	6	-1.8	-2.0	101911
Plekhm1	pleckstrin homology domain containing, family M (with RU	10391918	6	1.8	3.0	2443207
Serpinb9b	serine (or cysteine) peptidase inhibitor, clade B, mem	10404439	6	2.2	2.8	894668
Plk2	polo-like kinase 2 (Drosophila)	10407126	6	2.2	3.7	1099790
Il7r	interleukin 7 receptor	10427628	6	2.6	3.1	96562
Abcc5	ATP-binding cassette, sub-family C (CFTR	10438478	6	2.3	3.0	1351644
Plekho1	pleckstrin homology domain containing, family O member 1	10500295	6	1.9	2.3	1914470
BC004044	cDNA sequence BC004044	10526853	6	1.9	3.6	2136853
Plxna1	plexin A1	10546184	6	1.9	2.4	107685
Mtmr10	myotubularin related protein 10	10553897	6	1.8	2.1	2142292
Hmox1	heme oxygenase (decycling) 1	10572897	6	2.5	6.3	96163
Slc6a8	solute carrier family 6 (neurotransmitter transporter, cr	10600210	6	2.0	2.6	2147834
Centa2	centaurin, alpha 2	638602	24	-2.6	-3.9	2663075
Ms4a6b	membrane-spanning 4-domains, subfamily A, member 6B	920843	24	-3.5	-4.0	1917024

Table 17, continued.

Olfr112	olfactory receptor 112	690941	24	-6.1	-2.4	2177495
Pdxk	pyridoxal (pyridoxine, vitamin B6) kinase	480631	24	-2.7	-2.7	1351869
Tmem26	transmembrane protein 26	604942	24	-12.3	-2.6	2143537
8030453 O 22Rik	RIKEN cDNA 8030453O22 gene	769847	24	2.0	2.0	1924459
Blvra	biliverdin reductase A	664457	24	2.2	1.8	88170
Ephx1	epoxide hydrolase 1, microsomal	907012	24	3.6	3.2	95405
Hmgb1	high mobility group box 1	900889	24	2.1	2.7	96113
Metapl1	methionine aminopeptidase-like 1	536468	24	2.8	1.9	1913809
Phb	Prohibitin	392862	24	2.2	2.5	97572
Tuba4	tubulin, alpha 4	509694	24	1.9	2.5	1095410

[a] Genes consistently regulated 1.8-fold up or down ($p \leq 0.01$) at 6 or 24 h in BH- and HNE-treated RAW 264.7 cells. Fold changes (FC) represent the average of three independent biological experiments.

REFERENCES

1. *Fact Sheet 94*; World Health Organization: 2009.

2. Greenwood, B.; Mutabingwa, T., Malaria in 2002. *Nature* **2002,** 415, 670-672.

3. Weissbuch, I.; Leiserowitz, L., Interplay between malaria, crystalline hemozoin formation, and antimalarial drug action and design. *Chem. Rev.* **2008,** 108, 4899-4914.

4. Tan, S. Y.; Sung, H., Carlos Juan Finlay (1833-1915): of mosquitoes and yellow fever. *Singapore Med. J.* **2008,** 49, 370-371.

5. Chernin, E., Sir Ronald Ross, malaria, and the rewards of research. *Med. Hist.* **1988,** 32, 119-41.

6. Baldacci, P.; Menard, R., The elusive malaria sporozoite in the mammalian host. *Mol. Microbiol.* **2004,** 54, 298-306.

7. Francis, S. E.; Sullivan, D. J.; Goldberg, D. E., Hemoglobin metabolism in the malaria parasite *Plasmodium falciparum*. *Annu. Rev. Microbiol.* **1997,** 51, 97-123.

8. Chen, J.; Henderson, G. I.; Freeman, G. L., Role of 4-hydroxynonenal in modification of cytochrome C oxidase in ischemia/reperfused rat heart. *J. Mol. Cell. Cardiol.* **2001,** 33, 1919-1927.

9. Slater, A. F. G.; Swiggard, W. J.; Orton, B. R.; Flitter, W. D.; Goldberg, D. E.; Cerami, A.; Henderson, G. B., An iron-carboxylate bond links the heme units of malaria pigment. *Proc. Natl. Acad. Sci. U.S.A.* **1991,** 88, 325-329.

10. Schmitt, T. H.; Wilson A. Frezzatti, J.; Schreier, S., Hemin-induced lipid membrane disorder and increased permeability: a molecular model for the mechanism of cell lysis. *Arch. Biochem. Biophys.* **1993,** 307, 96-103.

11. Gluzman, I. Y.; Francis, S. E.; Oksman, A.; Smith, C. E.; Duffin, K. L.; Goldberg, D. E., Order and specificity of the *Plasmodium falciparum* hemoglobin degradation pathway. *J. Clin. Invest.* **1994,** 93, 1602-1608.

12. Egan, T. J.; Combrinck, J. M.; Egan, J.; Hearne, G. R.; Marques, H. M.; Ntenteni, S.; Sewell, B. T.; Smith, P. J.; Taylor, D.; VanSchalkwyk, D. A.; Walden, J. C., Fate of haem iron in the malaria parasite *Plasmodium falciparum*. *Biochem. J.* **2002,** 365, 343-347.

13. Sullivan, D. J., Jr.; Gluzman, I. Y.; Russell, D. G.; Goldberg, D. E., On the molecular mechanism of chloroquine's antimalarial action. *Proc. Natl. Acad. Sci. U.S.A.* **1996,** 93, 11865-11870.

14. Tripathi, A. K.; Khana, S. I.; Walkera, L. A.; Tekwani, B. L., Spectrophotometric determination of de novo hemozoin/β-hematin formation in an in vitro assay. *Anal. Biochem.* **2004,** 325, 85-91.

15. Goldberg, D. E.; Slater, A. F.; Cerami, A.; Henderson, G. B., Hemoglobin degradation in the malaria parasite *Plasmodium falciparum*: an ordered process in a unique organelle. *Proc. Natl. Acad. Sci. U.S.A.* **1990,** 87, 2931-2935.

16. Slater, A. F.; Swiggard, W. J.; Orton, B. R.; Flitter, W. D.; Goldberg, D. E.; Cerami, A.; Henderson, G. B., An iron-carboxylate bond links the heme units of malaria pigment. *Proc. Natl. Acad. Sci. U.S.A.* **1991,** 88, 325 - 329.

17. Pagola, S.; Stephens, P. W.; Bohle, D. S.; Kosar, A. D.; Madsen, S. K., The structure of malaria pigment β–haematin. *Nature* **2000,** 404, 307-310.

18. Slater, A. F. G.; Cerami, A., Inhibition by chloroquine of a novel haem polymerase enzyme activity in malaria trophozoites. *Nature* **1992,** 355, 167-9.

19. Liang, K. C.; Lee, C. W.; Lin, W. N.; Lin, C. C.; Wu, C. B.; Luo, S. F.; Yang, C. M., Interleukin-1beta induces MMP-9 expression via p42/p44 MAPK, p38 MAPK, JNK, and nuclear factor-kappaB signaling pathways in human tracheal smooth muscle cells. *J. Cell. Physiol.* **2007,** 211, 759-770.

20. Dorn, A.; Vippagunta, S. R.; Matile, H.; Bubendorf, A.; Vennerstrom, J. L.; Ridley, R. G., A comparison and analysis of several ways to promote haematin (haem) polymerisation and an assessment of its initiation in vitro. *Biochem. Pharmacol.* **1998,** 55, 737-47.

21. Sullivan, D. J., Jr.; Gluzman, I. Y.; Goldberg, D. E., *Plasmodium* hemozoin formation mediated by histidine-rich proteins. *Science* **1996,** 271, 219-222.

22. Ziegler, J.; Chang, R. T.; Wright, D. W., Multiple-antigenic peptides of histidine-rich protein II of *Plasmodium falciparum*: dendrimeric biomineralization templates. *J. Am. Chem. Soc.* **1999,** 121, 2395-2400.

23. Sullivan, D. J., Theories on malarial pigment formation and quinoline action. *Int. J. Parasitol.* **2002,** 32, 1645-1653.

24. Bendrat, K.; Berger, B. J.; Cerami, A., Haem polymerization in malaria. *Nature* **1995,** 378, 138-139.

25. Jackson, K. E.; Klonis, N.; Ferguson, D. J. P.; Adisa, A.; Dogovski, C.; Tilley, L., Food vacuole-associated lipid bodies and heterogeneous lipid environments in the malaria parasite, *Plasmodium falciparum*. *Mol. Microbiol.* **2004,** 54, 109-122.

26. Pisciotta, J. M.; Sullivan, D., Hemozoin: oil versus water. *Parasitol. Int.* **2008,** 57, 89-96.

27. Egan, T. J., Recent advances in understanding the mechanism of hemozoin (malaria pigment) formation. *J. Inorg. Biochem.* **2008,** 102, 1288-1299.

28. Fitch, C. D.; Kanjananggulpan, P., The state of ferriprotoporphyrin IX in malaria pigment. *J. Biol. Chem.* **1987,** 262, 15552-15555.

29. Coppens, I.; Vielemeyer, O., Insights into unique physiological features of neutral lipids in *Apicomplexa*: from storage to potential mediation in parasite metabolic activities. *Int. J. Parasitol.* **2005,** 35, 597-615.

30. Slater, A. F.; Swiggard, W. J.; Orton, B. R.; Flitter, W. D.; Goldberg, D. E.; Cerami, A.; Henderson, G. B., An iron-carboxylate bond links the heme units of malaria pigment. *Proc. Natl. Acad. Sci. U.S.A.* **1991,** 88, 325 - 329.

31. Goldie, P.; Roth, E. F., Jr.; Oppenheim, J.; Vanderberg, J. P., Biochemical characterization of *Plasmodium falciparum* hemozoin. *Am. J. Trop. Med. Hyg.* **1990,** 43, 584-596.

32. Schwarzer, E.; Kuhn, H.; Valente, E.; Arese, P., Malaria-parasitized erythrocytes and hemozoin nonenzymatically generate large amounts of hydroxy fatty acids that inhibit monocyte functions. *Blood* **2003,** 101, 722-728.

33. Schwarzer, E.; Turrini, F.; Ulliers, D.; Giribaldi, G.; Ginsburg, H.; Arese, P., Impairment of macrophage functions after ingestion of *Plasmodium falciparum*-infected erythrocytes or isolated malarial pigment. *J. Exp. Med.* **1992,** 176, 1033-1041.

34. Biswas, S.; Karmarkar, M. G.; Sharma, Y. D., Antibodies detected against *Plasmodium falciparum* haemozoin with inhibitory properties to cytokine production. *FEMS Microbiol. Lett.* **2001,** 194, 175-179.

35. Jaramillo, M.; Gowda, D. C.; Radzioch, D.; Olivier, M., Hemozoin increases IFN-gamma-inducible macrophage nitric oxide generation through extracellular signal-regulated kinase- and NF-kappa B-dependent pathways. *J. Immunol.* **2003,** 171, 4243 - 4253.

36. Taramelli, D.; Basilico, N.; Pagani, E.; Grande, R.; Monti, D.; Ghione, M.; Olliaro, P., The heme moiety of malaria pigment (β-hematin) mediates the inhibition of nitric oxide and tumor necrosis factor-α production by lipopolysaccharide-stimulated macrophages. *Exp. Parasitol.* **1995,** 81, 501-511.

37. Bohle, D. S.; Helms, J. B., Synthesis of β-hematin by dehydrohalogenation of hemin. *Biochem. Biophys. Res. Commun.* **1993,** 193, 504-508.

38. Slater, A. F.; Swiggard, W. J.; Orton, B. R.; Flitter, W. D.; Goldberg, D. E.; Cerami, A.; Henderson, G. B., An iron-carboxylate bond links the heme units of malaria pigment. *Proc Natl Acad Sci USA* **1991,** 88, 325 - 329.

39. Blauer, G.; Akkawi, M., Investigations of B- and β–Hematin. *J. Inorg. Biochem.* **1997,** 66, 145-152.

40. Jaramillo, M.; Plante, I.; Ouellet, N.; Vandal, K.; Tessier, P. A.; Olivier, M., Hemozoin-inducible proinflammatory events in vivo: potential role in malaria infection. *J. Immunol.* **2004,** 172, 3101-3110.

41. Bohle, D. S.; Dinnebier, R. E.; Madsen, S. K.; Stephens, P. W., Characterization of the products of the heme detoxification pathway in malarial late trophozoites by X-ray diffraction. *J. Biol. Chem.* **1997,** 272, 713-716.

42. Bohle, D. S.; Kosar, A. D.; Stephens, P. W., Phase Homogeneity and crystal morphology of the malaria pigment β–hematin. *Acta Cryst.* **2002,** D58, 1752-1756.

43. Noland, G.; Briones, N.; Sullivan, D. J. J., The shape and size of hemozoin crystals distinguishes diverse *Plasmodium* species. *Mol. Biochem. Parasitol.* **2003,** 130, 91-99.

44. Schrimpe, A. C.; Wright, D. W., Comparative analysis of gene expression changes mediated by individual constituents of hemozoin. *Chem. Res. Toxicol.* **2009,** 22, 433–445.

45. McGuire, W.; Hill, A. V.; Allsopp, C. E.; Greenwood, B. M.; Kwiatkowski, D., Variation in the TNF-alpha promoter region associated with susceptibility to cerebral malaria. *Nature* **1994,** 371, 508–10.

46. Luty, A. J.; Perkins, D. J.; Lell, B., Low interleukin-12 activity in severe *Plasmodium falciparum* malaria. *Infect. Immun.* **2000,** 68, 3909–15.

47. Odeh, M., The role of tumour necrosis factor-alpha in the pathogenesis of complicated falciparum malaria. *Cytokine* **2001,** 14, 11 - 18.

48. Grau, G. E.; Taylor, T. E.; Molyneux, M. E.; Wirima, J. J.; Vassalli, P.; Hommel, M.; Lambert, P. H., Tumor necrosis factor and disease severity in children with *falciparum* malaria. *N. Engl. J. Med.* **1989,** 320, 1586 - 1591.

49. Pichyangkul, S.; Saengkrai, P.; Webster, H. K., *Plasmodium falciparum* pigment induces monocytes to release high levels of tumor necrosis factor-a and interleukin-1b. *Am. J. Trop. Med. Hyg.* **1994,** 51, 430-435.

50. Karunaweera, N. D.; Grau, G. E.; Gamage, P.; Carter, R.; Mendis, K. N., Dynamics of fever and serum levels of tumor necrosis factor are closely associated during clinical paroxysms in *Plasmodium vivax* malaria. *Proc. Natl. Acad. Sci. U.S.A.* **1992,** 89, 3200-3203.

51. Kwiatkowski, D.; Molyneux, M. E.; Stephens, S.; Curtis, N.; Klein, N.; Pointaire, P.; Smit, M.; Allan, R.; Brewster, D. R.; Grau, G. E.; Greenwood, B. M., Anti-TNF therapy inhibits fever in cerebral malaria *Q. J. Med.* **1993,** 86, 91-98.

52. Ramasamy, R., Molecular basis for evasion of host immunity and pathogensis in malaria. *Biochim. Biophys. Acta* **1998,** 1406, 10-17.

53. Urquhart, A. D., Putative pathophysiological interactions of cytokines and phagocytic cells in severe human falciparum malaria. *Clin. Infect. Dis.* **1994,** 19, 117-31.

54. Ochiel, D. O.; Awandare, G. A.; Keller, C. C.; Hittner, J. B.; Kremsner, P. G.; Weinberg, J. B.; Perkins, D. J., Differential regulation of B–chemokines in children with *Plasmodium falciparum* malaria. *Infect. Immun.* **2005,** 73, 4190-4197.

55. McCall, M. B. B.; Netea, M. G.; Hermsen, C. C.; Jansen, T.; Jacobs, L.; Golenbock, D.; van der Ven, A. J. A. M.; Sauerwein, R. W., *Plasmodium falciparum* infection causes proinflammatory priming of human TLR responses. *J. Immunol.* **2007,** 179, 162-171.

56. Prakash, D.; Fesel, C.; Jain, R.; Cazenave, P.-A.; Mishra, Gyan C.; Pied, S., Clusters of cytokines determine malaria severity in *Plasmodium falciparum* infected patients from endemic areas of central India. *J. Infect. Dis.* **2006,** 194, 198-207.

57. Mohanty, S.; Patel, D. K.; Pati, S. S.; Mishra, S. K., Adjuvant therapy in cerebral malaria. *Indian J. Med. Res.* **2006,** 124, 245-260.

58. Boutlis, C. S.; Yeo, T. W.; Anstey, N. M., Malaria tolerance - For whom the cell tolls? *Trends Parasitol.* **2006,** 22, 371-377.

59. Day, N. P. J.; Diep, P. T.; Ly, P. T.; Sinh, D. X.; White, N. J., Clearance kinetics of parasites and pigment-containing leukocytes in severe malaria. *Blood* **1996,** 88, 4694-4700.

60. Schwarzer, E.; Bellomo, G.; Giribaldi, G.; Ulliers, D.; Arese, P., Phagocytosis of malarial pigment haemozoin by human monocytes: a confocal microscopy study. *Parasitology* **2001,** 123, 125-131.

61. Abbas, A.; Lichtman, A.; Pober, J., *Cellular and Molecular Immunology*. 4th ed.; Saunders Publishing Compny: 2000.

62. DeLeo, F. R.; Quinn, M. T., Assembly of the phagocyte NADPH oxidase: molecular interaction of oxidase proteins. *J. Leukocyte Biol.* **1996,** 60, 677-691.

63. Babior, B. M., NADPH oxidase: an update. *Blood* **1999,** 93, 1464-1476.

64. Vignais, P. V., The superoxide-generating NADPH oxidase: structural aspects and activation mechanism. *Cell. Mol. Life Sci.* **2002,** 59, 1428-1459.

65. MacMicking, J.; Xie, Q. W.; Nathan, C., Nitric Oxide and macrophage function. *Annu. Rev. Immunol.* **1997,** 15, 323-350.

66. Schwarzer, E.; Arese, P., Phagocytosis of malarial pigment hemozoin inhibits NADPH-oxidase activity in human monocyte-derived macrophages. *Biochim. Biophys. Acta* **1996,** 1316, 169-175.

67. Prada, J.; Malinowsky, J.; Muller, S.; Bienzle, U.; Kremsner, P. G., Effects of *Plasmodium vinckei* hemozoin on the production of oxygen radicals and nitrogen oxides in murine macrophages. *Am. J. Trop. Med. Hyg.* **1996,** 54, 620-624.

68. Carney, C. K.; Schrimpe, A. C.; Halfpenny, K.; Harry, R. S.; Miller, C. M.; Broncel, M.; Sewell, S. L.; Schaff, J. E.; Deol, R.; Carter, M. D.; Wright, D. W., The basis of the immunomodulatory activity of malaria pigment (hemozoin). *J. Biol. Inorg. Chem.* **2006,** 11, 917-929.

69. Nguyen, P. H.; Day, N.; Pram, T. D.; Ferguson, D. J.; White, N. J., Intraleucocytic malaria pigment and prognosis in severe malaria. *Trans. R. Soc. Trop. Med. Hyg.* **1995,** 89, 200-204.

70. Schwarzer, E.; Muller, O.; Arese, P.; Siems, W. G.; Grune, T., Increased levels of 4-hydroxynonenal in human monocytes fed with malarial pigment hemozoin. *FEBS Lett.* **1996,** 338, 119-122.

71. Poli, G.; Schaur, R. J.; Siems, W. G.; Leonarduzzi, G., 4-Hydroxynonenal: A membrane lipid oxidation product of medicinal interest. *Med. Res. Rev.* **2008,** 28, 569-631.

72. Schaur, R. J., Basic aspects of the biochemical reactivity of 4-hydroxynonenal. *Mol. Aspects Med.* **2003,** 24, 149-159.

73. Crabb, J. W.; O'Neil, J.; Miyagi, M.; West, K.; Hoff, H. F., Hydroxynonenal inactivates cathepsin B by forming Michael adducts with active site residues. *Protein Sci.* **2002,** 11, 831-840.

74. Ji, C.; Kozak, K. R.; Marnett, L. J., Ikappa B kinase, a molecular target for inhibition by 4-hydroxy-2-nonenal. *J. Biol. Chem.* **2001,** 276, 18223-18228.

75. Szweda, L. I.; Uchida, K.; Tsai, L.; Stadtman, E. R., Inactivation of glucose-6-phosphate dehydrogenase by 4-hydroxy-2- nonenal. Selective modification of an active-site lysine. *J. Biol. Chem.* **1993,** 268, 3342-3347.

76. Weigel, A. L.; Handa, J. T.; Hjelmeland, L. M., Microarray analysis of H_2O_2-, HNE, or tBH-treated Arpe-19 cells. *Free Radical Biol. Med.* **2002,** 33, 1419-1432.

77. West, J. D.; Marnett, L. J., Alterations in gene expression induced by the lipid peroxidation product, 4-hydroxy-2-nonenal. *Chem. Res. Toxicol.* **2005,** 18, 1642-1653.

78. Carter, M. D.; Reese Harry, S.; Wright, D. W., Identification of hydroxyeicosatetraenoic acid components of schistosomal hemozoin. *Biochem. Biophys. Res. Commun.* **2007,** 363, 867-872.

79. Praticò, D., Prostanoid and isoprostanoid pathways in atherogenesis. *Atherosclerosis* **2008,** 201, 8-16.

80. Schafer, F. Q.; Qian, S. Y.; Buettner, G. R., Iron and free radical oxidations in cell membranes. *Cell. Mol. Biol.* **2000,** 46, 657-62.

81. Spiteller, P.; Spiteller, G., Strong dependence of the lipid peroxidation product spectrum whether Fe2+/O2 or Fe3+/O2 is used as oxidant. *Biochim. Biophys. Acta* **1998,** 1392, 23-40.

82. Cheng, Z.; Li, Y., What Is Responsible for the Initiating Chemistry of Iron-Mediated Lipid Peroxidation: An Update. *Chem. Rev.* **2007,** 107, 748-766.

83. Curmi, P. A.; Gavet, O.; Charbaut, E.; Ozon, S.; Lachkar-Colmerauer, S.; Manceau, V.; Siavoshian, S.; Maucuer, A.; Sobel, A., Stathmin and its phosphoprotein family: general properties, biochemical and functional interaction with tubulin. *Cell Struct. Funct.* **1999,** 24, 345-57.

84. Schwarzer, E.; Alessio, M.; Ulliers, D.; Arese, P., Phagocytosis of the malarial pigment, hemozoin, impairs expression of major histocompatibility complex class II antigen, CD54, and CD11c in human monocytes. *Infect. Immun.* **1998,** 66, 1601-1606.

85. Prada, J.; Malinowski, J.; Muller, S.; Bienzle, U.; Kremsner, P. G., Hemozoin differentially modulates the production of interleukin 6 and tumor necrosis factor in murine malaria. *Eur. Cytokine Network* **1995,** 6, 109-112.

86. Green, M. D.; Xiao, L.; Lal, A. A., Formation of hydroxyeicosatetraenoic acids from hemozoin-catalyzed oxidation of arachidonic acid. *Mol. Biochem. Parasitol.* **1996,** 83, 183-188.

87. Pandey, A. V.; Tekwani, B. L., Formation of haemozoin/β-haematin under physiological conditions is not spontaneous. *FEBS Lett.* **1996,** 393, 189-192.

88. Miller, C. M.; Carney, C. K.; Schrimpe, A. C.; Wright, D. W., β–hematin (hemozoin) mediated decomposition of polyunsaturated fatty acids to 4-hydroxy-2-nonenal. *Inorg. Chem.* **2005,** 44, 2134-2136.

89. Delcarte, J.; Jacques, P.; Fauconnier, M.-L.; Hoyaux, P.; Matsui, K.; Marlier, M.; Thonart, P., The homolytic and heterolytic fatty acid hydroperoxide lyase-like activities of hematin. *Biochem. Biophys. Res. Commun.* **2001,** 286, 28-32.

90. Lee, S. H.; Blair, I. A., Characterization of 4-oxo-2-nonenal as a novel product of lipid peroxidation. *Chem. Res. Toxicol.* **2000,** 13, 698-702.

91. Lee, S. H.; Oe, T.; Blair, I. A., Vitamin C-induced decomposition of lipid hydroperoxides to endogenous genotoxins. *Science* **2001,** 292, 2083-2086.

92. Fridovich, S. E.; Porter, N. A., Oxidation of arachidonic acid in micelles by superoxide and hydrogen peroxide. *J. Biol. Chem.* **1981,** 256, 260-265.

93. Schneider, C.; Tallman, K. A.; Porter, N. A.; Brash, A. R., Two Distinct Pathways of Formation of 4-Hydroxynonenal. Mechanisms of Nonenzymatic Trandformation of the 9- and 13-Hydroperoxides of Linoleic Acid to 4-Hydroxyalkenals. *J. Biol. Chem.* **2001,** 276, 20831-20838.

94. Amarnath, V.; Amarnath, K.; Amarnath, K.; Davies, S.; Roberts, L. J., Pyridoxamine: an extremely potent scavenger of 1,4-dicarbonyls. *Chem. Res. Toxicol.* **2004,** 17, 410-415.

95. Davies, S. S.; Brantley, E. J.; Voziyan, P. A.; Amarnath, V.; Zagol-Ikapitte, I.; Boutaud, O.; Hudson, B. G.; Oates, J. A.; Roberts, L. J., Pyridoxamine analogues scavenge lipid-derived γ-ketoaldehydes and protect against H2O2-mediated cytotoxicity. *Biochemistry* **2006,** 45, 15756-15767.

96. Brame, C. J.; Boutaud, O.; Davies, S. S.; Yang, T.; Oates, J. A.; Roden, D.; Roberts, L. J., II, Modification of proteins by isoketal-containing oxidized phospholipids. *J. Biol. Chem.* **2004,** 279, 13447-13451.

97. Bernoud-Hubac, N.; Fay, L. B.; Armarnath, V.; Guichardant, M.; Bacot, S.; Davies, S. S.; Roberts, L. J.; LaGarde, M., Covalent binding of isoketals to ethanolamine phospholipids. *Free Radical Biol. Med.* **2004,** 37, 1064-1611.

98. Oliveira, M. F.; Timm, B. L.; Machado, E. A.; Miranda, K.; Attias, M.; Silva, J. R.; Dansa-Petretski, M.; de Oliveira, M. A.; de Souza, W.; Pinhal, N. M.; Sousa, J. J. F.; Vugman, N. V.; Oliveira, P. L., On the pro-oxidant effects of haemozoin. *FEBS Lett.* **2002,** 512, 139-144.

99. Miller, C. M. Hemozoin mediated oxidation of polyunsaturated fatty acids. Doctoral Dissertation, Vanderbilt University, Nashville, 2005.

100. Zagorski, M. G.; Salomon, R. G., Prostaglandin endoperoxides. Carboxylate catalysis and the effects of proton donors on the decomposition of 2,3-dioxabicyclo[2.2.1]heptane. *J. Am. Chem. Soc.* **1982,** 104, 3498-3503.

101. Skorokhod, O. A.; Alessio, M.; Mordmuller, B.; Arese, P.; Schwarzer, E., Hemozoin (malarial pigment) inhibits differentiation and maturation of human monocyte-derived dendritic cells: a peroxisome proliferator-activated receptor-γ-mediated effect. *J. Immunol.* **2004,** 173, 4066-4074.

102. Brame, C. J.; Salomon, R. G.; Morrow, J. D.; Roberts, L. J., II, Identification of extremely reactive gamma -ketoaldehydes (isolevuglandins) as products of the isoprostane pathway and characterization of their lysyl protein adducts. *J. Biol. Chem.* **1999,** 274, 13139-13146.

103. Davies, S. S.; Amarnath, V.; Roberts, L. J., Isoketals: highly reactive γ-ketoaldehydes formed from the H2-isoprostane pathway. *Chem. Phys. Lipids* **2004,** 128, 85-99.

104. Jaramillo, M.; Godbout, M.; Olivier, M., Hemozoin induces macrophage chemokine expression through oxidative stress-dependent and -independent mechanisms. *J. Immunol.* **2005,** 174, 475 - 484.

105. Taramelli, D.; Recalcati, S.; Basilico, N.; Olliaro, P.; Cairo, G., Macrophage preconditioning with synthetic malaria pigment reduces cytokine production via heme iron-dependent oxidative stress. *Lab. Invest.* **2000,** 80, 1781-1788.

106. Jaramillo, M.; Gowda, D. C.; Radzioch, D.; Olivier, M., Hemozoin increases IFN-gamma-inducible macrophage nitric oxide generation through extracellular signal-regulated kinase- and NF-kappa B-dependent pathways. *J. Immunol.* **2003,** 171, 4243 - 4253.

107. Schwarzer, E.; Arese, P., Phagocytosis of malarial pigment hemozoin inhibits NADPH-oxidase activity in human monocyte-derived macrophages. *Biochim. Biophys. Acta* **1996,** 1316, 169-175.

108. Dianzani, C.; Parrini, M.; Ferrara, C.; Fantozzi, R., Effect of 4-hydroxynonenal on superoxide anion production from primed human neutrophils. *Cell Biochem. Funct.* **1996,** 14, 193-200.

109. Carney, C. K. Hemozoin immunoreactivity. Doctoral Dissertation, Vanderbilt University, Nashville, 2006.

110. Liu, W.; Kato, M.; Itoigawa, M.; Murakami, H.; Yajima, M.; Wu, J.; Ishikawa, N.; Nakashima, I., Distinct involvement of NF-κB and p38 mitogen-activated protein kinase pathways in serum deprivation-mediated stimulation of inducible nitric oxide synthase and its inhibition by 4-hydroxynonenal. *J. Cell. Biochem.* **2001,** 83, 271-280.

111. Schwarzer, E.; Ludwig, P.; Valente, E.; Arese, P., 15(S)-hydroxyeicosatetraenoic acid (15-HETE), a product of arachidonic acid peroxidation, is an active component of hemozoin toxicity to monocytes. *Parassitologia* **1999,** 41, 199 - 202.

112. Shu, H.; Wong, B.; Zhou, G.; Li, Y.; Berger, J.; Woods, J. W.; Wright, S. D.; Cai, T.-Q., Activation of PPARα or γ reduces secretion of matrix metalloproteinase 9 but not interleukin 8 from human monocytic THP-1 cells. *Biochem. Biophys. Res. Commun.* **2000,** 267, 345-349.

113. Boyault, S.; Bianchi, A.; Moulin, D.; Morin, S.; Francois, M.; Netter, P.; Terlain, B.; Bordji, K., 15-Deoxy-Δ12,14-prostaglandin J2 inhibits IL-1β-induced IKK enzymatic activity and IκBα degradation in rat chondrocytes through a PPARγ-independent pathway. *FEBS Lett.* **2004,** 572, 33-40.

114. Schwarzer, E.; Skorokhod, O. A.; Barrera, V.; Arese, P., Hemozoin and the human monocyte--a brief review of their interactions. *Parassitologia* **2008,** 50, 143-5.

115. Prato, M.; Gallo, V.; Giribaldi, G.; Arese, P., Phagocytosis of haemozoin (malarial pigment) enhances metalloproteinase-9 activity in human adherent monocytes: Role of IL-1beta and 15-HETE. *Malar. J.* **2008,** 7, 157.

116. Spector, A. A.; Gordon, J. A.; Moore, S. A., Hydroxyeicosatetraenoic acids (HETEs). *Prog. Lipid Res.* **1988,** 27, 271-323.

117. Setty, B. N. Y.; Dampier, C. D.; Stuart, M. J., Arachidonic acid metabolites are involved in mediating red blood cell adherence to endothelium. *J. Lab. Clin. Med.* **1995,** 125, 608-617.

118. Al-Shahrour, F.; Minguez, P.; Vaquerizas, J. M.; Conde, L.; Dopazo, J., BABELOMICS: a suite of web tools for functional annotation and analysis of groups of genes in high-throughput experiments. *Nucleic Acids Res.* **2005,** 33, W460-464.

119. Ockenhouse, C. F.; Hu, W.-c.; Kester, K. E.; Cummings, J. F.; Stewart, A.; Heppner, D. G.; Jedlicka, A. E.; Scott, A. L.; Wolfe, N. D.; Vahey, M.; Burke, D. S., Common and divergent immune response signaling pathways discovered in peripheral blood mononuclear cell gene expression patterns in presymptomatic and clinically apparent malaria. *Infect. Immun.* **2006,** 74, 5561-5573.

120. Griffiths, M. J.; Mohammed, J. S.; Popper, S. J.; Hemingway, C. A.; Kortok, M. M.; Wathen, A.; Rockett, K. A.; Mott, R.; Levin, M.; Newton, C. R.; Marsh, K.; Relman, D. A.; Kwiatkowski, D. P., Genomewide analysis of the host response to malaria in Kenyan children. *J. Infect. Dis.* **2005,** 191, 1599-611.

121. Muehlenbachs, A.; Fried, M.; Lachowitzer, J.; Mutabingwa, T. K.; Duffy, P. E., Genome-wide expression analysis of placental malaria reveals features of lymphoid neogenesis during chronic infection. *J. Immunol.* **2007,** 179, 557-565.

122. Sexton, A. C.; Good, R. T.; Hansen, D. S.; D'Ombrain, M. C.; Buckingham, L.; Simpson, K.; Schofield, L., Transcriptional profiling reveals suppressed

erythropoiesis, up-regulated glycolysis, and interferon-associated responses in murine malaria. *J. Infect. Dis.* **2004,** 189, 1245-56.

123. Lovegrove, F. E.; Pena-Castillo, L.; Mohammad, N.; Liles, C.; Hughes, T. R.; Kain, K. C., Simultaneous host and parasite expression profiling identifies tissue-specific transcriptional programs associated with susceptibility or resistance to experimental cerebral malaria. *BMC Genomics* **2006,** 7, 295-311.

124. Schaecher, K.; Kumar, S.; Yadava, A.; Vahey, M.; Ockenhouse, C. F., Genome-wide expression profiling in malaria infection reveals transcriptional changes associated with lethal and nonlethal outcomes. *Infect. Immun.* **2005,** 73, 6091-6100.

125. Ylostalo, J.; Randall, A. C.; Myers, T. A.; Metzger, M.; Krogstad, D. J.; Cogswell, F. B., Transcriptome profiles of host gene expression in a monkey model of human malaria. *J. Infect. Dis.* **2005,** 191, 400-9.

126. Huy, N. T.; Trang, D. T. X.; Kariu, T.; Sasai, M.; Saida, K.; Harada, S.; Kamei, K., Leukocyte activation by malarial pigment. *Parasitol. Int.* **2006,** 55, 75-81.

127. Krämer, B.; Grobusch, M. P.; Suttorp, N.; Neukammer, J.; Rinneberg, H., Relative frequency of malaria pigment-carrying monocytes of nonimmune and semi-immune patients from flow cytometric depolarized side scatter. *Cytometry* **2001,** 45, 133-140.

128. Koster, J. F.; Slee, R. G.; Montfoort, A.; Lang, J.; Esterbauer, H., Comparison of the inactivation of microsomal glucose-6-phosphatase by in situ lipid peroxidation-derived 4-hydroxynonenal and exogenous 4-hydroxynonenal. *Free Radical Res.* **1986,** 1, 273 - 287.

129. Sherry, B. A.; Alava, G.; Tracey, K. J.; Martiney, J.; Cerami, A.; Slater, A. F., Malaria-specific metabolite hemozoin mediates the release of several potent endogenous pyrogens (TNF, MIP-1 alpha, and MIP-1 beta) in vitro, and altered thermoregulation in vivo. *J Inflamm* **1995,** 45, 85 - 96.

130. Douki, T.; Odin, F.; Caillat, S.; Favier, A.; Cadet, J., Predominance of the 1,N2-propano 2'-deoxyguanosine adduct among 4-hydroxy-2-nonenal-induced DNA lesions. *Free Radical Biol. Med.* **2004,** 37, 62-70.

131. Carbone, D. L.; Doorn, J. A.; Petersen, D. R., 4-Hydroxynonenal regulates 26S proteasomal degradation of alcohol dehydrogenase. *Free Radical Biol. Med.* **2004,** 37, 1430-1439.

132. Neely, M. D.; Boutte, A.; Milatovic, D.; Montine, T. J., Mechanisms of 4-hydroxynonenal-induced neuronal microtubule dysfunction. *Brain Res.* **2005,** 1037, 90-98.

133. Usatyuk, P. V.; Natarajan, V., Role of mitogen-activated protein kinases in 4-hydroxy-2-nonenal-induced actin remodeling and barrier function in endothelial cells. *J. Biol. Chem.* **2004,** 279, 11789-11797.

134. Montine, T. J.; Amarnath, V.; Martin, M. E.; Strittmatter, W. J.; Graham, D. G., E-4-hydroxy-2-nonenal is cytotoxic and cross-links cytoskeletal proteins in P19 neuroglial cultures. *Am. J. Pathol.* **1996,** 148, 89-93.

135. Jaramillo, M.; Godbout, M.; Olivier, M., Hemozoin induces macrophage chemokine expression through oxidative stress-dependent and -independent mechanisms. *J. Immunol.* **2005,** 174, 475-484.

136. Sherry, B. A.; Alava, G.; Tracey, K. J.; Martiney, J.; Cerami, A.; Slater, A. F., Malaria-specific metabolite hemozoin mediates the release of several potent endogenous pyrogens (TNF, MIP-1 alpha, and MIP-1 beta) in vitro, and altered thermoregulation in vivo. *J. Inflammation* **1995,** 45, 85 - 96.

137. Sinniah, R.; Rui-Mei, L.; Kara, A., Up-regulation of cytokines in glomerulonephritis associated with murine malaria infection. *Int. J. Exp. Pathol.* **1999,** 80, 87-95.

138. Wahlgren, M.; Abrams, J. S.; Fernandez, V.; Bejarano, M. T.; Azuma, M.; Torii, M.; Aikawa, M.; Howard, R. J., Adhesion of Plasmodium falciparum-infected erythrocytes to human cells and secretion of cytokines (IL-1-beta, IL-1RA, IL-6, IL-8, IL-10, TGF beta, TNF alpha, G-CSF, GM-CSF. *Scand. J. Immunol.* **1995,** 42, 626-636.

139. Millington, O. R.; Lorenzo, C. D.; Phillips, S.; Garside, P.; Brewer, J. M., Suppression of adaptive immunity to heterologous antigens during *Plasmodium* infection through hemozoin-induced failure of dendritic cell function. *J. Biol.* **2006,** 5, 5.

140. Ocaña-Morgner, C.; Wong, Kurt A.; Lega, F.; Dotor, J.; Borras-Cuesta, F.; Rodriguez, A., Role of TGF-beta and PGE2 in T cell responses during *Plasmodium yoelii* infection. *Eur. J. Immunol.* **2007,** 37, 1562-1574.

141. Skorokhod, O. A.; Schwarzer, E.; Ceretto, M.; Arese, P., Malarial pigment haemozoin, IFN-gamma, TNF-alpha, IL-1beta and LPS do not stimulate expression of inducible nitric oxide synthase and production of nitric oxide in immuno-purified human monocytes. *Malar. J.* **2007,** 6, 73-80.

142. Sullivan, A. D.; Ittarat, I.; Meshnick, S. R., Patterns of haemozoin accumulation in tissue. *Parasitology* **1996,** 112, 285-94.

143. Newton, C. R.; Taylor, T. E.; Whitten, R. O., Pathophysiology of fatal *falciparum* malaria in African children. *Am. J. Trop. Med. Hyg.* **1998,** 58, 673-683.

144. Adams, S.; Brown, H.; Turner, G., Breaking down the blood-brain barrier: signaling a path to cerebral malaria? *Trends Parasitol.* **2002,** 18, 360-366.

145. Mandal, M.; Mandal, A.; Das, S.; Chakraborti, T.; Chakraborti, S., Clinical implications of matrix metalloproteinases. *Mol. Cell. Biochem.* **2003,** 252, 305-29.

146. Prato, M.; Giribaldi, G.; Polimeni, M.; Gallo, V.; Arese, P., Phagocytosis of hemozoin enhances matrix metalloproteinase-9 activity and TNF-alpha production in human monocytes: role of matrix metalloproteinases in the pathogenesis of falciparum malaria. *J. Immunol.* **2005,** 175, 6436 - 6442.

147. Woo, C.-H.; Lim, J.-H.; Kim, J.-H., Lipopolysaccharide induces matrix metalloproteinase-9 expression via a mitochondrial reactive oxygen species-p38 kinase-activator protein-1 pathway in RAW 264.7 Cells. *J. Immunol.* **2004,** 173, 6973-6980.

148. Lai, W.-C.; Zhou, M.; Shankavaram, U.; Peng, G.; Wahl, L. M., Differential regulation of lipopolysaccharide-induced monocyte matrix metalloproteinase (MMP)-1 and MMP-9 by p38 and extracellular signal-regulated kinase 1/2 mitogen-activated protein kinases. *J. Immunol.* **2003,** 170, 6244-6249.

149. Rhee, J. W.; Lee, K. W.; Kim, D.; Lee, Y.; Jeon, O. H.; Kwon, H. J.; Kim, D. S., NF-kappaB-dependent regulation of matrix metalloproteinase-9 gene expression by lipopolysaccharide in a macrophage cell line RAW 264.7. *J. Biochem. Mol. Biol.* **2007,** 40, 88 - 94.

150. Gearing, A. J. H.; Beckett, P.; Christodoulou, M.; Churchill, M.; Clements, J.; Davidson, A. H.; Drummond, A. H.; Galloway, W. A.; Gilbert, R.; Gordon, J. L.; Leber, T. M.; Mangan, M.; Miller, K.; Nayee, P.; Owen, K.; Patel, S.; Thomas, W.; Wells, G.; Wood, L. M.; Woolley, K., Processing of tumour necrosis factor-α precursor by metalloproteinases. *Nature* **1994,** 370, 555-557.

151. Brown, H.; Turner, G.; Rogerson, S.; Tembo, M.; Mwenechanya, J.; Molyneux, M.; Taylor, T., Cytokine expression in the brain in human cerebral malaria. *J. Infect. Dis.* **1999,** 180, 1742-1746.

152. Armah, H.; Wiredu, E. K.; Dodoo, A. K.; Adjei, A. A.; Tettey, Y.; Gyasi, R., Cytokines and adhesion molecules expression in the brain in human cerebral malaria. *Int. J. Environ. Res. Public Health* **2005,** 2, 123-131.

153. Wassmer, S. C.; Combes, V.; Candal, F. J.; Juhan-Vague, I.; Grau, G. E., Platelets potentiate brain endothelial alterations induced by Plasmodium falciparum. *Infect. Immun.* **2006,** 74, 645-653.

154. Turner, G. D. H.; Morrison, H.; Jones, M.; Davis, T. M. E.; Looareesuwan, S.; Buley, I. D.; Gatter, K. C.; Newbold, C. I.; Pukritayakamee, S.; Nagachinta, B.; White, N. J.; Berendt, A. R., An immunohistochemical study of the pathology of fatal malaria: evidence for widespread endothelial activation and a potential role

for intercellular adhesion molecule-1 in cerebral sequestration. *Am. J. Pathol.* **1994,** 145, 1057-1069.

155. Silamut, K.; Phu, N. H.; Whitty, C.; Turner, G. D. H.; Louwrier, K.; Mai, N. T. H.; Simpson, J. A.; Hien, T. T.; White, N. J., A quantitative analysis of the microvascular sequestration of malaria parasites in the human brain. *Am. J. Pathol.* **1999,** 155, 395-410.

156. Van Oosten, M.; Van de Bilt, E.; De Vries, H. E.; Van Berkel, T. J.; Kuiper, J., Vascular adhesion molecule-1 and intercellular adhesion molecule-1 expression on rat liver cells after lipopolysaccharide administration in vivo. *Hepatology* **1995,** 22, 1538-46.

157. Mohan, K.; Stevenson, M., Dyserythropoiesis and severe anaemia associated with malaria correlate with deficient interleukin-12 production. *Br. J. Haematol.* **1998,** 103, 942-949.

158. Casals-Pascual, C.; Kai, O.; Cheung, J. O. P.; Williams, S.; Lowe, B.; Nyanoti, M.; Williams, T. N.; Maitland, K.; Molyneux, M.; Newton, C. R. J. C.; Peshu, N.; Watt, S. M.; Roberts, D. J., Suppression of erythropoiesis in malarial anemia is associated with hemozoin in vitro and in vivo. *Blood* **2006,** 108, 2569-2577.

159. Giribaldi, G.; Ulliers, D.; Schwarzer, E.; Roberts, I.; Piacibello, W.; Arese, P., Hemozoin- and 4-hydroxynonenal-mediated inhibition of erythropoiesis. Possible role in malarial dyserythropoiesis and anemia. *Haematologica* **2004,** 89, 492-493.

160. Were, T.; Hittner, J. B.; Ouma, C.; Otieno, R. O.; Orago, A. S.; Ong'echa, J. M.; Vulule, J. M.; Keller, C. C.; Perkins, D. J., Suppression of RANTES in children with *Plasmodium falciparum* malaria. *Haematologica* **2006,** 91, 1396-1399.

161. John, C. C.; Opika-Opoka, R.; Byarugaba, J.; Idro, R.; Boivin, M. J., Low levels of RANTES are associated with mortality in children with cerebral malaria. *J. Infect. Dis.* **2006,** 194, 837-845.

162. Schrimpe, A. C.; Wright, D. W., Differential gene expression mediated by 15-hydroxyeicosatetraenoic acid in LPS stimulated RAW 264.7 cells. *submitted* **2009**.

163. Ho, M.; White, N. J., Molecular mechanisms of cytoadherence in malaria. *Am. J. Physiol: Cell Physiol.* **1999,** 276, C1231-1242.

164. Bolick, D. T.; Orr, A. W.; Whetzel, A.; Srinivasan, S.; Hatley, M. E.; Schwartz, M. A.; Hedrick, C. C., 12/15-Lipoxygenase regulates intercellular adhesion molecule-1 expression and monocyte adhesion to endothelium through activation of RhoA and Nuclear Factor-{kappa}B. *Arterioscler. Thromb. Vasc. Biol.* **2005,** 25, 2301-2307.

165. Patricia, M. K.; Kim, J. A.; Harper, C. M.; Shih, P. T.; Berliner, J. A.; Natarajan, R.; Nadler, J. L.; Hedrick, C. C., Lipoxygenase products increase monocyte adhesion to human aortic endothelial cells. *Arterioscler. Thromb. Vasc. Biol.* **1999,** 19, 2615-2622.

166. Howard, R. J.; Gilladoga, A. D., Molecular studies related to the pathogenesis of cerebral malaria. *Blood* **1989,** 74, 2603-2618.

167. Patnaik, J. K.; Das, B. S.; Mishra, S. K.; Mohanty, S.; Satpathy, S. K.; Mohanty, D., Vascular clogging, mononuclear cell margination, and enhanced vascular permeability in the pathogenesis of human cerebral malaria. *Am. J. Trop. Med. Hyg.* **1994,** 51, 642-647.

168. Johnson, H.; McNee, M.; Sun, F., 15-Hydroxyeicosatetraenoic acid is a potent inflammatory mediator and agonist of canine tracheal mucus secretion. *Am. Rev. Respir. Dis.* **1985,** 131, 917-22.

169. Ricote, M.; Li, A. C.; Willson, T. M.; Kelly, C. J.; Glass, C. K., The peroxisome proliferator-activated receptor-γ is a negative regulator of macrophage activation. *Nature* **1998,** 391, 79-82.

170. Marx, N.; Schonbeck, U.; Lazar, M. A.; Libby, P.; Plutzky, J., Peroxisome proliferator-activated receptor gamma activators inhibit gene expression and migration in human vascular smooth muscle cells. *Circ. Res.* **1998,** 83, 1097-1103.

171. Marx, N.; Sukhova, G.; Murphy, C.; Libby, P.; Plutzky, J., Macrophages in human atheroma contain PPAR{gamma} : differentiation-dependent peroxisomal proliferator-activated receptor {gamma} (PPAR{gamma}) expression and reduction of MMP-9 activity through PPAR{gamma} activation in mononuclear phagocytes in vitro. *Am. J. Pathol.* **1998,** 153, 17-23.

172. Zambon, A.; Gervois, P.; Pauletto, P.; Fruchart, J.-C.; Staels, B., Modulation of hepatic inflammatory risk markers of cardiovascular diseases by PPAR-{alpha}activators: clinical and experimental evidence. *Arterioscler. Thromb. Vasc. Biol.* **2006,** 26, 977-986.

173. Jiang, C.; Ting, A. T.; Seed, B., PPAR-γ agonists inhibit production of monocyte inflammatory cytokines. *Nature* **1998,** 391, 82-86.

174. Reuben, P. M.; Cheung, H. S., Regulation of matrix metalloproteinase (MMP) gene expression by protein kinases. *Front. Biosci.* **2006,** 11, 1199-1215.

175. Yan, C.; Boyd, D. D., Regulation of matrix metalloproteinase gene expression. *J. Cell. Physiol.* **2007,** 211, 19 - 26.

176. Pandey, M. K.; Sung, B.; Kunnumakkara, A. B.; Sethi, G.; Chaturvedi, M. M.; Aggarwal, B. B., Berberine Modifies Cysteine 179 of I{kappa}B{alpha} Kinase,

Suppresses Nuclear Factor-{kappa}B-Regulated Antiapoptotic Gene Products, and Potentiates Apoptosis. *Cancer Research* **2008,** 68, 5370-5379.

177. Kapahi, P.; Takahashi, T.; Natoli, G.; Adams, S. R.; Chen, Y.; Tsien, R. Y.; Karin, M., Inhibition of NF-kappa B activation by arsenite through reaction with a critical cysteine in the activation Loop of Ikappa B kinase. *J. Biol. Chem.* **2000,** 275, 36062-36066.

178. Jeon, K. I.; Byun, M. S.; Jue, D. M., Gold compound auranofin inhibits IκB kinase (IKK) by modifying Cys-179 of IKKβ subunit *Exp. Mol. Med.* **2003,** 35, 61-66.

179. Jeon, K. I.; Jeong, J. Y.; Jue, D. M., Thiol-reactive metal compounds inhibit NF-{kappa}B activation by blocking I{kappa}B kinase. *J. Immunol.* **2000,** 164, 5981-5989.

180. Spreitzer, G.; Whitling, J. M.; Madura, J. D.; Wright, D. W., Peptide-encapsulated CdS nanoclusters from a combinatorial ligand library. *Chem. Commun.* **2000**, 209-210.

181. Morquette, B.; Shi, Q.; Lavigne, P.; Ranger, P.; Fernandes, J. C.; Benderdour, M., Production of lipid peroxidation products in osteoarthritic tissues: New evidence linking 4-hydroxynonenal to cartilage degradation. *Arthritis Rheum.* **2006,** 54, 271-281.

182. Ito, A.; Mukaiyama, A.; Itoh, Y.; Nagase, H.; Thogersen, I. B.; Enghild, J. J.; Sasaguri, Y.; Mori, Y., Degradation of interleukin 1 beta by matrix metalloproteinases. *J. Biol. Chem.* **1996,** 271, 14657-14660.

183. Mäkeläa, M.; Salob, T.; Larjava, H., MMP-9 from TNFα-stimulated keratinocytes binds to cell membranes and type I collagen: a cause for extended matrix degradation in inflammation? *Biochem. Biophys. Res. Commun.* **1998,** 253, 325-335

184. Page, S.; Fischer, C.; Baumgartner, B.; Haas, M.; Kreusel, U.; Loidl, G.; Hayn, M.; Ziegler-Heitbrock, H. W. L.; Neumeier, D.; Brand, K., 4-Hydroxynonenal prevents NF-{kappa}B activation and tumor necrosis factor expression by inhibiting I{kappa}B phosphorylation and subsequent proteolysis. *J. Biol. Chem.* **1999,** 274, 11611-11618.

185. Li, L.; Hamilton, R. F., Jr.; Holian, A., Effect of acrolein on human alveolar macrophage NF-kappa B activity. *Am. J. Physiol. Lung Cell. Mol. Physiol.* **1999,** 277, L550-557.

186. Castrillo, A.; Díaz-Guerra, M. J. M.; Hortelano, S.; Martín-Sanz, P.; Boscá, L., Inhibition of IκB kinase and IκB phosphorylation by 15-Deoxy-Δ12,14-prostaglandin J2 in activated murine macrophages. *Mol. Cell. Biol.* **2000,** 20 1692–1698.

187. May, M. J.; Ghosh, S., Signal transduction through NF-κB. *Immunol. Today* **1998,** 19, 80-88.

188. Jeon, K. I.; Byun, M. S.; Jue, D. M., Gold compound auranofin inhibits IκB kinase (IKK) by modifying Cys-179 of IKKβ subunit. *Exp. Mol. Med.* **2003,** 35, 61-66.

189. Hayden, M. S.; Ghosh, S., Signaling to NF-κB. *Genes Dev.* **2004,** 18, 2195-2224.

190. Lin, S.; Saxena, N. K.; Ding, X.; Stein, L. L.; Anania, F. A., Leptin increases tissue inhibitor of metalloproteinase I (TIMP-1) gene expression by a specificity protein 1/sgnal transducer and activator of transcription 3 mechanism. *Mol. Endocrinol.* **2006,** 20, 3376-3388.

191. Dien, J.; Amin, H. M.; Chiu, N.; Wong, W.; Frantz, C.; Chiu, B.; Mackey, J. R.; Lai, R., Signal transducers and activators of transcription-3 up-regulates tissue inhibitor of metalloproteinase-1 expression and decreases invasiveness of breast cancer. *Am. J. Pathol.* **2006,** 169, 633-642.

CURRICULUM VITAE

Alexandra Catherine Schrimpe Rutledge

Vanderbilt University
Department of Chemistry
Station B 351822
Nashville, TN 37235

Education

- Ph.D., Chemistry, Vanderbilt University; Nashville, TN — April 2009
  Advisor: David W. Wright — GPA: 3.962

- B.S., Forensic Chemistry, Eastern Kentucky University; Richmond, KY — May 2004
  Minors: Mathematics, Statistics — GPA: 3.97

Research Experience

2004 – Present — Graduate Research Assistant, Vanderbilt University
Department of Chemistry, Advisor: David W. Wright

- Studied lipid peroxidation mediated by the malaria pigment, hemozoin
- Explored the global impact of lipid peroxidation products on the function of macrophage-like cells
- Investigated protein adduction sites by tandem mass spectrometry
- Experienced in mammalian cell culture, RNA extraction and purification, protein isolation, protein digestion, gel electrophoresis, biological assays, western blotting, zymography, ELISA, flow cytometry, UV-Visible spectroscopy, HPLC, MALDI MS, LC-MS and LC-MS-MS (TSQ Quantum and LCQ/LTQ Ion Traps), microarray analysis, and biological pathway analysis (Ingenuity Pathway Analysis)

Summer 2003 — Internship, U.S. Food and Drug Administration
Forensic Chemistry Center, Cincinnati, OH
Advisor: Mark Witkowski

- Examined mock contamination on the surfaces of over-the-counter (OTC) pharmaceuticals using comparison microscopy, FT-IR spectroscopy, LC-UV and GC-MS

Summer 2002 — Undergraduate Research Assistant, University of Tennessee
Department of Chemistry, Knoxville, TN
Advisor: Kelsey D. Cook

- Explored the simultaneous analysis of xylene isomer mixtures using process (Pr)-mass spectrometry

Awards

- GAANN Fellowship September 2004-August 2005
- Senior GAANN Fellowship September 2005-August 2006
  January 2008-May 2008
- Scientist-in-the-Classroom Partnership Program Fellowship June 2008-May 2009

Publications

- Miller, C. M; Carney, C. K; **Schrimpe, A. C**; Wright, D. W. "Beta-Hematin (hemozoin) mediated decompostion of polyunsaturated fatty acids to 4-hydroxy-2-nonenal." Inorg. Chem. **2005**, *44*, 2134-6.

- Carney, C.K.; **Schrimpe, A.C**; Halfpenny, K; Harry, R. S; Miller, C. M; Broncel, M; Sewell, S. L; Schaff, J. E; Deol, R; Carter, M. D; Wright, D. W. "The basis of the immunomodulatory activity of malaria pigment (hemozoin)." J. Biol. Inorg. Chem. **2006**, *11*, 917-29.

- **Schrimpe, A.C**.; Wright, D. W. "Comparative analysis of gene expression changes mediated by individual constituents of hemozoin." Chem. Res. Toxicol. **2009,** *22*, 433-445.

- **Schrimpe, A.C**.; Wright, D. W. "Differential gene expression mediated by 15-hydroxyeicosatetraenoic acid in LPS stimulated RAW 264.7 cells." Submitted.

- **Schrimpe, A.C**.; Wright, D. W. "Effects of Lipid Peroxidation Products on Matrix Metalloproteinase-9 Regulation in LPS stimulated RAW 264.7 Cells." Submitted.

- **Schrimpe, A.C**.; Wright, D. W. "4-hydroxynonenal impairs LPS-mediated expression of inducible nitric oxide synthase in RAW 264.7 cells." In preparation.

Abstracts of Conference Presentations

- **Schrimpe, A. C**; Wright, D W. "Inhibition of macrophage function upon phagocytosis of lipidized hemozoin." **The 57th Southeast/61st Southwest Joint Regional Meeting of the American Chemical Society**, Memphis, TN, November 1-4, 2005.

- Halfpenny, K. C; **Schrimpe, A. C**; Wright, David W. "Hemozoin: Malaria's Trojan horse." **The 231st ACS National Meeting**, Atlanta, GA, March 26-30, 2006; INOR 117.

- **Schrimpe, A. C**; Wright, D. W. **"**Basis of hemozoin immunoreactivity." **The 234th ACS National Meeting**, Boston, MA, August 19-23, 2007; INOR 098.

- Schrimpe, A. C; **Wright, D W**. "Hemozoin-mediated lipid peroxidation and its biological impact." **Gordon Conference, Chemistry & Biology of Tetrapyrroles**, Salve Regina University, Newport, RI July 20-25, 2008.

- **Schrimpe, A. C**; Wright, D. W. "Biological effects of hemozoin-mediated lipid peroxidation in macrophage-like cells." **The 41st Annual Meeting of the Society for Leukocyte Biology**, Denver, CO, November 6-8, 2008.

- **Schrimpe, A. C**; Wright, D. W. **"**Effects of hemozoin constituents on matrix metalloproteinase-9 regulation." **The 60th Southeast Regional Meeting of the American Chemical Society**, Nashville, TN, November 12-15, 2008; SERM 172.

References

- Prof. David W. Wright
  Vanderbilt University, Department of Chemistry, Station B 351822, Nashville, TN, 37235
  (615) 322-2636, david.wright@vanderbilt.edu

- Prof. David E. Cliffel
  Vanderbilt University, Department of Chemistry, Station B 351822, Nashville, TN, 37235
  (615) 343-3937, d.cliffel@vanderbilt.edu

- Prof. Daniel C. Liebler
  Vanderbilt University, Departments of Biochemistry, Pharmacology and Biomedical Informatics, U1213 MRBIII, Nashville, TN, 37232
  (615) 322-3063, daniel.liebler@vanderbilt.edu

- Prof. Brian O. Bachmann
  Vanderbilt University, Department of Chemistry, Station B 351822, Nashville, TN, 37235
  (615) 322-8865, brian.o.bachmann@vanderbilt.edu